Sphingolipids as modulators of T cell function

Sphingolipide als Modulatoren der T-Zell-Funktion

Doctoral thesis for a doctoral degree
at the Graduate School of Life Sciences,
Julius-Maximilians-Universität Würzburg,

Section Infection and Immunity

submitted by

Paulina Cruz de Casas

from

Mérida, Yucatán, México

Würzburg, 2024

Submitted on: ……..……..

Members of the Thesis Committee

Chairperson: Prof. Dr. Carmen Villmann

Primary Supervisor: Prof. Dr. Wolfgang Kastenmüller

Supervisor (Second): PD Dr. med. Niklas Beyersdorf

Supervisor (Third): Prof. Dr. rer. nat. Thomas Rudel

Supervisor (Fourth): Prof. Dr. med Andreas Beilhack

Date of Public Defense:……

Date of Receipt of Certificates:……

Table of contents

Summary

The immune system is responsible for the preservation of homeostasis whenever a given organism is exposed to distinct kinds of perturbations. Given the complexity of certain organisms like mammals, and the diverse types of challenges that they encounter (e.g. infection or disease), the immune system evolved to harbor a great variety of distinct immune cell populations with specialized functions. For instance, the family of T cells is sub-divided into conventional (Tconv) and unconventional T cells (UTCs). Tconv form part of the adaptive arm of the immune system and are comprised of αβ $CD4^+$ or $CD8^+$ cells that differentiate from naïve to effector and memory populations upon activation and are essential during infection and cancer. Furthermore, UTCs, which include γδ T cells, NKT and MAIT, are involved in innate and adaptive immune responses, due to their dual mode of activation, through cytokines (innate-like) or TCR (adaptive), and function. Despite our understanding of the basic functions of T cells in several contexts, a great number of open questions related to their basic biology remain. For instance, the mechanism behind the differentiation of naïve $CD4^+$ and $CD8^+$ T cells into effector and memory populations is not fully understood. Moreover, the exact function and relevance of distinct UTC subpopulations in a physiological context have not been fully clarified.

Here, we investigated the factors mediating naïve $CD8^+$ T cell differentiation into effector and memory cells. By using flow cytometry, mass spectrometry, enzymatic assays, and transgenic mouse models, we found that the membrane bound enzyme sphingomyelin-phosphodiesterase acid-like 3b (Smpdl3b) is crucial for the maintenance of memory $CD8^+$ T cells. Our data show that the absence of Smpdl3b leads to diminished $CD8^+$ T cell memory, and a loss of stem-like memory populations due to an aggravated contraction. Our scRNA-seq data suggest that Smpdl3b could be involved in clathrin-mediated endocytosis through modulation of Huntingtin interacting protein 1 (Hip1) levels, likely regulating TCR-independent signaling events. Furthermore, in this study we explored the role of UTCs in lymph node-specific immune responses. By using transgenic mouse models for photolabeling, lymph node transplantation models, infection models and flow cytometry, we demonstrate that S1P regulates the migration of tissue-derived UTC from tissues to draining lymph nodes, resulting in heterogeneous immune responses mounted by lymph nodes draining different tissues. Moreover, our unbiased scRNA-seq and single lineage-deficient mouse models analysis revealed that all UTC lineages (γδ T cells, NKT and MAIT) are organized in functional units, based on transcriptional homogeneity, shared microanatomical location and migratory behavior, and numerical and functional redundancy.

Taken together, our studies describe additional cell intrinsic (Smpdl3b) and extrinsic (S1P-mediated migration) functions of sphingolipid metabolism modulating T cell biology. We propose the S1P/S1PR1/5 signaling axis as the potential survival pathway for $Smpdl3b^+$ memory $CD8^+$ T cells and UTCs, mainly in lymph nodes. Possibly, Smpdl3b regulates S1P/S1PR signaling by balancing ligand-receptor endocytosis, while UTCs migrate to lymph nodes during homeostasis to be exposed to specific levels of S1P that assure their maintenance. Our results are clinically relevant, since several drugs modulating the S1P/S1PR signaling axis or the levels of Smpdl3b are currently used to treat human diseases, such as multiple sclerosis and B cell-mediated diseases. We hope that our discoveries will inspire future studies focusing on sphingolipid metabolism in immune cell biology.

Zusammenfassung

Das Immunsystem ist für die Aufrechterhaltung der Homöostase verantwortlich, wenn ein bestimmter Organismus verschiedenen Arten von Störungen ausgesetzt ist. In Anbetracht der Komplexität bestimmter Organismen wie Säugetiere und der verschiedenen Arten von Störungen, denen sie ausgesetzt sein können (z. B. Infektionen oder Krankheiten), hat sich das Immunsystem so entwickelt, dass es eine große Vielfalt verschiedener Immunzellpopulationen mit spezialisierten Funktionen beherbergt. So wird beispielsweise die Familie der T-Zellen in konventionelle (Tconv) und unkonventionelle T-Zellen (UTC) unterteilt. Tconv sind Teil des adaptiven Arms des Immunsystems und bestehen aus αβ-$CD4^+$- oder $CD8^+$-Zellen, die sich bei der Aktivierung von naiven zu Effektor- und Gedächtnispopulationen differenzieren und bei Infektionen und Krebs eine wichtige Rolle spielen. Darüber hinaus sind UTCs, zu denen γδ-T-Zellen, NKT und MAIT gehören, aufgrund ihrer dualen Aktivierungsweise durch Zytokine (angeboren) oder TCR (adaptiv) und ihrer Funktion an angeborenen und adaptiven Immunantworten beteiligt. Trotz unseres Verständnisses der grundlegenden Funktionen von T-Zellen in verschiedenen Zusammenhängen gibt es nach wie vor eine große Anzahl offener Fragen im Zusammenhang mit ihrer grundlegenden Biologie. So ist beispielsweise der Mechanismus der Differenzierung naiver $CD4^+$ und $CD8^+$ T-Zellen in Effektor- und Gedächtnispopulationen noch nicht ausreichend verstanden. Auch die genaue Funktion und Bedeutung der verschiedenen UTC-Subpopulationen im physiologischen Kontext sind noch nicht vollständig geklärt.

Wir haben die Faktoren untersucht, die die Differenzierung naiver CD8+ T-Zellen in Effektor- und Gedächtniszellen vermitteln. Mithilfe von Durchflusszytometrie, Massenspektrometrie, enzymatischen Assays und transgenen Mausmodellen konnten wir feststellen, dass das membrangebundene Enzym Sphingomyelin-Phosphodiesterase acid-like 3b (Smpdl3b) für die Aufrechterhaltung der $CD8^+$ T-Zell-Gedächtnisfunktion entscheidend ist. Unsere Daten zeigen, dass das Fehlen von Smpdl3b zu einer verminderten Anzahl and $CD8^+$ T Gedächtniszellen durch eine verstärke Kontraktion sowie einem Verlust von stammzellartigen Gedächtnispopulationen führt. Unsere scRNA-seq-Daten deuten jedoch darauf hin, dass Smpdl3b an der Clathrin-vermittelten Endozytose beteiligt sein könnte, indem es die Spiegel des Huntingtin interacting protein 1 (Hip1) moduliert und wahrscheinlich TCR-unabhängige Signalereignisse reguliert. Darüber hinaus untersuchten wir in dieser Studie die Rolle von UTCs bei lymphknotenspezifischen Immunantworten. Mit Hilfe von transgenen Mausmodellen für Photolabeling, Lymphknotentransplantationsmodellen, Infektionsmodellen und Durchflusszytometrie konnten wir zeigen, dass S1P die Migration von UTCs aus dem Gewebe in die drainierenden Lymphknoten reguliert, was zu heterogenen Immunantworten in den Lymphknoten führt, die verschiedene Gewebe drainieren. Ausserdem ergab unsere Analyse von scRNA-seq-Daten, sowie Mausmodelle mit einer genetischen Defizienz einzelner UTC-Linien (γδ-T-Zellen, NKT und MAIT), dass diese zusammen in funktionellen Einheiten organisiert sind, die auf transkriptioneller Homogenität, gemeinsamer mikroanatomischer Lage und Migrationsverhalten sowie numerischer und funktioneller Redundanz basieren.

Zusammengenommen beschreiben unsere Studien zusätzliche zellinterne (Smpdl3b) und -externe (S1P-vermittelte Migration) Funktionen des Sphingolipid-Stoffwechsels, welche die T-Zell-Biologie modulieren. Wir schlagen die S1P/S1PR1/5-Signalachse als potenziellen Überlebensweg für $Smpdl3b^+$ Gedächtnis-$CD8^+$-T-Zellen und UTCs ausschließlich in Lymphknoten vor. Möglicherweise

reguliert Smpdl3b die S1P/S1PR-Signalübertragung, indem es die Endozytose des Liganden-Rezeptors reguliert. Dadurch könnte deren Exposition zu bestimmten S1P-Mengen in der Homöostase im Lymphknoten reguliert werden, die wiederum das Überleben der UTC steuern. Unsere Ergebnisse sind klinisch relevant, da mehrere Medikamente, die die S1P/S1PR-Signalachse oder die Smpdl3b-Konzentration modulieren, derzeit zur Behandlung menschlicher Krankheiten eingesetzt werden, z. B. bei Multipler Sklerose und B-Zell-vermittelten Krankheiten. Wir hoffen, dass unsere Entdeckungen zukünftige Studien anregen werden, die sich auf den Sphingolipid-Stoffwechsel in der Immunzellbiologie konzentrieren.

Introduction

The immune system

The immune system (IS) is often referred to as the organism's defense and tolerogenic system against pathogens and commensal microorganisms, respectively. However, several other functions have been identified in recent years, such as tissue repair, healing and regeneration[1-3], organ development and remodeling[4-6], and fighting diseases such as cancer[7,8]. Overall, the ultimate goal of the immune system is to preserve, or restore the organism's homeostatic state, particularly when certain perturbations occur.

In order to achieve its varied functions, the mammalian IS is comprised by a heterogeneous pool of cell types and organs that are widely distributed throughout the body. Owing to their purpose, the organs forming part of the IS have been divided into primary (bone marrow (BM) and thymus) and secondary (spleen, lymph nodes (LNs)) lymphoid organs. Primary lymphoid organs (PLO) are responsible for the generation and development of immune cells, whereas secondary lymphoid organs (SLO) are important for maintenance and activation of certain naïve immune populations. Additionally, cells are categorized into myeloid and lymphoid cells. Myeloid cells are comprised of dendritic cells (DCs), macrophages, monocytes, and granulocytes (neutrophils, eosinophils, and basophils). Lymphoid cells include B cells, T cells, natural killer (NK) cells and innate lymphoid cells (ILCs)[9]. Evidently, the cellular compartment of the IS is exceptionally diverse, with each cell type having a unique biology and function. However, the core aim of these diverse cell types is to constantly discern the status of the organism (homeostasis, inflammation, infection, or disease) and, when necessary, mount the adequate immune responses to reestablish homeostasis. To achieve this, immune cells mainly rely on cell-to-cell communication with other immune and non-immune cells in a contact-dependent or independent fashion. Contact-independent intercellular communication materializes in the form of cytokines[10] and chemokines[11], which are proteins produced by immune and non-immune cells in a context-dependent manner. Cytokines maintain, activate, differentiate, or suppress immune cells. For instance, interleukin-7 (IL-7) and IL-15 are survival cytokines produced by DCs, monocytes and epithelial cells during homeostasis[10]. IL-7 and IL-15 maintain T and NK cells, whereas IL-1β and IL-6, produced by macrophages and fibroblasts during inflammation, activate macrophages, B and T cells[10]. IL-10 acts as a suppressor cytokine to diminish an immune response[10]. Likewise, chemokines are produced by a variety of immune and non-immune cells in homeostatic or inflammatory conditions. Chemokines, together with integrins, are predominantly responsible for determining the location of cells within specific tissues or areas of these tissues[12,13]. In brief, distinct immune cell types express their own plethora of cytokine and chemokine receptors, and integrins. Together, these molecules largely define the migratory behavior, location and function of immune cells[14].

Each immune cell type follows a particular developmental pathway and is characteristically distributed throughout the organism. For instance, some macrophage and monocyte populations originate in the yolk sac or the fetal liver[9,15]. Late during development, monocyte populations[9,15], DCs[9,16], granulocytes[9,17], NK cells[9,18] and B cells[9,19] develop in the BM, whereas T cells arise in the thymus[9,20,21]. Following their development, immune cells exit the aforementioned organs through the bloodstream. Certain populations occupy lymphoid and non-lymphoid tissues, where they finalize their maturation and become tissue-resident cells. As an example, BM-derived precursors of DCs (preDCs) can finalize their

maturation in LNs or in peripheral tissues (skin and mucosal organs), where they become LN-resident DCs[22] or immature migratory DCs (migDCs)[23], respectively. Furthermore, macrophages, ILCs and unconventional T cells (UTCs) populate tissues pre- or neonatally[24-27]. Conversely, immune cells such as naïve lymphocytes, continuously circulate between SLO[9], while monocytes circulate within the bloodstream[28]. The tissue-resident or migratory phenotype of immune cells is related to the functional specialization of each population and will be discussed below. Namely, DCs are professional antigen presenting cells (APCs) that constantly capture antigens during homeostasis and inflammation, present them to lymphocytes and either induce tolerance or activation[29]. Therefore, LN-resident and migDCs continuously phagocytose and present soluble and cell-associated autoantigens to maintain tolerance. Based on their strategical position, they can also rapidly gain access to foreign antigens following infections. Naïve circulating lymphocytes specific for one particular foreign antigen (antigenic determinant) are scarce (less than 1 in 10000)[9]. Hence, these limited antigen-specific lymphocytes recirculate to maximize the probability of encountering their cognate foreign antigen by "scanning" APCs throughout SLO draining distinct tissues.

Concisely, the IS is a highly organized system comprised by a heterogeneous pool of specialized immune cells. Their differing migratory patterns and location, which will be further discussed in the following sections, are determined by the expression of chemokine receptors and integrins, which in turn are regulated by the differentiation state of the cell and reflect their functional specialization.

The lymphatic system and lymphatic organs

The cardiovascular and lymphatic systems are essential for immune cell trafficking between distinct lymphoid organs. The lymphatic system is formed by lymphatic vessels that originate in peripheral tissues. These vessels are responsible for collecting interstitial fluid (ISF), which is referred to as lymph once it enters the lymphatics and transports it in a unidirectional manner towards the blood circulation. Lymphatic drainage of ISF from tissues and its return to the bloodstream are crucial to maintain peripheral tissue homeostasis, by removing excess extracellular fluid and waste products from the organs[30,31]. Moreover, lymph also acts as a means of transportation for tissue-derived migratory immune cells[32-34].

Each tissue is connected to its draining lymph node(s) (dLN) via the lymphatic vessels. Hence, the lymph drained from tissues will be temporarily collected in dLNs before its return to the bloodstream. Importantly, dLNs are the meeting venue for various LN-resident and migratory cells. Owing to these characteristics, dLNs are the optimal site for continuous sampling and purification of lymph before it enters the bloodstream. For instance, LN-resident macrophages are essential for phagocytosing molecules or pathogens present in the lymph to avoid their systemic spread[35]. Moreover, LN-resident and migDCs can present tissue- or pathogen-derived antigens and activate lymphocytes in dLNs[36]. Therefore, the main functions of LNs are to act as filters that prevent systemic pathogen spreading[37], to orchestrate the induction of tolerance, and to mount the appropriate immune response in case of infection or disease. To fulfill these purposes, immune cells in LNs express specific chemokine receptors that segregate them into specific areas, to ensure efficient cell-to-cell interactions and antigen accessibility. In particular, $CXCR5^+$ B cells and $CXCL13^+$ follicular dendritic cells (FDCs), a cell type that

can store antigen for long periods of time[38], are organized into follicle structures referred to as B cell follicles. Furthermore, CCL19/21$^+$ fibroblastic reticular cells (FRCs) located in the LN paracortex define the T cell zone, the area where the CCR7$^+$ conventional T cells (Tconv) and CCR7$^+$ DCs are positioned[39]. Additionally, UTCs and ILCs are located between B cell follicles[34,40,41], while NK cells are also found in the interfollicular area and, primarily, in the LN medulla[42]. Finally, macrophages are more dispersed within LNs, distributed in the subcapsular and medullary sinus, medullary cord, and the T cell zone[43-45].

In contrast to LNs, the spleen is a secondary lymphoid organ that lacks connection to lymphatic vessels. Hence, the main roles of the spleen are to filter blood-derived pathogens, antigens, and aged erythrocytes. Furthermore, similarly to LNs, the spleen also facilitates interactions between distinct immune cell types[46]. Structurally, the spleen is divided into red pulp, the marginal zone (the zone between the red and the white pulp) and the white pulp. The red pulp owes its name to being the area of the spleen where the blood is delivered to, whereas the white pulp is usually referred to as a LN-like structure[46,47]. Various immune cell populations inhabit or circulate throughout the spleen and collectively mount immune responses against blood-borne pathogens. The red pulp harbors macrophages, which are responsible for phagocytosing aged-erythrocytes and blood-borne antigens. Additionally, neutrophils, monocytes, DCs and UTCs are found in the red pulp. Within the white pulp, CCR7$^+$ naïve T cells, CCR7$^+$ DCs and CCL21$^+$ FRCs are located in the T cell zone, whereas CXCL13$^+$ FDCs and CXCR5$^+$ B cells form the spleen follicles. Finally, the marginal zone harbors macrophages, LFA-1$^+$ α4β7$^+$ innate-like B cells and LFA-1$^+$ α4β7$^+$ DCs[46,47].

Together, LNs and spleen function as specialized filtering organs that facilitate close interactions between resident and migratory immune cells, promoting the generation of immune responses tailored against specific microbial challenges, tissue damage or disease.

Immune cell migration patterns

As noted above, immune cells can settle in tissues to become tissue-resident, or they can transiently access organs by recirculating within the blood and lymphatic vessels. Furthermore, some cells migrate from peripheral tissues to dLNs via the lymphatics. The location and migratory pattern pursued by the diverse immune cell populations reflect their functional role. However, the resident or migratory phenotype of each immune cell population is strategically designed to optimize the adequate activation or suppression of the immune response(s) to ensure homeostasis of the organism as a whole.

Tissue-resident immune cells

Tissue-resident immune cells are strategically positioned to be the first line of defense of the organism. Therefore, these cells can be rapidly activated to recruit and activate other immune cells by producing anti- or pro-inflammatory cytokines. Additionally, tissue-resident APCs can rapidly acquire and present antigens locally for the induction of tolerance or inflammation. Examples of tissue-resident myeloid cells are macrophages and DCs, whereas tissue-resident lymphocytes include ILCs, UTCs and memory T-, B- and NK-resident cells.

Macrophages are myeloid cells that initially derive from the yolk-sac and the fetal liver early during development, and seed developing organs in the perinatal period. In certain organs,

macrophages are imprinted by the tissue where they reside, and become long-lived self-renewing tissue-resident populations. However, other tissues rely on constant replenishment of the macrophage population by blood-derived monocytes that further differentiate into tissue-resident macrophages. The functions of tissue-resident macrophages are diverse and organ-specific, ranging from organ development, regeneration and maintenance to phagocytosis and removal of cell debris, dying cells, pathogens, and antigens. By their location and diverse functions, macrophages are essential for starting the adequate immune response cascade that will recruit other immune cells by producing anti-inflammatory cytokines such as IL-10, or pro-inflammatory cytokines, including IL-1β, IL-6 and IL-12[9,24,48,49]. An additional myeloid cell lineage that gives rise to tissue-resident populations are the aforementioned DCs. DCs develop as preDCs in the BM, then exit via the bloodstream and some enter LNs through medullary high endothelial venules[22]. These cells establish residency in the LN medulla and further develop into mature LN-resident DCs. Their location allows them to constantly scan lymph-derived soluble antigens transported by the conduit system (maximum 70kDa) and rapidly present them to T cells positioned in the paracortex T cell zone[50,51].

"Innate-like" lymphocytes that are considered tissue-resident are ILCs and UTCs. Both lineages develop from common lymphoid progenitors (CLP) early during development, seeding lymphoid and non-lymphoid tissues. ILCs and UTCs are considered "innate-like" because they can be rapidly activated in a cytokine-mediated manner due to their effector-like differentiation state in tissues. Furthermore, their location in tissues renders them as part of the first line of defense of the organism. ILCs lack antigen-specific receptors and differentiate into Th1-, Th2- or Th17-like cells, producing IFNγ, IL-5 and IL-13, and IL-17, respectively[27,52]. On the other hand, UTCs are a heterogeneous group of T cells comprised by γδ T cells, mucosal-associated invariant T cells (MAIT) and natural killer T cells (NKT), which are also differentiated into Th1-, Th2- or Th-17 like subpopulations and can be activated in a TCR-independent manner to rapidly produce IFNγ and IL-17[27,53].

Closely related to ILCs are the recently identified tissue-resident NK cells. These cells settle in the skin or salivary glands upon acute or chronic infections, respectively, but are also found in certain tissues (e.g. salivary glands) during early life in the absence of infection[54,55]. During an acute infection, tissue-resident NK cells accelerate the immune response by producing pro-inflammatory cytokines to clear the infection[54]. In a chronic infection setting, tissue-resident NK cells play a protective role to maintain tissue homeostasis[55]. Similarly to skin tissue-resident NK cells[54], tissue-resident memory T cells (TRM) arise and persist in non-lymphoid tissues following an acute infection. Antigen-specific T cells seed the site of infection and persist as long-lived antigen-specific memory populations. Therefore, their location and phenotype allow them to be rapidly activated in the context of a secondary infection with the same pathogen, without the need of being recruited from the circulation as their naïve counterparts[56].

In summary, tissue-resident myeloid and lymphoid immune cell populations provide prompt local immunity in the tissues that they inhabit by executing rapid effector functions and by recruiting and activating other immune cells.

Recirculating immune cells

Various immune cell populations recirculate between SLO via the bloodstream with the purpose of i) surveilling and having rapid access to potentially injured or infected tissues, or ii) to increase the possibility of encountering their cognate antigen and become activated in SLO. Monocytes, neutrophils, and NK cells constantly circulate in the blood to facilitate and accelerate their recruitment to sites where inflammation occurs. However, naïve and memory B and T cells recirculate between SLO, to scan APC in the quest of their cognate antigen.

Monocytes are short-lived myeloid cells that can be categorized into $Ly6C^+$ $CCR2^+$ "classical" and $Ly6C^-$ $CX3CR1^+$ "non-classical" monocytes. Several studies suggest that $Ly6C^+$ monocytes downregulate this molecule and give rise to $Ly6C^-$ monocytes, yet it is also possible that these two subsets develop independently in the BM. Both populations circulate in the bloodstream. Circulating classical monocytes extravasate into affected tissues and differentiate into tissue-resident macrophages or DCs, whereas non-classical monocytes rather patrol the vasculature in homeostatic and inflammatory conditions. Importantly, patrolling non-classical monocytes migrate slower than classical monocytes, independently of the blood flow direction, removing cell debris and apoptotic cells from the vasculature[28,57,58]. Besides monocytes, neutrophils are additional short-lived myeloid cells that exit the BM succeeding their development and integrate the blood circulation. Neutrophils are the most abundant immune cell type in the blood. Smaller in size than macrophages, neutrophils are described as circulating granulocytes with a phagocytic capacity. These cells are constantly patrolling the blood and are rapidly recruited to tissues upon inflammatory scenarios, where they release numerous antimicrobial molecules, inflammatory cytokines and phagocytose pathogens[59]. Furthermore, recent studies suggest that circulating neutrophils are capable of accessing certain tissues during homeostasis, as part of the circadian cycle, and likely regulate tissue physiology[60].

Circulating lymphoid cells include NK, B and T cells. NK cells access the bloodstream following their development in the BM and have the capacity to circulate accessing organs such as spleen, lungs, and liver. Upon inflammation, circulating NK cells can be recruited to several tissues to exert their effector functions[61]. Hence, being in the blood circulation facilitates NK recruitment when and where required. Importantly, as previously mentioned, blood recirculation is not only crucial for accelerating immune cell recruitment, but also to increase the possibility for lymphocytes expressing antigen-specific receptors to encounter their cognate antigen. Only a low frequency of B and T cells that recognize distinct antigens or peptide-MHC molecules, respectively, are generated, selected and egress the bone marrow (B cells) or thymus (T cells) as mature cells. Therefore, they require constant accessibility to different LNs and the spleen to augment the chance of encountering their cognate antigen[9,37,62]. Naïve lymphocyte recirculation is a process regulated in a circadian-manner[63], and similarly mimicked by certain subsets of memory T cells[64].

In brief, immune cell recirculation is essential for facilitating immune cell recruitment into affected organs and, together with the anatomical structure of SLO, to ease the activation of antigen-specific lymphocytes by encountering of their cognate antigen.

Migratory non-recirculating immune cells

Besides tissue-resident and recirculating cells, certain subsets of immune populations have been identified as tissue-derived migratory cells. Particularly, the route of migration followed by these populations is from tissues to dLNs via the lymphatics. Immune cells that follow this unidirectional migration route connecting tissues and LNs include migDCs, a subset of γδ T cells, Langerhans cells, Langerhans-like DCs, and ILC/DC-like APCs.

Immature migDCs are a subset of myeloid cells which can be activated in their residing non-lymphoid tissues once they encounter certain tissue-specific or pathogen-derived antigens. Then, the activated antigen-bearing DCs migrate via the lymphatics to the dLN, where they interact with lymphocytes[23]. The phenotype of migDCs is imprinted by their tissue of origin. Interestingly, dLNs co-draining several tissues have a mixture of phenotypically heterogeneous migratory DC populations[65]. Consequently, migDCs will activate, polarize, and instruct lymphocytes to i) become inflammatory or tolerogenic, and ii) home to the tissue of origin of the DCs, where they will encounter their cognate antigen[65-67]. Similarly to migDCs, a subset of skin γδ T cells has been shown to migrate from skin to dLNs during homeostatic conditions[33,68,69]. Additional cell types that also migrate via the lymph to dLNs are skin Langerhans cells (LCs)[23,27,70], skin LC-like DCs[71] and a newly identified population of ILC/DC-like APCs which migrate from skin or mucosal tissues to dLNs[72].

Aside from migDCs, the physiological function that underlies the lymphatic migration of γδ T cells, LCs, LC-like DCs and ILC/DC-like APCs is yet to be discerned. However, it is clear that these tissue-derived non-recirculating immune cell populations act as a direct connection between non-lymphoid tissues and dLNs. Hence, they act as a source of information to report the status of peripheral tissues to resident or transiently visiting immune cells in LNs.

Innate and adaptive immunity

Evidently, the cellular elements of the immune system are highly dynamic and functionally heterogeneous. As noted, their location within organs and their migratory behavior are part of their specific roles in immunity. In general, the immune system and its cell types can be segregated into innate and adaptive arms of the IS. The innate immune system is often described as a conserved immediate response initiated when non-self-antigens are encountered within an organism. The discrimination between self and non-self is achieved by the expression of pattern-recognition receptors (PRRs), whose ligands are pathogen-associated molecular patterns (PAMPs) or damage-associated molecular patterns (DAMPs). PAMPs and DAMPs may be proteins, nucleotides or lipids that constitute the pathogen, or that are released upon cellular damage and death[73]. These “danger signals” are conserved among species and can be recognized by numerous germline encoded receptors such as Toll-like receptors (TLR)[74], retinoid acid-inducible gene I (RIG-I)-like receptors[75], AIM2-like receptors (ALRs)[76], and nucleotide-binding oligomerization domain (NOD)-like receptors[77]. The activation of certain PRRs will lead to the release of antimicrobial peptides, autophagy or phagocytosis, and the production of pro-inflammatory cytokines and chemokines[78,79].

Immune cells orchestrating innate responses comprise tissue-resident and circulatory myeloid or lymphoid cells. This cellular diversity is required to achieve an efficient coordinated innate immune

response, that will lead to the initiation of an equally efficient adaptive immune response. Examples of cells involved in the innate immune response include macrophages, monocytes, ILCs, NK cells and neutrophils. Macrophages are present in nearly every organ and express various PRRs, therefore can be rapidly activated by pathogens or tissue damage. Activated macrophages will exert diverse innate functions, such as phagocytosis and secretion of pro-inflammatory molecules that will further activate and recruit other immune cells[9,24,48,49,80,81]. The local innate response typically driven by macrophages is amplified by additional resident populations, such as ILCs activated by macrophage-derived pro-inflammatory cytokines[82]. Furthermore, the enhanced inflammatory environment in the tissue will recruit additional immune cells from the circulation, like neutrophils, monocytes, and NK cells[28,57-59,61]. Together, the innate immune response is orchestrated by various immune cell populations whose main purposes are to i) clear or locally contain the pathogen, ii) promote tissue healing and repair, and iii) set the stage for the initiation of the adaptive immune response.

Adaptive immunity is a fine-tuned immune response that complements innate responses to establish complete immune protection. An important distinction between innate and adaptive immunity is that the receptors expressed by adaptive immune cells are not germline encoded. Adaptive immune cells include lymphocytes expressing B or T cell receptors (BRC; TCR). During B and T cell development, BCRs and TCRs undergo somatic diversification, a process in which site-specific DNA recombination occurs. The somatic recombination of BCR and TCR is responsible for the particular antigen-specificity of each receptor, or clone. Hence, individual pathogen-specific BCR or TCR can recognize a different antigens, epitopes or peptide/MHC molecules[9,83,84]. Immune cells critically participating in adaptive immune responses are DCs, B and T cells. As previously noted, DCs can be subdivided in to resident or migratory populations. Both DC subsets express PRRs and can, therefore, be activated by PAMPs and DAMPs. DCs will acquire and process both, commensal- and pathogen-derived antigens, and induce tolerogenic or inflammatory lymphocytes, respectively[22,23,29]. In addition to pathogen recognition, the inflammatory environment caused by the innate response will accelerate DC maturation[22]. DCs are essential for antigen presentation to T cells[84], whereas BCRs can recognize native soluble or membrane-bound antigens[85]. Proceeding activation with the respective cognate antigen, activated B and T cell clones proliferate and generate a great number of cells with an identical BCR or TCR. Furthermore, the progeny of these activated cells will differentiate into short-lived effector and long-lived memory populations[85,86]. Effector and memory B cell populations are important for the generation of antibody-mediated immunity (humoral response)[87], whereas diverse T cell populations exert different functions as part of the cellular immune response[53,88,89].

Overall, the innate and adaptive arms of the immune system complement one another to mount short and long term, highly specific immune responses. During an acute challenge (microbial infection or injury), the innate and adaptive immune cells mount a coordinated response to restore homeostasis. In the context of infection, once the primary challenge has been resolved by the innate and adaptive effector populations, long-lived pathogen-experienced populations, which are epigenetically distinct from their naïve counterparts, remain. If the same pathogen is encountered, these long-lived innate and adaptive populations exert enhanced effector functions as in comparison to the primary infection. This is referred to as “trained immunity” for innate cells, such as macrophages and monocytes, and as “immune memory” for lymphocytes, such as NK cells, B and T cells[54,85,86,90-92].

The family of T cells: conventional and unconventional T cells

The family of T cells is comprised by a heterogeneous pool group of lymphoid cells which develop from BM-derived progenitor cells that migrate to the thymus. In the thymus, these T cell progenitors, referred to as thymocytes, undergo distinct developmental stages from which separate T cell lineages emerge. CD4 CD8 double negative (DN) thymocytes initiate TCR-gene assembly through a process known as V(D)J recombination, which gives rise to the expression of γδ or β TCR chains. DN thymocytes that successfully recombine a β chain, upregulate CD4 and CD8 co-receptors and further mature to become double positive (DP) thymocytes. At the DP stage, the genes coding for the TCR α chain begin to recombine, and give rise to a functional αβ TCR[93]. DP thymocytes containing a functional αβ TCR are submitted to a quality control process known as "positive selection". During positive selection, the capacity of the newly generated TCRs to interact with antigen presenting molecules (APM) is tested. Cortical thymic epithelial cells express the APM major histocompatibility complex (MHC) glycoproteins. DP thymocytes whose TCR recognizes and interacts with MHC molecules are positively selected, whereas those who fail to interact with MHC molecules die via apoptosis (death by neglect). At this stage, lineage commitment to become a CD4 or CD8 single positive (SP) T cell arises, as CD8 T cells interact with MHC-I and CD4 T cells interact with MHC-II. Therefore, downregulation of CD4 or CD8 occurs and the SP thymocytes migrate into the thymus medulla. Medullary thymic epithelial cells are responsible for an additional quality control step known as negative selection. During negative selection, medullary thymic epithelial cells present endogenous antigens in the form of peptides via MHC-I and II. SP thymocytes with a high affinity towards self-antigens will i) succumb to clonal deletion to prevent autoimmunity, or ii) further develop into MHC-II-dependent $CD4^+$ regulatory T cells (Treg) that control or suppress immune responses[21]. $CD4^+$ αβ T cells, $CD8^+$ αβ T cells and Treg that survived positive and negative selection will further mature, leave the thymus and enter the bloodstream as functional naïve recirculating Tconv.

As previously stated, some DN thymocytes will randomly recombine the γ and δ TCR chains and will further develop into γδ T cells. To date, no APM have been identified for γδ T cells, leaving unclear whether they undergo analogous positive and negative selection processes like αβ Tconv. However, subsets of innate-like γδ T cells are "agonist selected" by strongly binding to endogenous ligands (self-agonists), similar to Treg[21,94]. Moreover, phosphoantigens have been identified as γδ TCR antigens[95], and an "antibody-like" mode of antigen recognition has been postulated for the γδ TCR[96]. However, it has been shown that αβ DP thymocytes regulate γδ T cell development through various molecules such as lymphotoxin[97-99]. Additional αβ T cell lineages whose developmental pathway differs from Tconv are NKT and MAIT. Commitment to the NKT or MAIT lineages occurs when the TCR of DP thymocytes is capable of interacting with the non-polymorphic APM CD1d or MR1, respectively. CD1d and MR1 are non-polymorphic APM whose function is analog to MHC molecules. Yet, CD1d presents lipids and MR1 presents small microbial-derived metabolites rather than protein-derived antigens[100]. CD1d and MR1 in the thymus are expressed by DP thymocytes, instead of cortical epithelial cells. Hence, NKT and MAIT selection involves DP-DP thymocyte interactions through CD1d or MR1, and strong binding of self-lipids and commensal microbial metabolites (agonist selection), respectively[99,101-103]. In summary, the developmental pathway, APM-dependency and class of antigens recognized by γδ

T cells, NKT and MAIT differ from Tconv. These are some of the various reasons why these T cell lineages are referred to as unconventional T cells (UTCs)[89].

An additional factor differing between Tconv and UTCs is their differentiation state when exiting the thymus. Mature Tconv exit the thymus as naïve cells that will be activated upon antigen presentation in SLO[21,104]. In the periphery, naïve $CD4^+$ T cells recognize extracellular antigens loaded into MHC-II molecules expressed by phagocytic APCs, such as DCs and macrophages[105]. Then, activated naïve $CD4^+$ T cells proliferate and differentiate into T helper (Th) cells with a differing phenotype, based on the cytokine environment created during the innate immune response to a specific pathogen[106]. For instance, Th1 cells are IFNγ producers that arise from an IL-12-rich environment during viral or intracellular bacterial infections[107], whereas Th2 cells are induced by alarmins, IL-25 and IL-33, and produce IL-4 and IL-13 to control parasitic infections[108,109]. Th17 cells are essential for the immune response mounted against extracellular bacteria and fungi by producing IL-17[106,110]. The term "helper" is attributed to differentiated $CD4^+$ T cells due to their various functions regulating other immune cells, like macrophages, DCs and B cells for the germinal center reaction[103]. Also in the periphery, naïve $CD8^+$ T cells must be activated by professional APCs, namely DCs, presenting antigen via MHC-I[111,112]. Activated $CD8^+$ clonally expand and differentiate into cytotoxic lymphocytes (CTL) and memory cells[113]. Following activation, CTL are able to recognize intracellular antigens presented by MHC-I in the surface of almost all nucleated cells, hence identifying infected or malignant cells and directly killing them[9,114]. In brief, Tconv leave the thymus as naïve populations that require antigen presentation to exert their helper and cytotoxic functions. Similarly to $CD4^+$ T cells, UTCs differentiate into Th1-, Th2- and Th17-like cells. However, UTC differentiation occurs already in the thymus prior to their exit and can be activated in a TCR-independent cytokine-mediated manner[53,99]. Interestingly, effector-like UTCs do not recirculate between SLO as naïve Tconv following thymic egress. Instead, they seed diverse non-lymphoid tissues early during development and establish tissue-residency[53,115,116]. Importantly, the tissue seeding of UTCs is a highly coordinated process in which cells expressing a specific TCR chains (e.g. Vγ6) will seed specific organs during distinct developmental windows (e.g. skin and lung)[103,115,117].

Naturally, the distinct T cell lineages have specialized roles during homeostasis or an immune response. Briefly, $CD4^+$ Th subsets contribute to pathogen-specific and anti-tumor immune responses, mainly by producing the required cytokines and regulating other immune cells, including $CD8^+$ CTL. Treg are essential for controlling autoimmunity and to regulate inflammation by suppressing immune responses via diverse mechanisms. $CD8^+$ T cells are the killer cells that clear infected or malignant cancer cells[118]. UTCs have varied TCR-dependent and independent roles in wound healing, tissue repair, nutrient sensing, thermogenesis, and infection[53,89]. Although our understanding of basic T cell biology is profound, several open questions regarding individual lineages remain. Namely, the mechanisms underlying Tconv differentiation from naïve into effector and memory populations are still topics of active research[113,119]. Moreover, the missing insights regarding the antigen-specificity of the individual UTC lineages in physiological conditions limit our understanding of their function in diverse settings.

Sphingolipids and T cells

Sphingolipids (SLs) are defined as a major class of lipids mainly present in eukaryotic cells. This group of lipids is comprised by more or less complex species that are structurally related to each other. SLs are distributed along nearly every cellular compartment across cell types, including the plasma membrane (PM), endoplasmic reticulum (ER), Golgi apparatus, lysosomes, mitochondria, and even the extracellular space. Moreover, certain SL species have been described as bioactive lipids due to their involvement in cellular signaling pathways such as cell death, proliferation, differentiation, survival, and migration, among others[120]. Their ubiquitous abundance as structural and bioactive molecules have positioned SLs in the focus of various studies over the last decades.

The metabolic pathway of SL is highly interconnected due to a great variety of synthetizing and degrading enzymes present along the pathway, and to their similar structure between the SL species (Chapter 1: Role of Smpdl3b in CD8$^+$ T cells. Figure 1A)[120,121]. The SL *de novo* synthesis pathway begins with the condensation of L-serine and palmitoyl-CoA by the enzyme serine palmitoyltransferase (SPT), giving rise to 3-ketosphinganine (KS). Then, KS is subsequently converted to dihydrosphingosine, which further generates dihydroceramide (dhCer). dhCer is next reduced to ceramide (Cer), the core species in the SL metabolism pathway. Alternative sources of Cer are the salvage pathway, in which complex SL and sphingosine are degraded or converted back into Cer, respectively[122]. Cer acts as the backbone of more complex SL species, such as sphingomyelin (SM), glycosphingolipids and gangliosides, among others. Additionally, it can be converted to sphingosine and sphingosine-1-phosphate (S1P)[120,123,124]. The bioactive function of SL depends on their location within cells[120,122], with differing intra- and extracellular roles, and on the studied cell types, including T cells[125,126]. Importantly, membrane-associated SL such as glycosphingolipids, SM and Cer form part of highly organized domains, known as lipid rafts, and lipid-enriched platforms. These SL-enriched structures serve as sites for receptor clustering, enhancing signal transduction[127,128]. For instance, Cer generated from SM degradation by sphingomyelinases (SMases) in the PM forms Cer-enriched platforms that enhance receptor signaling events and modulate membrane fluidity[122,129-131], whilst mitochondrial Cer modulates cell death via apoptosis[132-134].

An important discovery in T cell biology was the regulation of lymphocyte egress from lymphoid organs via the S1P/S1PR signaling pathway. Sphingosine-1-phosphate receptors (S1PRs) are G-protein coupled receptors whose ligand is S1P. Each receptor has a distinct downstream signaling pathway[135]. T cells mainly rely on S1P-receptor 1 (S1PR1) to sense the abundance of S1P in the local milieu[136,137]. The highest concentration of extracellular S1P is found in the blood and it is also abundant in the lymph. Blood S1P is mainly synthetized by red blood cells (RBCs), and to a lesser degree endothelial cells, whereas lymph S1P is produced by lymphatic endothelial cells (LECs)[138,139]. Mature Tconv exit the thymus to the bloodstream in an S1P/S1PR1-dependent manner, by following the high concentration of S1P[21,136,138]. Importantly, S1P levels within lymphoid organs and tissues are lower than in the blood and lymph due to the activity of the S1P-degrading enzyme S1P-lyase. S1P-lyase expression is absent in blood and lymph, while active in lymphoid and non-lymphoid tissues, and is responsible for creating the S1P gradient[140,141]. To prevent prolonged retention in blood, T cells downregulate S1PR1, a process known as S1PR1 desensitization[137,142,143]. Following desensitization, Tconv access SLO through high endothelial venules. Within SLO, the levels of S1P are low, leading to

the upregulation of S1PR1 on the circulating lymphocytes[138,143]. Finally, S1PR1$^+$ Tconv egress SLO by following the increasing S1P gradient towards the lymph (LNs) or blood (spleen)[136,138]. Similarly to Tconv, UTCs upregulate S1PR1 in the thymus and follow the S1P gradient towards the bloodstream[144,145], to then seed their respective tissues[53,115,116]. Interestingly, recent studies found that S1PR2 is involved in the retention of a subset of γδ T cells in the skin, together with the retention molecule CD69. However, the homeostatic downregulation of CD69 and the upregulation of S1PR1 regulate the lymphatic migration of skin γδ T cells to the dLNs[33,68,69].

During inflammatory conditions, a balance between retention and egress is essential to assure proper Tconv activation and rapid egress to the site of infection. CD69 expression is promptly induced in lymphocytes exposed to type I interferons, present in the inflamed LNs, and TCR-mediated activation[146,147]. CD69 blocks S1P-mediated T cell egress from SLO by inducing the degradation of S1PR1[148], hence retaining and accumulating polyclonal recirculating T cells in LNs[146]. Likely, the initial retention of lymphocytes in LNs by type I interferon induced CD69 is important to assure APC-T cell interactions, increasing the probability of cognate antigen encounter[136,138]. Furthermore, the levels of CD69 induction upon TCR activation might be influenced by the TCR-ligand affinity since high affinity antigens induce higher levels of CD69 and lower levels of S1PR1. Conversely, low affinity antigens induce lower levels of CD69 and higher levels of S1PR1, favoring egress and migration to other SLO to continue the quest of the cognate antigen[149]. Moreover, CD69 is transiently upregulated during the first hours following TCR activation to assure sufficient APC-DC interactions and proper activation[147,150]. Importantly, S1P levels in LNs increase upon inflammation, with the main producers being monocytes. Together with CD69 upregulation for retention, monocyte-derived S1P might support the downregulation of S1PR1 to increase the retention time of T cells within LNs[151]. In summary, the S1P/S1PR signaling axis exerts a crucial role governing basic T cell function in homeostatic or inflammatory conditions. Notably, elucidating this pathway led to the development of drugs that modulate this signaling axis to treat specific human autoimmune conditions. For instance, Fingolimod (also known as FTY720), Siponimod and Ozanimod are agonists of S1P used to treat multiple sclerosis (MS). Fingolimod agonizes S1PRs 1, 3, 4, and 5, whereas Siponimod and Ozanimod are more specific and act on S1PRs 1 and 5[136,152-155]. MS is an autoimmune disease in which autoimmune T and B cells infiltrate the central nervous system (CNS) to cause demyelination and local inflammation[153,156]. Therefore, by treating patients with S1P agonists mimicking the S1P/S1PR signaling axis, lymphocytes are not able to leave lymphoid organs due to being desensitized to the S1P gradient in the organism and are not able to exert their effector functions in the CNS[152].

Besides the well characterized extracellular role of S1P on T cells, some intracellular functions of SL have been reported. For instance, LEC-derived S1P signaling through S1PR1 acts as a survival molecule for naïve Tconv by assuring mitochondrial fitness and regulating proteins from the Bcl-2 family, independently of its chemoattractant role in T cell migration[157,158]. Furthermore, the S1P/S1P1 signaling axis also regulates Treg development and maintenance[159] and CD4$^+$ T cell differentiation into Th1 or Th17 cells[160,161]. An additional SL species with important cell-intrinsic functions in T cells is Cer. Upon TCR stimulation, neutral and acid SMases are activated, hence increasing the levels of SM-derived Cer. Increased Cer levels influence T cell activation, proliferation, differentiation, cytokine secretion and cytotoxicity[162-172]. Moreover, a recent study found how the regulation of short- or long-chained Cer

species impacts T cell senescence[173], and more complex SL such as gangliosides also affect TCR-mediated activation[174]. Overall, the cell intrinsic roles of the distinct SL species are a consequence of signaling modulation by receptor clustering on lipid rafts or Cer-enriched platforms[127,128]. Accordingly, the size and abundance of lipid rafts influence TCR signal transduction[175,176], while Cer-enriched platforms favor induction of apoptosis[177].

Evidently, SL metabolism is a crucial element of T cell biology, ranging from extrinsic modulation of their distribution within the organism, to intrinsically regulating diverse signaling events impacting their survival and function. Thus, in-depth characterization of the SL metabolism in T cell development, differentiation, and function during homeostatic, inflammatory and disease contexts is of high interest. Here, we aimed to further expand our knowledge on the cell intrinsic and extrinsic roles of SLs in T cells. First, we investigated the role of the PM SL in $CD8^+$ T cell differentiation. To date, the predominant emphasis in the field has been given to transcription factors, receptors, metabolism, and genetics[113], with relatively limited attention towards lipid composition. We hypothesized that the SL composition at the PM could differ between $CD8^+$ T cells with distinct differentiation states, due to their differing phenotypes. Hence, we made use of mass spectrometry and an acute infection model (LCMV Armstrong) to compare the SL profile between naïve, effector and memory $CD8^+$ T cells. Moreover, by using flow scRNA-seq, flow cytometry, acute infection models (LCMV Armstrong and Vaccinia virus G2), and knock-out (KO) and TCR transgenic mouse models, we found that the PM-bound enzyme sphingomyelin phosphodiesterase acid-like 3b (Smpdl3b) is involved in memory $CD8^+$ T cell maintenance. In the first chapter, the intrinsic role of the Smpdl3b in $CD8^+$ T cells will be discussed. Second, we focused on UTCs and their migratory behavior. Growing evidence suggests that the different UTC lineages (γδ T cells, MAIT and NKT) have overlapping functions and a similar biology[53,104,178]. For that reason, we hypothesized that UTC lineages operate as functional units with shared transcriptome, migratory behavior and function. Hence, we speculated that the S1P/S1PR1 axis would also modulate the migratory behavior of NKT and MAIT cells in tissues, similarly to dermal γδ T cells[33,68,69]. By employing photoconvertible mouse models, LN transplantation models and flow cytometry, we found that all UTC lineages migrate via the S1P/S1PR axis from tissues to dLNs during homeostatic conditions. Moreover, we used single-lineage KO mouse models, bacterial and viral infection models (*Staphyloccocus aureus* (*S. aureus*), *Salmonella typhimurium* (*S. typhimurium*) and Vaccinia virus), scRNA-seq and flow cytometry to show that UTCs are organized in functional units. The second chapter will focus on the extrinsic role of S1P in the migration of these UTC functional units from tissues to dLNs and their impact in the heterogeneous immune responses mounted by LNs draining distinct tissues.

In summary, our studies revealed novel intrinsic and extrinsic roles of SL in distinct T cell lineages. Naturally, these findings are of great importance because they accentuate the relevance of SL metabolism as a crucial component of T cell biology and function. Importantly, various drugs modulating the SL pathway are currently in use in humans or being developed[152,179-182]. Thus, a comprehensive study of how SL specifically modulate the individual T cell lineages in a context-dependent manner will certainly improve the design of therapeutic strategies targeting this pathway.

Chapter I

“The role of Smpdl3b in CD8^{+} T cells”

The role of Smpdl3b in CD8⁺ T cells

Paulina Cruz de Casas[1,5], Dominik Wigger[2], Fabian Schumacher[2], Fabian Imdahl[3], Antoine-Emmanuel Saliba[3], Leonhard Heinz[4], Burkhard Kleuser[2] and Wolfgang Kastenmüller[1,5,6]

[1] Würzburg Institute of Systems Immunology, Max Planck Research Group at the Julius-Maximilians-Universität Würzburg, 97078, Germany

[2] Institute of Pharmacy, Department of Pharmacology and Toxicology, Freie Universität Berlin, 14195, Germany

[3] Division of Rheumatology, Medical University of Vienna, Vienna, Austria

[4] Helmholtz Institute for RNA-based Infection Research (HIRI), Helmholtz-Center for Infection Research (HZI), 97078, Würzburg, Germany

[5] corresponding authors

[6] lead contact

Corresponding authors:

Wolfgang Kastenmüller, Professor, M.D.

Office Phone: +49 (0) 931 31 81816

e-mail: wolfgang.kastenmueller@uni-wuerzburg.de

Paulina Cruz de Casas

e-mail: paucruzdec@gmail.com

One sentence summary:

Sphingomyelin phosphodiesterase acid-like 3b (Smpdl3b) regulates CD8⁺ T cell contraction phase following acute infections.

Abstract

The mechanism behind the differentiation of a naïve CD8$^+$ to become an effector or memory cell during an acute infection is not completely understood. Here, we inquired whether the plasma membrane plays a role in this process. We found that Smpdl3b, a supposed sphingomyelin-metabolizing enzyme, plays an essential role in memory CD8$^+$ T cell development. By using transgenic (knock-out and TCR transgenic) mouse models, adoptive cell transfer models, and LCMV infections we discovered that the memory CD8$^+$ T cell pool is dramatically reduced in the absence of Smpdl3b. While the remaining Smpdl3b-deficient cells did not show an altered cytokine production or failure to re-expand following rechallenge, we observed a predominant loss CX3CR1-expressing peripheral memory T cells. Mechanistically, our data point to a role of Smpdl3b in modulating endocytosis via Hip1. In summary, we describe an important function of Smpdl3b in regulating CD8$^+$ T cell survival. The location of Smpdl3b in the outer leaflet of the plasma membrane may foster pharmacological targeting to modulate cellular immunity in the contact of immunotherapy and vaccination.

Main

One of the main roles of CD8$^+$ T cells is to eradicate cells that are infected with viruses or intracellular pathogens, or cancerous cells. Antigen presenting cells (APCs) and infected cells present antigens to CD8$^+$ T cells via the antigen presenting molecule MHC-I (major histocompatibility complex class I), which interacts with the CD8 protein. For a naïve antigen-specific CD8$^+$ T cell to be exert its cytotoxic function towards infected cells, they must previously be activated by professional APCs via cross-presentation, which is a process in which non-infected dendritic cells present exogenous antigen to CD8$^+$ T cells[1]. Following their activation with their cognate antigen, naïve antigen-specific CD8$^+$ T cells proliferate exponentially, a process that is referred to as “clonal expansion”. Consequently, in an acute infection setting, these high numbers of activated, antigen-specific CD8$^+$ T cells are able to clear the infection by eliminating the infected cells. Next, the clonally expanded antigen-specific CD8$^+$ T cell population dies via apoptosis (contraction phase), and only a small fraction (5-10%) survives and remains as memory cells[2].

Importantly, within the expansion, contraction and memory phases of the CD8$^+$ T cell response in an acute infection, CD8$^+$ T cells with distinct differentiation states are found. For instance, terminally differentiated short-lived effector cells (SLEC) and effector memory cells (TEM) can be found during the acute and memory phases of the infection, respectively. Additionally, stem-like memory precursor cells (MPEC) and central memory cells (TCM) are additional subpopulations present in the acute and memory pools. These populations can be distinguished by the expression of KLRG1 and CX3CR1, by the terminally differentiated SLEC and TEM subpopulations, and IL-7Rα, by the stem-like MPEC and TCM populations[3,4]. Intuitively, cells with a distinct differentiation state also differ in their function. For instance, CX3CR1$^+$ TEM cells are constantly patrolling the blood stream and spleen, whereas the IL-7Rα$^+$ TCM cells recirculate between lymph nodes, spleen and blood vessels, and are capable of self-renewing. Moreover, a CX3CR1^{int} IL-7Rα$^+$ population, denominated peripheral memory (TPM), can be found in the blood, spleen and peripheral non-lymphoid tissues[4].

Distinct models such as the linear model[5], asymmetric cell division cell fate model[6], or the signal-strength and decreasing potential models[2,7], have been proposed to describe how naïve CD8$^+$ T cells differentiate into effector and/or memory cells. Furthermore, naïve, effector and memory (sub)populations differ in the expression of certain chemokine and cytokine receptors (e.g. KLRG1, CX3CR1, IL-7Rα, CD44), transcription factors (T-bet, Eomes, TCF1, BLIMP1, BCL-6) or even their metabolism[2,8,9]. Interestingly, not much attention has been given to the changes in the plasma membrane (PM) composition, and more specifically the lipid components of it, of CD8$^+$ T cells that differ in their differentiation state. Mainly, studies of the PM lipidome of CD8$^+$ T cells have focused on signaling events succeeding T cell receptor (TCR) activation[10,11], but not on the lipid composition itself.

Sphingomyelin (SM) is a sphingolipid (SL) mostly found in the outer leaflet of the PM and enriched in highly ordered microdomains known as "lipid rafts"[12,13]. In addition to SM, lipid rafts are also composed by cholesterol and glycosylphosphatidylinositol (GPI)-anchored proteins, and have been shown to play a role in receptor clustering and signal transduction enhancement upon TCR activation[10,14]. Here, we investigated the SL composition in distinct CD8$^+$ T cell subpopulations. We found that Sphingomyelin phosphodiesterase acid-like 3b (Smpdl3b), a GPI-anchored lipid raft-associated enzyme with supposed SM-degrading activity[15-17], is highly expressed by effector and memory CD8$^+$ T cells, but absent in their naïve counterparts. Therefore, we hypothesized that modulation of the SM content in the PM and lipid rafts by Smpdl3b could influence CD8$^+$ T cell differentiation and function. Importantly, Smpdl3b has been described as a regulator of innate immunity by modulating membrane fluidity and affecting toll-like receptor (TLR) 3 and TLR4 signaling[16,18]. Here, we show that Smpdl3b is essential for the maintenance of CD8$^+$ T cells with a less differentiated state (MPEC, TPM, TCM) in a sphingomyelin-independent manner. In addition, we found that Smpdl3b-deficient cells have no functional defects. We propose that Smpdl3b is an essential player for memory CD8$^+$ T cell development, likely by modulating endocytosis and possibly signaling in CD8$^+$ T cells.

Results

The sphingolipid profile of CD8$^+$ T cell differs along with their differentiation trajectory.

How naïve CD8$^+$ T cell differentiate into effector (T_{eff}) or memory (T_{mem}) cells is not fully resolved. Distinct models, such as asymmetric division or signal strength models, have been proposed[2,5-7]. Additionally, an exhaustive characterization of differences in the phenotype and genotype between these populations exists[2], mainly focusing on receptors, transcription factors, epigenetics and metabolism, in order to distinguish these subsets. However, the role of the plasma membrane (PM) and its lipid composition in CD8$^+$ T cells with distinct differentiation states and its biological implications remain understudied. Previous studies have highlighted the importance of the PM lipids for TCR signaling and activation in T cells[10,11,19,20-29]. Here, we set out to investigate the sphingolipid (SL) composition of CD8$^+$ T cells, since they compose around 10-20% of the PM[30,31] and only a few studies have looked into their cell intrinsic roles in T cells[32-42].

We speculated that the SL profile (Figure 1A) of CD8$^+$ T cells might differ based on their differentiation state. To test this, we acutely infected C57BL/6J wild-type mice with LCMV Armstrong and

isolated naïve, effector central and effector memory CD8$^+$ T cells at 0, 8 and 22 days post-infection. Next, we performed an in-depth mass spectrometry lipidomics analysis. We indeed found that the amount of the total ceramides (Cer), dihydrosphingomyelins (dhSM), sphingomyelins (SM) and more complex sphingolipids, such as lactosylceramides (lacCer) and hexosylceramides (hexCer), was altered in the terminally differentiated effector and effector memory (TEM) CD8$^+$ T cells compared to their naïve and central memory (TCM) counterparts (Figure 1B). Moreover, we found that Cer 16:0 and 24:1 were the most altered species in the effector and TEM populations (Supplementary Figure 1B). Since the SL metabolism is very complex and highly interconnected (Figure 1A), depicting the origin of the observed alterations in the pathway is not evident. Moreover, SM is the most abundant SL species, therefore the detection of small differences when comparing distinct cell populations is challenging. To circumvent this, we calculated the ratio of the total or individual species of SM and Cer to determine the conversion rate of SM into Cer, a process mediated by sphingomyelinases (SMases). Indeed, we found that for the total and individual species, the SM/Cer ratios were reduced in the effector and TEM populations (Figure 1C), highlighting the activity of SMases on the distinct SM species. SMase activity generating Cer from SM seemed to be a distinctive trait of terminally differentiated effector and TEM CD8$^+$ T cells. Together, our data revealed a differing SL composition between stem-like and terminally differentiated CD8$^+$ T cell subpopulations. Importantly, these differences were mainly SMase-mediated.

Sphingomyelin phosphodiesterase acid-like 3b (Smpdl3b) is not expressed or active in naïve, but in effector and memory CD8$^+$ T cells.

In order to reveal the mechanistic basis for the observed differences in the SL composition of CD8$^+$ T cells (Figure 1), we focused on SMases. The family of SMases is composed by 7 enzymes coded by the genes *Smpd1, Smpd2, Smpd3, Smpd4, Smpd5, Smpdl3a* and *Smpdl3b.* "Smpd" stands for **S**phingo**M**yelin **P**hospho**D**iesterase, whereas "Smpdl" corresponds to **S**phingo**M**yelin **P**hospho**D**iesterase **A**cid-**L**ike. The name of each enzyme coded by these genes is determined by the pH in which they catalyze the conversion of SM into Cer and phosphatidylcholine more efficiently (Figure 2A). As an exception, the enzyme coded by the *Smpdl3b* gene better exerts its function at a neutral pH[16]. To determine which enzyme(s) is responsible for the sphingolipid profile seen in T_{eff} and T_{mem} subsets, we made use of a published single-cell RNA sequencing (scRNA-seq) data set in which T cell receptor (TCR)-transgenic gp33-specific (P14) naïve, effector, memory and exhausted CD8$^+$ T cells from acutely (LCMV Armstrong) or chronically (LCMV clone 13) infected mice were sequenced[43]. The temporal expression pattern of *Smpd1, Smpd2*, *Smpdl3a and Smpdl3b* was consistent with a role in T cell differentiation peaking at around d8 (*Smpd1, Smpd2*) after infection or in the memory phase (*Smpd5*). By contrast, *Smpd4* was already highly expressed in naïve CD8$^+$ T cells, while *Smpd3* was not expressed at any timepoint (Figure 2B; Supplementary Figure 2C). Interestingly, *Smpdl3b* was the only SMase not expressed in the naïve cluster, yet present in the other clusters (Figure 2B; Supplementary Figure 2A). We corroborated the expression patterns of *Smpdl3b* by using the RNA sequencing (RNA-seq) browser from the Immgen database[44] (Supplementary Figure 2B). To further support these results, we analyzed an additional scRNA-seq data set in which splenic P14 were sequenced at days 3, 4, 5, 6, 7 and 32 after acute infection (Figure 2C)[45]. The data showed that *Smpdl3b*

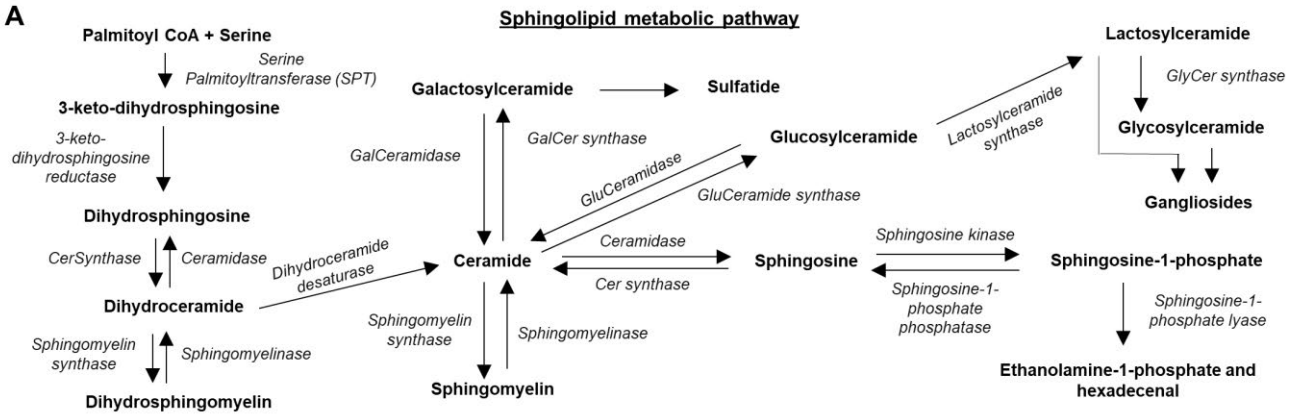
A
Sphingolipid metabolic pathway
Palmitoyl CoA + Serine
Serine Palmitoyltransferase (SPT)
3-keto-dihydrosphingosine
3-keto-dihydrosphingosine reductase
Dihydrosphingosine
CerSynthase
Ceramidase
Dihydroceramide desaturase
Dihydroceramide
Sphingomyelin synthase
Sphingomyelinase
Dihydrosphingomyelin
Galactosylceramide
Sulfatide
GalCeramidase
GalCer synthase
Glucosylceramide
GluCeramidase
GluCeramide synthase
Ceramide
Ceramidase
Cer synthase
Sphingomyelin synthase
Sphingomyelinase
Sphingomyelin
Lactosylceramide
Lactosylceramide synthase
GlyCer synthase
Glycosylceramide
Gangliosides
Sphingosine kinase
Sphingosine
Sphingosine-1-phosphate
Sphingosine-1-phosphate phosphatase
Sphingosine-1-phosphate lyase
Ethanolamine-1-phosphate and hexadecenal

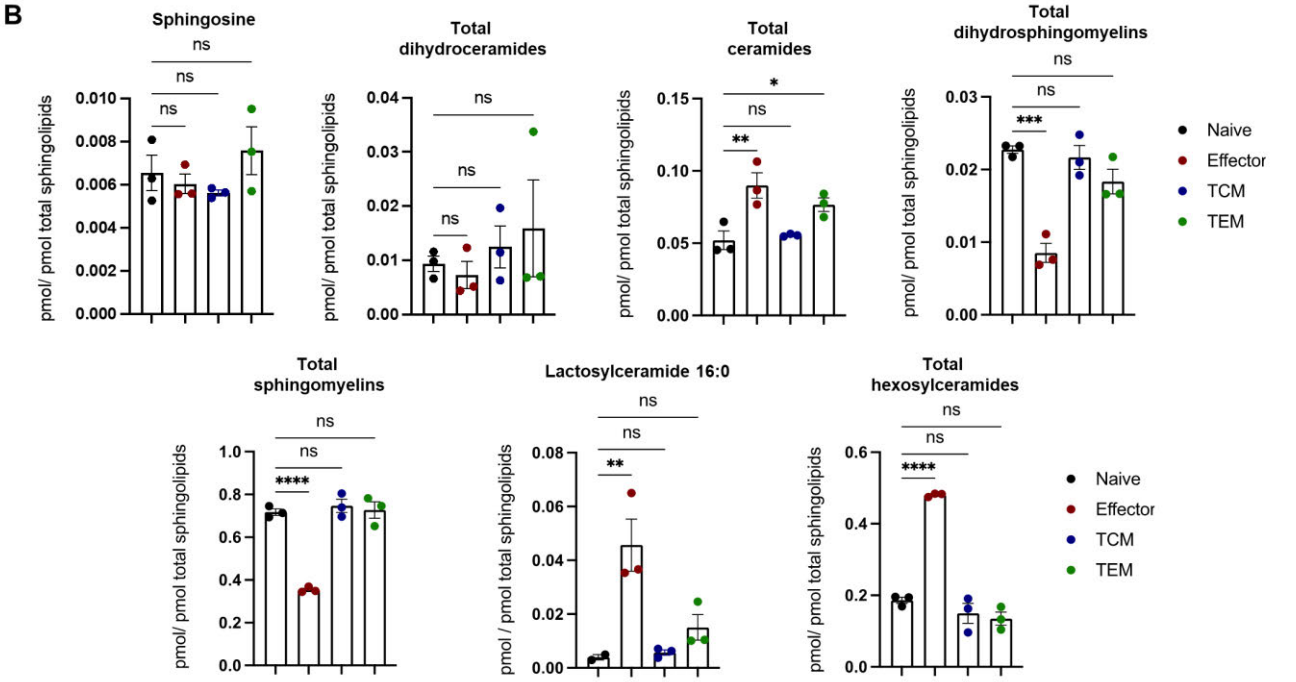
B
Sphingosine
Total dihydroceramides
Total ceramides
Total dihydrosphingomyelins
Total sphingomyelins
Lactosylceramide 16:0
Total hexosylceramides
pmol/ pmol total sphingolipids
pmol / pmol total sphingolipids
Naive
Effector
TCM
TEM

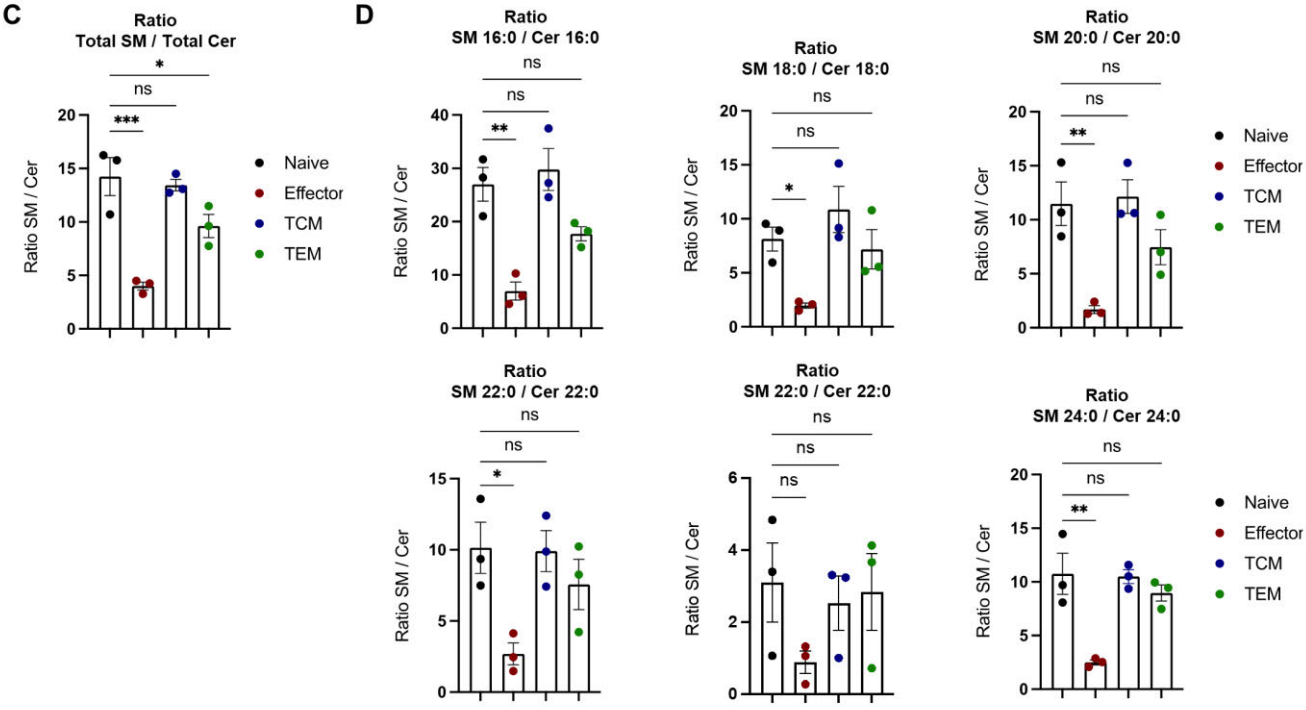
C
Ratio
Total SM / Total Cer
Ratio SM / Cer
D
Ratio
SM 16:0 / Cer 16:0
SM 18:0 / Cer 18:0
SM 20:0 / Cer 20:0
SM 22:0 / Cer 22:0
SM 22:0 / Cer 22:0
SM 24:0 / Cer 24:0
Naive
Effector
TCM
TEM

Figure 1. The sphingolipid profile of CD8⁺ T cell differs along with their differentiation trajectory. A) Schematic of the sphingolipid metabolism pathway. Adaptation from Mielke, M. M., *et al.* (2011)[46]. B) Comparison of the sphingolipid profile of CD8⁺ T cells with distinct differentiation status, normalized to total measured sphingolipids. C) Ratio of total sphingomyelin (SM) and total ceramide (Cer) present in distinct subpopulations of CD8⁺ T cells, calculated from the values shown in B. D) Ratio of the individual species of SM and Cer present in distinct subpopulations of CD8⁺ T cells, calculated from the values of the individual species (shown in Supplementary Figure 1). Cells are derived and sorted from the spleen of non-infected (naive) or LCMV Armstrong (acutely) infected C57BL/6J mice for 8 (effector) or 22 days (TCM: central memory; TEM: effector memory) for B-D. Data represent 3 of 3 independent experiments with n = 2 pooled mice per experiment for naïve, n = 2 pooled mice per experiment for effector and n = 3 or 6 pooled mice per experiment for TCM and TEM. Bar graphs represent the mean values and error bars represent SEM. Comparison between groups was calculated using one-way ANOVA and Dunnett's multiple comparisons test (B-D). ns = non-significant ($p > 0.05$); * $p < 0.05$; ** $p < 0.01$; *** $p < 0.001$; **** $p < 0.0001$.

expression was detected from day 5 post-infection (Figure 2D; Supplementary Figure C) and its expression seems to be maintained at acute and memory timepoints. Next, we wished to validate the expression of Smpdl3b on a protein level. Given the lack of suitable antibodies, we decided to measure its enzymatic activity. Specifically, we employed a phosphodiesterase activity assay that has been used to measure the activity of Smpdl3b, due to its similar structure to other phosphodiesterases[16,17]. Importantly, this assay would detect the enzymatic activity of any phosphodiesterase expressed by CD8⁺ T cells. Hence, we compared *Smpdl3b*$^{+/-}$ (heterozygous) with *Smpdl3b*$^{-/-}$ (Smpdl3b knockout (KO)) to be able to discriminate the specific activity of Smpdl3b. We acutely infected heterozygous or Smpdl3b KO mice for 7 and 32 days, then sorted the naïve, effector and memory (central memory (TCM) and effector memory (TEM)) CD8⁺ T cells and assessed the phosphodiesterase activity. In accordance with the scRNA-seq data, we detected enzymatic activity of Smpdl3b at days 7 and 32, while its was absent in naïve CD8⁺ T cells (Figure 2F). We were also able to quantify and compare the enzymatic 4-Nitrophenol (pNP) production by Smpdl3b, showing that highest expression is found in T_{eff} and TEM cells (Supplementary Figure D-E). In summary, these results revealed that the transcriptional expression kinetics of the distinct SMases in CD8⁺ T cells differ. Importantly, *Smpd1*, *Smpd2*, *Smpd5* and *Smpdl3a* are expressed by naïve CD8⁺ T cells, whereas Smpdl3b is not. Importantly, by being the sole SMase absent in naïve CD8⁺ T cells and expressed from day 5 post-infection onwards in T_{eff} and T_{mem}, suggests that Smpdl3b is exclusively required by already differentiated CD8⁺ T cells. Furthermore, additional factors that elicited our interest on Smpdl3b over other SMases were its yet unknown physiological substrate[16,17,47], and its modulation of TLR-dependent innate immunity[16,18] and cell migration[48-51]. Hence, we decided to investigate the potential role of Smpdl3b in CD8⁺ T cell function and differentiation from naïve to T_{eff} and T_{mem}.

A

Gene	Enzyme name (sphingomyelinase)
Smpd1	Acid sphingomyelinase (ASM)
Smpd2	Neutral sphingomyelinase 1 (NSM1)
Smpd3	Neutral sphingomyelinase 2 (NSM2)
Smpd4	Neutral sphingomyelinase 3 (NSM3)
Smpd5	Neutral sphingomyelinase 4 (NSM4)
Smpdl3a	Sphingomyelinase phosphodiesterase acid-like 3a
Smpdl3b	Sphingomyelinase phosphodiesterase acid-like 3b

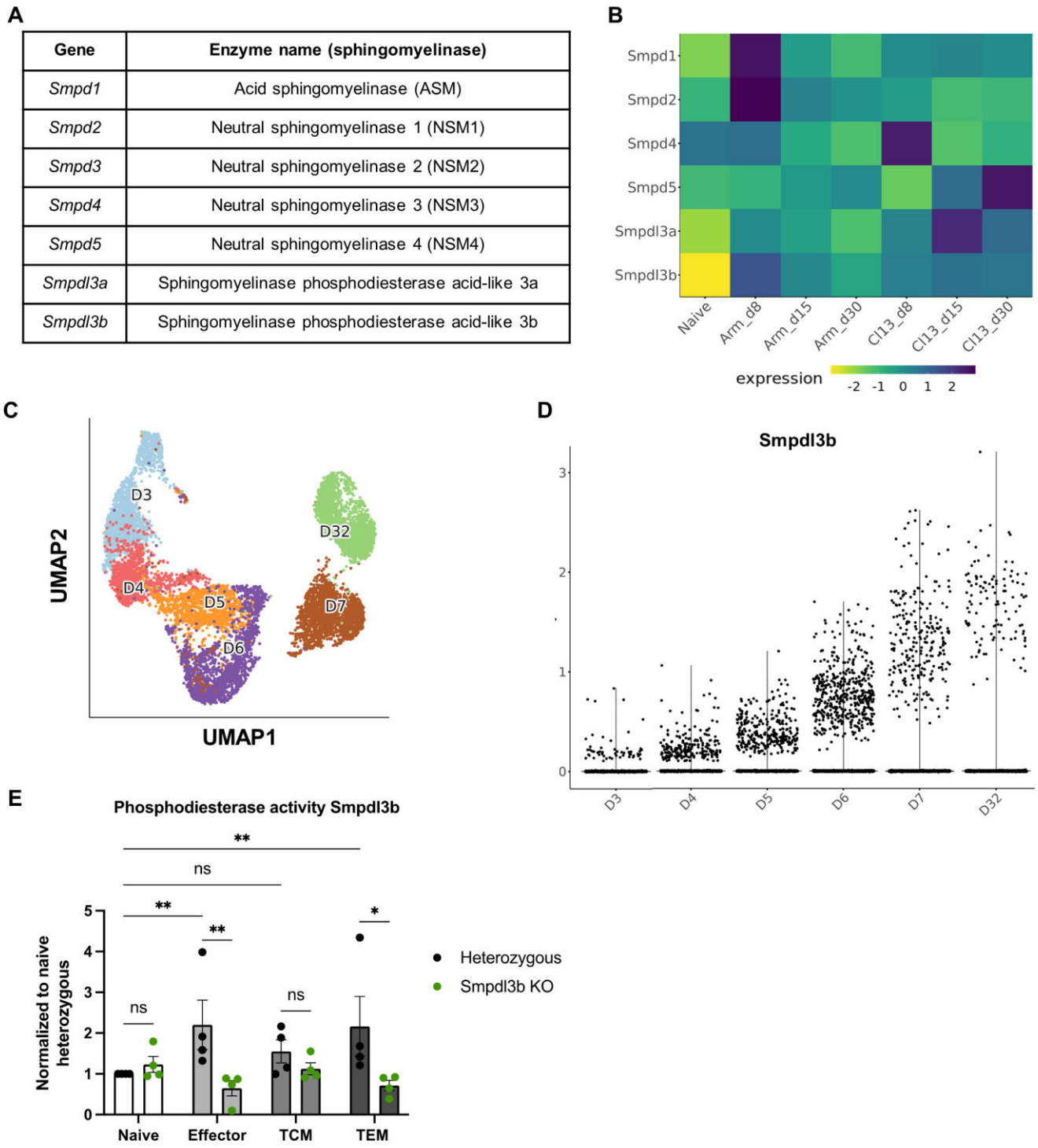

Figure 2. Sphingomyelin phosphodiesterase acid-like 3b (Smpdl3b) is not expressed or active in naïve, but in effector and memory CD8⁺ T cells. A) Table showing the genes expressing the sphingomyelin-degrading enzymes (sphingomyelinases). B) Heatmap displaying the expression of the distinct sphingomyelinases in distinct timepoints and infection settings. The data was obtained from the scRNA-seq data set published by Giles, J.R., *et al.* (2022)[43] and uploaded to our Institute's Shiny app, in which 30289 single cells were sequenced at distinct timepoints during acute or chronic infection. C) UMAP projection of 9896 single cells from scRNA-seq, color code based on the clusters per timepoint. The UMAP was generated from the data set published by Kurd, N.S., *et al.* (2020)[45] and uploaded into our Institute's Shiny app. D) Violin plot comparing the expression of Smpdl3b in CD8⁺ T cell populations with distinct differentiation status per timepoint. The Violin plot was generated the same way as for C. E) Quantitative analysis of the phosphodiesterase activity of Smpdl3b in *Smpdl3b*$^{+/-}$ (Heterozygous) and *Smpdl3b*$^{-/-}$ (Smpdl3b KO) CD8⁺ T cell subpopulations. Cells were isolated and sorted from the spleen of

non-infected (naive) or LCMV Armstrong (acutely) infected mice for 7 (effector) or 32 days (TCM: central memory; TEM: effector memory) for E. Data represent 4 of 4 independent experiments with n = 4 mice for naïve Heterozygous, naïve Smpdl3b KO, effector Heterozygous and effector Smpdl3b KO, and n = 12 mice for Heterozygous memory (TCM and TEM) and Smpdl3b KO memory (TCM and TEM). Bar graphs represent the mean values and error bars represent SEM. Comparison between groups was calculated using two-way ANOVA and uncorrected Fisher's LSD multiple comparisons test. ns = non-significant ($p > 0.05$); * $p < 0.05$; ** $p < 0.01$; *** $p < 0.001$; **** $p < 0.0001$.

Smpdl3b is necessary for the survival of stem-like CD8$^+$ T cell memory populations at acute and memory timepoints.

Based on the expression pattern of Smpdl3b, we hypothesized an involvement in the differentiation of naive CD8$^+$ T cells into T_{eff} and T_{mem} during an acute immune response. In order to test this hypothesis *in vivo*, we isolated cells from wild-type (WT) tdTomato P14 and *Smpdl3b*$^{-/-}$ Venus (Smpdl3b KO) P14 mice and co-transferred them into the same C57BL/6J WT recipient mice at a 1:1 ratio. We then acutely infected the recipient mice with LCMV Armstrong and tracked the transferred cells in the blood at the acute (day 7), contraction (day 12-15), and memory (day 22-29) phases via flow cytometry. Surprisingly, we found that the *Smpdl3b* KO P14 cells were reduced in frequencies starting from day 7 post-infection and further aggravated over time (Figure 3A). Moreover, this phenotype was present in lymphoid (spleen, inguinal lymph node and mesenteric lymph node) and non-lymphoid (small intestine and salivary glands) organs (Figure 3B-D; Supplementary Figure A). Intrigued by this quantitative loss of the Smpdl3b KO cells, we further characterized their effector (KLRG1$^+$ IL-7Rα$^-$ (CD127) CX3CR1$^+$) or memory (KLRG1$^-$ IL-7Rα$^+$) phenotype at the acute (day 8) and memory (day 30) timepoints. Interestingly, at day 8 post-infection the Smpdl3b KO cells had a slight increase in the frequency of short-lived effector cells (SLEC; KLRG1$^+$ IL-7Rα$^-$), whereas the memory precursor cells (MPEC; KLRG1$^-$ IL-7Rα$^+$) were reduced in both, frequencies and numbers (Figure 3E; Supplementary Figure 3B). Furthermore, at a memory timepoint (day 30 post-infection) the frequency of IL-7Rα$^+$ CX3CR1$^-$ central memory (TCM) and IL-7Rα$^+$ CX3CR1$^+$ peripheral memory (TPM) cells were also reduced within the Smpdl3b KO population, while the IL-7Rα$^-$ CX3CR1$^+$ effector memory (TEM) cells were increased (Figure 3F). Next, to test whether the observed phenotype was due to a competitive disadvantage of the co-transferred Smpdl3b KO P14 cells against the WT P14 cells, we transferred WT KO P14 cells into independent C57BL/6J WT recipient mice that were then acutely infected and analyzed similarly to the co-transferred setting mice. We found a matching quantitative and qualitative phenotype in the Smpdl3b KO cells, regardless of the competitive setting (Supplementary Figure 3C-F). Together, our data suggests that Smpdl3b is required for the survival of memory CD8$^+$ T cells. To test this notion, we investigated the protein levels of a well-characterized pro-apoptotic factor, Bim (*Bcl2l11*), which is known to play an important role in the contraction phase of the CD8$^+$ T cell response[52-54]. Bim levels did not seem to differ between WT and Smpdl3b KO cells at any analyzed timepoint after infection (Figure 3G). In summary, our data indicates that Smpdl3b plays a Bim-independent role in maintaining CD8$^+$ memory T cells. Moreover, its absence seems to favor the presence of terminally differentiated over stem-like subpopulations.

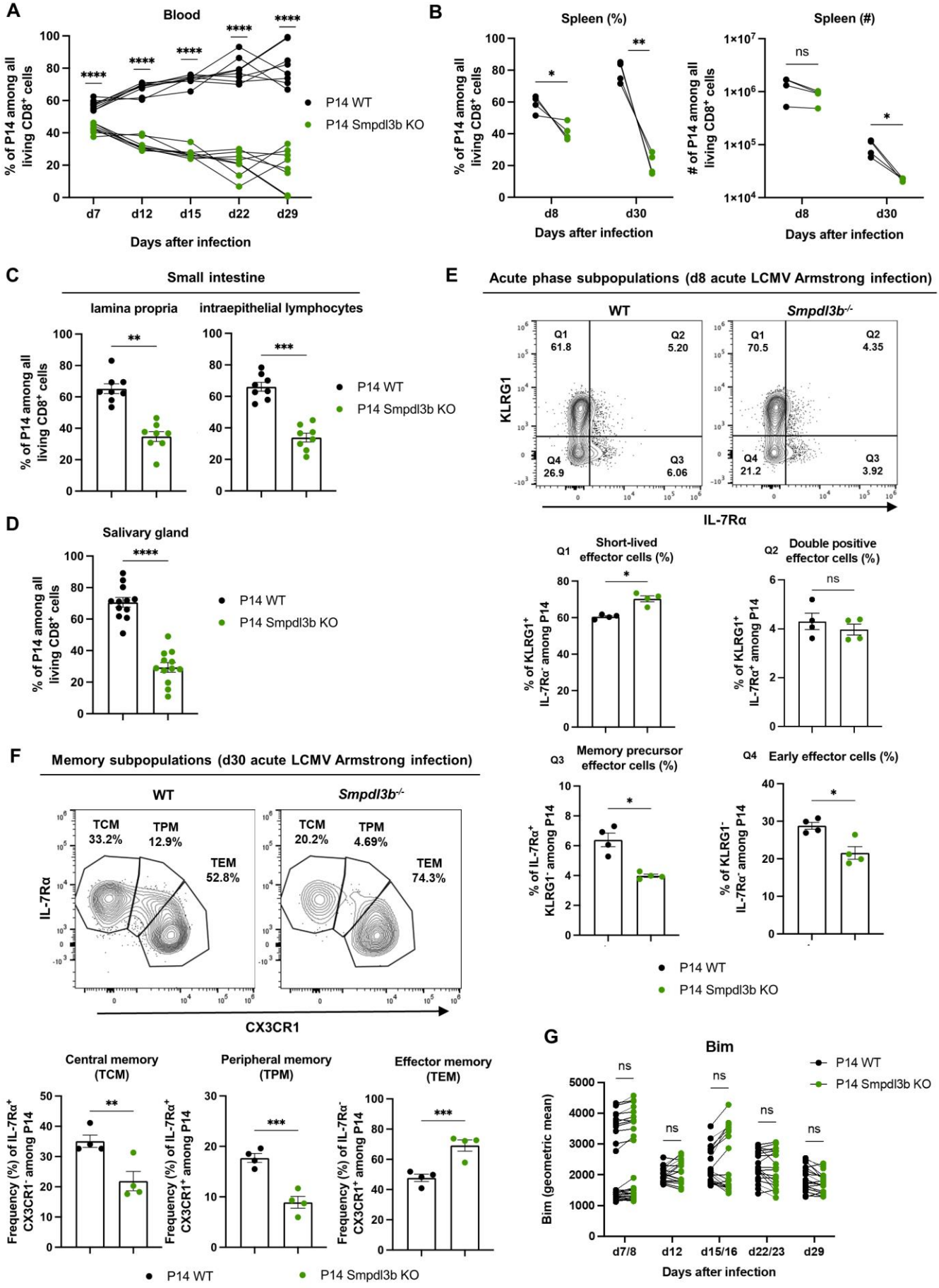
A
Blood
% of P14 among all living CD8+ cells
Days after infection
d7
d12
d15
d22
d29
P14 WT
P14 Smpdl3b KO
B
Spleen (%)
Spleen (#)
# of P14 among all living CD8+ cells
d8
d30
ns
C
Small intestine
lamina propria
intraepithelial lymphocytes
D
Salivary gland
E
Acute phase subpopulations (d8 acute LCMV Armstrong infection)
WT
Smpdl3b-/-
KLRG1
IL-7Rα
Q1 61.8
Q2 5.20
Q4 26.9
Q3 6.06
Q1 70.5
Q2 4.35
Q4 21.2
Q3 3.92
Short-lived effector cells (%)
Double positive effector cells (%)
Memory precursor effector cells (%)
Early effector cells (%)
F
Memory subpopulations (d30 acute LCMV Armstrong infection)
TCM 33.2%
TPM 12.9%
TEM 52.8%
TCM 20.2%
TPM 4.69%
TEM 74.3%
CX3CR1
Central memory (TCM)
Peripheral memory (TPM)
Effector memory (TEM)
G
Bim
Bim (geometric mean)

Figure 3. Smpdl3b is necessary for the formation of stem-like CD8+ T cell memory populations at acute and memory timepoints. A-D) Quantitative analysis of the frequency (and numbers for spleen) of wild-type (WT) P14 and *Smpdl3b*$^{-/-}$ P14 (Smpdl3b KO) in the blood (A), spleen (B), small intestine lamina propria (LP) and intraepithelial lymphocytes (IELs) (C), and salivary gland (SG) (D) of C57BL/6J WT recipient mice into which WT P14 and Smpdl3b KO P14 were co-transferred in a 1:1 ratio and that were acutely infected with LCMV Armstrong for 8 (blood and spleen) or 30 days (blood, spleen, LP, IELs, SG). E-F) Representative flow cytometry plots and quantitative analysis of the phenotype of WT and Smpdl3b KO P14 at acute (E) or memory (F) timepoints. G) Quantitative analysis of Bim expression in WT and Smpdl3b KO P14 CD8$^+$ T cells from the blood of mice acutely infected with LCMV Armstrong for 8 and 30 days. Data represent 1 of 2 (A-B), or 1 of 3 (E-F), or 2 of 2 (C and G) or 3 of 3 (D) independent experiments with n = 27 mice (G day 7/8), n = 19 mice (days 12-29), n = 12 mice (A day 7; D), n = 8 mice (A day 12-29; C), n = 4 mice (B, E-F). Bar graphs represent the mean values and error bars represent SEM. Comparison between groups was calculated using paired multiple comparisons two-way ANOVA with uncorrected Fisher's LSD for mixed effects analysis (A), multiple T test (B and G) or student T test (C-F). ns = non-significant ($p > 0.05$); * $p < 0.05$; ** $p < 0.01$; *** $p < 0.001$; **** $p < 0.0001$. TCM: central memory; TPM: peripheral memory; TEM: effector memory.

Smpdl3b is dispensable for CD8$^+$ T cell TCR- or cytokine-mediated functions.

Next, we wondered whether the function of CD8$^+$ T cells would also be impaired by the absence of Smpdl3b. Smpdl3b is supposedly a lipid-modifying enzyme forming part of lipid rafts[16], which are highly ordered nanodomains rich in SM, and it has been shown that lipid rafts play an essential role in membrane signaling events[10,55]. Additionally, Cer-enriched platforms, formed after catabolizing SM into Cer, also play a role in receptor clustering and signaling[56]. Thus, we hypothesized that Smpdl3b could play a role in signal transduction via modulation of the SM composition in the PM (e.g. modulating the abundance of lipid rafts and ceramide-enriched platforms). Importantly, it has been shown that antigen specific memory cells contain more lipid rafts than their naïve counterparts and are thus more sensitive to TCR stimulation[10]. In order to test this hypothesis, we compared distinct signaling pathways between WT and Smpdl3b KO cells by using several concentrations of stimulating compounds. We co-transferred WT and Smpdl3b KO P14 cells into WT recipients, acutely infected them with LCMV Armstrong and analyzed splenocytes on 8 or 30 days later. Single-cell suspensions were platted and stimulated for 4 h with diverse concentrations of gp33 peptide, for TCR stimulation, or IL-18/IL-12, for cytokine (TCR independent) stimulation. After stimulation, we compared the interferon-γ (IFNγ), interleukin-2 (IL-2) and tumor necrosis factor α (TNFα) production via flow cytometry. When stimulated with gp33 peptide, we did not detect significant differences in IFNγ nor TNFα production at any concentration or timepoint (Figure 4A; Supplementary Figure 4A). We observed a tendency for a lesser IL-2 production by Smpdl3b KO P14 cells at day 30 (Figure 4A), in line with the reduced frequencies of the IL-7Rα$^+$ CX3CR1$^-$ TCM (Figure 3F), which are the main IL-2 producers within the CD8$^+$ T cell memory pool[4]. Similarly, we observed no difference in the IFNγ produced after IL-18/IL-12 stimulation (Figure 4B-C; Supplementary Figure 4B-C). In conclusion, these data showed that the absence of Smpdl3b did not affect TCR-dependent and independent cytokine production in effector or memory CD8$^+$ T cells. Furthermore, we did not detect differences in lipid raft abundance between WT and KO cells when measuring the levels of asialo-GM1 (data not shown).

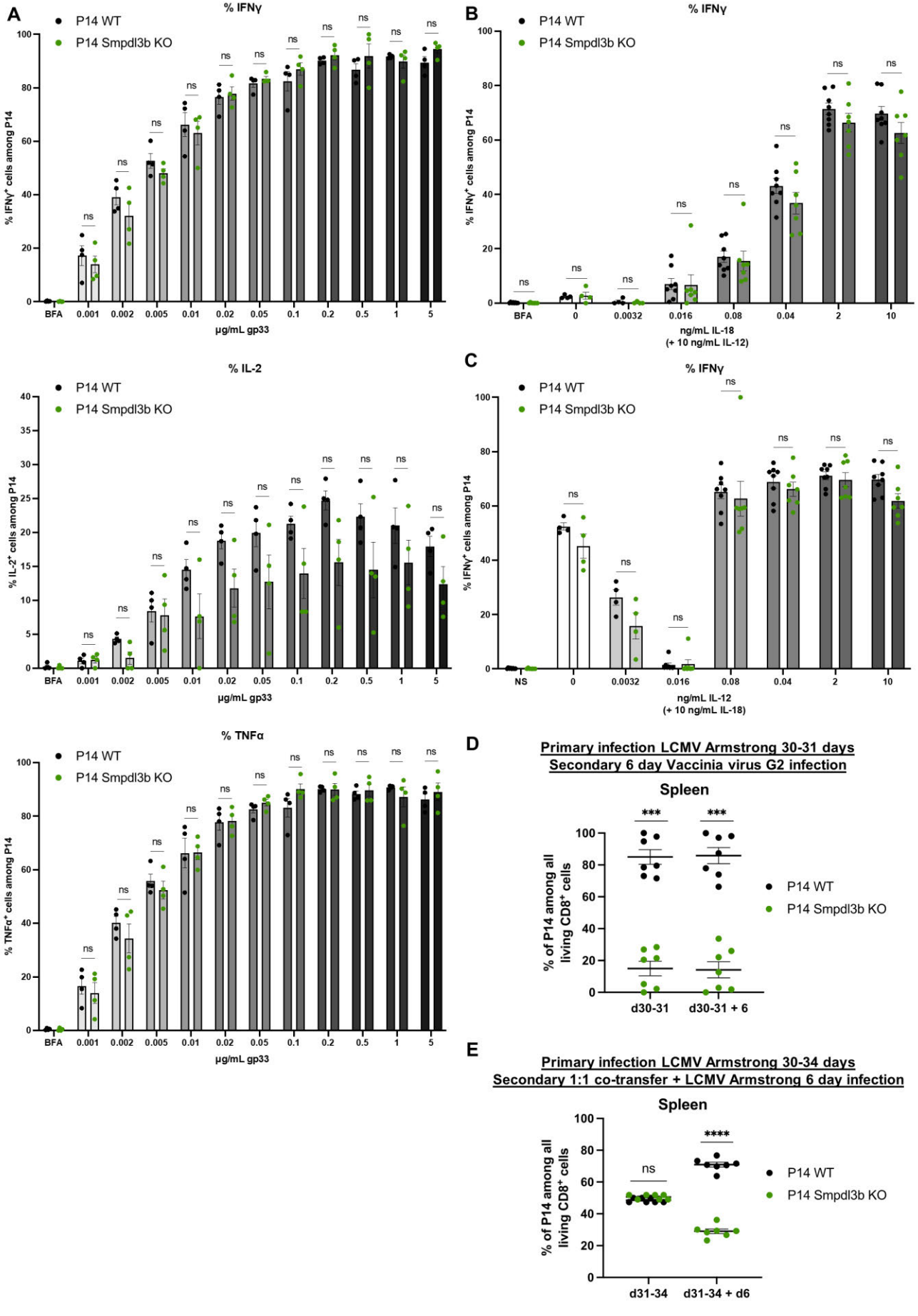
A
% IFNγ
P14 WT
P14 Smpdl3b KO
% IFNγ+ cells among P14
BFA
0.001
0.002
0.005
0.01
0.02
0.05
0.1
0.2
0.5
1
5
µg/mL gp33
B
% IFNγ
P14 WT
P14 Smpdl3b KO
% IFNγ+ cells among P14
BFA
0
0.0032
0.016
0.08
0.04
2
10
ng/mL IL-18
(+ 10 ng/mL IL-12)
% IL-2
P14 WT
P14 Smpdl3b KO
% IL-2+ cells among P14
µg/mL gp33
C
% IFNγ
P14 WT
P14 Smpdl3b KO
% IFNγ+ cells among P14
NS
ng/mL IL-12
(+ 10 ng/mL IL-18)
% TNFα
P14 WT
P14 Smpdl3b KO
% TNFα+ cells among P14
µg/mL gp33
D
Primary infection LCMV Armstrong 30-31 days
Secondary 6 day Vaccinia virus G2 infection
Spleen
% of P14 among all living CD8+ cells
d30-31
d30-31 + 6
P14 WT
P14 Smpdl3b KO
E
Primary infection LCMV Armstrong 30-34 days
Secondary 1:1 co-transfer + LCMV Armstrong 6 day infection
Spleen
% of P14 among all living CD8+ cells
d31-34
d31-34 + d6
P14 WT
P14 Smpdl3b KO

Figure 4. Smpdl3b is dispensable for CD8⁺ T cell TCR- or cytokine-mediated functions. A-C) Quantitative analysis of the frequency cytokines produced by wild-type (WT) P14 or *Smpdl3b*$^{-/-}$ P14 (Smpdl3b KO) isolated from the spleen of C57BL/6J mice infected for 30 days with LCMV Armstrong, after stimulating them *in vitro* for 4 hours with distinct concentrations of (A) gp33 peptide (TCR stimulation) with Brefeldin A (BFA), (B-C) IL-18 and IL-12. D) Quantitative analysis of the frequency of WT P14 or Smpdl3b KO P14 in the blood and spleen of mice that were infected with LCMV Armstrong for 30-31 days (primary infection) and then rechallenged with Vaccinia virus G2 (modified strain expressing gp33) for 6 days, respectively. E) Quantitative analysis of the frequency of WT P14 or Smpdl3b KO P14 present in the spleen of secondary recipient mice that were infected for 6 days with LCMV Armstrong. Previously, the cells were isolated and sorted from the spleen of primary recipient mice infected with LCMV Armstrong for 30-34 days, then co-transferred in a 1:1 ratio into the secondary recipients. Data represent 1 of 2 (A), or 2 of 2 (B-C, E) or 2 of 3 (D) independent experiments with n = 8 mice (B-C), n = 7 mice (D-E), n = 4 mice (A). Bar graphs represent the mean values and error bars represent SEM. Comparison between groups was calculated using paired multiple T test. ns = non-significant ($p > 0.05$); * $p < 0.05$; ** $p < 0.01$; *** $p < 0.001$; **** $p < 0.0001$.

An additional crucial function of memory CD8⁺ T cells is rapid clonal expansion upon antigen re-encounter[57]. To test this, we performed recall experiments in various experimental settings. As a baseline for all settings, we co-transferred WT and Smpdl3b KO P14 cells into C57BL/6J WT recipient mice that were subsequently infected with LCMV Armstrong for 30-34 days. Our first test was to re-infect these “memory mice” for 6 days in a heterologous prime-boost setting with a gp33-expressing strain of Vaccinia virus (VVG2). Surprisingly, we saw no skewing in the frequencies of WT and Smpdl3b KO in the spleen nor in the blood of the re-challenged mice (Figure 4D; Supplementary Figure 4D). These data suggested that the Smpdl3b KO P14 cells that survived until the memory phase, were similarly able to re-expand as their WT counterparts. Importantly, in this first setup we compared very low numbers of memory P14 cells, hence any potential differences could have been missed. Moreover, at d30-31 we merely analyzed the frequency of P14 cells in the blood of mice before boost. To account for differences in cell numbers, we sorted the memory WT and Smpdl3b KO P14 cells from “memory mice”, re-adjusted the ratio 1:1 and transferred them into non-infected C57BL/6J WT secondary recipient mice. We then infected these recipient mice for six days with either LCMV Armstrong or VVG2. Interestingly, in this experimental set-up where cell numbers where normalized before transfer, we did see that the frequencies of WT and Smpdl3b KO P14 cells shifted in the spleen and blood from 50-50% to 65-35% (Figure 4E; Supplementary Figure E-F). Overall, these results demonstrate that the absence of Smpdl3b does not impair memory TCR-dependent and independent cytokine production in a cell-to-cell basis. Yet, the capacity of re-expansion is hindered in Smpdl3b KO cells, in line with the pronounced gradual loss of memory cells (Figure 3; Supplementary Figure 3).

The sphingolipid profile of CD8⁺ T cells is not altered in the absence of Smpdl3b.

Next, we wished to uncover the mechanism how Smpdl3b regulates CD8⁺ T cell survival during the transition to memory. To this end, we first compared the SL profile of WT and Smpdl3b KO P14 cells, since, as previously stated, the SL metabolism pathway is tightly interconnected (Figure 1A), and potential compensatory mechanisms might maintain the homeostatic levels of certain species, when one part of the pathway is altered. Therefore, by looking at the pathway as a whole, we would be able

to detect subtle differences due to the absence of Smpdl3b. To this end, we isolated WT or Smpdl3b KO P14 cells, transferred them individually into C57BL/6J WT recipient mice, and acutely infected them for

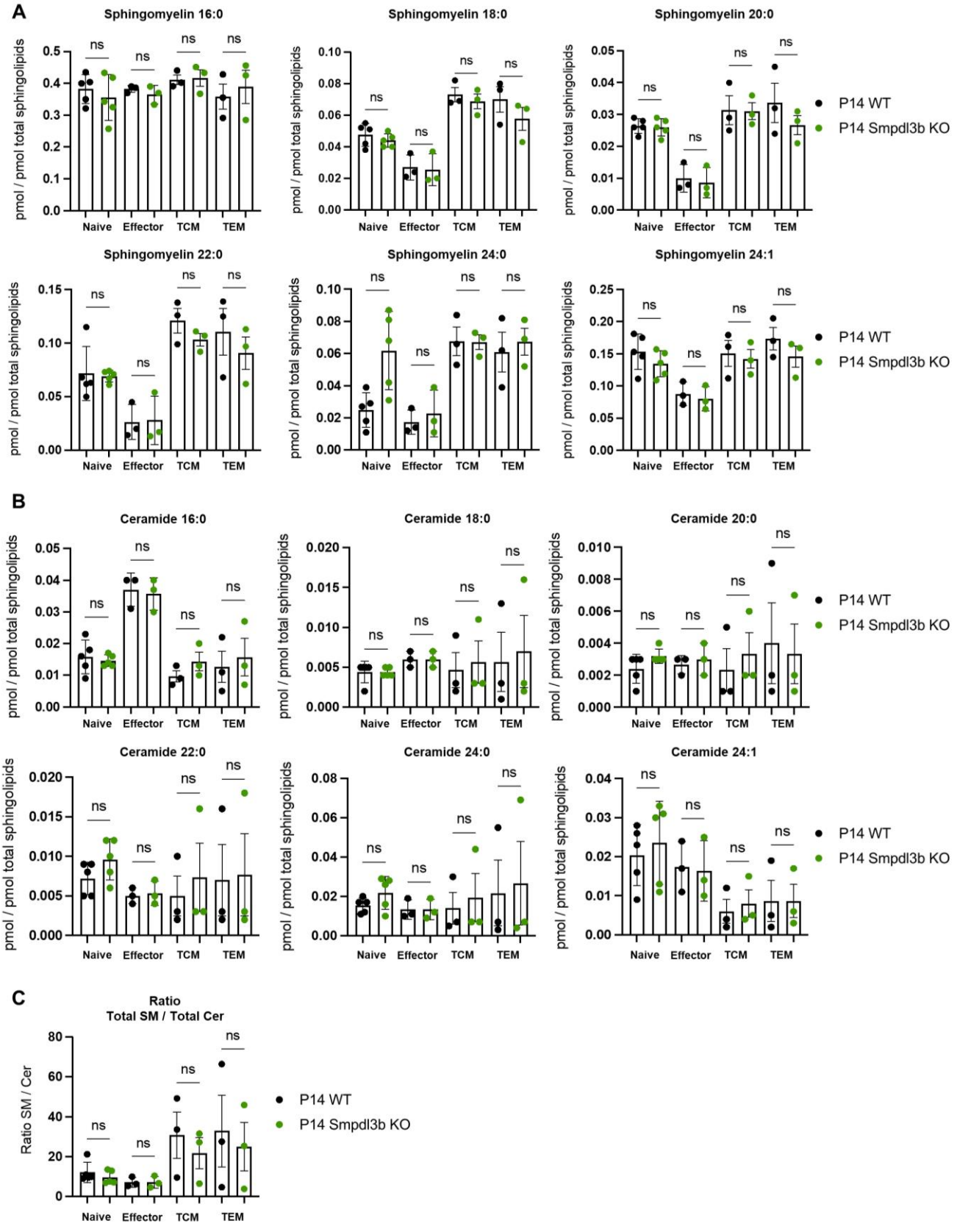

Figure 5. The sphingolipid profile of CD8$^+$ T cells is not altered in the absence of Smpdl3b. A-B) Comparison of the individual sphingomyelin (A) and ceramide (B) species between wild-type (WT) or Smpdl3b$^{-/-}$ (Smpdl3b KO) P14 CD8$^+$ T cells with distinct differentiation status, normalized to total measured sphingolipids. C) Ratio of total sphingomyelin (SM) and total ceramide (Cer) present in distinct subpopulations of WT or Smpdl3b KO P14 CD8$^+$ T cells, calculated from the values shown in A-B. Cells are derived and sorted from the spleen of non-infected (naive) or LCMV Armstrong (acutely) infected C57BL/6J mice for 8 (T_{eff}) or 22 (TCM: central memory; TEM: effector memory) days for A-C. Data represent 3 of 3 independent experiments (Teff, T_{CM} and TEM) or 5 of 5 independent experiments (naïve) with n = 1 mouse per experiment for naïve WT, n = 1 mouse per experiment for naïve Smpdl3b KO, n = 1 or 2 mice per experiment for WT T_{eff}, n = 1 or 2 mice per experiment for Smpdl3b T_{eff}, n = 5 pooled mice per experiment for WT TCM and TEM, and n = 15 pooled mice per experiment for Smpdl3b KO TCM and TEM. Bar graphs represent the mean values and error bars represent SEM. Comparison between groups was calculated using one-way ANOVA and Dunnett's multiple comparisons test (B-D). ns = non-significant ($p > 0.05$); * $p < 0.05$; ** $p < 0.01$; *** $p < 0.001$; **** $p < 0.0001$.

8 and 22 days. Afterwards, we sorted the WT and KO cells, and assessed their SL composition. Surprisingly, we were not able to detect any differences in individual SL nor Cer species (Figure 5A-B), nor in any other SL species (data not shown). Importantly, we also did not detect differences in the conversion rate of SM to Cer (Supplementary Figure 5). In summary, our data shows that the overall SL pathway is not affected by absence of Smpdl3b and therefore questions a significant SMase activity.

Single-cell sequencing suggests that *Smpdl3b*$^{-/-}$ CD8$^+$ T cells could undergo apoptosis at a higher rate and present enhanced endocytosis.

Since our data strongly argued against a possible function of Smpdl3b as a lipid modifying enzyme, we next performed single-cell RNA sequencing (scRNA-seq) on WT and *Smpdl3b*$^{-/-}$ P14 cells to elucidate its function. We isolated WT and Smpdl3b KO P14 cells and co-transferred them in a 1:1 ratio into C57BL/6J WT recipient mice that were acutely infected with LCMV Armstrong. We then performed comparative scRNA-seq of WT and Smpdl3b KO cells at days 7 (acute phase), 13 (contraction phase) and 22 (memory phase) post-infection, by using hashtag antibodies for each timepoint. Our unbiased analysis identified 9 separate clusters, mainly segregating by timepoints, but not by genotype (Figure 6A; Supplementary Figure 6A-B). We found a fairly similar distribution of WT and Smpdl3b KO cells within the identified clusters (Figure 6B-C). Differentially expressed genes (DEGs) analysis comparing the genotype, independent of the clustering and timepoint, revealed minor differences (Figure 6D-E). Importantly, several of the DEGs were actually related to the genotype or the background of the donor mice. For instance, *tdTomato* and *Venus* are just reflecting the fluorescent proteins expressed by the WT or Smpdl3b KO cells, respectively. Moreover, *Ctse* has been identified as one of the DEG between CD45.1 and CD45.2 mouse strains[58], whereas expression of *Ide*, *Btaf1* and *Gzma* differs between C57BL/6J (WT) and C57BL/6N (Smpdl3b KO) mice[59]. Further, the expression of *Il7r* was reduced in Smpdl3b KO cells, whereas *Cx3cr1* was increased, confirming the phenotype observed at a protein level via flow cytometry analysis (Figure 3E-F). One of the DEGs that caught our attention was *Bcl2*, due to its role as an anti-apoptotic protein[60]. Therefore, we speculated that the phenotype of the Smpdl3b KO cells could be caused by a reduced expression of *Bcl2*, thus increased

apoptosis in a Bim-independent manner (Figure 3G). Therefore, we compared the Annexin V$^+$ cells and the caspase 8 activity among co-transferred WT and Smpdl3b KO cells that were isolated from the spleen at 13 days post-LCMV Armstrong infection (data not shown), but did not detect any differences. Another DEG that intrigued us due to its upregulation in the Smpdl3b KO cells was *Hip1* (Figure 6E). This gene codes for the Huntington's interacting protein 1 (Hip1), which is involved in clathrin-mediated endocytosis processes[61-63] and neuronal apoptosis[64-67]. Based on our sequencing analysis, we hypothesized that the absence of Smpdl3b could enhance clathrin-mediated endocytosis, thus the accumulation of Hip1.

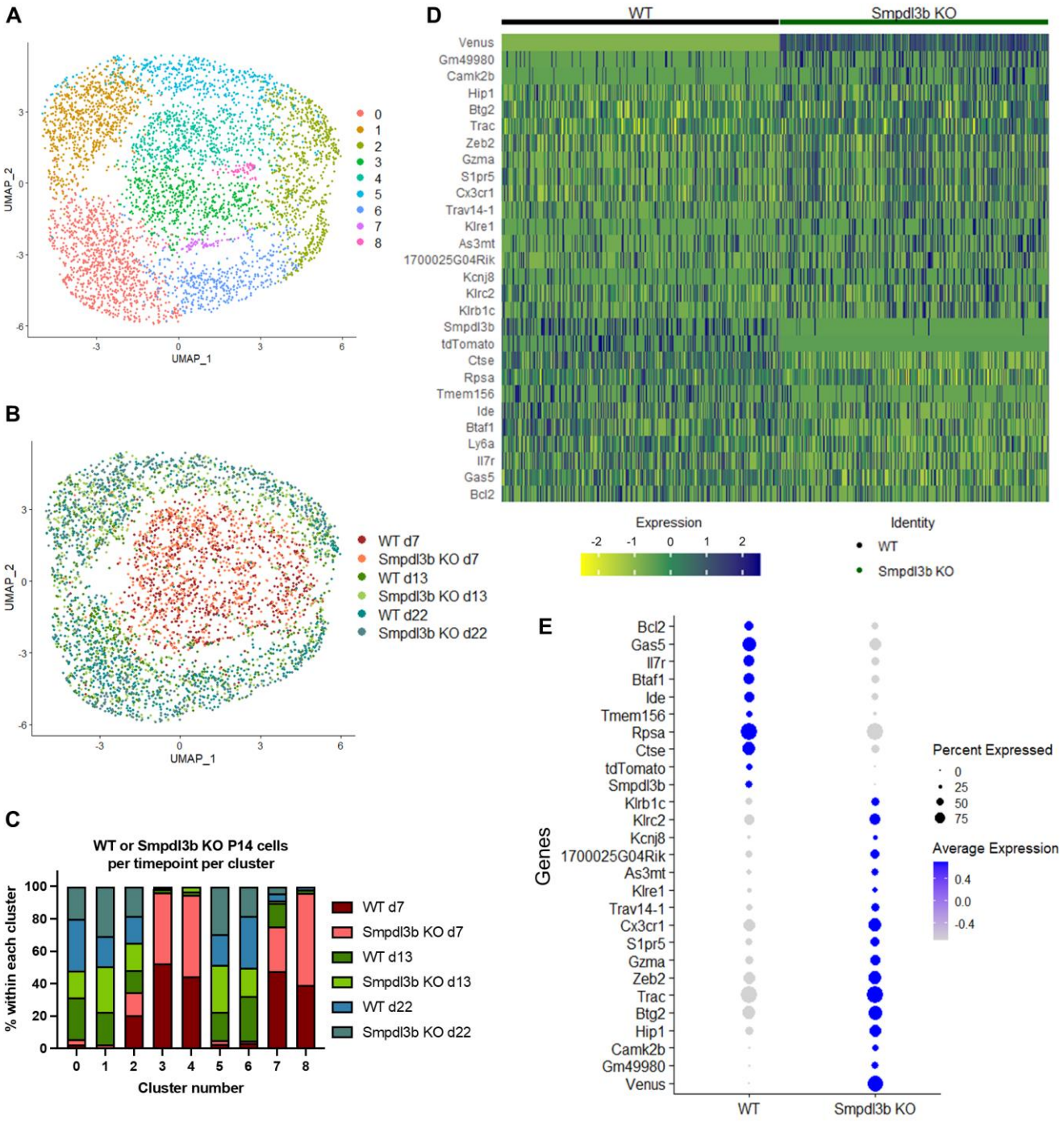

Figure 6. Single-cell sequencing suggests that *Smpdl3b*$^{-/-}$ CD8^{+} T cells could undergo apoptosis at a higher rate and present enhanced endocytosis. A-B) UMAP projections of 4258 single cells, color code based on cluster identity (A) or genotype + timepoint identity (B). C) Quantitative analysis of the genotype + timepoint identity distribution within all clusters, as represented in B. D) Heatmap displaying the differentially expressed genes (DEGs) between wild-type (WT) and *Smpdl3b*$^{-/-}$ (Smpdl3b KO) P14 CD8^{+} T cells. Color represents z-score mean expression values per cell. E) Dot plot of the DEGs between WT and Smpdl3b KO P14 CD8^{+} T cells. Color represents the z-score mean expression values per cell.

In summary, the DEGs between WT and Smpdl3b KO CD8^{+} T cells revealed minor differences. For this reason, we compared the DEGs between WT and Smpdl3b KO within each cluster (Figure 6A), since some seemed to be slightly enriched (1, 4, 5, 8) or reduced (0, 3, 6, 7) in Smpdl3b KO cells (Figure 6C). Yet again, we found the same DEGs as in the cluster-independent comparison (data not shown; Figure D-E). In conclusion, our transcriptional comparison suggests that Smpdl3b-deficient cells might be more apoptotic and have a higher endocytosolic activity than their WT-counterparts. This supposed increase in the endocytosolic capacity of Smpdl3b KO cells could lead to i) the ingestion of unwanted molecules, ii) attenuated survival signaling events, iii) enhanced death signaling cascades, which could eventually lead to heightened mortality of CD8^{+} T cells. Evidently, the substrate of Smpdl3b, the pathway leading to the accumulation of Hip1 and the involved mechanism leading to T_{mem} cell death should urgently be depicted.

Discussion

In our study, we found that SM degradation to produce Cer is conserved in terminally differentiated CD8^{+} T cells (T_{eff} and TEM) when compared to their stem-like counterparts (naïve and TCM). In line with our results, it has been shown that a higher Cer content in CD8^{+} T cells is required for their cytotoxic function[37,68]. Moreover, Cer-enriched platforms generated by the degradation of SM have been associated with apoptosis induction[69], which is required for the contraction phase of the terminally differentiated populations after the resolution of the infection. These results led us to study Smpdl3b as a potential candidate for Cer generation in differentiated CD8^{+} T cells. However, we and others (data not shown; Figure 5;[16,17]) have failed to show any direct SMase activity of Smpdl3b in *in vitro* and *in vivo* settings. Instead, we identified Smpdl3b as an essential enzyme for the maintenance of CD8^{+} T cell memory. Unfortunately, we were unable to elucidate its mechanism of action. Other studies have linked the activity of Smpdl3b to innate immunity, by modulating TLR signaling in podocytes, liver cells and macrophages[16,18,70]. Moreover, Smpdl3b has been described as a potential prognosis marker in cancer[49-51] and nephrotic syndrome[71]. Furthermore, several studies in podocytes have established that Smpdl3b could indirectly modulate the levels of ceramide-1-phosphate (C1P) in these cells[48,72-75,76]. Also, Smpdl3b has been reported to enhance DNA double-strand breaks and reduce apoptosis in podocytes, protecting them from ionizing radiation[73,77,78], or even increase the apoptosis in glomerular endothelial cells during irradiation[79]. Further indirect roles attributed to Smpdl3b have been the modulation of lipid droplet abundance in podocytes[80], viral entry and replication of porcine reproductive and respiratory syndrome virus (PRRSV)[81], and murine embryonic stem cell neural differentiation[82]. Interestingly, all of these studies seem to observe context-dependent functions, and potential substrates,

of Smpdl3b. In our hands, using our knock-out mouse model and overexpressing systems (data not shown), we were, however, not able to reproduce the reported alterations in SM or Cer species detected in knock-down models[16].

In our study, we found that Smpdl3b exerts a cell intrinsic function in sustaining memory CD8$^+$ T cells, and more specifically less terminally differentiated cells, during an acute infection setting. The relatively late (day 5) expression of Smpdl3b in comparison to antigen presentation and activation, together with our data, indicate that it is crucial following the resolution of the primary infection[2]. In line with our results (Figure 3; Supplementary Figure 3), our survival phenotype suggested that memory Smpdl3b KO cells might fail to mount an efficient recall response and therefore only mediate an insufficient protective cellular immunity. Importantly, the remaining Smpdl3b-deficient CD8$^+$ T cells do not seem to have any functional defects in cytokine production. Nonetheless, we did observe a dampened capacity for re-expansion upon recall. This could be explained by the bias towards increased terminally differentiated IL-7Rα$^-$ CX3CR1$^+$ TEM cells when Smpdl3b is absent, whose proliferative capacity is reduced compared to IL-7Rα$^+$ CX3CR1$^-$ TCM cells[4,83]. Moreover, an alternative explanation to the observed differences between the re-infection and the re-transfer settings could be that, perhaps, TEM cells are less good at engrafting when competing with their TCM counterparts in a post-sorting transfer setting. Likely, co-transferring WT and Smpdl3b KO memory cells into non-infected recipient mice and comparing their ratio after 6 days would clarify the potentially reduced engraftment capacity of the TEM population. Whether there are differences in viral control between WT and Smpdl3b KO mice in a recall setting should be elucidated.

Unfortunately, the lack of commercially available antibodies for flow cytometry and the reduced number of cells, specially at a memory timepoint, limit our possibilities for performing screening assays in order to find Smpdl3b's physiological substrate. Concisely, our lipidomics and transcriptomics data together advocate for a molecule in the extracellular milieu being the substrate of Smpdl3b. A recent study suggested that the homolog protein Smpdl3a modulates innate immunity via the cGAS-STING innate pathway[84] by cleaving extracellular cGAMP. Moreover, we and others have shown a phosphodiesterase activity of Smpdl3b (Figure 2E; [16,17]) and its capacity to cleave ADP and ATP, similarly to its paralog Smpdl3a[85-87]. This in addition to the structural resemblance between Smpdl3a with Smpdl3b[17], lead us to hypothesize the physiological substrate of Smpdl3b are not (sphingo)lipid species, but rather nucleotides. Furthermore, the connection of Smpdl3a to lipid metabolism is the induction of its expression through liver X receptor (LXR), whose ligands are cholesterol metabolites[88]. Therefore, studying the nuclease function of Smpdl3b in CD8$^+$ T cells would be an opportunity to understand its physiological role and mechanism of action.

Importantly, the topology of Smpdl3a and Smpdl3b differs, since Smpdl3a is mainly secreted and Smpdl3b is GPI-anchored[15,88]. Nonetheless, they are both exposed to the extracellular milieu. Distinct publications have shown how cGAMP produced in dying cancer or infected cells can be secreted into the extracellular space, which is where Smpdl3a and other enzymes, such as ectonucleotide pyrophosphatase/phosphodiesterase I (ENPP1) exert their nuclease function[84,89-91]. Interestingly, ENPP1 can be membrane bound or secreted[92], as an analogy to Smpdl3b and Smpdl3a, respectively. Extracellular cGAMP has been described as an immune cell activator in response to tumours[93-96].

Therefore, its degradation by ENPP1 results in suppressed anti-tumour responses[89,90,97]. Likely, cGAMP and other cyclic dinucleotides (CDNs) are released to the extracellular space by dying apoptotic cells[98], as it has been proven for other nucleotides[99-101]. Consequently, during the contraction phase of a $CD8^+$ T cell response to an acute infection, 90-95% of the expanded clones will die via apoptosis[2] and release their intracellular content, including nucleotides and CDNs. Additionally, the dying infected cells in our infection setting might also release the aforementioned species. Therefore, the local extracellular milieu could be rich with these molecules. Notably, extracellular cGAMP can cross the PM through the transporters SLC19A1 and SLC46A2, clathrin-mediated endocytosis, GAP junctions or volume-activated LRRC8A anion channels[94,98,102-107]. Despite elucidating the effects of extracellular CDNs in $CD8^+$ T cells, it is known that these cells are capable of endocytosing distinct molecules (e.g. TCR or other receptors) via clathrin-dependent and independent mechanisms[108-110]. Furthermore, it has been shown that STING activation in $CD8^+$ T cells elicits cell death via apoptosis during the contraction phase of the acute response for clones with high-affinity for the antigen[111,112]. Similarly, the kinetics observed in the Smpdl3b KO cells aggravates from the contraction phase onwards (Figure 3). Remarkably, the increased expression of *Hip1* in Smpdl3b KO cells suggests an increased clathrin-mediated endocytosis capacity in these cells[61-63]. Possibly, the lack of the phosphodiesterase activity of Smpdl3b in the KO cells allows them to endocytose the abundant extracellular CDNs (e.g. cGAMP) released by the great number of apoptotic cells mainly during the contraction phase, leading to STING- and Hip1-mediated apoptosis[64-67,112]. Importantly, we did not find any differences in the levels of Bim (Figure 3G), Annexin V or caspase 8 (data not shown) between WT and Smpdl3b KO cells. Yet, the KO cells express less Bcl-2 (Figure 6E), in line with increased apoptosis. Notably, delineating the physiological substrate of Smpdl3b is critical for determining its modulating function over Hip1.

Alternatively, the aggravated loss of Smpdl3b KO cells could be based on altered IL-7 and IL-15 signaling, since antigen specific memory cells mainly rely on these signaling pathways for survival and homeostatic proliferation[113,114]. On one hand, CD127/IL-7Rα is internalized as part of a negative feedback loop once it encounters IL-7, in order to signal and consecutive degradation by the proteasome. This process has been shown to be clathrin-mediated endocytosis-dependent[110,115]. On the other hand, the predominant signaling pathway of IL-15 occurs via trans-presentation from the APC to the T cells[116-118]. This model establishes that a complex of IL-15Rα – IL-15 is present in the APCs and presented to, for example, $CD8^+$ T cells expressing the IL-2Rβ and IL-2Rγ chains. Potentially, the mechanism leading to an enhanced endocytosis in the Smpdl3b KO $CD8^+$ T cells could increase endocytosis of IL-7Rα or affect the surface levels of the IL-15Rβ and γ chains, impairing these signaling pathways, proliferation and survival. Whether the IL-2Rβ and γ chains are being internalized via clathrin-mediated endocytosis should be the focus of future studies.

In summary, in this study we identified a role of Smpdl3b as a protector of memory $CD8^+$ T cell longevity. Likely, the role of Smpdl3b in safeguarding memory $CD8^+$ T cell relies on the hydrolysis of cytotoxic extracellular CDNs, such as cGAMP, released by the numerous dying cells during the resolution phase of an acute infection. This is consistent with its expression kinetics at later timepoints after activation and with the bias towards more terminally differentiated cells in its absence. Therefore, we propose that Smpdl3b is upregulated as a shielding mechanism in order to protect the memory cells

from a harmful environment that likely occurs during the massive cell death during the contraction phase. Alternatively, Smpdl3b could be essential for maintaining T_{mem} survival signaling pathways by modulating Hip1-mediated endocytosis, since certain receptors are endocytosed in order to attenuate signaling, whereas others require this internalization as part of their signaling pathway[108,119]. Given its location in the extracellular leaflet of the PM and its supposed function, understanding the mechanism of action of Smpdl3b will make it a suitable candidate for improving T cell memory in vaccination strategies. For instance, Smpdl3b is stabilized in the PM by being an off-target of anti-CD20 (Rituximab)[120]. In the context of focal segmental glomerulosclerosis (FSGS) it has been shown that the Rituximab-dependent stabilization of Smpdl3b in podocytes protects them from apoptosis[76].

Supplementary Figures

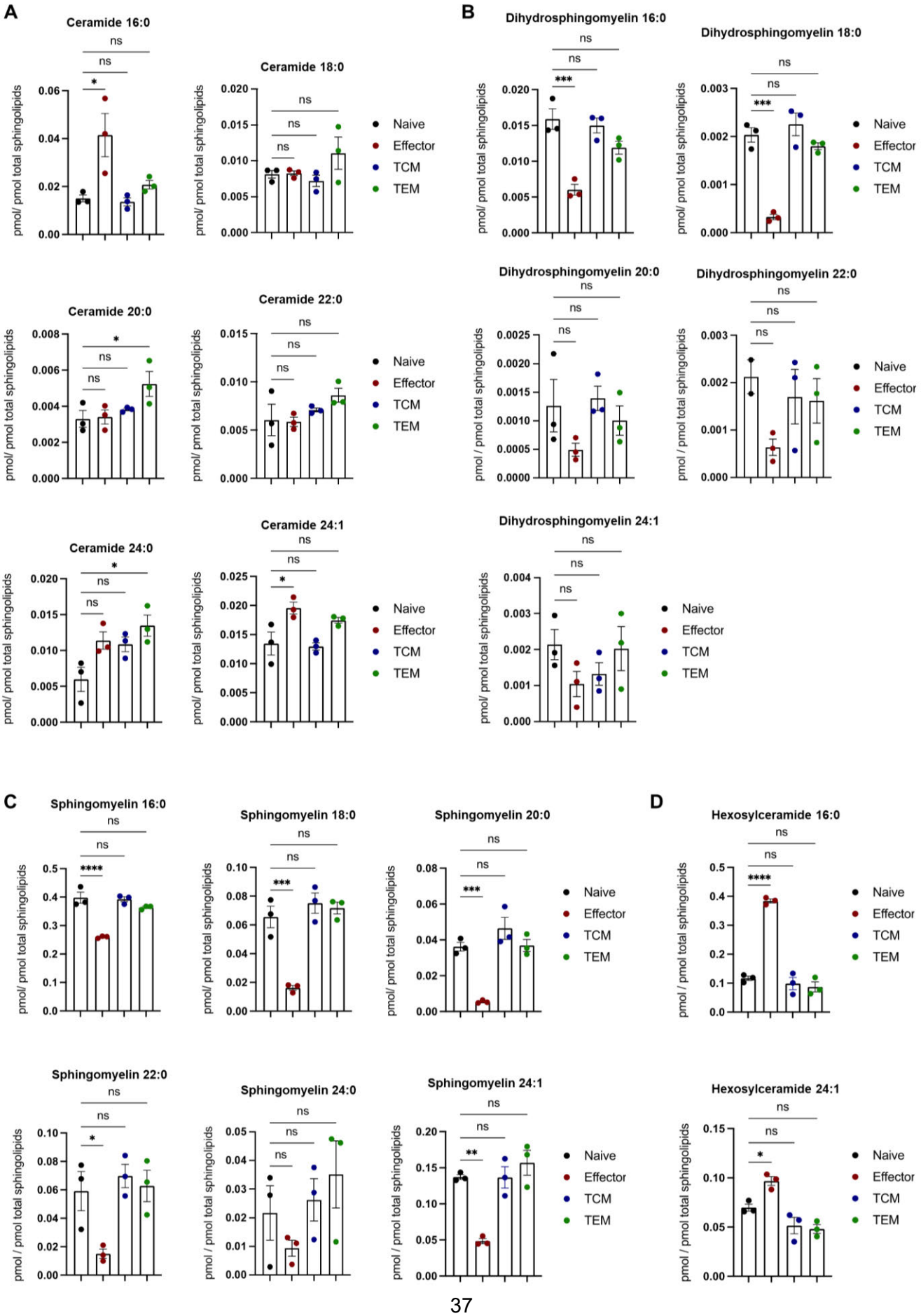

Supplementary Figure 1 (related to Figure 1). The sphingolipid profile of CD8$^+$ T cell differs along with their differentiation trajectory. A) Individual ceramide species' profile present in CD8$^+$ T cells with distinct differentiation status, normalized to total measured sphingolipids. B) Individual dihydrosphingomyelin species' profile present in CD8$^+$ T cells with distinct differentiation status, normalized to total measured sphingolipids. C) Individual sphingomyelin species' profile present CD8$^+$ T cells with distinct differentiation status. D) Individual hexosylceramide species' profile present CD8$^+$ T cells with distinct differentiation status. Cells are derived and sorted from the spleen of non-infected (naive) or LCMV Armstrong (acutely) infected mice for 8 (effector) or 22 days (TCM: central memory; TEM: effector memory) for A-D. Data represent 3 of 3 independent experiments with n = 2 pooled mice per experiment for naïve, n = 2 pooled mice per experiment for effector and n = 3 or 6 pooled mice per experiment for TCM and TEM. Bar graphs represent the mean values and error bars represent SEM. Comparison between groups was calculated using one-way ANOVA and Dunnett's multiple comparisons test (A-D). ns = non-significant ($p > 0.05$); * $p < 0.05$; ** $p < 0.01$; *** $p < 0.001$; **** $p < 0.0001$.

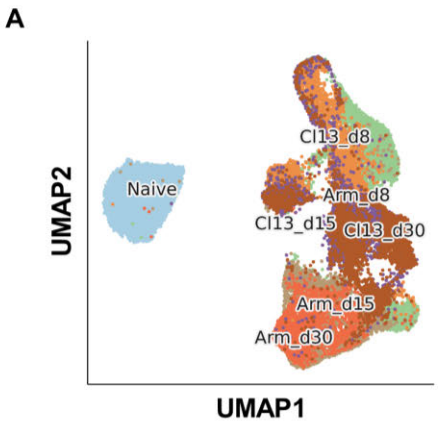

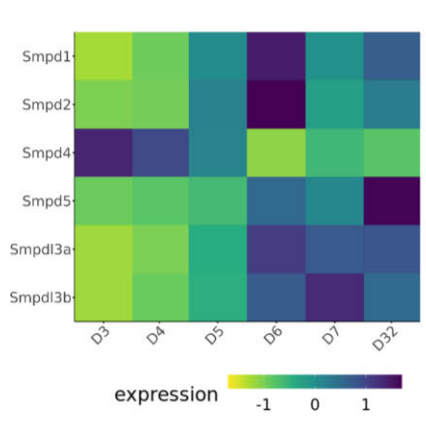

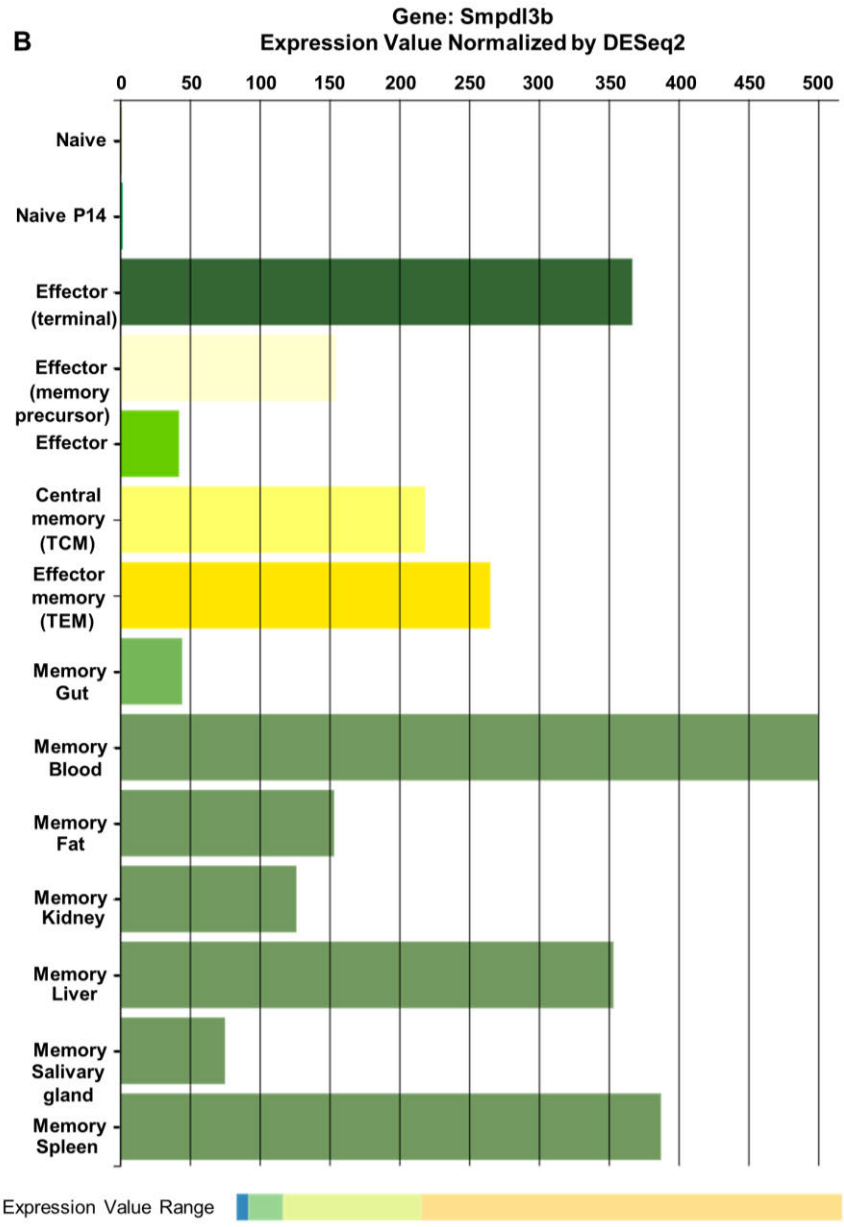

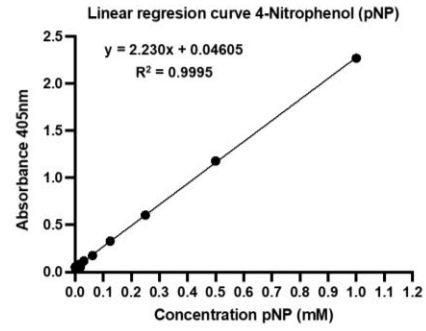

E

Population	Amount of pNP produced (mM)
Naive WT	0,266151
Naive KO	0,2878935
Effector WT	0,363156
Effector KO	0,252548
TEM WT	0,360703
TEM KO	0,256785
TCM WT	0,310751
TCM KO	0,258123
HEK WT	0,750061
HEK OE Smpdl3b	8,830168667

Supplementary Figure 2 (related to Figure 2). Sphingomyelin phosphodiesterase acid-like 3b (Smpdl3b) is not expressed or active in naïve, but in effector and memory CD8$^+$ T cells. A) UMAP projection of 30289 single cells from single-cell RNA sequencing, color code based on the cluster timepoint (Naïve, day 8 (d8), day 15 (d15) and day 30 (d30)) and type of infection (acute: Arm; chronic: Cl13). The UMAP was generated using from the data set published by Giles, J.R., *et al.* (2022)[43] and uploaded into our Institute's Shiny app. B) Bar graph showing the expression value of *Smpdl3b* in CD8$^+$ T cells with distinct differentiation states, including tissue-resident populations. The graph was generated in the Immgen Consortium website (immgen.org) using the Gene Skyline ULI-RNA seq Data Browser[44]. C) Heatmap displaying the expression of the distinct sphingomyelinases in the distinct identity clusters shown in Figure 2C[45]. D) Linear regression curve generated as a calibration curve to further quantify the amount of 4-Nitrophenol (pNP) produced by the distinct *Smpdl3b*$^{+/-}$(WT) and *Smpdl3b*$^{-/-}$ (KO) CD8$^+$ T cell subpopulations. E) Table showing the amount of pNP produced by the distinct control (HEK293T WT, HEK293T overexpressing (OE) Smpdl3b) and CD8$^+$ T cell subpopulations. Data for E and F represent 1 of 4 independent experiments with n = 1 mouse for naïve het, naïve KO, effector het and effector KO, and n = 3 mice for het memory (TCM and TEM) and KO memory (TCM and TEM).

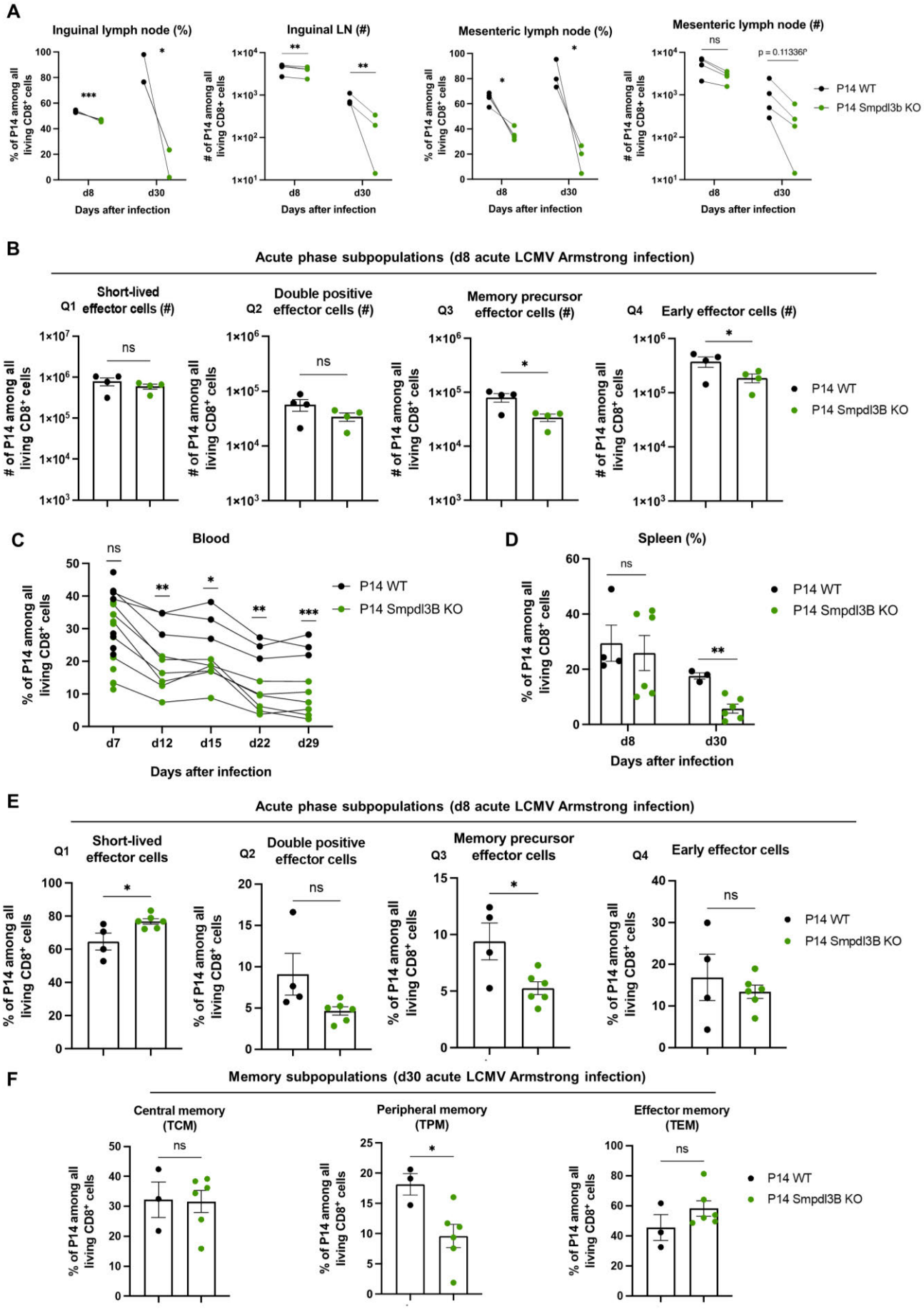
A
Inguinal lymph node (%)
Inguinal LN (#)
Mesenteric lymph node (%)
Mesenteric lymph node (#)
% of P14 among all living CD8+ cells
# of P14 among all living CD8+ cells
Days after infection
d8
d30
ns
p = 0.11336
P14 WT
P14 Smpdl3b KO
B
Acute phase subpopulations (d8 acute LCMV Armstrong infection)
Q1 Short-lived effector cells (#)
Q2 Double positive effector cells (#)
Q3 Memory precursor effector cells (#)
Q4 Early effector cells (#)
P14 Smpdl3B KO
C
Blood
D
Spleen (%)
d7
d12
d15
d22
d29
E
Acute phase subpopulations (d8 acute LCMV Armstrong infection)
Q1 Short-lived effector cells
Q2 Double positive effector cells
Q3 Memory precursor effector cells
Q4 Early effector cells
F
Memory subpopulations (d30 acute LCMV Armstrong infection)
Central memory (TCM)
Peripheral memory (TPM)
Effector memory (TEM)

Supplementary Figure 3 (related to Figure 3). Smpdl3b is necessary for the formation of stem-like CD8+ T cell memory populations at acute and memory timepoints. A) Quantitative analysis of the frequency and numbers of wild-type (WT) P14 and *Smpdl3b*$^{-/-}$ P14 (Smpdl3b KO) in the inguinal (iLN) and mesenteric (mesLN) lymph nodes of C57BL/6J WT recipient mice into which WT P14 and Smpdl3b KO P14 were co-transferred in a 1:1 ratio and that were acutely infected with LCMV Armstrong for 8 or 30 days. B) Quantitative analysis (numbers) of the phenotype of wild-type (WT) P14 and *Smpdl3b*$^{-/-}$ P14 (Smpdl3b KO) in the spleen of C57BL/6J WT recipient mice into which WT P14 and Smpdl3b KO P14 were co-transferred in a 1:1 ratio and that were acutely infected with LCMV Armstrong for 8 or 30 days. C-F) Quantitative analysis of the frequency and phenotype of WT P14 and Smpdl3b KO P14 in the blood (C) and spleen (D-F) of C57BL/6J WT recipient mice into which WT P14 or Smpdl3b KO P14 were transferred (single transfers) and that were acutely infected with LCMV Armstrong for 8 or 30 days. Data represent 1 of 1 (A), or 1 of 3 (B), 2 of 3 (C-F) independent experiments with n = 12 mice (C Smpdl3b KO d7), n = 8 mice (C WT d7), n = 6 (C Smpdl3b KO d12-29, D-F Smpdl3b KO d8 and d30), n = 4 mice (A d8, B, D-F WT d8), n = 3 (A d30, C WT d12-29, D-F WT d30). Bar graphs represent the mean values and error bars represent SEM. Comparison between groups was calculated using two-way ANOVA with uncorrected Fisher's LSD test for mixed effects analysis (C), multiple paired T test (A) or unpaired student T test (B, E-F). ns = non-significant ($p > 0.05$); * $p < 0.05$; ** $p < 0.01$; *** $p < 0.001$; **** $p < 0.0001$.

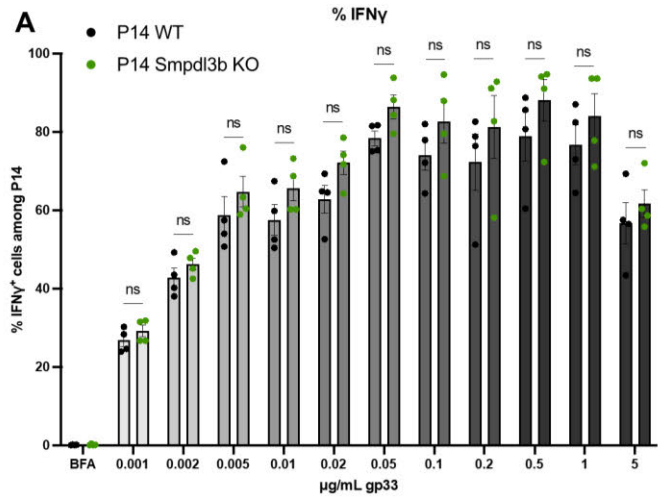
A
% IFNγ
P14 WT
P14 Smpdl3b KO
% IFNγ+ cells among P14
BFA
0.001
0.002
0.005
0.01
0.02
0.05
0.1
0.2
0.5
1
5
µg/mL gp33
ns

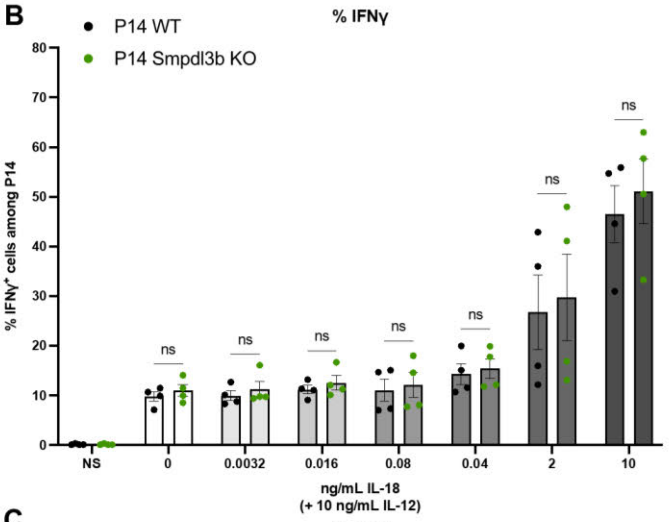
B
% IFNγ
P14 WT
P14 Smpdl3b KO
% IFNγ+ cells among P14
NS
0
0.0032
0.016
0.08
0.04
2
10
ng/mL IL-18
(+ 10 ng/mL IL-12)
ns

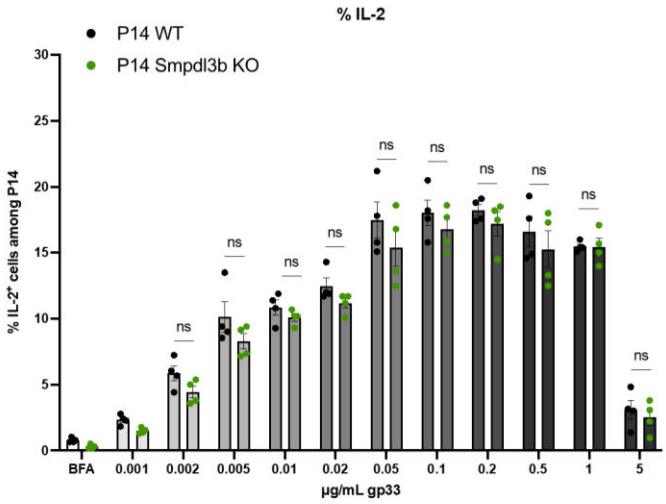
% IL-2
P14 WT
P14 Smpdl3b KO
% IL-2+ cells among P14
BFA
0.001
0.002
0.005
0.01
0.02
0.05
0.1
0.2
0.5
1
5
µg/mL gp33
ns

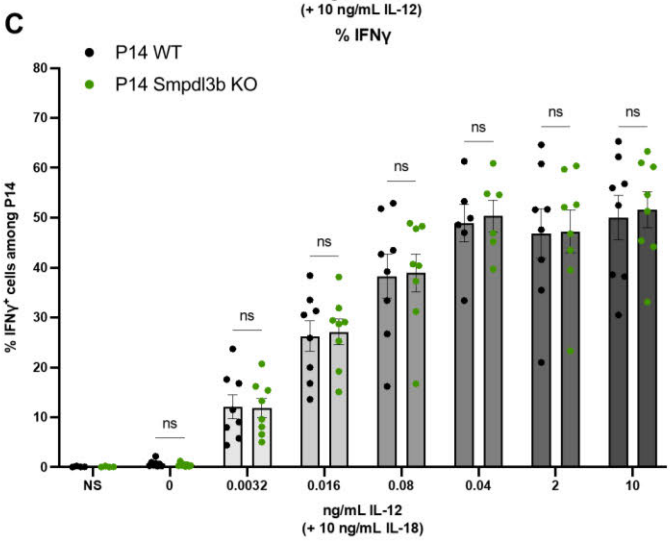
C
% IFNγ
P14 WT
P14 Smpdl3b KO
% IFNγ+ cells among P14
NS
0
0.0032
0.016
0.08
0.04
2
10
ng/mL IL-12
(+ 10 ng/mL IL-18)
ns

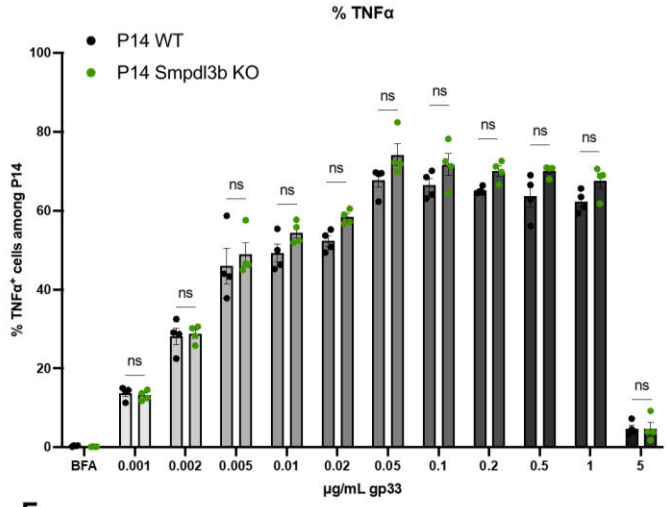
% TNFα
P14 WT
P14 Smpdl3b KO
% TNFα+ cells among P14
BFA
0.001
0.002
0.005
0.01
0.02
0.05
0.1
0.2
0.5
1
5
µg/mL gp33
ns

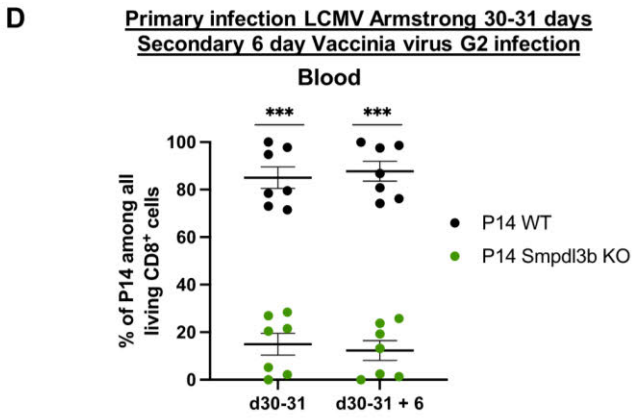
D
Primary infection LCMV Armstrong 30-31 days
Secondary 6 day Vaccinia virus G2 infection
Blood
% of P14 among all living CD8+ cells
d30-31
d30-31 + 6
***
P14 WT
P14 Smpdl3b KO

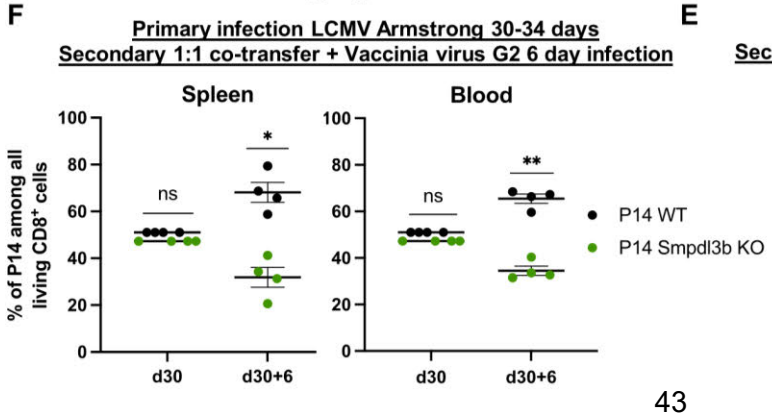
F
Primary infection LCMV Armstrong 30-34 days
Secondary 1:1 co-transfer + Vaccinia virus G2 6 day infection
Spleen
Blood
% of P14 among all living CD8+ cells
d30
d30+6
ns
*
**
P14 WT
P14 Smpdl3b KO

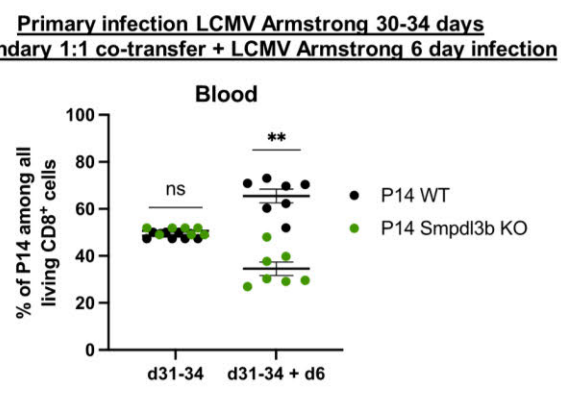
E
Primary infection LCMV Armstrong 30-34 days
Secondary 1:1 co-transfer + LCMV Armstrong 6 day infection
Blood
% of P14 among all living CD8+ cells
d31-34
d31-34 + d6
ns
**
P14 WT
P14 Smpdl3b KO

Supplementary Figure 4 (related to Figure 4). Smpdl3b is dispensable for CD8$^+$ T cell TCR- or cytokine-mediated functions. A-C) Quantitative analysis of the frequency cytokines produced by wild-type (WT) P14 or *Smpdl3b*$^{-/-}$ P14 (Smpdl3b KO) isolated from the spleen of C57BL/6J mice infected for 8 days with LCMV Armstrong, after stimulating them *in vitro* for 4 hours with distinct concentrations of (A) gp33 peptide (TCR stimulation) with Brefeldin A (BFA), (B-C) IL-18 and IL-12. D) Quantitative analysis of the frequency of WT P14 or Smpdl3b KO P14 in the blood of mice that were infected with LCMV Armstrong for 30-31 days (primary infection) and then rechallenged with Vaccinia virus G2 (modified strain expressing gp33) for 6 days. E) Quantitative analysis of the frequency of WT P14 or Smpdl3b KO P14 present in the blood of secondary recipient mice that were infected for 6 days with LCMV Armstrong. Previously, the cells were isolated and sorted from the spleen of primary recipient mice infected with LCMV Armstrong for 30-34 days, then co-transferred in a 1:1 ratio into the secondary recipients. F) Quantitative analysis of the frequency of WT P14 or Smpdl3b KO P14 present in the blood and spleen of secondary recipient mice that were infected for 6 days with Vaccinia virus G2. Previously, the cells were isolated and sorted from the spleen of primary recipient mice infected with LCMV Armstrong for 30-34 days, then co-transferred in a 1:1 ratio into the secondary recipients. Data represent 1 of 1 (F), 1 of 2 (A-B), or 2 of 2 (C, E) or 2 of 3 (D) independent experiments with n = 8 mice (C), n = 7 mice (D-E), n = 4 mice (A-B, F). Bar graphs represent the mean values and error bars represent SEM. Comparison between groups was calculated using paired multiple T test. ns = non-significant ($p > 0.05$); * $p < 0.05$; ** $p < 0.01$; *** $p < 0.001$; **** $p < 0.0001$.

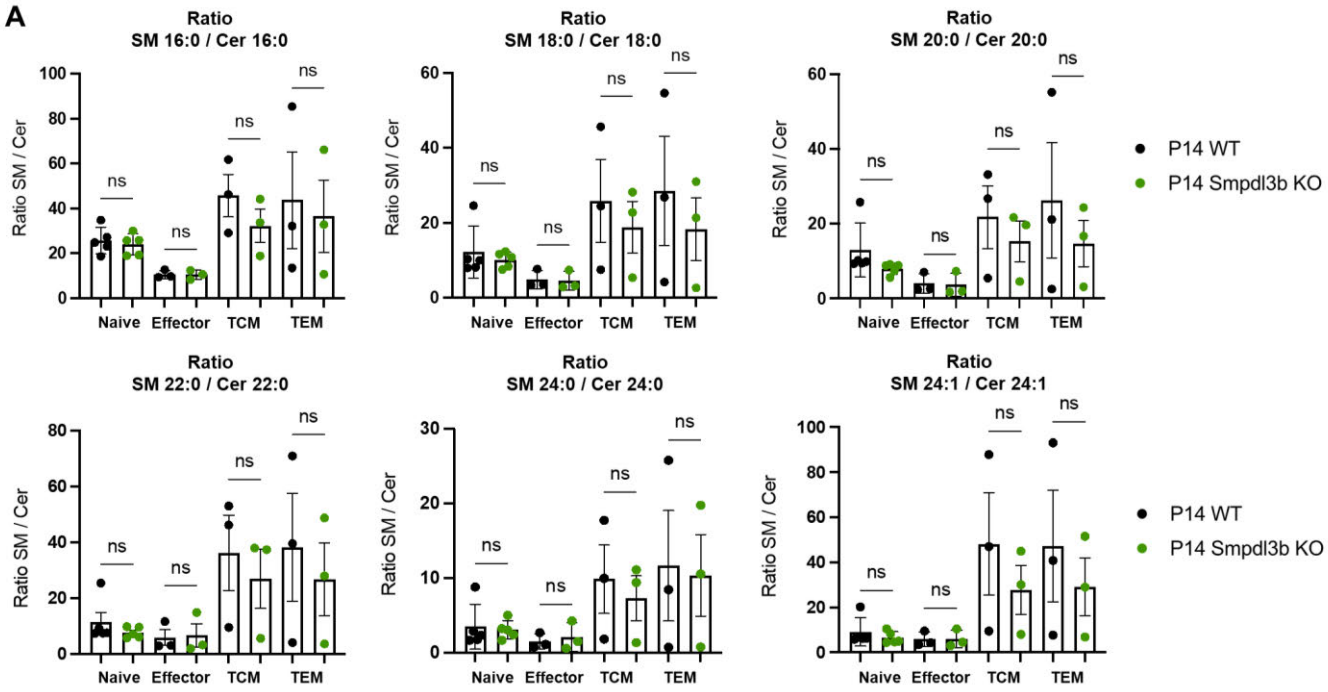

Supplementary Figure 5 (related to Figure 5). Smpdl3b shows no activity towards sphingomyelin. A) Ratio of total individual sphingomyelin (SM) and ceramide (Cer) species present in distinct subpopulations of WT or Smpdl3b KO P14 CD8$^+$ T cells, calculated from the values of the individual species shown in Figure 5A-B. Cells are derived and sorted from the spleen of non-infected (naive) or LCMV Armstrong (acutely) infected C57BL/6J mice for 8 (effector) or 22 (TCM: central memory; TEM: effector memory) days for A-C. Data represent 3 of 3 independent experiments (effector, TCM and TEM) or 5 of 5 independent experiments (naïve) with n = 1 mouse per experiment for naïve WT, n = 1 mouse per experiment for naïve Smpdl3b KO, n = 1 or 2 mice per experiment for WT effector, n = 1 or 2 mice per experiment for Smpdl3b effector, n = 5 pooled mice per experiment for WT TCM and TEM, and n = 15 pooled mice per experiment for Smpdl3b KO TCM and TEM. Bar graphs represent the mean values and error bars represent SEM. Comparison between groups was calculated using one-way ANOVA and Dunnett's multiple comparisons test (B-D). ns = non-significant ($p > 0.05$); * $p < 0.05$; ** $p < 0.01$; *** $p < 0.001$; **** $p < 0.0001$.

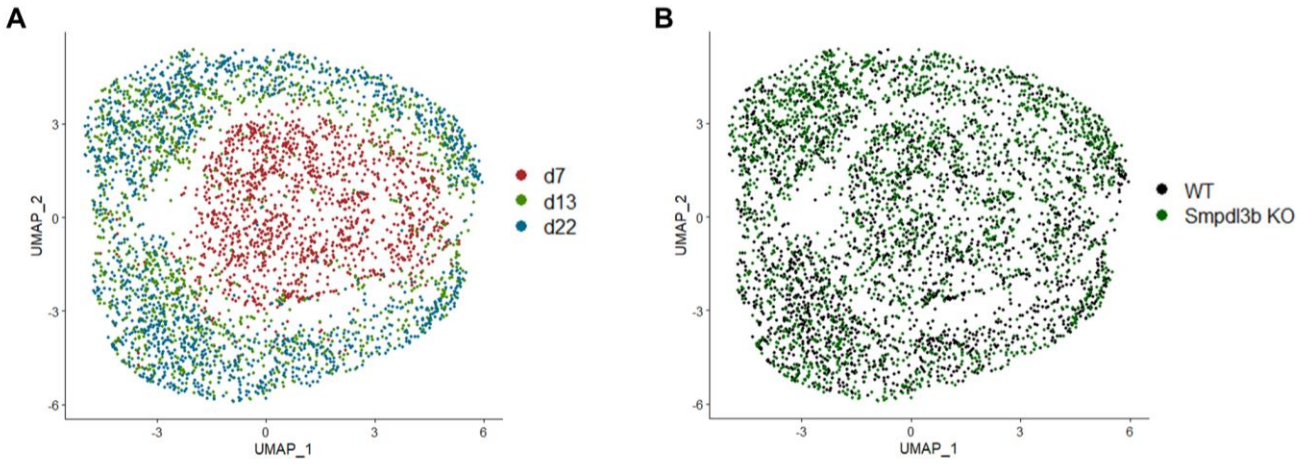

Supplementary Figure 6 (related to Figure 6). Single-cell sequencing suggests that *Smpdl3b*$^{-/-}$ CD8$^+$ T cells could undergo apoptosis at a higher rate and present enhanced endocytosis. A-B) UMAP projections of 4258 single cells, color code based on timepoint identity (A) or genotype identity (B).

Material and methods

Material

Table 1. Equipment

Device	Name and Company
1290 Infinity II HPLC	Agilent Technologies, Waldbronn, Germany
6495C triple-quadrupole mass spectrometer	Agilent Technologies, Waldbronn, Germany
Autoclave	HX-430, Systec, Linden, Germany
Balance	CP2201, Sartorius, Göttingen, Germany
Cell separator magnet	EasyEights™ EasySep™ Magnet, Vancouver, British Columbia, Canada
Cell sorter Aria II	Becton-Dickinson, Franklin Lakes, NJ, USA
Centrifuge	Thermo Fisher Scientific, Waltham, MA, USA
FlexStation 3 Multi-Mode Microplate Reader	Molecular Devices
Flow cytometers	Attune NxT Flow Cytometer, Thermo Fisher Scientific, Waltham, MA, USA Cytek Aurora 5-Laser, Cytek Biosciences, Amsterdam, The Netherlands
Freezer -20 °C	Liebherr, Biberach, Germany
Freezer -80 °C	VIP ECO ULT freezer, Panasonic, Avon Cedex, France
Freezer -150°C (Ultra-Low Temperature Freezer)	Panasonic, Etten Leur, Netherlands
Ice machine	Ziegra, Isernhagen, Germany
Incubator cells	Binder, Tuttlingen, Germany
Incubator bacteria	MaxQ, Thermo Fisher Scientific, Waltham, MA, USA
IVC mice cage	Tecniplast Smartflow, Hohenpeißenberg, Germany
NanoPhotometer	Implen, Munich, Germany
Neubauer chamber	Assistent, Karl Hecht GmbH, Sondheim, Germany
Pipette boy	Integra Biosciences, Biebertal, Germany
Pipette	Research plus (10, 20, 200, 1000), Eppendorf, Hamburg, Germany
Poroshell 120 EC-C8 column (3.0 × 150 mm, 2.7 µm)	Agilent Technologies, Waldbronn, Germany
Preparation instruments	F.S.T., Heidelberg, Germany
Refrigerator	Liebherr, Biberach, Germany
Sieves, steel	Mechanical Workshop, University Hospital Bonn, Germany
Table centrifuge Micro Star 17R	VWR, Leuven, Belgium
Thermo-Shaker	Thermo Fisher Scientific , Schwerte, Germany
Vacuum Pump	Integra Biosciences, Biebertal, Germany
Vortex	Neolab, Heidelberg, Germany
Water bath	Memmert, Schwabach, Germany
Workbench, sterile	Envair ECO, ENVAIR GmbH, Emmendingen, Germany

Table 2. Consumables

Consumable	Company	Catalog number
Cell culture flask 75 cm^2 (T75) and 175 cm^2	Greiner Bio-one	658175; 660175
Cell strainer (70 and 100um)	Falcon, VWR	734-0003; 734-0004
Cryo-container Mr. Frosty	Carl Roth	AC96.1
Cryo.S, 2 ml	Greiner Bio-one	122263
F-bottom 96-well plate Cellstar	Greiner Bio-one	655180
FACS tubes	Sarstedt	55.1579
Falcon tubes (15 and 50 ml)	Greiner Bio-one	188271; 227261

Injection needles (20G, 25G, 27G)	BD Microlance or Sterican	-
Nylon gauze	Labomedic	-
Parafilm	Hartenstein	PF10
Pipette tips (10 µl, 20 µl, 200 µl, 1000 µl)	Sarstedt	701130600; 70.3021; 70.3030; 70.3050
Pasteur-Plast Pipette 3 ml 150 mm	VWR	612-1755
Pasteurpipetten, 230 mm	Carl Roth	4522.1
Plates suspension culture (6, 12, 24 and 48 wells)	Greiner Bio-one	657185; 665102; 662102; 677102
Petri dish 92x16mm	Sarstedt	82.1473
Pipette bulk pack (5, 10, 25 ml)	Greiner Bio-one	606107; 607107; 760107
Pipette single pack (5, 10, 25, 50 ml)	Greiner Bio-one	606180; 607180; 760180; 768180
Syringe Inject, Luer, 5 ml, sterile	Carl Roth	0057.1
Syringes Omnican (U-50, 0.5ml and U-100, 1ml)	Carl Roth	AKN9.1; AKP0.1
Tubes, 0.5 ml, 1.5 ml, 2 ml SafeSeal, PP	Sarstedt	72704; 70.706; 72695500
Tubes PCR strip of 8, flat cap	Sarstedt	72.991.002
U-bottom 96-well plate Cellstar	Greiner Bio-one	650180
V-bottom 96-well plate and lids	VWR	732-0191; 734-2184

Table 3. Chemicals, reagents, cytokines, peptides

Product	**Company**	**Catalog number**
2-Propanol	Sigma-Aldrich	59300-1L
4-Nitrophenol	Sigma-Aldrich	1048-5G
ß-mercaptoethanol (cell culture)	Gibco	31350010
ß-mercaptoethanol (molecular biology)	Applichem	UN2966
Agar agar, Kobe I	Carl Roth	5210.1
Agarose, Low Melting Point, Analytical Grade	Promega	V2111
Ampicillin	Sigma Aldrich	A0166-5G
Bis(p-nitrophenyl) phosphate sodium salt	Sigma-Aldrich	N3002-100G
Blasticidin	Sigma Aldrich	203350-25mg
Bovine Serum Albumin (BSA)	Carl Roth	8076.3
Braun distilled water	VWR	LOCA0082479E
Brefeldin A (BFA)	Sigma Aldrich	B7651-5MG
C16:0 Ceramide (external calibration)	Avanti Polar Lipids	860516P
C17:0 Ceramide (internal standard)	Avanti Polar Lipids	860517P
C18:0 Ceramide (external calibration)	Avanti Polar Lipids	860518P
C20:0 Ceramide (external calibration)	Avanti Polar Lipids	860520P
C22:0 Ceramide (external calibration)	Avanti Polar Lipids	860501P
C24:0 Ceramide (external calibration)	Avanti Polar Lipids	860524P
C24:1 Ceramide (external calibration)	Avanti Polar Lipids	860525P
C16:0 Sphingomyelin (external calibration)	Avanti Polar Lipids	860584P
C18:0 Sphingomyelin (external calibration)	Avanti Polar Lipids	860586P
C20:0 Sphingomyelin (external calibration)	Cayman Chemicals	24450
C22:0 Sphingomyelin (external calibration)	Cayman Chemicals	24451
C24:0 Sphingomyelin (external calibration)	Avanti Polar Lipids	860592P
C24:1 Sphingomyelin (external calibration)	Avanti Polar Lipids	860593P
C17:0 Glucosylceramide (internal standard)	Avanti Polar Lipids	860569P
C17:0 Lactosylceramide (internal standard)	Avanti Polar Lipids	860595P
Chloroform (lipidomics)	Carl Roth	7331.2
Collagenase D	Roche	11088882001
d_7-Sphingosine (internal standard)	Avanti Polar Lipids	860657P

d_7-Sphingosine-1-phosphate (internal standard)	Avanti Polar Lipids	860659P
d_{31}-C16:0 Sphingomyelin (internal standard)	Avanti Polar Lipids	868584P
Dimethylsulfoxid (DMSO)	Sigma Aldrich	D2650-100ML
DNase I	Sigma Aldrich	DN25
Dispase II	Roche	04942078001
DMEM medium	Thermo Fisher Scientific	41965-039
Diethiothreitol (DTT)	Sigma Aldrich	1.11474
DPBS, Calcium, Magnesium	Thermo Fischer Scientific	14040133
EDTA	Carl Roth	8043.2
Ethanol 96%	Carl Roth	5054.2
Fetal Bovine Serum	Sigma Aldrich	F7524-500ML
Ftl3L	BioLegend	550706
GeneRuler DNA Ladder Mix and 6X Purple Loading dye	Thermo Fisher Scientific	SM0331
Glycerol	Sigma Aldrich	G5516-500ML
Hydrochloric Acid (HCl)	Sigma Aldrich	H1758-100ML
HD Green Plus DNA stain	Intas	ISII-HDGreen Plus
Heparin sodium (25000 IU)	Ratiopharm	-
HEPES	Sigma-Aldrich	H0887-100ML
Human Normal Immunoglobulin (IVIG)	Privigen	-
IC Fixation Buffer	eBioscience	00-8222-49
IL-6	BioLegend	575706
IL-7	BioLegend	577804
LB Broth Base	Invitrogen	12780029
LCMV GP33 33-41 (H2-D(b))	Peptides and Elephants	EP11847
Methanol	Carl Roth	4627.5
Methanol 99.9%	Sigma Aldrich	34860-1L-R
NaCl	Sigma Aldrich	S9888-1KG
NaOH	Carl Roth	6771.3
Normal Rat Serum	StemCell Technologies	13551
Penicillin/Streptomycin	Sigma-Aldrich	P4333
Percoll	Sigma-Aldrich	P1644-1L
Permeabilization Buffer	Invitrogen	00-8333-56
Polybrene	Santa Cruz Biotechnology	sc-134220
Poly-L-Lysin	Thermo Fischer Scientific	A3890401
Puromycin	Thermo Fischer Scientific	A1113803
RPMI 1640 medium	Gibco	72400021
SCF	BioLegend	579706
S.O.C. Medium	Thermo Fischer Scientific	15544034
Sphingosine-1-phosphate	Avanti Polar Lipids	860492P
Tris	Carl Roth	AE15.3
Trypan Blue Solution, 0.4%	Thermo Fisher Scientific	15250061
Trypsin-EDTA (0.05%), phenol red	Thermo Fisher Scientific	25300054
UltraComp eBeads™ Compensation Beads	Thermo Fischer Scientific	01-2222-42

Table 4. Commercial assays

Product	**Company**	**Catalog number**
GenJet DNA Transfection reagent (Ver.II)	Tebu-Bio	SL100489-1ml
Mojo Sort Mouse CD8 T cell isolation Kit	BioLegend	480008
MojoSort™ Streptavidin Nanobeads	BioLegend	480016

NucleoBond Xtra Midi kit for transfection-grade plasmid DNA	Macherey-Nagel	740410.50
NucleoSpin Plasmid, Mini kit for plasmid DNA	Macherey-Nagel	740588.250
ScaI-HF®	New England Biolabs	R3122S
Zombie NIR™ Fixable Viability Kit	BioLegend	423106

Table 5. Buffers, media and solutions

Buffer, media, solution	**Composition**
1% Heparin	1:100 dilution of Heparin soidium 25000 IU in PBS
1X TBS	10 mM Tris.HCl 150 mM NaCl pH 7.5
1X Ammonium-Chloride-Potassium (ACK) lysis buffer (erythrocyte lysis buffer)	10X ACK lysis buffer diluted in distilled water
10X Ammonium-Chloride-Potassium (ACK) lysis buffer (erythrocyte lysis buffer)	1.5 M NH_4Cl 100 mM $KHCO_3$ 10 mM EDTA-Na_2 in distilled water (pH value 7.2)
40% Percoll	40% of 100% Percoll 60% DMEM or RPMI media
80% Percoll	20% 1X PBS 80% of 100% Percoll
100% Percoll	1/9 10X PBS 8/9 Percoll (Sigma-Aldrich)
Cell culture media (HEK293T cells)	10 % heat-inactivated FBS 100 U/ml Penicillin 100 µg/ml Streptomycin in DMEM media
Easy Sep buffer	2% (v/v) FBS 1mM EDTA In 1X PBS
FACS buffer	2 % (v/v) FBS in 1X PBS
Freezing media	20% DMSO 40% heat-inactivated FBS 40% cell culture media (see above)
Glycerol stock media	50% Glycerol 50% LB media (see below)
Intestine media 1	2% FBS in RPMI 1640 medium
Intestine digestion media 2	1 mM EDTA 10 mM HEPES 0.15 % (w/v) DTT in RPMI 1640 medium preparation directly before use
Intestine digestion media 3	1 mM EDTA 10 mM HEPES in RPMI 1640 medium
Intestine digestion media 4	2 % (v/v) FBS 1.5 mg/ml Collagenase D 0.5 mg/ml Dispase 20 µg/ml DNase 1 1 mM EDTA 10 mM HEPES

	in RPMI 1640 medium preparation directly before use
LB media	0.1 mg/ml Ampicillin 20 g LB broth base 1 L Braun distilled water
LB plates	0.1 mg/ml Ampicillin 15 g Agar 20 g LB broth base 1 L Braun distilled water
Salivary gland digestion media	10 mM HEPES 1 mg/ml Collagenase D 20 µg/ml DNase 1 in DMEM media
Selection media (for transfected HEK293T)	10 % heat-inactivated FBS 100 U/ml Penicillin 100 µg/ml Streptomycin 1 µg/mL Puromycin in DMEM media
Stop solution	ß-mercaptoethanol (molecular biology) in 1X PBS
T cell media	10 % heat-inactivated FBS 50 µM ß-mercaptoethanol (cell culture) 100 U/ml Penicillin 100 µg/ml Streptomycin in RPMI 1640 media

Table 6. Antibodies for flow cytometry

Antigen	Conjugate	Clone	Catalog #	Company
asialo-GM1	AF647	Poly21460	146004	BioLegend
B220 (CD45R)	AF700	RA3-6B2	103232	BioLegend
B220 (CD45R)	APC Cy7	RA3-6B2	103224	BioLegend
Bim	Unconjugated	C34C5	2933s	Cell Signaling
CD3	BV785	17A2	100232	BioLegend
CD3	AF700	17A2	100216	BioLegend
CD4	Biotin	GK1.5	100404	BioLegend
CD8α	BV421	53-6.7	100738	BioLegend
CD8α	BV510	53-6.7	100752	BioLegend
CD8α	BV605	53-6.7	100744	BioLegend
CD8α	BV650	53-6.7	100742	BioLegend
CD8α	BV711	53-6.7	100759	BioLegend
CD8α	APC	53-6.7	553035	BD Biosciences
CD8α	AF700	53-6.7	100730	BioLegend
CD8α	PE	53-6.7	100708	BioLegend
CD19	Biotin	6D5	115504	BioLegend
CD44	PerCP Cy5.5	IM7	103032	BioLegend
CD44	BV510	IM7	103044	BioLegend
CD44	BV785	IM7	103059	BioLegend
CD44	BV786	IM7	563736	BD Biosciences
CD44	PE Cy7	IM7	25-0441-82	Thermo Fischer Scientific
CD45.2	BV510	104	109837	BioLegend
CD62L	BV510	MEL-14	104441	BioLegend
CD62L	APC	MEL-14	104412	BioLegend

CD69	PE Cy7	H1.2F3	104512	BioLegend
CD69	BV711	H1.2F3	104537	BioLegend
CD103	PE Cy7	2E7	121426	BioLegend
CD127 (IL-7Rα)	BV421	A7R34	135027	BioLegend
CD127 (IL-7Rα)	PE Cy7	A7R34	25-1271-82	Thermo Fisher Scientific
CX3CR1	BV421	SA011F11	149023	BioLegend
CX3CR1	BV650	SA011F11	149033	BioLegend
CX3CR1	BV785	SA011F11	149029	BioLegend
CX3CR1	APC	SA011F11	149008	BioLegend
Donkey anti-rabbit IgG	AF647	Polyclonal	A31573	Invitrogen
IFNγ	BV605	XMG1.2	505839	BioLegend
IFNγ	BV421	XMG1.2	505830	BioLegend
IL-2	APC	JES6-5H4	17-7021-182	Thermo Fischer Scientific
KLRG1	BV421	2F1	562897	BD Biosciences
KLRG1	BV605	2F1	138419	BioLegend
KLRG1	BV711	2F1	138427	BioLegend
KLRG1	PE Cy7	2F1	25-5893-82	Thermo Fischer Scientific
NK1.1	BV711	PK136	108745	BioLegend
NK1.1	Biotin	PK136	108704	BioLegend
Thy1.1 (CD90.1)	PE	OX-7	202523	BioLegend
Thy1.1 (CD90.1)	AF700	OX-7	202528	BioLegend
TNFα	PE Cy7	MP6-XT22	506324	BioLegend
TotalSeq™-A0178 anti-mouse CD45.1	-	A20	110753	BioLegend
TotalSeq™-A0157 anti-mouse CD45.2	-	104	109853	BioLegend
Va2	Pacific Blue	B20.1	127816	BioLegend
Va2	AF700	B20.1	127824	BioLegend
TotalSeq™-A0301 anti-mouse Hashtag 1	-	M1/42 30-F11	155801	BioLegend
TotalSeq™-A0302 anti-mouse Hashtag 2	-	M1/42 30-F11	155803	BioLegend
TotalSeq™-A0303 anti-mouse Hashtag 3	-	M1/42 30-F11	155805	BioLegend
TruStain FcX	-	93	101320	BioLegend

Table 7. Viruses

Viruses	Description and Reference
Lymphocytic choriomeningitis virus (LCMV) Armstrong	Wu, H., *et al.* 2023[121]. Kind gift from Dr. Martin Väth
Vaccinia virus (VV) G2 (expressing LCMV-GP protein)	Kind gift from Prof. Dr. Annette Oxenius

Mouse strains

All mice used were maintained under specific pathogen-free conditions in accordance with institutional animal guidelines at certified Association for Assessment and Accreditation of Laboratory Animal Care-accredited animal facilities (animal facility at the Institute of Systems Immunology Würzburg or at the Center of Experimental and Molecular Medicine (ZEMM) of the University of Würzburg). Female and male mice were used for all experiments, aged 8-30 weeks. Gender and age matched mice were used in each individual experiment. Used mouse strains are listed below (Table 8).

Table 8.

Mouse strain	Description	Source and/or reference
C57BL/6J	C57BL/6J non-transgenic mice were purchased from Janvier Laboratories and used as wildtype (WT) controls	Janvier Laboratories
B6.Cg-Tcra^{tm1Mom} Tg(TcrLCMV)327Sdz/TacMmjax x B6.tg (tdTomato)	Mouse model in which all CD8$^+$ T cells express a transgenic TCR recognizing the LCMV GP33 33-41 (H2-D(b)) peptide. This TCR clone is referred to as P14 cells. Additionally, every cell of this mouse model expresses the fluorescent protein tdTomato in order to identify the cells in adoptive transfer settings	The Jackson Laboratories #037394-JAX / Kastenmüller, W., *et al.* 2013[122]
B6.Cg-Tcra^{tm1Mom} Tg(TcrLCMV)327Sdz/TacMmjax x B6.tg (Venus)	Mouse model in which all CD8$^+$ T cells express a transgenic TCR recognizing the LCMV GP33 33-41 (H2-D(b)) peptide. This TCR clone is referred to as P14 cells. Additionally, every cell of this mouse model expresses the fluorescent protein Venus in order to identify the cells in adoptive transfer settings	The Jackson Laboratories #037394-JAX / Swanson, P.A., *et al.* 2016[123]
B6.Cg-Tcra^{tm1Mom} Tg(TcrLCMV)327Sdz/TacMmjax x B6.SJL-Ptprca Pepcb/BoyJ	Mouse model in which all CD8$^+$ T cells express a transgenic TCR recognizing the LCMV GP33 33-41 (H2-D(b)) peptide. This TCR clone is referred to as P14 cells. Additionally, every immune of this mouse model expresses the congenic marker CD45.1 in order to identify the cells in adoptive transfer settings	The Jackson Laboratories #037394-JAX / JAX 002014
B6N;B6N-Smpdl3btm1a(EUCOMM)Wtsi/H Smpdl3b$^{-/-}$ x B6.tg (Venus)	Mouse model in which all cells are deficient in Smpdl3b due to the insertion of a knock-out first construct (PMID: 21677750). In the presence of the enzyme flipase, the KO would be inverted to give rise to WT-floxed alleles. If crossed to a specific Cre, we can have cell specific knock-out mouse models. Additionally, every cell of this mouse model expresses the fluorescent protein Venus in order to identify the cells in adoptive transfer settings	EUCOMM Kastenmüller lab (crossing of Smpdl3b KO mouse line to Venus mouse line)
B6N;B6N-Smpdl3btm1a(EUCOMM)Wtsi/H Smpdl3b$^{-/-}$ x B6.Cg-Tcra^{tm1Mom} Tg(TcrLCMV)327Sdz x B6.tg (Venus) x B6.tg (Venus)	Mouse model in which all cells are deficient in Smpdl3b due to the insertion of a knock-out first construct (PMID: 21677750). In the presence of the enzyme flipase,	EUCOMM Kastenmüller lab (crossing of Smpdl3b KO mouse line to P14 Venus mouse line)

	the KO would be inverted to give rise to WT-floxed alleles. If crossed to a specific Cre, we can have cell specific knock-out mouse models. Additionally, all $CD8^+$ T cells express a transgenic TCR recognizing the LCMV GP33 33-41 (H2-D(b)) peptide. This TCR clone is referred to as P14 cells. Moreover, every cell of this mouse model expresses the fluorescent protein Venus in order to identify the cells in adoptive transfer settings	

Table 9. Cell lines

Cell line	Mutations	Name and explanation
HEK293T	-	HEK293T WT
HEK293T pMSCV gw mSmpdl3b	Murine Smpdl3b overexpression	HEK293T murine Smpdl3b; cell line overexpressing the WT murine version of Smpdl3b
HEK293T pMSCV gw mSmpdl3b H135A	Murine functional mutant Smpdl3b overexpression	HEK293T murine Smpdl3b H135A; cell line overexpressing a functional mutant version of murine Smpdl3b that renders the enzyme inactive. H135A interacts with the phosphate group of the substrate in the active site of Smpdl3b

Table 10. Plasmids

Plasmid name	Company or source	Identifier and explanation
pMSCV gw mSmpdl3b	Kind gift from Dr. Leonhard Heinz	Retroviral plasmid that allows the overexpression of the murine version of Smpdl3b. Additionally, this plasmid contains an HA-tag
pMSCV gw mSmpdl3b H135A	Kind gift from Dr. Leonhard Heinz	Retroviral plasmid that allows the overexpression of the murine version of Smpdl3b containing a mutation in its active site (H135A), therefore reducing the enzyme's activity Additionally, this plasmid contains an HA-tag

Table 11. Software and algorithms

Software and algorithm	Company or source
Attune NxT Software	Thermo Fisher Scientific
BD FACS Diva Software	BD Biosciences
Biorender	Biorender

EndNote 20.6	Clarivate
Flowjo v10	BD Biosciences
GraphPad Prism 8	GraphPad Software
MassHunter Quantitative Analysis Software (version 10.1)	Agilent Technologies
Microsoft Excel	Microsoft
Microsoft PowerPoint	Microsoft
Microsoft Word	Microsoft
RStudio	RStudio
Seurat	Stuart *et al*., 2019[124].
Softmax Pro 7.1	Molecular Devices
SpectroFlo Software	Cytek Biosciences

Methods

Organ harvest and lymphocyte isolation

Mice were mainly sacrificed by cervical dislocation, except for re-call experiments in which blood was collected 6 days post-secondary infection. Here, CO_2 asphyxiation was utilized to avoid internal bleeding and blood clotting.

Lymph nodes

Inguinal, brachial, axillary, and mesenteric lymph nodes were harvested from donor mice and placed into 1.5 ml Eppendorf tubes containing 200 µl of cold FACS buffer on ice until further processing. Lymph nodes were a) mashed together with the spleen over a metal sieve into a 50 ml tube (see “Spleen” section below for further details), or b) mashed in the tubes using a pestle to create a single cell suspension and transferred into a 96-well V-bottom plate for staining and flow cytometry analysis (see see section “Antibody staining for flow cytometry and cell sorting”).

Spleen

The spleen was harvested and placed into 1.5 Eppendorf tubes containing 500 µl of cold FACS buffer on ice until further processing. A single cell suspension was created by mashing the spleen, and lymph nodes when applicable, over a metal sieve into a 50 ml Falcon tube. The sieve was washed with 20 ml FACS buffer and afterwards the cells were pelleted by centrifuging for 8 min at 1600 rpm 4°C. After discarding the supernatant, the pellet was resuspended in 2 ml of 1X ACK buffer to lyse erythrocytes. The 1X ACK was pre-warmed at room temperature (RT) while harvesting the organs. After a 5 min incubation at room temperature, 20 ml of PBS were added to stop the lysis. Then, the cells were filtered into a new 50 ml Falcon tube and centrifuged for 8 min at 1600 rpm 4°C. The pellet was resuspended in the required volume of PBS, FACS buffer or Easy Sep buffer for a) transferring a fraction into a 96-well V-bottom plate for staining and flow cytometry analysis, b) isolation or enrichment of $CD8^+$ T cells for transfers or sorting, c) *in vitro* peptide or cytokine stimulation, respectively.

Blood

Blood for kinetics analysis was collected by puncturing the submandibular (facial) vein (slightly behind the mandible) using a lancet. One or two drops were collected into a 1.5 Eppendorf tube containing 80 µl of 1% Heparin. 200 µl of cold PBS were added to the tubes and the volume was transferred to a 96-well V bottom plate. The plate was centrifuged at 1600 rpm 3 min at 4°C, the supernatant was discarded and pellets were resuspended in 200 µl of room temperature 1X ACK buffer to lyse erythrocytes. The samples were incubated for 10 min at room temperature. The cells were centrifuged at 1600 rpm 3 min 4°C. The supernatants were discarded and the ACK lysis was repeated for 10 min. The samples were again centrifuged at 1600 rpm 3 min 4°C, the supernatants were discarded and the pellets were resuspended in the needed volume of surface antibody mix (see section “Antibody staining for flow cytometry and cell sorting”).

Blood for day 6 after secondary infection or recall of memory cells was collected by inserting a U-50 Omnican syringe into the chest of the mice (sacrificed by CO_2 asphyxiation), where the heart is located. 400-700 µl of blood were collected into 15 ml Falcon tubes containing 300 µl of 1% Heparin. 3 ml of room temperature 1X ACK buffer was added to lyse erythrocytes by incubating for 10 min at room temperature. The cells were centrifuged for 6 min 1600 rpm room temperature and the supernatants were discarded. The pellets were resuspended once more in 3 ml 1X ACK buffer and incubated for 10 minutes at room temperature. The cells were centrifuged for 6 min 1600 rpm room temperature, the supernatants were discarded and the pellets were resuspended in the needed volume of FACS buffer. 200 µl of the blood sample were transferred to 96-well V-bottom plates to proceed with surface antibody staining (see section “Antibody staining for flow cytometry and cell sorting”).

Salivary gland

The salivary glands were harvested and placed in ice cold PBS until further processing. Afterwards, they were transferred into a 5 ml tube and cut into small pieces with scissors, until no visible clumps remained. 2 ml of salivary gland digestion media were added to the tube and incubated for 40 min 37°C 80 rpm. The digestion was stopped by mashing the samples with a syringe plunger through a 70 µm cell strainer into a 50 ml Falcon and adding 20 ml of stop solution. Cells were centrifuged for 8 min 1600 rpm 4°C and resuspended in 4 ml 40% Percoll (see “Percoll gradient” section).

Small intestine

The small intestine was harvested and placed in ice cold PBS until further processing. Fat tissue was carefully removed (avoid tearing the tissue) and the intestine was transferred to ice cold intestine media 1. Afterwards, Payer’s patches and the feces were removed, and the intestine was washed in intestine media 1. The intestine was cut longitudinally in order to expose the internal side and washed in intestine media 1. Then, the intestine was cut into 0.5 – 1 cm fragments and transferred into a 50 ml Falcon tube containing 20 ml of pre-warmed intestine digestion buffer 2. Samples were incubated for 30 min at 37°C 120 rpm. Next, the intestine fragments were vigorously shaken for 10-15 seconds, and the pieces poured out into a Petri dish on ice. The pieces were transferred to a new 50 ml tube with 15 ml of cold intestine digestion media 3, whereas the supernatant was collected in a fresh tube labeled intraepithelial lymphocytes (IELs). The shaking of the fragments and collection of supernatants were repeated. IELs were kept on ice until the lamina propria (LP) lymphocytes were isolated. The small intestine pieces were transferred into a 1.5 ml Eppendorf tube and rapidly chopped into very small pieces. The pieces were transferred back into a 50 ml Falcon tube containing 25 ml of pre-warmed intestine digestion media 4 and incubated for 30 min 37°C 120 rpm. The digestion was stopped by adding 25 ml of cold intestine media 1. Afterwards, the mixture of LP lymphocytes was filtered into a 50 ml Falcon tube using a 70 µm cell strainer and meshed with a syringe plunger. IELs and LP lymphocytes were centrifuged for 6 min 350G 4°C and resuspended in 4 ml 40% Percoll (see “Percoll gradient” section).

Percoll gradient

The single cell suspensions of the different tissues were resuspended in 4 ml 40% Percoll and carefully transferred into a 15 ml Falcon tube containing 4 ml of 80% Percoll. For the density gradient centrifugation, the cells were centrifuged at 20-22°C 20 min 2500 rpm. The acceleration was set to 1 and deacceleration to 0. Afterwards, the top floating layer of cells was removed, and the interface was collected and diluted in 6 ml cold FACS buffer in a 15 ml Falcon tube. The cell suspensions were centrifuged for 6 min 350G 4°C. Afterwards, the pellets were resuspended in FACS buffer (volume determined by the size of the pellet), transferred into a 96-well V-bottom plate, and further processed for flow cytometry analysis (see section “Antibody staining for flow cytometry and cell sorting”).

$CD8^+$ T cell isolation or enrichment from lymphoid organs

Isolation (for adoptive transfers)

Single cell suspensions from pooled spleen and lymph nodes were counted (see section “Cell counting Neubauer chamber” for further details), resuspended in 1 ml of sterile Easy Sep buffer and transferred into FACS tubes. By using the Mojo Sort Mouse CD8 T cell isolation Kit (BioLegend, 480008) and following the manufacturer’s instructions, 10 µl of Normal Rat Serum and the biotinylated antibody cocktail were added per $1x10^7$ cells in the suspension and incubated for 15 min on ice. Afterwards, the streptavidin beads were vortexed for 30 seconds and 10 µl per $1x10^7$ cells were added to the suspension. After a 15 min incubation on ice, the volume of the suspension was completed to 2.5 ml using sterile Easy Sep buffer. The FACS tubes were placed on the magnetic holder and incubated for 5 min at room temperature. The supernatant was collected in a 15 ml tube containing 7.5 ml of cold sterile FACS buffer. The isolated $CD8^+$ T cells were counted (see section “Cell counting Neubauer chamber” for further details) and centrifuged 8 min 1600 rpm 4°C. The cell pellet was resuspended into the needed volume and concentration for adoptive cell single or co-transfer.

Enrichment (for cell sorting)

Single cell suspensions from pooled spleen and lymph nodes were counted (see section “Cell counting Neubauer chamber” for further details), resuspended in 1 ml of sterile Easy Sep buffer and transferred into FACS tubes. By adapting the Mojo Sort Mouse CD8 T cell isolation Kit’s (BioLegend, 480008) protocol, 10 µl of Normal Rat Serum were added to the suspension per $1x10^7$ cells and 5 µl of CD4, CD19 and NK1.1 biotinylated antibodies (1:200 dilution each) were added to the suspension. After a 15 min incubation on ice, the streptavidin beads were vortexed for 30 seconds, and 10 µl were added per $1x10^7$ cells were added to the cell suspension. After a 15 min incubation on ice, the volume of the suspension was completed to 2.5 ml using sterile Easy Sep buffer. The FACS tubes were placed on the magnetic holder and incubated for 5 min at room temperature. The supernatant was collected in a 15 ml Falcon tube containing 7.5 ml of cold sterile FACS buffer, the cells were counted counted (see section “Cell counting Neubauer chamber” for further details) and centrifuged 8 min 1600 rpm. The cell pellet was resuspended in the antibody mix for cell sorting (see sections “Extracellular staining for cell sorting” and “Cell sorting” for further details).

Cell counting Neubauer chamber

10 µl of the cell suspension were diluted in 90 µl of 1:10 pre-diluted Trypan Blue to create a 1:10 dilution. Afterwards, 10 µl of the 1:10 cell dilution were diluted in 90 µl of 1:10 pre-diluted Trypan Blue to create a 1:100 dilution. 10 µl of the 1:10 and 1:100 cell dilutions were loaded into the Neubauer chamber. The four quadrants were counted and the average value was calculated. The cell numbers were determined following the manufacturer’s instructions.

Adoptive T cell transfers

Primary adoptive cell transfer

P14 cells were isolated from inguinal, brachial, axillary, cervical and mesenteric lymph nodes and spleen of WT P14 tdTomato (B6.Cg-Tcra^{tm1Mom} Tg(TcrLCMV)327Sdz/TacMmjax x B6.tg (tdTomato) or B6.Cg-Tcra^{tm1Mom} Tg(TcrLCMV)327Sdz/TacMmjax x B6.SJL-Ptprca Pepcb/BoyJ) or Smpdl3b KO P14 Venus (B6N;B6N-Smpdl3btm1a(EUCOMM)Wtsi/H Smpdl3b$^{-/-}$ x B6.Cg-Tcratm1Mom Tg(TcrLCMV)327Sdz x B6.tg (Venus)) mice using the Mojo Sort Mouse CD8 T cell isolation Kit (BioLegend, 480008) and following the manufacturer's instructions. The concentration of the WT and Smpdl3b KO cell suspensions were adjusted to 10x10^4 cells/ml in PBS. A total of 100µl containing 10x10^3 WT or Smpdl3b KO cells were injected intravenously (tail vein) to each mouse using a U-50 Omnican syringe.

Primary adoptive cell co-transfer

P14 cells were isolated from inguinal, brachial, axillary, cervical and mesenteric lymph nodes and spleen of WT P14 tdTomato (B6.Cg-Tcra^{tm1Mom} Tg(TcrLCMV)327Sdz/TacMmjax x B6.tg (tdTomato) or B6.Cg-Tcra^{tm1Mom} Tg(TcrLCMV)327Sdz/TacMmjax x B6.SJL-Ptprca Pepcb/BoyJ) or Smpdl3b KO P14 Venus (B6N;B6N-Smpdl3btm1a(EUCOMM)Wtsi/H Smpdl3b$^{-/-}$ x B6.Cg-Tcra^{tm1Mom} Tg(TcrLCMV)327Sdz x B6.tg (Venus)) mice using the Mojo Sort Mouse CD8 T cell isolation Kit (BioLegend, 480008) and following the manufacturer's instructions. The concentration of the WT and Smpdl3b KO cell suspensions were adjusted in order to have 1x10^6 cells/ml in PBS. Subsequently, the WT and Smpdl3b KO cells were mixed in a 1:1 ratio to have 5x10^4 cells/ml per genotype. The 1:1 ratio was verified by aliquoting 10-20 µl of the mix and measuring in a flow cytometer. A total of 100 µl containing 10x10^3 cells (5x10^3 WT and 5x10^3 Smpdl3b KO) were injected intravenously (tail vein) to each mouse using a U-50 Omnican syringe.

Secondary adoptive cell co-transfer

CD8$^+$ T cells were enriched from inguinal, brachial, axillary, cervical and mesenteric lymph nodes, and spleen of C57BL/6J mice that previously received primary adoptive cell co-transfer and LCMV Armstrong infection for 30-36 days. All WT and Smpdl3b KO P14 cells were sorted (see sections "Extracellular staining for cell sorting" and "Cell sorting" for further details) and counted. The same number of WT cells was added to the Smpdl3b KO cell suspension in order to have a 1:1 ratio in the needed volume to inject 100 µl per mouse. The 1:1 ratio was verified by aliquoting 10-20 µl of the mix and measuring in a flow cytometer. In this setting, all sorted Smpdl3b KO cells and the equivalent number of WT cells were transferred. Finally, 100 µl the whole mix was transferred intravenously into secondary non-infected C57BL/6J recipient mice.

Virus preparation

Lymphocytic choriomeningitis virus (LCMV) Armstrong strain or Vaccinia virus (VV) G2 were stored at -80 °C in PCR Tubes strip of 8 or cryo-conservation tubes, respectively. For usage, the virus stocks were diluted in sterile PBS to have an infectious dose of 2x10^6 plaque forming units (PFU) per ml of LCMV Armstrong or 1x10^7 PFU per ml of VVG2.

Infections

Primary infection

Each mouse was infected intraperitoneally with 100 µl of $2x10^6$ PFU/ml LCMV Armstrong ($2x10^5$ PFU per mouse) 16-20 hours following adoptive cell transfer for 6, 7, 8, 13, 22, 30, 32 or 36 days, or 100 µl of $1x10^7$ PFU/ml VVG2 ($1x10^6$ PFU per mouse) 16-20 hours following adoptive cell transfer for 6 days.

Secondary infection

Mice previously infected with LCMV Armstrong for 30-36 days were infected intraperitoneally with 100µl of $1x10^7$ PFU/ml VVG2 ($1x10^6$ PFU per mouse) for 6 days.

In vitro stimulation for cytokine production

Peptide stimulation: GP33 titration curve

Lymphocytes were isolated from the spleen as described above and adjusted to a concentration of $2x10^7$ cells/ml in T cell media. 100 µl of the cell suspensions were plated in a F-bottom 96-well plate and stimulated with increasing concentrations of 100 µl LCMV GP33 33-41 (H2-D(b)) peptide (0.001, 0.002, 0.005, 0.01, 0.02, 0.05, 0.1, 0.2, 0.5, 1, 5 µg/ml) and 1 mg/ml Brefeldin A (BFA) for 4 hours at 37°C 5% CO_2. Control conditions were no stimulated cells (T cell media only) and cells without peptide and only 1 mg/ml BFA. After the 4 hours incubation, cells were further processed for surface and intracellular staining for flow cytometry.

Cytokine stimulation: IL-18 and IL-12 titration curve

Lymphocytes were isolated from the spleen as described above and adjusted to a concentration of $2x10^7$ cells/ml in T cell media. 100 µl of the cell suspensions were plated in a flat bottom 96-well plate and stimulated with a) 100 µl murine IL-18 peptide (0, 0.0032, 0.016, 0.08, 0.4, 2, 10 ng/ml) with 10ng/mL murine IL-12 with or without 1 mg/ml Brefeldin A (BFA) for 4 hours at 37°C 5% CO_2, or b) 100 µl murine IL-12 peptide (0, 0.0032, 0.016, 0.08, 0.4, 2, 10 ng/ml) with 10ng/mL murine IL-18 with or without 1 mg/ml Brefeldin A (BFA) for 4 hours at 37°C 5% CO_2. Control conditions were no stimulated cells (T cell media only) and cells without peptide and only 1 mg/ml BFA. After the 4 hours incubation, cells were further processed for surface and intracellular staining for flow cytometry.

Antibody staining for flow cytometry and cell sorting

Surface staining for flow cytometry

For staining surface markers for flow cytometry analysis, cells were transferred into a 96-well V-bottom plate and centrifuged for 3 min 1600 rpm 4°C. The pellets were resuspended in 40-50 µl staining solution (surface antibody mix and Human Normal Immunoglobulin (Fc block; 1:66 dilution) diluted in FACS buffer) and incubated on ice or in the fridge (4°C) for 30 min in the dark. Afterwards, 150 µl of FACS buffer were added to the wells and the plates were centrifuged for 3 min 1600 rpm 4°C. Finally, the pellets were a) resuspended in 200 µl FACS buffer, transferred into adequate tubes by filtering through nylon gauze, washed with additional 200 µl FACS buffer and analyzed using Attune or Cytek flow cytometers, or b) furthered processed for intracellular staining (see below).

Intracellular staining for flow cytometry

For intracellular marker staining, once the last centrifugation step of the surface marker staining protocol was done, the cells were resuspended in 40-50 µl of IC Fixation Buffer to be fixed and incubated on ice or in the fridge (4°C) for 30 min in the dark. 150 µl Permeabilization Buffer were added to the wells and the cells were centrifuged for 3 min 1600 rpm 4°C. The pellets were resuspended in 40-50 µl staining solution (intracellular antibody mix diluted in Permeabilization Buffer) and incubated on ice or in the fridge (4°C) for 30 min in the dark. To wash, 150 µl of Permeabilization Buffer were added to the wells and the plates were centrifuged for 3 min 1600 rpm 4°C. Finally, the pellets were resuspended in 200 µl FACS buffer and transferred into adequate tubes by filtering through nylon gauze. The wells were washed with additional 200 µl FACS buffer, also filtered, and the samples were analyzed using Attune or Cytek flow cytometers.

Extracellular staining for cell sorting

For staining for cell sorting, enriched cells were transferred into 1.5 ml Eppendorf tubes and centrifuged for 4 min 2000 rpm 4°C. The pellets were resuspended in 200 µl staining solution (surface antibody mix diluted and Human Normal Immunoglobulin (Fc block; 1:66 dilution) diluted in FACS buffer) and incubated on ice or in the fridge (4°C) for 30 min in the dark. Afterwards, 500 µl of FACS buffer were added to the wells and the tubes were centrifuged for 4 min 1600 rpm 4°C. Finally, the pellets were resuspended in the needed volume of FACS buffer and filtered into 15 ml Falcon tubes using the nylon gauze. The tubes were washed with additional FACS buffer, also filtered.

For the scRNA-seq experiment TruStain FcX (1:1000 dilution) was used instead of Fc block. See the “Single cell RNA sequencing (scRNA-seq)” for further details about the experimental set up.

Cell sorting

Lymph node and spleen $CD8^+$ T cells were enriched and stained as described above. Afterwards, the populations of interest were sorted using a FACS Aria II cell sorter and a 100 µm filter. The cells were sorted into 1.5 ml or 2 ml Eppendorf tubes containing 200-300 µl of FACS buffer. The cells were then counted and further processed for a) HPLC-MS/MS, b) phosphodiesterase activity, or c) scRNA-sequencing assays. Importantly, for the scRNA-seq experiment the tubes into which the cells were sorted were 1.5 ml Eppendorf tubes coated overnight 4°C with 0.1% BSA diluted in PBS (to avoid that the cells attach to the tube). See the “Single cell RNA sequencing (scRNA-seq)” for further details about the experimental set up.

Intracellular sphingolipid quantification by HPLC-MS/MS

WT and Smpdl3b KO naïve, T_{eff}, TEM and TCM $CD8^+$ T cells were enriched and sorted as described above. After sorting, the cells were counted, centrifuged 4 min 2000 rpm 4°C and resuspended in 500 µl of methanol. The sphingolipid extraction was performed as previously described[125]. Briefly, 1.5 ml methanol/chloroform (2:1, v:v) was added to the samples containing 500 µl of methanol and were incubated overnight at 48°C 120 rpm. Internal standards (pmol in 10 µl injection volume) were part of the extraction solvent: 0.25 pmol d_7-sphingosine (d_7-Sph), 0.125 pmol d_7-dihydrosphingosine (d_7-dhSph), 0.125 pmol d_7-sphingosine 1-phosphate (d_7-S1P), 2.5 pmol C17:0 ceramide (C17:0 Cer), 2.5 pmol d_{31}-C16:0 sphingomyelin (d_{31}-C16:0 SM), 0.25 pmol C17:0 glucosylceramide and 0.25 pmol C17:0 lactosylceramide (all Avanti Polar Lipids, Alabaster, USA). After addition of 150 µl KOH (1 M in MeOH) and incubation for 2 h at 37°C 120 rpm, the lipid extract was neutralized with 12 µl glacial acetic acid. After centrifugation (2.200 G, 5 min, 4°C), the organic phase was transferred to new extraction vessels and evaporated to dryness under vacuum. The following HPLC-MS/MS analysis was carried out under already published conditions[126]. The lipid extract was

chromatographically separated using a 1290 Infinity II HPLC (Agilent Technologies, Waldbronn, Germany) equipped with a Poroshell 120 EC-C8 column (3.0 × 150 mm, 2.7 µm; Agilent Technologies). Analysis in MS/MS mode was performed using a 6495C triple-quadrupole mass spectrometer (Agilent Technologies) in positive electrospray ionization mode (ESI+). The analyzed SL species, their mass transitions as well as their retention times are listed in Table 12. While Sph and S1P were quantified directly in relation to their deuterated internal standards, an external calibration had to be performed for dhCer, Cer, dhSM, SM, lactosyl-Cer and hexosyl-Cer. Integration and quantification were determined using MassHunter Quantitative Analysis Software (version 10.1, Agilent Technologies).

Table 12. HPLC-MS/MS parameters

Compound	Precursor ion (*m/z*)	Product ion (*m/z*) [a]	Retention time (min)	Calibration Reference Compound	Internal Standards
d_7-Sph	307.3	**289.3 (8)** / 259.3 (20)	5.5		
d_7-S1P	387.3	**271.3 (20)** / 82.1 (36)	6.8		
Sph	300.3	**282.3 (8)** / 252.3 (16)	5.5		d_7-Sph
S1P	380.3	**264.3 (20)** / 82.1 (32)	6.8		d_7-S1P
C16:0 dhCer	540.5	**522.6 (20)** / 284.3 (28)	14.2		C17:0 Cer
C18:0 dhCer	568.5	**550.5 (20)** / 284.3 (28)	16.3		C17:0 Cer
C20:0 dhCer	596.6	**578.6 (22)** / 284.3 (32)	18.9		C17:0 Cer
C22:0 dhCer	624.6	**606.6 (22)** / 284.3 (32)	22.1		C17:0 Cer
C24:0 dhCer	652.7	**634.6 (24)** / 284.3 (36)	25.7		C17:0 Cer
C24:1 dhCer	650.7	**632.7 (24)** / 284.3 (36)	22.6		C17:0 Cer
C17:0 Cer	534.5	**264.3 (24)** / 282.3 (28)	14.6		
C16:0 Cer	520.5	**264.3 (24)** / 282.3 (24)	13.7		C17:0 Cer
C18:0 Cer	548.5	**264.2 (24)** / 282.3 (28)	15.6		C17:0 Cer
C20:0 Cer	576.6	**264.3 (32)** / 282.3 (28)	18.0		C17:0 Cer
C22:0 Cer	604.6	**264.3 (34)** / 282.3 (30)	21.0		C17:0 Cer
C24:0 Cer	632.6	**264.3 (36)** / 282.3 (28)	24.5		C17:0 Cer
C24:1 Cer	630.6	**264.3 (36)** / 282.3 (32)	21.2		C17:0 Cer
C16:0 dhSM	705.6	**184.0 (8)** / 86.1 (76)	13.5	C16:0 SM	d_{31}-C16:0 SM
C18:0 dhSM	733.6	**184.0 (28)** / 86.1 (76)	15.6	C18:0 SM	d_{31}-C16:0 SM
C20:0 dhSM	761.6	**184.0 (28)** / 86.1 (78)	18.0	C20:0 SM	d_{31}-C16:0 SM
C22:0 dhSM	789.7	**184.0 (28)** / 86.1 (78)	20.9	C22:0 SM	d_{31}-C16:0 SM
C24:0 dhSM	817.7	**184.0 (28)** / 86.1 (80)	24.5	C24:0 SM	d_{31}-C16:0 SM
C24:1 dhSM	815.7	184.0 (8) / **86.1 (80)**	20.9	C24:1 SM	d_{31}-C16:0 SM
d_{31}-C16:0 SM	734.6	**184.0 (28)** / 86.1 (76)	12.7		
C16:0 SM	703.6	**184.0 (8)** / 86.1 (76)	12.8		d_{31}-C16:0 SM
C18:0 SM	731.6	**184.0 (28)** / 86.1 (76)	14.7		d_{31}-C16:0 SM
C20:0 SM	759.6	**184.0 (28)** / 86.1 (78)	17.0		d_{31}-C16:0 SM
C22:0 SM	787.7	**184.0 (28)** / 86.1 (78)	19.4		d_{31}-C16:0 SM
C24:0 SM	815.7	**184.0 (28)** / 86.1 (80)	22.7		d_{31}-C16:0 SM
C24:1 SM	813.7	184.0 (8) / **86.1 (80)**	19.5		d_{31}-C16:0 SM
C17:0 Glucosyl-Cer	714.6	**264.2 (44)** / 696.6 (12)	13.2		
C16:0 Hexosyl-Cer	700.6	**264.2 (40)** / 682.6 (12)	12.5		C17:0 Glucosyl-Cer
C24:1 Hexosyl-Cer	810.7	**264.2 (40)** / 792.7 (16)	18.8		C17:0 Glucosyl-Cer
C17:0 Lactosyl-Cer	876.6	**264.3 (52)** / 534.5 (24)	12.6		
C16:0 Lactosyl-Cer	862.6	**264.3 (48)** / 520.5 (20)	12.1		C17:0 Lactosyl-Cer
C24:1 Lactosyl-Cer	972.7	**264.3 (56)** / 630.7 (28)	17.8		C17:0 Lactosyl-Cer

Quantifiers are given in bold. Collision energies (in eV) are shown in parentheses.

Phosphodiesterase activity assay

A F-bottom 96-well plate was precoated with 50 ul / well of a 0.1 mg/ml Poly-L-Lysin solution 16-24h before use and kept at 4°C. The Poly-L-Lysin was then recovered to be reused. $CD8^+$ T cells were enriched from inguinal, axillary, brachial, and mesenteric lymph nodes, and spleen of B6N;B6N-Smpdl3btm1a(EUCOMM)Wtsi/H Smpdl3b$^{+/+}$ x B6.tg (Venus) or B6N;B6N-Smpdl3btm1a(EUCOMM)Wtsi/H Smpdl3b$^{-/-}$ x B6.tg (Venus), stained, and sorted as described above. The cells were counted after sort, and the concentration was adjusted to $2x10^6$ cells / ml using T cell media. 200 µl containing $4x10^5$ cells per WT or Smpdl3b KO population (naïve (Zombie NIR^- $CD8^+$ $CD44^-$), effector (Zombie NIR^- $CD8^+$ $CD44^+$ $KLRG1^+$), TCM (Zombie NIR^- $CD8^+$ $CD44^+$ $CD127^+$ $CX3CR1^-$)) and TEM (Zombie NIR^- $CD8^+$ $CD44^+$ $CD127^-$ $CX3CR1^+$)) were plated. Cells were incubated for 4 h at 37°C 5% CO_2, in order for them to adhere to the bottom of the well. The media was removed and 100 µl of 1 mM bis-pNPP in 1X TBS was added to each well. The cells were incubated for 2 h at 37°C 5% CO_2. Afterwards, 80 µl of the supernatant were transferred to a F-bottom 96-well plate and 20 µl of 2M NaOH were added to each well to increase the intensity of the yellow color. Additionally, a serial dilution of pNP diluted in 1X TBS ($4.88x10^{-4}$ mM, $9.77x10^{-4}$ mM, $1.95x10^{-3}$ mM, $3.90x10^{-3}$ mM, $7.80x10^{-3}$ mM, $1.56x10^{-2}$ mM, $3.125x10^{-2}$ mM, $6.25x10^{-2}$ mM, 0.125 mM, 0.25 mM, 0.5 mM, 1mM) was prepared to make a standard curve. 80 µl of each concentration were added to the flat bottom plate plus additional 20 µl of 2M NaOH. The absorbance was measured at 405 nm in a microplate reader (FlexStation 3 Multi-Mode Microplate Reader; temperature 20-25°C, no shaking, no compound transfer). As controls, $1x10^4$ of WT, murine Smpdl3b overexpressing or murine Smpdl3b H135A overexpressing HEK293T cells were plated in non-coated wells and incubated for 3.5 h for them to adhere to the bottom of the wells. H135A refers to a point mutation in the enzyme's active site that renders Smpdl3b inactive[16].

Single cell RNA sequencing (scRNA-seq)

The single-cell RNA-sequencing was performed with the help of the Helmholtz Institute for RNA-based Infection Research in Würzburg, the Core Unit Systems Medicine of the University of Würzburg and the Helmholtz Centre for Infection Research in Braunschweig.

To cover the distinct phases of the $CD8^+$ T cell immune response (acute, contraction and memory), we co-transferred the WT and KO cells in a 1:1 ratio into C57BL/6J WT recipient mice, and acutely infected them for 7 (acute phase), 13 (contraction phase) or 22 (memory phase) days, as described above. The spleen and lymph nodes (inguinal, brachial, axillary, cervical and mesenteric) of these mice were harvested, and the $CD8^+$ T cells were enriched and sorted as described above ((WT: $tdTomato^+$ $CD45.1^+$ $Venus^-$; KO: $tdTomato^-$ $CD45.1^-$ $Venus^+$).

Hashtagging and CITE-seq antibodies for scRNA-seq

Cells derived from mice infected for 7, 13 or 22 days were treated as three distinct samples. Each sample was stained separately (see section "Extracellular staining for cell sorting") separately with 200 µl of the same antibody mix, including the **C**ellular **I**ndexing of **T**ranscriptomes and **E**pitopes (CITE-seq) antibodies CD45.1 (1:500 dilution) and CD45.2 (1:125 dilution) to discriminate between WT and Smpdl3b KO cells, respectively. CITE-seq antibodies are conjugated to a unique oligonucleotide that will be sequenced and correlate the transcriptional and protein expression of a certain protein. Next, we hashtagged each sample using independent TotalSeq™-A antibodies (1:200 dilution; BioLegend). Each of these hashtag antibodies are monoclonal antibodies targeting CD45 and MHC-I, conjugated with a unique oligonucleotide. Therefore, each sample hashtagged with a distinct hashtag antibody can be identified during the analysis. Following the staining, the three samples were filtered into a 15 ml Falcon tube through a nylon gauze. $10x10^3$ cells were sorted per genotype (WT or Smpdl3b KO) per timepoint (days 7, 13, 22) into the 0.1% BSA coated 1.5 ml Eppendorf tube.

Dropseq

The single cells were encapsulated into droplets with the ChromiumTM Controller and processed following manufacturer's specifications. Transcripts captured in all the cells encapsulated with a bead were uniquely barcoded using a combination of a 16 bp 10x Barcode and a 10 bp unique molecular identifier (UMI). To generate complementary desoxyribonucleic acid (cDNA) libraries the Chromium™ Single Cell 3' Library & Gel Bead Kit was used following the detailed protocol provided by the manufacturer. Libraries were quantified by QubitTM 3.0 Fluometer and quality was checked using 2100 Bioanalyzer with High Sensitivity DNA kit. Libraries were sequenced in 50 base pair paired-end mode with the NovaSeq 6000 platform. The sequencing data was demultiplexed using CellRanger software (version 2.0.2). The reads were aligned to mouse mm10 reference genome using STAR aligner. Aligned reads were used to quantify the expression level of mouse genes and generation of gene-barcode

scRNA-seq analysis

scRNA-seq analysis workflow

Quality control was performed, and viable cells were selected by excluding cells with UMI counts lower than 1000 and above 5000, as well as cells having more than 5% of mitochondrial transcripts. A total of 451 transcripts were excluded. 2000 most variable genes were used for downstream analysis to calculate principal components, after log-normalization and scaling. Principle component analysis (PCA) was used for dimensionality reduction and to visualize a uniform manifold approximation and projection (UMAP) of the identified clusters.

Sample demultiplexing and doublet identification

To demultiplex hashing tags for each cell HTODemux function in Seurat package was used with standard parameters. Cross-sample doublet cell or "empty" (no bound hashtag) detection was performed based on hashtag signal. Cells that were classified as "singlet" and identified by hashtags were retained and used for downstream analysis (Stuart, T., *et al.* 2019[124])

Sample identity based on CITE-seq antibodies and fluorescent protein expression

Samples were classified as WT or Smpdl3b KO based on the CITE-seq antibodies CD45.1 and CD45.2, and on the expression tdTomato and Venus proteins. WT cells were defined as CD45.1 and tdTomato single or double positive, CD45.2 and Venus double negative. Smpdl3b KO cells were identified as CD45.2 and Venus single or double positive, CD45.1 and tdTomato double negative. Cells that were negative for all the aforementioned markers were excluded for downstream analysis.

Creating stable polyclonal Smpdl3b-overexpressing HEK293T cell lines

Preparing the cells

5-7 days before the transfection, HEK293T cells were maintained in cell culture media. 3 days before the transfection, the cells were split and $1x10^6$ cells were plated in a T75 cell culture flask and cultured at 37°C 5% CO_2 until 70% confluence was reached (around 3 days after splitting the cells).

Digesting the plasmids

The plasmids pMSCV gw mSmpdl3b and pMSCV gw mSmpdl3b H135A were linearized by digesting them with 5 units of the enzyme ScaI-HF (New England Biolabs) and following the manufacturer's instructions. The plasmids and digestion mix were incubated at 37°C for 1 h, and then 65°C for 20 min to inactivate the restriction enzyme. To test whether the digestion worked, a small volume of the digested and non-digested plasmids was loaded to a 0.8% agarose gel with 1:20 dilution of HD Green Plus (Intas) and ran for 1 h 120V. The samples were stained with 6X Purple Loading dye (Thermo Fischer Scientific) in order to be visible in the gel and GeneRuler DNA Ladder Mix (Thermo Fischer Scientific) was used to determine the size of each band.

Transfection

At least 30 min before transfection, cells were supplemented with fresh cell culture media. The transfection media was prepared by mixing in one tube (tube 1) 5 µg of the pMSCV gw mSmpdl3b plasmid or pMSCV gw mSmpdl3b H135A plasmid, and up to 250 µl of DMEM media per flask, and on a second tube (tube 2) 15 µl of GenJet DNA Transfection reagent and 235 µl of DMEM media per flask. Afterwards, tube 2 was mixed into tube 1 (total volume 500 µl per flask) and briefly vortexed. The transfection mix was incubated at room temperature for 10 min and added in a drop-wise fashion over the HEK293T cells. Cells were incubated 37°C 5% CO_2 for 48 h. Then, the media was removed and exchanged with 10 ml of fresh cell culture media. 24 h later, the media was removed and 10 ml of selection media were added to the flasks. The exchange of media to fresh selection media was repeated daily for 7 days. Afterwards, when the flasks reached 80% confluence, the cells were frozen as polyclonal cell lines using 500 µl freezing media and 500 µl cell culture media. The tubes were kept in the Mr. Frosty cryo-container for 24 h in a -80°C freezer, and later moved to a -150°C freezer. Cell aliquots were saved for flow cytometry and phosphoactivity assay analysis.

Statistical analysis

Data, with the exception of scRNA-seq data, were analyzed using GraphPad Prism 10. Paired and non-paired Student t-test (two-tailed) were used to determine statistical significance between two groups (WT and Smpdl3b KO), one-way Anova was used for more than three groups (naïve, effector, central and effector memory), and multiple T tests or two-way Anova were used to determine statistical significance between two groups (WT and Smpdl3b KO) when comparing different timepoints or concentrations. Stars indicate significances (* $p < 0.05$; ** $p < 0.01$; *** $p < 0.001$; **** $p < 0.0001$) and ns indicates "no significance". Error bars indicate the standard error of the mean (SEM).

References

1 Joffre, O. P., Segura, E., Savina, A. & Amigorena, S. Cross-presentation by dendritic cells. *Nat Rev Immunol* **12**, 557-569 (2012). https://doi.org:10.1038/nri3254

2 Kaech, S. M. & Cui, W. Transcriptional control of effector and memory CD8+ T cell differentiation. *Nat Rev Immunol* **12**, 749-761 (2012). https://doi.org:10.1038/nri3307

3 Kaech, S. M. *et al.* Selective expression of the interleukin 7 receptor identifies effector CD8 T cells that give rise to long-lived memory cells. *Nat Immunol* **4**, 1191-1198 (2003). https://doi.org:10.1038/ni1009

4 Gerlach, C. *et al.* The Chemokine Receptor CX3CR1 Defines Three Antigen-Experienced CD8 T Cell Subsets with Distinct Roles in Immune Surveillance and Homeostasis. *Immunity* **45**, 1270-1284 (2016). https://doi.org:10.1016/j.immuni.2016.10.018

5 Opferman, J. T., Ober, B. T. & Ashton-Rickardt, P. G. Linear differentiation of cytotoxic effectors into memory T lymphocytes. *Science* **283**, 1745-1748 (1999). https://doi.org:10.1126/science.283.5408.1745

6 Chang, J. T. *et al.* Asymmetric T lymphocyte division in the initiation of adaptive immune responses. *Science* **315**, 1687-1691 (2007). https://doi.org:10.1126/science.1139393

7 Lanzavecchia, A. & Sallusto, F. Progressive differentiation and selection of the fittest in the immune response. *Nat Rev Immunol* **2**, 982-987 (2002). https://doi.org:10.1038/nri959

8 Michalek, R. D. & Rathmell, J. C. The metabolic life and times of a T-cell. *Immunol Rev* **236**, 190-202 (2010). https://doi.org:10.1111/j.1600-065X.2010.00911.x

9 MacIver, N. J., Michalek, R. D. & Rathmell, J. C. Metabolic regulation of T lymphocytes. *Annu Rev Immunol* **31**, 259-283 (2013). https://doi.org:10.1146/annurev-immunol-032712-095956

10 Kersh, E. N. *et al.* TCR signal transduction in antigen-specific memory CD8 T cells. *J Immunol* **170**, 5455-5463 (2003). https://doi.org:10.4049/jimmunol.170.11.5455

11 Edwards-Hicks, J. *et al.* Phosphoinositide acyl chain saturation drives CD8(+) effector T cell signaling and function. *Nat Immunol* **24**, 516-530 (2023). https://doi.org:10.1038/s41590-023-01419-y

12 Slotte, J. P. Biological functions of sphingomyelins. *Prog Lipid Res* **52**, 424-437 (2013). https://doi.org:10.1016/j.plipres.2013.05.001

13 Milhas, D., Clarke, C. J. & Hannun, Y. A. Sphingomyelin metabolism at the plasma membrane: implications for bioactive sphingolipids. *FEBS Lett* **584**, 1887-1894 (2010). https://doi.org:10.1016/j.febslet.2009.10.058

14 Miceli, M. C. *et al.* Co-stimulation and counter-stimulation: lipid raft clustering controls TCR signaling and functional outcomes. *Semin Immunol* **13**, 115-128 (2001). https://doi.org:10.1006/smim.2000.0303

15 Masuishi, Y. *et al.* Mass spectrometric identification of glycosylphosphatidylinositol-anchored peptides. *J Proteome Res* **12**, 4617-4626 (2013). https://doi.org:10.1021/pr4004807

16 Heinz, L. X. *et al.* The Lipid-Modifying Enzyme SMPDL3B Negatively Regulates Innate Immunity. *Cell Rep* **11**, 1919-1928 (2015). https://doi.org:10.1016/j.celrep.2015.05.006

17 Gorelik, A., Heinz, L. X., Illes, K., Superti-Furga, G. & Nagar, B. Crystal Structure of the Acid Sphingomyelinase-like Phosphodiesterase SMPDL3B Provides Insights into Determinants of Substrate Specificity. *J Biol Chem* **291**, 24054-24064 (2016). https://doi.org:10.1074/jbc.M116.755801

18 Watanabe, S. *et al.* Sphingomyelin Phosphodiesterase Acid-Like 3b is Essential for Toll-Like Receptor 3 Signaling in Human Podocytes. *J Membr Biol* **255**, 117-122 (2022). https://doi.org:10.1007/s00232-021-00206-w

19 Harder, T. The T Cell Plasma Membrane Lipid Bilayer Stages TCR-proximal Signaling Events. *Front Immunol* **3**, 50 (2012). https://doi.org:10.3389/fimmu.2012.00050

20 Zech, T. *et al.* Accumulation of raft lipids in T-cell plasma membrane domains engaged in TCR signalling. *EMBO J* **28**, 466-476 (2009). https://doi.org:10.1038/emboj.2009.6

21 Dinic, J., Riehl, A., Adler, J. & Parmryd, I. The T cell receptor resides in ordered plasma membrane nanodomains that aggregate upon patching of the receptor. *Sci Rep* **5**, 10082 (2015). https://doi.org:10.1038/srep10082

22 Al-Aghbar, M. A., Jainarayanan, A. K., Dustin, M. L. & Roffler, S. R. The interplay between membrane topology and mechanical forces in regulating T cell receptor activity. *Commun Biol* **5**, 40 (2022). https://doi.org:10.1038/s42003-021-02995-1

23 Urbancic, I. *et al.* Aggregation and mobility of membrane proteins interplay with local lipid order in the plasma membrane of T cells. *FEBS Lett* **595**, 2127-2146 (2021). https://doi.org:10.1002/1873-3468.14153

24 Robinson, G. A., Waddington, K. E., Pineda-Torra, I. & Jury, E. C. Transcriptional Regulation of T-Cell Lipid Metabolism: Implications for Plasma Membrane Lipid Rafts and T-Cell Function. *Front Immunol* **8**, 1636 (2017). https://doi.org:10.3389/fimmu.2017.01636
25 Farrell, M. V., Webster, S., Gaus, K. & Goyette, J. T Cell Membrane Heterogeneity Aids Antigen Recognition and T Cell Activation. *Front Cell Dev Biol* **8**, 609 (2020). https://doi.org:10.3389/fcell.2020.00609
26 Manes, S. & Viola, A. Lipid rafts in lymphocyte activation and migration. *Mol Membr Biol* **23**, 59-69 (2006). https://doi.org:10.1080/09687860500430069
27 Schieffer, D., Naware, S., Bakun, W. & Bamezai, A. K. Lipid raft-based membrane order is important for antigen-specific clonal expansion of CD4(+) T lymphocytes. *BMC Immunol* **15**, 58 (2014). https://doi.org:10.1186/s12865-014-0058-8
28 Yang, W. *et al.* Potentiating the antitumour response of CD8(+) T cells by modulating cholesterol metabolism. *Nature* **531**, 651-655 (2016). https://doi.org:10.1038/nature17412
29 Tonnetti, L., Verí, M.-C., Bonvini, E. & D'Adamio, L. A Role for Neutral Sphingomyelinase-mediated Ceramide Production in T Cell Receptor–induced Apoptosis and Mitogen-activated Protein Kinase–mediated Signal Transduction. *The Journal of Experimental Medicine* **189**, 1581-1589 (1999). https://doi.org:10.1084/jem.189.10.1581
30 Breslow, D. K. & Weissman, J. S. Membranes in balance: mechanisms of sphingolipid homeostasis. *Mol Cell* **40**, 267-279 (2010). https://doi.org:10.1016/j.molcel.2010.10.005
31 Gault, C. R., Obeid, L. M. & Hannun, Y. A. An overview of sphingolipid metabolism: from synthesis to breakdown. *Adv Exp Med Biol* **688**, 1-23 (2010). https://doi.org:10.1007/978-1-4419-6741-1_1
32 Hollmann, C. *et al.* Translational Approaches Targeting Ceramide Generation From Sphingomyelin in T Cells to Modulate Immunity in Humans. *Front Immunol* **10**, 2363 (2019). https://doi.org:10.3389/fimmu.2019.02363
33 Tischner, D. *et al.* Acid sphingomyelinase is required for protection of effector memory T cells against glucocorticoid-induced cell death. *J Immunol* **187**, 4509-4516 (2011). https://doi.org:10.4049/jimmunol.1100911
34 Hose, M. *et al.* T Cell-Specific Overexpression of Acid Sphingomyelinase Results in Elevated T Cell Activation and Reduced Parasitemia During Plasmodium yoelii Infection. *Front Immunol* **10**, 1225 (2019). https://doi.org:10.3389/fimmu.2019.01225
35 Wiese, T. *et al.* Inhibition of acid sphingomyelinase increases regulatory T cells in humans. *Brain Commun* **3**, fcab020 (2021). https://doi.org:10.1093/braincomms/fcab020
36 Bai, A., Kokkotou, E., Zheng, Y. & Robson, S. C. Role of acid sphingomyelinase bioactivity in human CD4+ T-cell activation and immune responses. *Cell Death Dis* **6**, e1828 (2015). https://doi.org:10.1038/cddis.2015.178
37 Hose, M. *et al.* Cell-intrinsic ceramides determine T cell function during melanoma progression. *Elife* **11** (2022). https://doi.org:10.7554/eLife.83073
38 Hartel, J. C., Merz, N. & Grosch, S. How sphingolipids affect T cells in the resolution of inflammation. *Front Pharmacol* **13**, 1002915 (2022). https://doi.org:10.3389/fphar.2022.1002915
39 Avota, E., de Lira, M. N. & Schneider-Schaulies, S. Sphingomyelin Breakdown in T Cells: Role of Membrane Compartmentalization in T Cell Signaling and Interference by a Pathogen. *Front Cell Dev Biol* **7**, 152 (2019). https://doi.org:10.3389/fcell.2019.00152
40 Lee, M., Lee, S. Y. & Bae, Y. S. Functional roles of sphingolipids in immunity and their implication in disease. *Exp Mol Med* **55**, 1110-1130 (2023). https://doi.org:10.1038/s12276-023-01018-9
41 Lim, S. A., Su, W., Chapman, N. M. & Chi, H. Lipid metabolism in T cell signaling and function. *Nat Chem Biol* **18**, 470-481 (2022). https://doi.org:10.1038/s41589-022-01017-3
42 Hollmann, C. *et al.* Inhibition of Acid Sphingomyelinase Allows for Selective Targeting of CD4+ Conventional versus Foxp3+ Regulatory T Cells. *J Immunol* **197**, 3130-3141 (2016). https://doi.org:10.4049/jimmunol.1600691
43 Giles, J. R. *et al.* Shared and distinct biological circuits in effector, memory and exhausted CD8(+) T cells revealed by temporal single-cell transcriptomics and epigenetics. *Nat Immunol* **23**, 1600-1613 (2022). https://doi.org:10.1038/s41590-022-01338-4
44 ImmGen, C. Open-source ImmGen: mononuclear phagocytes. *Nat Immunol* **17**, 741 (2016). https://doi.org:10.1038/ni.3478
45 Kurd, N. S. *et al.* Early precursors and molecular determinants of tissue-resident memory CD8(+) T lymphocytes revealed by single-cell RNA sequencing. *Sci Immunol* **5** (2020). https://doi.org:10.1126/sciimmunol.aaz6894
46 Mielke, M. M. *et al.* Plasma Sphingomyelins are Associated with Cognitive Progression in Alzheimer's Disease. *Journal of Alzheimer's Disease* **27**, 259-269 (2011). https://doi.org:10.3233/jad-2011-110405

47 Mitrofanova, A., Drexler, Y., Merscher, S. & Fornoni, A. Role of Sphingolipid Signaling in Glomerular Diseases: Focus on DKD and FSGS. *J Cell Signal* **1**, 56-69 (2020). https://doi.org:10.33696/Signaling.1.013
48 Yoo, T. H. *et al.* Sphingomyelinase-like phosphodiesterase 3b expression levels determine podocyte injury phenotypes in glomerular disease. *J Am Soc Nephrol* **26**, 133-147 (2015). https://doi.org:10.1681/ASN.2013111213
49 Waldbillig, F. *et al.* Phosphodiesterase SMPDL3B Gene Expression as Independent Outcome Prediction Marker in Localized Prostate Cancer. *Int J Mol Sci* **21** (2020). https://doi.org:10.3390/ijms21124373
50 Liu, B., Xiao, J., Dong, M., Qiu, Z. & Jin, J. Human alkaline ceramidase 2 promotes the growth, invasion, and migration of hepatocellular carcinoma cells via sphingomyelin phosphodiesterase acid-like 3B. *Cancer Sci* **111**, 2259-2274 (2020). https://doi.org:10.1111/cas.14453
51 Qu, H. & Zhu, Y. SMPDL3B Predicts Poor Prognosis and Contributes to Development of Acute Myeloid Leukemia. *Front Mol Biosci* **8**, 695601 (2021). https://doi.org:10.3389/fmolb.2021.695601
52 D'Cruz, L. M., Rubinstein, M. P. & Goldrath, A. W. Surviving the crash: transitioning from effector to memory CD8+ T cell. *Semin Immunol* **21**, 92-98 (2009). https://doi.org:10.1016/j.smim.2009.02.002
53 Hughes, P. D. *et al.* Apoptosis regulators Fas and Bim cooperate in shutdown of chronic immune responses and prevention of autoimmunity. *Immunity* **28**, 197-205 (2008). https://doi.org:10.1016/j.immuni.2007.12.017
54 Weant, A. E. *et al.* Apoptosis regulators Bim and Fas function concurrently to control autoimmunity and CD8+ T cell contraction. *Immunity* **28**, 218-230 (2008). https://doi.org:10.1016/j.immuni.2007.12.014
55 Lingwood, D. & Simons, K. Lipid rafts as a membrane-organizing principle. *Science* **327**, 46-50 (2010). https://doi.org:10.1126/science.1174621
56 Zhang, Y., Li, X., Becker, K. A. & Gulbins, E. Ceramide-enriched membrane domains--structure and function. *Biochim Biophys Acta* **1788**, 178-183 (2009). https://doi.org:10.1016/j.bbamem.2008.07.030
57 Turner, S. J., Bennett, T. J. & La Gruta, N. L. CD8(+) T-Cell Memory: The Why, the When, and the How. *Cold Spring Harb Perspect Biol* **13** (2021). https://doi.org:10.1101/cshperspect.a038661
58 Chisolm, D. A. *et al.* Defining Genetic Variation in Widely Used Congenic and Backcrossed Mouse Models Reveals Varied Regulation of Genes Important for Immune Responses. *Immunity* **51**, 155-168 e155 (2019). https://doi.org:10.1016/j.immuni.2019.05.006
59 Nemoto, S., Kubota, T. & Ohno, H. Metabolic differences and differentially expressed genes between C57BL/6J and C57BL/6N mice substrains. *PLoS One* **17**, e0271651 (2022). https://doi.org:10.1371/journal.pone.0271651
60 Opferman, J. T. & Kothari, A. Anti-apoptotic BCL-2 family members in development. *Cell Death Differ* **25**, 37-45 (2018). https://doi.org:10.1038/cdd.2017.170
61 Metzler, M. *et al.* HIP1 Functions in Clathrin-mediated Endocytosis through Binding to Clathrin and Adaptor Protein 2. *Journal of Biological Chemistry* **276**, 39271-39276 (2001). https://doi.org:10.1074/jbc.c100401200
62 Waelter, S. *et al.* The huntingtin interacting protein HIP1 is a clathrin and alpha-adaptin-binding protein involved in receptor-mediated endocytosis. *Hum Mol Genet* **10**, 1807-1817 (2001). https://doi.org:10.1093/hmg/10.17.1807
63 Gottfried, I., Ehrlich, M. & Ashery, U. The Sla2p/HIP1/HIP1R family: similar structure, similar function in endocytosis? *Biochem Soc Trans* **38**, 187-191 (2010). https://doi.org:10.1042/BST0380187
64 Wanker, E. E. Hip1 and Hippi participate in a novel cell death-signaling pathway. *Dev Cell* **2**, 126-128 (2002). https://doi.org:10.1016/s1534-5807(02)00121-1
65 Bhattacharyya, N. P., Banerjee, M. & Majumder, P. Huntington's disease: roles of huntingtin-interacting protein 1 (HIP-1) and its molecular partner HIPPI in the regulation of apoptosis and transcription. *FEBS J* **275**, 4271-4279 (2008). https://doi.org:10.1111/j.1742-4658.2008.06563.x
66 Choi, S. A., Kim, S. J. & Chung, K. C. Huntingtin-interacting protein 1-mediated neuronal cell death occurs through intrinsic apoptotic pathways and mitochondrial alterations. *FEBS Lett* **580**, 5275-5282 (2006). https://doi.org:10.1016/j.febslet.2006.08.076
67 Hackam, A. S. *et al.* Huntingtin interacting protein 1 induces apoptosis via a novel caspase-dependent death effector domain. *J Biol Chem* **275**, 41299-41308 (2000). https://doi.org:10.1074/jbc.M008408200
68 Herz, J. *et al.* Acid sphingomyelinase is a key regulator of cytotoxic granule secretion by primary T lymphocytes. *Nat Immunol* **10**, 761-768 (2009). https://doi.org:10.1038/ni.1757

69 Grassme, H., Cremesti, A., Kolesnick, R. & Gulbins, E. Ceramide-mediated clustering is required for CD95-DISC formation. *Oncogene* **22**, 5457-5470 (2003). https://doi.org:10.1038/sj.onc.1206540
70 Gwag, T. *et al.* Macrophage-derived thrombospondin 1 promotes obesity-associated non-alcoholic fatty liver disease. *JHEP Rep* **3**, 100193 (2021). https://doi.org:10.1016/j.jhepr.2020.100193
71 Kaya, M. *et al.* The Importance of Sphingomyelin Phosphodiesterase Acid-Like 3b (SMPDL-3b) Levels in Kidney Biopsy Specimens of Children With Nephrotic Syndrome. *Fetal Pediatr Pathol* **42**, 936-949 (2023). https://doi.org:10.1080/15513815.2023.2267683
72 Mitrofanova, A. *et al.* SMPDL3b modulates insulin receptor signaling in diabetic kidney disease. *Nat Commun* **10**, 2692 (2019). https://doi.org:10.1038/s41467-019-10584-4
73 Francis, M. *et al.* SMPDL3b modulates radiation-induced DNA damage response in renal podocytes. *FASEB J* **36**, e22545 (2022). https://doi.org:10.1096/fj.202100186RR
74 Mallela, S. K., Mitrofanova, A., Merscher, S. & Fornoni, A. Regulation of the amount of ceramide-1-phosphate synthesized in differentiated human podocytes. *Biochim Biophys Acta Mol Cell Biol Lipids* **1864**, 158517 (2019). https://doi.org:10.1016/j.bbalip.2019.158517
75 Merscher, S. & Fornoni, A. Podocyte pathology and nephropathy - sphingolipids in glomerular diseases. *Front Endocrinol (Lausanne)* **5**, 127 (2014). https://doi.org:10.3389/fendo.2014.00127
76 Fornoni, A. *et al.* Rituximab targets podocytes in recurrent focal segmental glomerulosclerosis. *Sci Transl Med* **3**, 85ra46 (2011). https://doi.org:10.1126/scitranslmed.3002231
77 Azzam, P. *et al.* Crosstalk Between SMPDL3b and NADPH Oxidases Mediates Radiation-Induced Damage of Renal Podocytes. *Front Med (Lausanne)* **8**, 732528 (2021). https://doi.org:10.3389/fmed.2021.732528
78 Ahmad, A. *et al.* Sphingomyelinase-like phosphodiesterase 3b mediates radiation-induced damage of renal podocytes. *FASEB J* **31**, 771-780 (2017). https://doi.org:10.1096/fj.201600618R
79 Abou Daher, A. *et al.* Modulation of radiation-induced damage of human glomerular endothelial cells by SMPDL3B. *FASEB J* **34**, 7915-7926 (2020). https://doi.org:10.1096/fj.201902179R
80 Mallela, S. K. *et al.* Sphingomyelin phosphodiesterase acid like 3B (SMPDL3b) regulates Perilipin5 (PLIN5) expression and mediates lipid droplet formation. *Genes Dis* **9**, 1397-1400 (2022). https://doi.org:10.1016/j.gendis.2021.12.014
81 Shen, H. H. *et al.* Porcine reproductive and respiratory syndrome virus upregulates SMPDL3B to promote viral replication by modulating lipid metabolism. *iScience* **26**, 107450 (2023). https://doi.org:10.1016/j.isci.2023.107450
82 Fan, W. *et al.* SIRT1 regulates sphingolipid metabolism and neural differentiation of mouse embryonic stem cells through c-Myc-SMPDL3B. *Elife* **10** (2021). https://doi.org:10.7554/eLife.67452
83 Wherry, E. J. *et al.* Lineage relationship and protective immunity of memory CD8 T cell subsets. *Nat Immunol* **4**, 225-234 (2003). https://doi.org:10.1038/ni889
84 Hou, Y. *et al.* SMPDL3A is a cGAMP-degrading enzyme induced by LXR-mediated lipid metabolism to restrict cGAS-STING DNA sensing. *Immunity* **56**, 2492-2507 e2410 (2023). https://doi.org:10.1016/j.immuni.2023.10.001
85 Lim, S. M., Yeung, K., Trésaugues, L., Ling, T. H. & Nordlund, P. The structure and catalytic mechanism of human sphingomyelin phosphodiesterase like 3a – an acid sphingomyelinase homologue with a novel nucleotide hydrolase activity. *The FEBS Journal* **283**, 1107-1123 (2016). https://doi.org:10.1111/febs.13655
86 Gorelik, A., Illes, K., Superti-Furga, G. & Nagar, B. Structural Basis for Nucleotide Hydrolysis by the Acid Sphingomyelinase-like Phosphodiesterase SMPDL3A. *Journal of Biological Chemistry* **291**, 6376-6385 (2016). https://doi.org:10.1074/jbc.m115.711085
87 Traini, M. *et al.* Sphingomyelin Phosphodiesterase Acid-like 3A (SMPDL3A) Is a Novel Nucleotide Phosphodiesterase Regulated by Cholesterol in Human Macrophages. *Journal of Biological Chemistry* **289**, 32895-32913 (2014). https://doi.org:10.1074/jbc.m114.612341
88 Noto, P. B. *et al.* Regulation of Sphingomyelin Phosphodiesterase Acid-Like 3A Gene (SMPDL3A) by Liver X Receptors. *Molecular Pharmacology* **82**, 719-727 (2012). https://doi.org:10.1124/mol.112.078865
89 Carozza, J. A. *et al.* Extracellular cGAMP is a cancer cell-produced immunotransmitter involved in radiation-induced anti-cancer immunity. *Nat Cancer* **1**, 184-196 (2020). https://doi.org:10.1038/s43018-020-0028-4
90 Li, J. *et al.* Metastasis and Immune Evasion from Extracellular cGAMP Hydrolysis. *Cancer Discovery* **11**, 1212-1227 (2021). https://doi.org:10.1158/2159-8290.cd-20-0387

91 Carozza, J. A. *et al.* ENPP1's regulation of extracellular cGAMP is a ubiquitous mechanism of attenuating STING signaling. *Proceedings of the National Academy of Sciences* **119** (2022). https://doi.org:10.1073/pnas.2119189119
92 Li, L. *et al.* Hydrolysis of 2′3′-cGAMP by ENPP1 and design of nonhydrolyzable analogs. *Nature Chemical Biology* **10**, 1043-1048 (2014). https://doi.org:10.1038/nchembio.1661
93 Zhou, Y. *et al.* Blockade of the Phagocytic Receptor MerTK on Tumor-Associated Macrophages Enhances P2X7R-Dependent STING Activation by Tumor-Derived cGAMP. *Immunity* **52**, 357-373.e359 (2020). https://doi.org:10.1016/j.immuni.2020.01.014
94 Cordova, A. F., Ritchie, C., Bohnert, V. & Li, L. Human SLC46A2 Is the Dominant cGAMP Importer in Extracellular cGAMP-Sensing Macrophages and Monocytes. *ACS Cent Sci* **7**, 1073-1088 (2021). https://doi.org:10.1021/acscentsci.1c00440
95 Marcus, A. *et al.* Tumor-Derived cGAMP Triggers a STING-Mediated Interferon Response in Non-tumor Cells to Activate the NK Cell Response. *Immunity* **49**, 754-763.e754 (2018). https://doi.org:10.1016/j.immuni.2018.09.016
96 Schadt, L. *et al.* Cancer-Cell-Intrinsic cGAS Expression Mediates Tumor Immunogenicity. *Cell Reports* **29**, 1236-1248.e1237 (2019). https://doi.org:10.1016/j.celrep.2019.09.065
97 Carozza, J. A. *et al.* Structure-Aided Development of Small-Molecule Inhibitors of ENPP1, the Extracellular Phosphodiesterase of the Immunotransmitter cGAMP. *Cell Chemical Biology* **27**, 1347-1358.e1345 (2020). https://doi.org:10.1016/j.chembiol.2020.07.007
98 Liu, H. *et al.* cGAS facilitates sensing of extracellular cyclic dinucleotides to activate innate immunity. *EMBO Rep* **20** (2019). https://doi.org:10.15252/embr.201846293
99 Chekeni, F. B. *et al.* Pannexin 1 channels mediate 'find-me' signal release and membrane permeability during apoptosis. *Nature* **467**, 863-867 (2010). https://doi.org:10.1038/nature09413
100 Elliott, M. R. *et al.* Nucleotides released by apoptotic cells act as a find-me signal to promote phagocytic clearance. *Nature* **461**, 282-286 (2009). https://doi.org:10.1038/nature08296
101 Yamaguchi, H., Maruyama, T., Urade, Y. & Nagata, S. Immunosuppression via adenosine receptor activation by adenosine monophosphate released from apoptotic cells. *Elife* **3**, e02172 (2014). https://doi.org:10.7554/eLife.02172
102 Gao, P. *et al.* Structure-Function Analysis of STING Activation by c[G(2′,5′)pA(3′,5′)p] and Targeting by Antiviral DMXAA. *Cell* **154**, 748-762 (2013). https://doi.org:10.1016/j.cell.2013.07.023
103 Corrales, L. *et al.* Direct Activation of STING in the Tumor Microenvironment Leads to Potent and Systemic Tumor Regression and Immunity. *Cell Reports* **11**, 1018-1030 (2015). https://doi.org:10.1016/j.celrep.2015.04.031
104 Ritchie, C., Cordova, A. F., Hess, G. T., Bassik, M. C. & Li, L. SLC19A1 Is an Importer of the Immunotransmitter cGAMP. *Molecular Cell* **75**, 372-381.e375 (2019). https://doi.org:10.1016/j.molcel.2019.05.006
105 Ablasser, A. *et al.* Cell intrinsic immunity spreads to bystander cells via the intercellular transfer of cGAMP. *Nature* **503**, 530-534 (2013). https://doi.org:10.1038/nature12640
106 Zhou, C. *et al.* Transfer of cGAMP into Bystander Cells via LRRC8 Volume-Regulated Anion Channels Augments STING-Mediated Interferon Responses and Anti-viral Immunity. *Immunity* **52**, 767-781.e766 (2020). https://doi.org:10.1016/j.immuni.2020.03.016
107 Luteijn, R. D. *et al.* SLC19A1 transports immunoreactive cyclic dinucleotides. *Nature* **573**, 434-438 (2019). https://doi.org:10.1038/s41586-019-1553-0
108 Charpentier, J. C. & King, P. D. Mechanisms and functions of endocytosis in T cells. *Cell Communication and Signaling* **19** (2021). https://doi.org:10.1186/s12964-021-00766-3
109 Evnouchidou, I., Caillens, V., Koumantou, D. & Saveanu, L. The role of endocytic trafficking in antigen T cell receptor activation. *Biomed J* **45**, 310-320 (2022). https://doi.org:10.1016/j.bj.2021.09.004
110 Faller, E. M., Ghazawi, F. M., Cavar, M. & Macpherson, P. A. IL-7 induces clathrin-mediated endocytosis of CD127 and subsequent degradation by the proteasome in primary human CD8 T cells. *Immunology & Cell Biology* **94**, 196-207 (2016). https://doi.org:10.1038/icb.2015.80
111 Larkin, B. *et al.* Cutting Edge: Activation of STING in T Cells Induces Type I IFN Responses and Cell Death. *The Journal of Immunology* **199**, 397-402 (2017). https://doi.org:10.4049/jimmunol.1601999
112 Quaney, M. J. *et al.* STING controls T cell memory fitness during infection through T cell-intrinsic and IDO-dependent mechanisms. *Proceedings of the National Academy of Sciences* **120** (2023). https://doi.org:10.1073/pnas.2205049120
113 Surh, C. D. & Sprent, J. Homeostasis of Naive and Memory T Cells. *Immunity* **29**, 848-862 (2008). https://doi.org:10.1016/j.immuni.2008.11.002

114 Nolz, J. C. & Richer, M. J. Control of memory CD8+ T cell longevity and effector functions by IL-15. *Molecular Immunology* **117**, 180-188 (2020). https://doi.org:10.1016/j.molimm.2019.11.011
115 Henriques, C. M., Rino, J., Nibbs, R. J., Graham, G. J. & Barata, J. T. IL-7 induces rapid clathrin-mediated internalization and JAK3-dependent degradation of IL-7Rα in T cells. *Blood* **115**, 3269-3277 (2010). https://doi.org:10.1182/blood-2009-10-246876
116 Dubois, S., Mariner, J., Waldmann, T. A. & Tagaya, Y. IL-15Rα Recycles and Presents IL-15 In trans to Neighboring Cells. *Immunity* **17**, 537-547 (2002). https://doi.org:10.1016/s1074-7613(02)00429-6
117 Waldmann, T. A., Miljkovic, M. D. & Conlon, K. C. Interleukin-15 (dys)regulation of lymphoid homeostasis: Implications for therapy of autoimmunity and cancer. *Journal of Experimental Medicine* **217** (2020). https://doi.org:10.1084/jem.20191062
118 Desbois, M. *et al.* IL-15 Trans-Signaling with the Superagonist RLI Promotes Effector/Memory CD8+ T Cell Responses and Enhances Antitumor Activity of PD-1 Antagonists. *The Journal of Immunology* **197**, 168-178 (2016). https://doi.org:10.4049/jimmunol.1600019
119 Sorkin, A. & Von Zastrow, M. Endocytosis and signalling: intertwining molecular networks. *Nature Reviews Molecular Cell Biology* **10**, 609-622 (2009). https://doi.org:10.1038/nrm2748
120 Perosa, F., Favoino, E., Caragnano, M. A. & Dammacco, F. Generation of biologically active linear and cyclic peptides has revealed a unique fine specificity of rituximab and its possible cross-reactivity with acid sphingomyelinase-like phosphodiesterase 3b precursor. *Blood* **107**, 1070-1077 (2006). https://doi.org:10.1182/blood-2005-04-1769
121 Wu, H. *et al.* Mitochondrial dysfunction promotes the transition of precursor to terminally exhausted T cells through HIF-1α-mediated glycolytic reprogramming. *Nature Communications* **14** (2023). https://doi.org:10.1038/s41467-023-42634-3
122 Kastenmüller, W. *et al.* Peripheral Prepositioning and Local CXCL9 Chemokine-Mediated Guidance Orchestrate Rapid Memory CD8+ T Cell Responses in the Lymph Node. *Immunity* **38**, 502-513 (2013). https://doi.org:10.1016/j.immuni.2012.11.012
123 Swanson, P. A. *et al.* CD8+ T Cells Induce Fatal Brainstem Pathology during Cerebral Malaria via Luminal Antigen-Specific Engagement of Brain Vasculature. *PLOS Pathogens* **12**, e1006022 (2016). https://doi.org:10.1371/journal.ppat.1006022
124 Stuart, T. *et al.* Comprehensive Integration of Single-Cell Data. *Cell* **177**, 1888-1902.e1821 (2019). https://doi.org:10.1016/j.cell.2019.05.031
125 Gulbins, A. *et al.* Antidepressants act by inducing autophagy controlled by sphingomyelin–ceramide. *Molecular Psychiatry* **23**, 2324-2346 (2018). https://doi.org:10.1038/s41380-018-0090-9
126 Naser, E. *et al.* Characterization of the small molecule ARC39, a direct and specific inhibitor of acid sphingomyelinase in vitro. *Journal of Lipid Research* **61**, 896-910 (2020). https://doi.org:10.1194/jlr.ra120000682

Statement of individual author contributions and of legal second publication rights to manuscript "The role of Smpdl3b in CD8⁺ T cells" included in the dissertation

Manuscript 1 (complete reference): Cruz de Casas, P., Wigger, D., Schumacher, F., Imdahl, F., Saliba, A. E., Heinz, L., Kleuser, B., Kastenmüller, W.; The role of Smpdl3b in CD8⁺ T cells (in preparation)					
Participated in	**Author Initials,** Responsibility decreasing from left to right				
Study Design Methods Development	WK, PCC	FS, DW, BB	LH		
Data Collection	PCC	DW, FS	FI, AES		
Data Analysis and Interpretation	PCC	FS, DW			
Manuscript Writing Writing of Introduction Writing of Materials & Methods Writing of Discussion Writing of First Draft	PCC, WK PCC, WK PCC, WK PCC, WK PCC, WK	DW			

Explanations (if applicable):

- PCC is the first author and WK is the primary supervisor.

The doctoral researcher and the primary supervisor confirm the correctness of the above mentioned assessment.

Paulina Cruz de Casas

Doctoral Researcher's Name	Date	Place	Signature

Prof. Dr. med. Wolfgang Kastenmüller

Primary Supervisor's Name	Date	Place	Signature

Statement of individual author contributions to figures/tables of manuscript "The role of Smpdl3b in CD8⁺ T cells"

Manuscript 1 (complete reference): Cruz de Casas, P., Wigger, D., Schumacher, F., Imdahl, F., Saliba, A. E., Heinz, L., Kleuser, B., Kastenmüller, W.; The role of Smpdl3b in CD8⁺ T cells (in preparation)					
Figure	**Author Initials,** Responsibility decreasing from left to right				
1	PCC	WK			
2	PCC	WK			
3	PCC	WK			
4	PCC	WK			
5	PCC	WK			

Explanations (if applicable):

- All Figures for the manuscript "The role of Smpdl3b in CD8⁺ T cells" were done by PCC and supervised by WK.
- The manuscript is still in preparation

The doctoral researcher and the primary supervisor confirm the correctness of the above mentioned assessment.

Paulina Cruz de Casas

Doctoral Researcher's Name	Date	Place	Signature

Prof. Dr. med. Wolfgang Kastenmüller

Primary Supervisor's Name	Date	Place	Signature

Chapter II

“Lymphatic migration of unconventional T cells promotes site-specific immunity in distinct lymph nodes”[183]

Immunity

Lymphatic migration of unconventional T cells promotes site-specific immunity in distinct lymph nodes

Graphical abstract

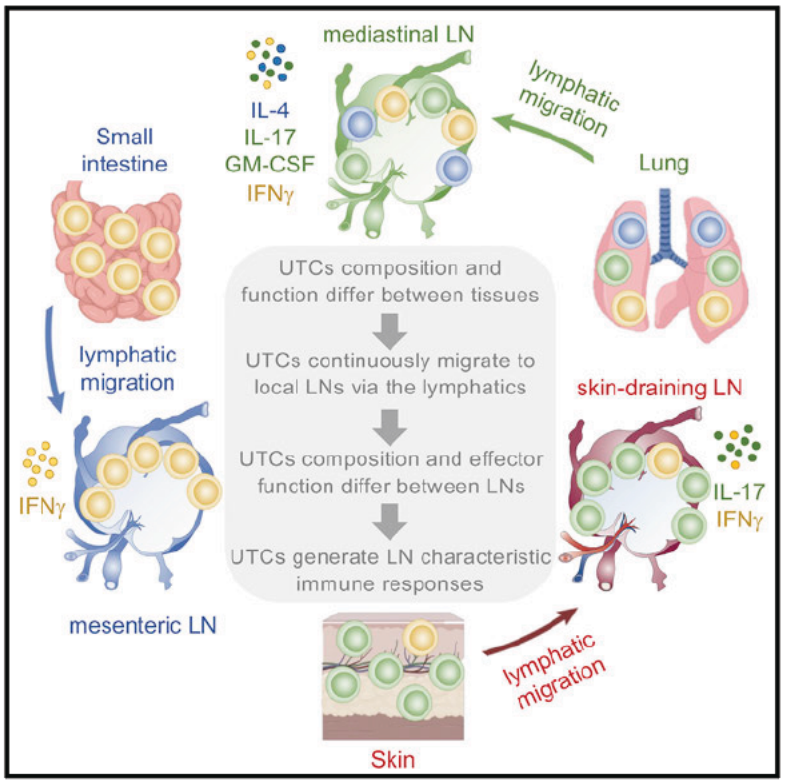

Highlights

- Lymph nodes contain non-circulating, tissue-derived UTCs that immigrate via lymphatics
- Heterogeneity of tissue-derived UTCs imprints immune responses in lymph nodes
- UTCs form functional units across TCR-based lineages
- UTCs within functional units share location, function, and homeostatic niche

Authors

Marco A. Ataide, Konrad Knöpper, Paulina Cruz de Casas, ..., Antoine-Emmanuel Saliba, Georg Gasteiger, Wolfgang Kastenmüller

Correspondence

ataideimmuno@gmail.com (M.A.A.), wolfgang.kastenmueller@uni-wuerzburg.de (W.K.)

In brief

Lymphatic vessels are immunological highways that connect lymph nodes to peripheral tissues. Ataide et al. found that tissue-derived UTCs also continuously migrate via this route. This migration pattern leads to characteristic innate and adaptive immune responses that differ between lymph nodes, mirrors the drained tissue, and is based on the immediate effector function of UTCs.

Ataide et al., 2022, Immunity 55, 1813–1828
October 11, 2022
https://doi.org/10.1016/j.immuni.2022.07.019

Immunity

CellPress

Article

Lymphatic migration of unconventional T cells promotes site-specific immunity in distinct lymph nodes

Marco A. Ataide,[1,10,*] Konrad Knöpper,[1,10] Paulina Cruz de Casas,[1,10] Milas Ugur,[1] Sarah Eickhoff,[1] Mangge Zou,[2] Haroon Shaikh,[3] Apurwa Trivedi,[4] Anika Grafen,[1] Tao Yang,[5] Immo Prinz,[6] Knut Ohlsen,[7] Mercedes Gomez de Agüero,[1] Andreas Beilhack,[3] Jochen Huehn,[2,8] Mauro Gaya,[4] Antoine-Emmanuel Saliba,[9] Georg Gasteiger,[1] and Wolfgang Kastenmüller[1,11,*]

[1]Würzburg Institute of Systems Immunology, Max Planck Research Group at the Julius-Maximilians-Universität Würzburg, 97078 Würzburg, Germany
[2]Experimental Immunology, Helmholtz Centre for Infection Research, 38124 Braunschweig, Germany
[3]Department of Medicine II and Pediatrics, Würzburg University Hospital, ZEMM, 97078 Würzburg, Germany
[4]Centre d'Immunologie de Marseille-Luminy (CIML), Department of Immunology, 13288 Marseille, France
[5]Institute of Immunology, Hannover Medical School, 30625 Hannover, Germany
[6]Institute of Systems Immunology, University Medical Center Hamburg-Eppendorf, 20251 Hamburg, Germany
[7]Institute for Molecular Infection Biology (IMIB), 97078 Würzburg, Germany
[8]Cluster of Excellence RESIST (EXC 2155), Hannover Medical School, 30625 Hannover, Germany
[9]Helmholtz Institute for RNA-Based Infection Research (HIRI), Helmholtz-Center for Infection Research (HZI), 97078 Würzburg, Germany
[10]These authors contributed equally
[11]Lead contact
*Correspondence: ataideimmuno@gmail.com (M.A.A.), wolfgang.kastenmueller@uni-wuerzburg.de (W.K.)
https://doi.org/10.1016/j.immuni.2022.07.019

SUMMARY

Lymphatic transport of molecules and migration of myeloid cells to lymph nodes (LNs) continuously inform lymphocytes on changes in drained tissues. Here, using LN transplantation, single-cell RNA-seq, spectral flow cytometry, and a transgenic mouse model for photolabeling, we showed that tissue-derived unconventional T cells (UTCs) migrate via the lymphatic route to locally draining LNs. As each tissue harbored a distinct spectrum of UTCs with locally adapted differentiation states and distinct T cell receptor repertoires, every draining LN was thus populated by a distinctive tissue-determined mix of these lymphocytes. By making use of single UTC lineage-deficient mouse models, we found that UTCs functionally cooperated in interconnected units and generated and shaped characteristic innate and adaptive immune responses that differed between LNs that drained distinct tissues. Lymphatic migration of UTCs is, therefore, a key determinant of site-specific immunity initiated in distinct LNs with potential implications for vaccination strategies and immunotherapeutic approaches.

INTRODUCTION

Lymph nodes (LNs) are specialized organs that bring together various cell types, such as dendritic cells, macrophages, natural killer (NK) cells, and B and T lymphocytes, to effectively initiate adaptive immune responses against pathogens (Qi et al., 2014). A key element for the function of LNs is their connection to the lymphatic system allowing them to integrate information from the peripheral tissues that they drain (Roozendaal et al., 2008). In principle, this information in the form of metabolites, cytokines, chemokines, microbial products, or pathogens can passively drain or can be actively transported by migratory dendritic cells via the lymph (Girard et al., 2012; Thomas et al., 2016). Importantly, this information is not only used to initiate and scale an immune response but also to shape its quality, which is adapted to the tissue that is drained by the respective LN. As such, it has been shown that conventional dendritic cells (cDCs) that migrate from distinct tissues optimize the polarization and expression of adhesion molecules in the lymphocytes they interact with. Thereby, they adjust the function of T and B cells and promote their recruitment to the target tissue from which these cDCs emigrated (Campbell and Butcher, 2002; Everson et al., 1996; Johansson-Lindbom et al., 2003; Mora et al., 2005). A specific challenge is the orchestration of immune responses in the LNs, which drain barrier tissues, because the inflammatory responses against pathogens need to be balanced against tolerance toward commensal bacteria and, in the intestine, against food antigens. In the intestine, specific requirements on local tissue immunity are solved by compartmentalizing the lymphatic drainage. Here, the lymph transports the

regional information to LNs that harbor adapted stromal and immigrated dendritic cell populations that in turn depend on the local tissue environment and microbial communities (Cording et al., 2014; Esterházy et al., 2019; Hammerschmidt et al., 2008; Houston et al., 2016; Pezoldt et al., 2018; Worbs et al., 2006). Together these data established the paradigm that dendritic cells not only report the tissue status to lymphocytes in the draining LNs (dLNs) but additionally generate and fine-tune immune responses that are optimized to the tissue that they drain. Whether and how other immune cells have functions in determining the tissue status and transport this information to dLNs to generate site-specific immune responses is currently not known.

Here, we asked whether unconventional T cells (UTCs) could have such a role in linking tissue immunity to lymph node function given their tissue-specific distribution patterns, their capacity to exhibit early innate cytokine production, and their ability to sense cellular stress (Godfrey et al., 2015). These features would, in principle, qualify them as cells that can relay tissue-specific information and translate them into characteristic and tissue-adapted immune responses.

UTCs consist of three major lineages—gamma delta (γδ), MR1-restricted (e.g., mucosal-associated invariant T cells [MAIT]), and CD1d-restricted T cells (e.g., natural killer T cells [NKT]), which all display a T cell receptor (TCR) repertoire of limited diversity. These cells are selected by non-polymorphic antigen-presenting molecules, such as CD1 and MR1, and typically recognize endogenous lipids or microbial metabolites bound to these surface proteins (Legoux et al., 2019; Pellicci et al., 2020). They differentiate into polarized effector cells already in the thymus (Lee et al., 2020) with properties similar to those of specialized CD4 T cell subsets and seed organs in developmental waves (Bendelac et al., 2007; Ribot et al., 2021; Salou et al., 2019). In the tissues, they may be localized within the parenchyma, close to or within the epithelium, or reside within the microvasculature, as in the lungs or the liver (Geissmann et al., 2005; Scanlon et al., 2011; Thomas et al., 2011). UTCs that populate barrier tissues are, based on parabiosis experiments, considered to be tissue-resident lymphocytes (Scanlon et al., 2011). UTC populations that are found in the blood and secondary lymphoid organs recirculate similar to those found in the conventional T cells (Ugur et al., 2018). However, some UTCs in LNs also appear to be tissue resident (Audemard-Verger et al., 2017). Whether the populations present in secondary lymphoid organs and those in tissues are related is incompletely understood (Gray et al., 2012). On a functional level, UTCs interact with the commensal microbiome, maintain tissue homeostasis, and participate in tissue healing and pathogen defense (Ansaldo et al., 2021; Constantinides et al., 2019). To execute these functions, UTCs can be activated in two ways. One mechanism is dual cytokine stimulation, with one mediator being an IL-1 family member (IL-1β, IL-18, and IL-33) and the other signal being a STAT-activating cytokine (e.g., IL-2, IL-4, IL-12, IL-23, and IFNI) (McGinty and von Moltke, 2020). The second activation mode is executed via their specific TCR, and some effector functions may depend on this mode of activation and are not induced by cytokines alone, as demonstrated for the secretion of IL-4 (Brigl et al., 2011). However, only a limited number of exogenous pathogen-associated TCR ligands have been identified (Chien and Konigshofer, 2007; McWilliam and Villadangos, 2017).

When addressing whether UTCs could play a role in linking tissue immunity with LN function, we found that the local composition as well as the cytokine production capacity of UTCs diverged among LNs, which had a substantial impact on the immune responses that were generated. These local differences were a consequence of continuous migration of UTCs via the lymphatic route to locally draining LNs, establishing tissue-specific UTC composition in draining LNs. This migratory behavior was conserved across TCR-based lineages (NKT, MAIT, and γδ T cells) and effector states, suggesting shared, interconnected functions of these cells. Testing their function in further depth, we demonstrated their common cytokine-dependent innate response within shared homeostatic and microanatomical niches, supporting the concept that UTCs form locally diverse yet interconnected populations—functional units. Together, we show that UTCs continuously migrate via the lymphatic route to locally draining LNs where they form functional units that generate characteristic, site-specific immune responses and, thereby, link tissue immunity to lymph node function.

RESULTS

Different LNs generate characteristic UTC-dependent immune responses

To investigate whether lymph nodes (LNs) that drain distinct tissue sites generate characteristic immune responses we globally activated (PMA/ionomycin) single-cell suspensions from different LNs (skin-draining [sd], mediastinal [med], and mesenteric [mes]) and measured the resulting cytokines that were released in the culture supernatant. We focused on signature cytokines IFNγ, IL-4, IL-17 and GM-CSF that represent a polarized immune response against intracellular pathogens (Th1), parasites (Th2), or extracellular bacteria and fungi (Th17). We found that the pattern and number of cytokines that we detected significantly differed between LNs draining different tissues. The highest IL-17 response was detected from cells derived from sdLNs and medLNs (Figure 1A), although these LNs differed in their capacity to produce GM-CSF, another Th17 signature cytokine. IL-4 was particularly prominent in supernatants from medLNs, whereas IFNγ was particularly high in supernatants from sdLNs (Figure 1A). To identify the cellular source of these cytokines, we performed intracellular cytokine staining and flow cytometric analysis. This approach revealed UTCs that included γδ T cells, NKT, and MAIT cells but were globally defined as $CD3^{+}$ $CD4/CD8^{int\text{-}DN}$, as major producers of IL-17, GM-CSF, and IL-4 (Figures 1B and S1A–S1D).

To confirm our results *in vivo*, we performed vaccinia virus (VV) infection because both the lungs and the skin are natural routes of infection for this pathogen. Consistent with our *in vitro* activation data, we observed significantly more IL4-producing cells in the medLN as compared with the sdLN, 3 days after local infection of IL-4 reporter mice (Figure 1C). The main IL-4 producers were NKT cells that were also overall more abundant in medLNs as compared with sdLN (Figures 1D and 1E). Functionally, it has been shown that this rapid CD1d-dependent and, hence, TCR-dependent IL-4 production by NKT cells accelerates and

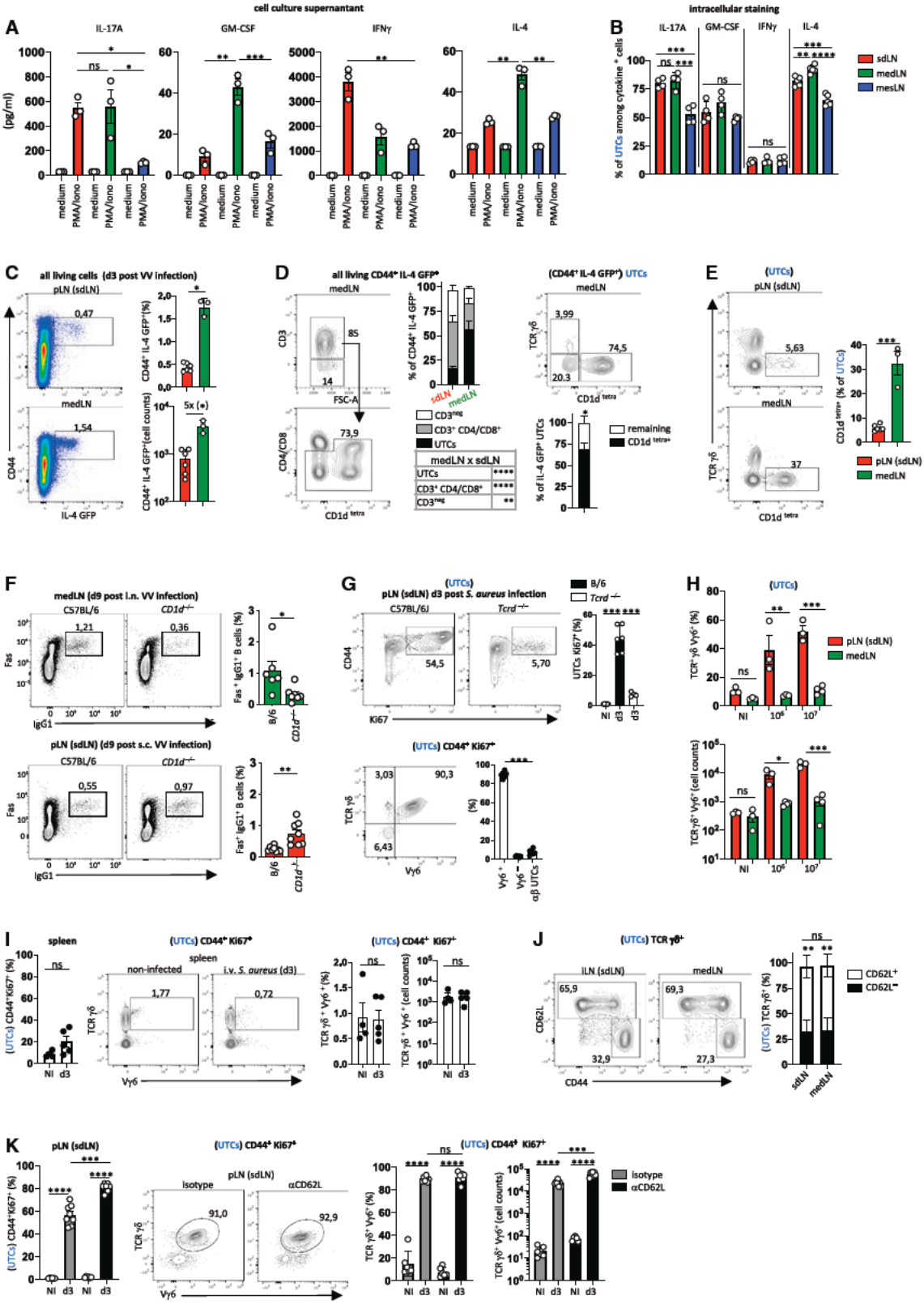

(legend on next page)

enhances germinal center reactions in the medLN during influenza infections of the lungs (Gaya et al., 2018). Thereby, NKT cells are critical for the formation of IgG1 by providing an early source of IL-4 at the T/B cell border. Consistently, we also observed a significant reduction of IgG1-producing germinal center B cells in medLNs after pulmonary VV infection in CD1d-deficient (*Cd1d*$^{-/-}$) mice as compared with wild-type (WT) mice. By contrast, NKT cells were not critical for the generation of IgG1-producing germinal center B cells in the sdLN after VV infection of the skin (Figure 1F). Importantly, activation of CD4 T_{FH} cells was similar in sdLNs of WT and *Cd1d*$^{-/-}$ mice (Figure S1E). Next, we focused on γδ T cells that represent a distinct lineage within UTCs. A subset of γδ T cells specifically responds by clonal TCR-dependent expansion after *S. aureus* infection of the skin (Dillen et al., 2018). After expansion in the sdLN, these γδ T cells migrate to the site of infection where they mediate protection (Marchitto et al., 2019). Similarly, we observed an expansion of γδ T cells in the skin-draining LN 3 days after subcutaneous (s.c.) or topical infection with *S. aureus* (Figures 1G and S1F). These γδ T cells expressed the TCR-chain Vγ6 and showed Ki67 expression indicative of recent proliferation. Importantly, IL23R-, Myd88-, and Trif-mediated signaling was dispensable for this proliferation (Figure S1G), and other UTCs in the same dLN did not show such a vigorous expansion or Ki67 expression, arguing that this response by γδ T cells was TCR dependent (Figure 1G). Next, we tested whether a similar γδ T cell response was generated in the medLN after *S. aureus* of the lungs. The lungs are a clinically relevant site of *S. aureus* infections, and, similar to sdLNs, the medLN harbors a sizable population of IL-17-polarized UTCs (Figure 1A). However, we did not detect an expansion of γδ T cells or other UTCs in the medLN on d3, even using a 10-fold higher infection dose than in the skin and despite a similar abundance of Vγ6$^+$ γδ T cells in the skin and the lungs (Figures 1H, S1H, and S1I). By contrast, we found a similar increase in Ki67$^+$ conventional T cells and similar absolute numbers of RORγt$^+$ expressing non-UTCs in both, skin-draining LN and medLN, on d3 post *S. aureus* infection (Figures S1J and S1K). Also, we detected an IL-17 response by UTCs in the lung 6 h post-intranasal (i.n.) infection with *S. aureus* (Figure S1L) confirming that UTCs do get activated during this early, innate phase of the infection. Next, we asked whether the LN-characteristic response by γδ T cells can be induced in the medLN using repeat or simultaneous infections at different sites. To test this question, we infected mice s.c. or i.n. or simultaneously at both sites with *S. aureus* and rechallenged these mice i.n. 20 days after the primary infection. However, we still failed to detect the expansion γδ T cells in the medLN under this experimental condition (Figure S1M). Similarly, we did not detect an expansion of γδ T cells in the spleen following intravenous (i.v.) infection (Figure 1I). Therefore, we speculated that the divergent UTC-driven immune responses between these secondary lymphoid organs (SLOs) are based on a distinct cellular composition of UTCs among LNs and the spleen. This on the other hand implied that some UTCs are not recirculating between SLOs. Because CD62L is a key adhesion molecule that mediates recirculation via the blood (Girard et al., 2012), we first asked whether both CD62L$^+$ and (non-recirculating) CD62L$^-$ γδ T cells are present in LNs. Indeed, about 30% of γδ T cells in sdLNs and medLNs did not express CD62L (Figure 1J). To determine whether the response was driven by recirculating γδ T cells, we blocked the entry of these cells using anti-CD62L antibody for 5 days. We found that the expansion of Vγ6$^+$ γδ T cells in sdLN on d3 post-infection and continued CD62L blockade remained unaltered (Figures 1K and S1N). This argued that the responding γδ T cells in sdLN are not recirculating via the blood. Consistently, Vγ6$^+$ γδ T cells in sdLN were CD62L$^-$ before infection. Together, our data suggested that LNs draining different tissues harbored a unique composition of local UTCs, which generated characteristic cellular and supported distinct humoral immune responses.

scRNA-seq reveals major differences in UTC composition among lymph nodes

To further investigate this finding, and to gain an unbiased view of the exact composition of these UTCs, we compared LNs

Figure 1. Different LNs generate characteristic UTC-dependent immune responses

(A and B) Leukocytes from skin-draining LN (sdLN), mediastinal LN (medLN), and mesenteric LN (mesLN) were isolated and stimulated with PMA (0.250 mg/mL) plus ionomycin (1 mg/mL) for 4 h. Flow cytometric quantification of cytokine abundance of (A) the supernatant and (B) intracellular staining displayed as a percentage of cytokine-producing UTCs (Figures S1A, S1B, and S1D) among all cytokine-producing lymphocytes.

(C and D) Flow cytometric quantification and statistical analysis of (C) IL-4 produced and (D) (left) IL-4-producing cells in the popliteal LNs (sdLN) and medLN on day 3 (D3) post-subcutaneous (s.c.) or -intranasal (i.n.) infection with 200 PFU vaccinia virus (VV) of IL-4^{GFP} reporter mice. (Right) The relative frequency of UTC lineages among the IL-4$^+$ cells.

(E) Quantification of CD1d^{tetra+} cells in sdLN and medLN in steady state.

(F) Flow cytometric quantification and statistical analysis of germinal center B cells producing IgG1 (GC IgG1$^+$) in the sdLN and medLN at d9 post-s.c. or -i.n. infection, respectively, with 2 × 10^3 PFU VV of C57BL/6J and *Cd1d*$^{-/-}$ mice.

(G) Flow cytometric quantification and statistical analysis of proliferating (Ki67$^+$) UTCs in the sdLN of *Tcrd*$^{-/-}$ and littermate control mice at d3 post-s.c. infection with 10^7 *S. aureus.*

(H) Flow cytometric quantification and statistical analysis of the Vγ6$^+$ γδ T cells in the sdLN and medLN 3 days after s.c. or i.n. infection with 10^6 or 10^7 CFU *S. aureus* of C57BL/6J mice.

(I) Flow cytometric and statistical analysis of the proliferating UTCs in the spleen of C57BL/6J mice 3 days after intravenous (i.v.) infection with 10^7 CFU *S. aureus*.

(J) Flow cytometric quantification and statistical analysis of CD62L expression among γδ T cells from the sdLN and medLN of C57BL/6J mice.

(K) Flow cytometric quantification and statistical analysis of the proliferating UTCs upon intraperitoneal (i.p.) treatment with anti-CD62L (MEL-14) and s.c. infection of C57BL/6J mice with 10^7 *S. aureus* for 3 days. NI, noninfected. Data are showing one representative of two independent experiments (A, n = 3; B, n = 4–5; C, medLN, n = 3; pLN (sdLN), n = 6; D, pLN (sdLN), n = 6; medLN, n = 3; E, pLN, n = 6; medLN, n = 3; F, B/6 pLN (sdLN), n = 8 and medLN, n = 6; *Cd1d*$^{-/-}$ pLN (sdLN), n = 8 and medLN, n = 7; G, B/6, n = 6; *Tcrd*$^{-/-}$, n = 3; H, pLN, n = 3; medLN, n = 4; I, spleen NI, n = 4; d3, n = 5; J, inguinal LN (sdLN), n = 6; medLN n = 3; K, NI, n = 6; d3 n = 8). Error bars indicate the mean ± SEM. Comparison between groups (A, B, D [left], G, H, J, and K) was calculated using the one-way ANOVA test. * $p \leq 0.01$; ** $p \leq 0.001$; *** $p \leq 0.0001$; **** $p < 0.0001$ and (C, D [right], E, F, and I) using the unpaired Mann-Whitney test * $p \leq 0.01$, ** $p \leq 0.001$.

See also Figure S1.

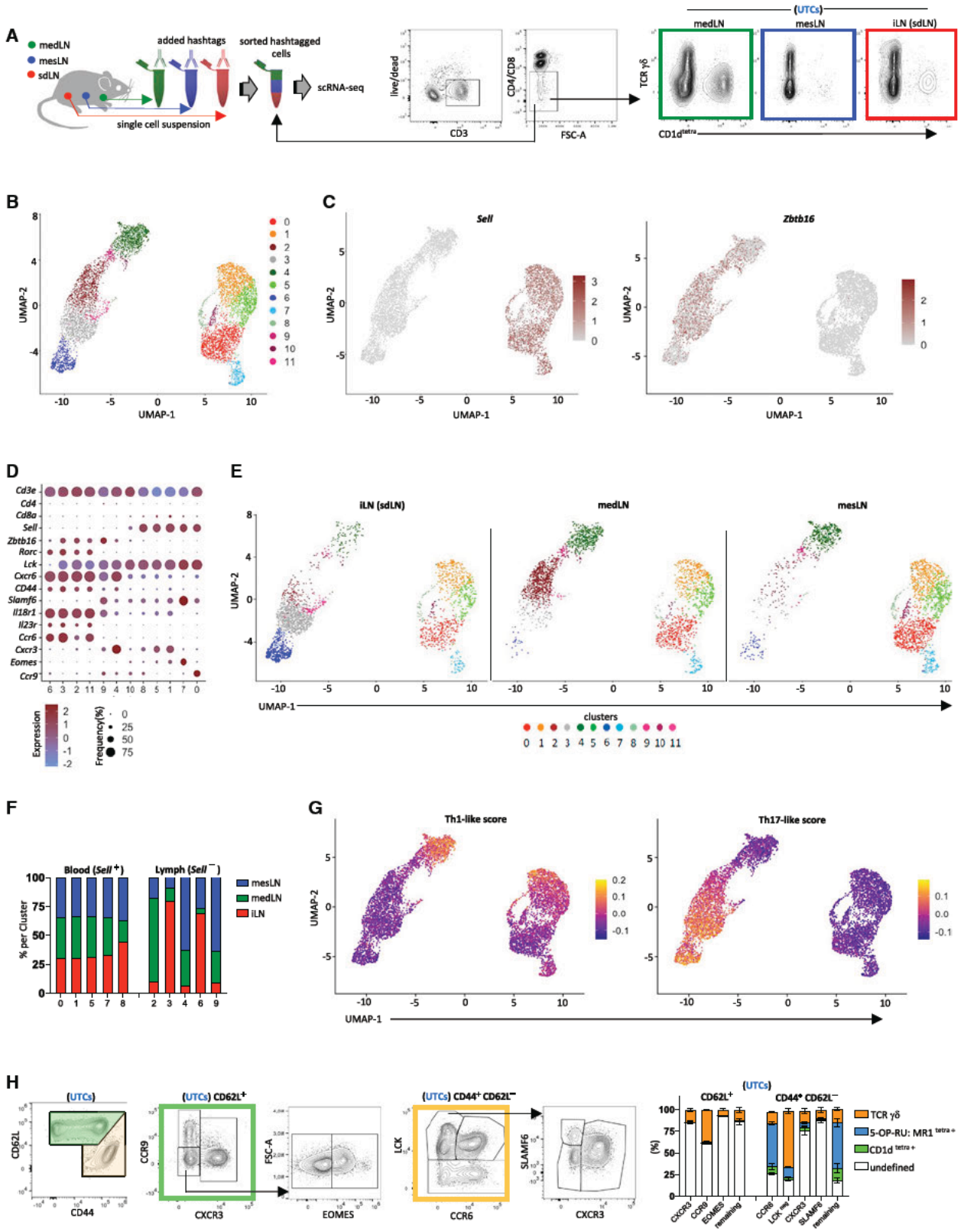

Figure 2. scRNA-seq reveals major differences in UTC composition among lymph nodes

(A) Schematic and sorting strategy for comparative scRNA-seq of UTCs from different LNs (color code applies to A and F).

(B) UMAP displaying 7,041 scRNA-seq transcriptomes clustered in 12 different clusters (color code applies to B, E, and G).

(legend continued on next page)

that drain different tissues using scRNA-seq. Therefore, we tagged and sorted UTCs from sdLNs, medLNs, and mesLNs, draining three major barrier tissues (skin, lungs, and gut), and analyzed these cells via scRNA-seq (Figure 2A). In our sorting strategy, we gated on $CD3^+$, $CD4/CD8^{DN/int}$ T cells, which covered >90% of all major UTC lineages across LNs while avoiding TCR activation upon tetramer binding (Figure 2A). The fraction of $CD4^+/CD8^+$ UTCs, specifically NKT cells, that were excluded by this sorting strategy was overall minimal (Figures S2A and S2B). Supporting the notion that the UTC composition differed between LNs, we noted substantial differences when analyzing the frequency of specific TCR-based lineages (Figure 2A). Unbiased analysis of the transcriptional data set revealed two major clusters of cells that were segregated by the expression of *Zbtb16* (PLZF), an important transcription factor that controls UTC differentiation in the thymus and *Sell* (CD62L) (Figures 2B and 2C) (Pellicci et al., 2020). Thus, irrespective of their differentiation (Th1-like and Th17-like) and lineage affiliation ($\gamma\delta$ T cells, MR1-restricted, or CD1d-restricted T cells), UTCs can be segregated into recirculating versus non-recirculating subsets (Figures 1J, 2C, and S2C; Table S1A). In line with this interpretation, $CD62L^+$ UTCs were equally represented in all LNs, whereas $CD62L^-$ cells showed a characteristic composition and transcriptional landscape that differed between LNs draining different tissues (Figures 2D–2F).

Focusing on UTC effector differentiation, we detected Th1-polarized UTCs among both recirculating and non-recirculating subsets, whereas Th17-polarized cells (Arlehamn et al., 2014) were restricted to $CD62L^-$ cells (Figure 2G). Notably, Th17-polarized UTCs diverged at the detailed transcriptional level between those in the medLN (cluster 2) and sdLN (clusters 3 and 6) (Figures 2D and 2E). In the sdLN, Th17-polarized UTCs further split up into two populations that differed in the expression of *Lck*. In the mesLN, Th17-polarized UTCs were largely absent, consistent with our prior results (Figures 1A, 1B, 2D, and 2E). By contrast, Th1-polarized UTCs (clusters 4 and 9) were prominent in the medLN and mesLN (Figures 2D, 2E, and S2C). Unlike in the thymus, we did not detect a distinct subset of Th2-polarized UTCs based on *Gata3*, *Zbtb16*, and *Il4* expression (Lee et al., 2013). Instead, the capacity to produce IL-4 seemed to be present within Th17- and dominantly in Th1-polarized NKT (Figure S2D). The transcriptional profile of Th1-polarized UTCs largely overlapped between LNs but segregated from the recirculating population (Figures 2D and 2E). In particular, the differential expression of *Id3*, *Id2*, *Eomes*, and *Ccl5* separated Th1-polarized UTCs with distinct expression of *Sell* (Figure S2C). Among the recirculating population, we identified four major populations based on the expression of *Cxcr3*, *Ccr9*, and *Eomes* (Figures 2D and 2E). Most of these cells had an expression pattern consistent with a Th1-polarization, whereas one cluster (cluster 0) seemed largely non-polarized, expressed *Ccr9*, and was negative for *Cd44*. Notably, neither *Il4*- nor *Rorc*-expressing UTCs seemed to be present in the recirculating compartment (Figures 2D, 2E, and S2C).

We next used multiparameter spectral flow cytometry to validate these populations based on the protein expression mean fluorescent intensity (MFI) and combined it with staining for TCR-based lineages. Classical flow cytometry gating readily recapitulated both circulating ($CD62L^+$) and non-recirculating UTCs ($CD62L^-$ and $CD44^+$) and all previously identified subpopulations using scRNA-seq (Figure 2H). Every cluster consisted of multiple TCR-based UTC lineages (Figure 2H). Notably, a significant fraction of non-$\gamma\delta$ T cells could not be assigned to either MAIT or NKT cells due to the lack of tetramer binding but likely represent CD1d and MR1 restricted UTCs (Figure 2H). $CD4^+$ NKT cells that were omitted from our scRNA-seq analysis fully overlapped with all other UTC clusters based on our multiparameter flow cytometry panel (Figure S2E). Together, these results revealed that every lymph node harbors two major groups of UTCs based on their CD62L expression and independent of their classical TCR-based lineage affiliation. Although $CD62L^+$ UTCs are recirculating and equally represented among different LNs, $CD62L^-$ UTCs substantially differed between LNs draining different tissues.

UTCs continuously migrate from tissues to draining lymph nodes

Next, we wished to investigate how the characteristic composition of $CD62L^-$ UTCs is developing among distinct LNs. UTCs differentiate in the thymus and seed tissues as effector cells in developmental waves. This process is currently incompletely understood; yet, it is known that specific TCRs are associated with the homing/retention of UTCs in specific tissues (Parker and Ciofani, 2020; Pellicci et al., 2020). We speculated that UTCs may not be strictly resident but instead continuously seed LNs by migrating from the tissue via the lymph. We have been geared toward this possibility because it has been previously shown that dermal Th-17 polarized $\gamma\delta$ T cells emigrate from the skin to the sdLN via the lymph (Gray et al., 2012; Nakamizo et al., 2015). To test this idea, we first examined if the subset distribution of UTCs in tissues generally mirrors the composition of $CD62L^-$ UTCs in the associated dLNs. We combined the use of CXCR3 reporter mice as a surrogate to detect Th1-like cells with staining for CCR6, a chemokine receptor indicative for Th17-like cells. As anticipated, the composition of UTCs in the tissue (lungs, gut, and skin) was largely mirrored by the respective dLNs (medLN, mesLN, and sdLN) (Figure 3A).

(C) UMAP displaying the mRNA expression of *Sell* (CD62L) and *Zbtb16* (PLZF).
(D) Dot plot of representative marker genes associated with the identified clusters. The color indicates the Z score mean of the expression values across clusters and dot size represents the fraction of cells in the cluster expressing the respective genes.
(E) UMAP plots showing the cluster prevalence in different LNs.
(F) Quantitative analysis showing the cluster prevalence in different LNs of scRNA sequencing data.
(G) UMAP of 7,041 scRNA-seq transcriptomes colored according to Th1-like and Th17-like score.
(H) Flow-cytometry-derived plots showing UTC clusters among $CD62L^+$ (green) and $CD62L^-$ (yellow) UTCs in LNs of C57BL/6J mice. Quantitative analysis showing the TCR lineage prevalence in the different clusters via flow cytometry. Data are showing one experiment from pooled mice (B–G) (n = 10) or one representative of three independent experiments (H) (n = 3). Error bars indicate the mean ± SEM.
See also Figure S2 and Table S1A.

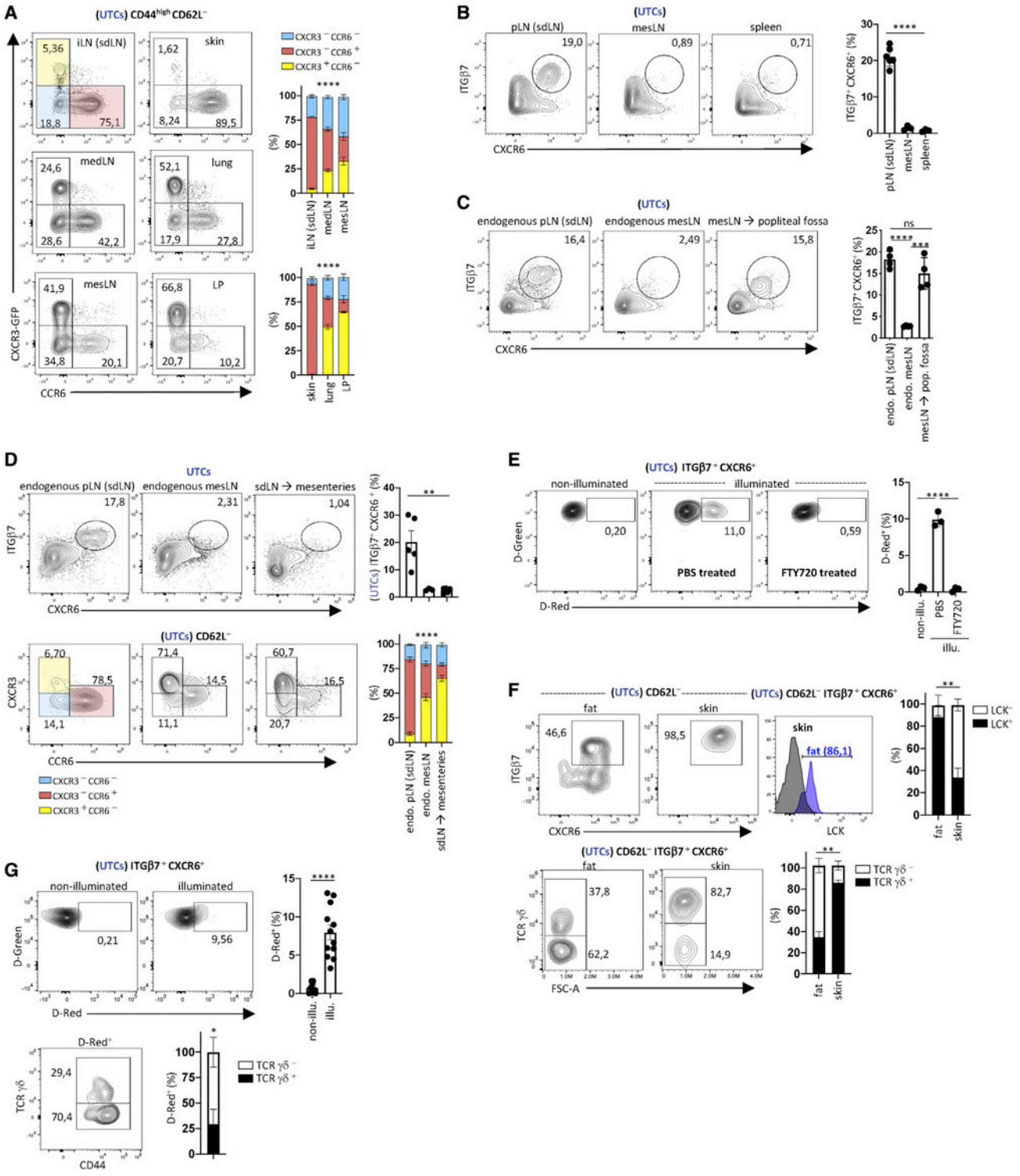

Figure 3. UTCs continuously migrate from tissues to draining lymph nodes

(A) Flow cytometric quantification and statistical analysis of the CD44^{high} CD62L^{-} UTCs from different tissues (skin, lungs, and small intestine [lamina propria, LP]) and their respective draining LNs (inguinal LN, sdLN; mediastinal LN, medLN; and mesenteric LN, mesLN) based on the expression of CXCR3 and CCR6 in CXCR3^{GFP} reporter mice.

(B) Flow cytometric quantification and statistical analysis of the frequency of the ITGβ7^{+} CXCR6^{+} cells in the popliteal LN (sdLN), mesLN, and the spleen of C57BL/6J mice.

(C) Flow cytometric quantification and statistical analysis of the ITGβ7^{+} CXCR6^{+} cells from the endogenous pLN (sdLN) and mesLN, and the donor-derived mesLN transplanted into the popliteal fossa. The LNs were harvested and analyzed 8 weeks post-transplantation.

(legend continued on next page)

Based on our scRNA-seq analysis, we employed the adhesion molecule ITGβ7 and the chemokine receptor CXCR6 as markers to identify IL-17-like cells (Figure S3A) (clusters 2, 3, and 6) (Figures 2D, 2G, and S2C)—a marker combination that refined our previous gating strategy based on CCR6 (Figure S3B). Consistently, this group of UTCs was largely absent in the mesLN and spleen (Figure 3B). Also, we did not detect this group of cells (UTCs ITGβ7$^+$, CXCR6$^+$) in the blood of mice; in the sdLN, these cells lacked the expression of CD62L (Figure S3C). To investigate whether these UTCs migrate to the dLN via the lymph, we transplanted mesLNs into the fossa of the popliteal lymph node that receives drainage from the leg. Conversely, we also transplanted sdLNs from GFP transgenic mice into the mesenteries of recipient mice. We anticipated that the transplanted LNs would harbor UTCs that matched the endogenous LNs that drained the same tissue. 8 weeks after transplantation, we analyzed the transplanted mesLN and detected the previously missing UTCs population (ITGβ7$^+$ and CXCR6$^+$) (Figure 3C). Vice versa, the donor sdLNs that previously harbored this UTC population (ITGβ7$^+$ and CXCR6$^+$) before transplantation lacked these cells after transplantation to the mesenteries and instead were populated by recipient (GFP negative) UTCs. These recipient UTCs matched those of endogenous mesLNs, based on CXCR3 and CCR6 expression (Figures 3D and S3D). Together, these results suggested that LNs were continuously populated by UTCs that migrated via lymphatic vessels.

Next, we photoconverted the skin of Dendra2 transgenic mice, which leads to a switch from green to red fluorescence in light-exposed cells. 24 h later, we analyzed CD62L$^-$ UTCs in the dLNs and found 10% of such cells were photoswitched/Dendra red (Figure 3E). The migration of all UTCs from the skin to the dLN was dependent on S1P because treatment with FTY720, which downregulates S1PR, prevented the arrival of photoswitched cells in the dLN (Figure 3E), consistent with prior studies on γδ T cells (Laidlaw et al., 2019; Zhang et al., 2016). Notably, also αβ T cells migrated from the skin, showing that this migration was not an exclusive property of γδ T cells (Figure S3E). However, although the photoswitched UTCs in the sdLN mirrored the UTCs population in the skin, they were not representative for all CD62L$^-$ UTCs in the sdLN identified in our scRNA-seq analysis. In particular, LCK$^+$ αβ T cells representing cluster 3 were largely underrepresented (Figures 2D–2F and S3F) (Fiala et al., 2019). The absence of the LCK$^+$ subset in the skin on the other hand implied that the LCK$^+$ UTCs found in sdLNs were migrating from another tissue that is also drained by this LN. To identify the tissue of origin, we digested adipose tissue lodging between muscle layers and surrounding the lymph nodes. Indeed, we detected UTCs in this fat tissue that phenotypically matched those found in sdLN. These cells expressed ITGβ7, CXCR6, and LCK and predominantly consisted of αβ T cells (Figure 3F). Therefore, we conclude that the two clusters (clusters 3 and 6) of IL-17-producing UTCs that we discovered in the sdLN using scRNA-seq (Figures 2D and 2E) represented populations that migrated from different tissues. Finally, we photoactivated the oral cavity of Dendra2 transgenic mice and analyzed the dLNs 24 h later. As anticipated, we detected photoswitched UTCs in cervical LNs that consisted predominantly of αβ UTCs (Figure 3G). Together, these data supported the concept that tissue-derived UTCs, irrespective of their TCR-based lineage affiliation or effector polarization (Th1- and Th17-like) continuously migrated via the lymph to the tissue-draining LNs where they generated characteristic and divergent immune responses.

UTCs share the same homeostatic niche across lineages

The shared lymphatic migration of UTCs across TCR-based lineage affiliations (Figure 3) as well as their shared transcriptional identity (Figure 2) suggested further interconnections between UTCs. To test this notion, we first focused on the sdLN and performed scRNA-seq using a sorting strategy that included all Th17-polarized UTCs of sdLNs. We identified a minimal marker combination (CD44 and CXCR6) that included all IL-17 polarized cells (Figure S4A). This approach revealed two cell clusters of UTCs distinguished by *Lck* expression as identified before and one additional small cluster that expressed *Cxcr3* (Figures 2B, 4A, and S4B; Table S1B). To confirm these data based on the protein expression MFI, we stained for LCK and CXCR3, in addition to γδ TCR, CD1d, and MR1 tetramers to identify scRNA-seq-based UTC clusters as well as UTC lineages (Figures 4B and S4C). We found that these clusters did not represent the three lineages of UTCs but instead were composed of at least two different UTC lineages (Figure S4C). This shows that on a single-cell transcriptional level, different lineages of UTCs with the same differentiation state appear to be largely indistinguishable (Figures 2, 4A, 4B, S4B, and S4C).

Next, we investigated whether different lineages of UTCs share a common homeostatic niche. To address this, we analyzed Th17-polarized UTCs in sdLN (ITGβ7$^+$ and CXCR6$^+$) in lineage-deficient mice (*Tcrd*$^{-/-}$, *Mr1*$^{-/-}$, and *Cd1d*$^{-/-}$). As anticipated, the relative composition of UTCs changed between lineage-deficient mice with regard to lineage proportion (Figures S4C and S4D). Also, we found all the three clusters in these lineage-deficient mice arguing that none of the observed transcriptional states are unique within a specific lineage

(D) Flow cytometric quantification and statistical analysis of the UTCs from the endogenous pLN (sdLN) and control mesLN, and the donor-derived sdLN transplanted into the mesenteries. The LNs were harvested and analyzed 8 weeks post-transplantation.
(E) Flow cytometric quantification and statistical analysis of sdLN 24 h after photoswitching (Dendra green to Dendra red) of the footpad skin of PBS- or FTY720-treated Dendra2 mice.
(F) Flow cytometric quantification and statistical analysis of CD44^{high} CD62L$^-$ UTCs in the skin and adipose tissue of C57BL/6J mice. Histograms show the LCK expression among the ITGβ7$^+$ CXCR6$^+$ population.
(G) Flow cytometric quantification and statistical analysis of the cervical LN and mandibular LN 24 h after photoswitching (Dendra green to Dendra red) the oral cavity and the tongue of Dendra2 mice. Data are showing one representative of three independent experiments (A, n = 3; B, pLN [sdLN], n = 6, mesLN, n = 3, and spleen, n = 3) or two (C and F, n = 4; D, n = 5; E, n = 3; G, n = 3 mice and 4 LN/mouse). Error bars indicate the mean ± SEM. Comparison between groups was calculated (A, D (lower), and F) using the two-way ANOVA, ** p = 0.001; **** p < 0.0001; or (B–D [upper], and E) the one-way ANOVA, ** p = 0.001; *** p = 0.0001; **** p < 0.0001; and (G) using the unpaired Mann-Whitney test * p ≤ 0.01 **** p < 0.0001.
See also Figure S3.

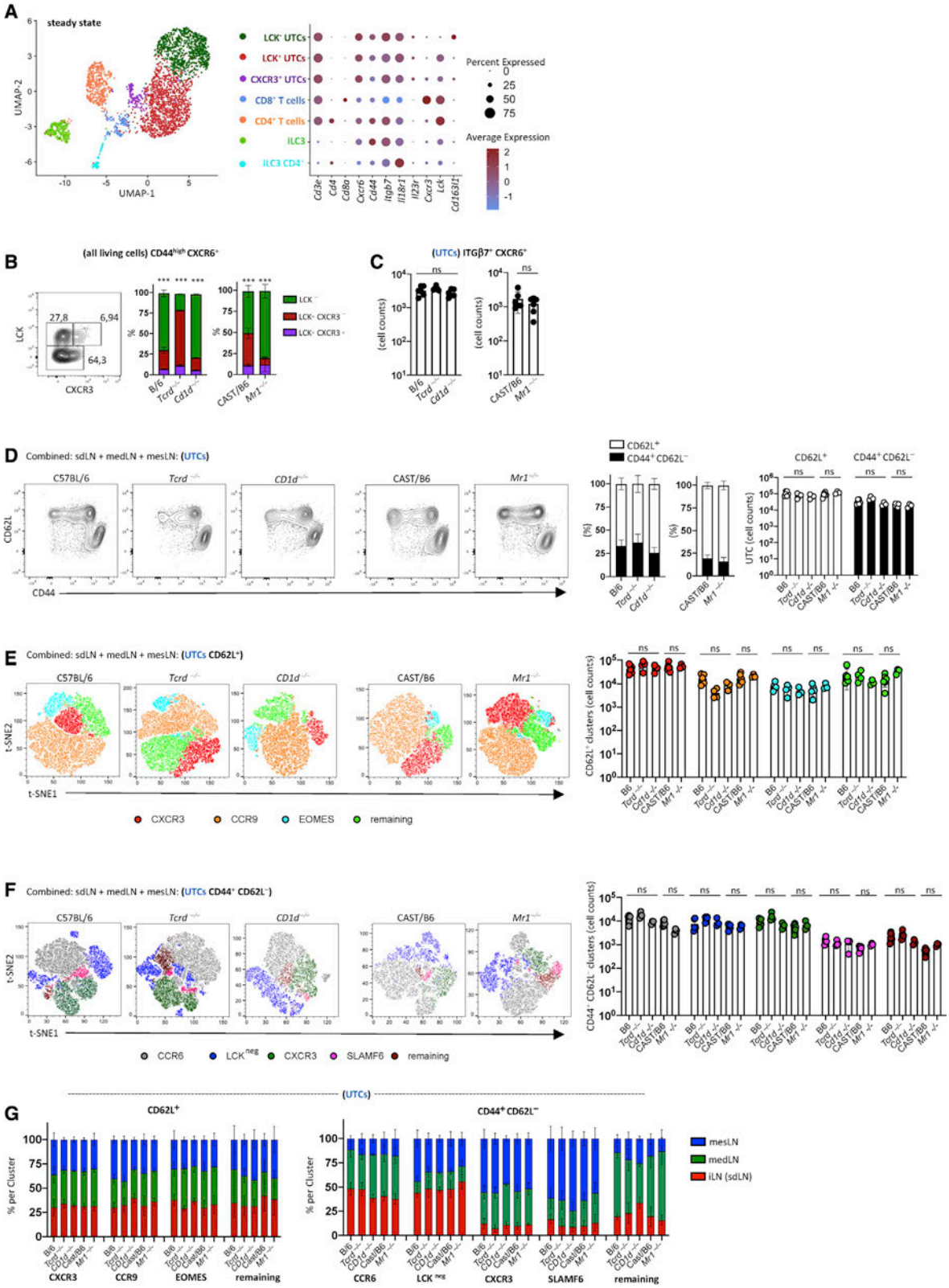

Figure 4. UTCs share the same homeostatic niche across lineages

(A) (Left) UMAP of 3032 scRNA-seq transcriptomes colored according to cluster classification of CD44^{high} CXCR6^{GFP+} sorted cells from sdLNs (Figure S4A). (Right) Dot plot of representative marker genes associated with the identified clusters. Color indicates Z score mean expression values across clusters; dot size represents fraction of cells in the cluster expressing respective genes.

(legend continued on next page)

(Figures 4B and S4C). Moreover, the total numbers of Th17-polarized UTCs in sdLN remained unaltered when compared with WT or littermate controls (Figures 4C and S4D). This result suggested that Th17-polarized UTCs together formed an interconnected population that was maintained as a whole, rather than in separate TCR-based populations. To test whether this applies to all UTCs across polarization states and migratory patterns (recirculating and non-recirculating), we applied our previously established multicolor flow panel to identify all UTC subsets (Figure 2H) on lineage-deficient mice (*Tcrd*$^{-/-}$, *Mr1*$^{-/-}$, and *Cd1d*$^{-/-}$). To provide a visual overview on the cluster distribution and representation, we generated a t-distributed stochastic neighbor embedding (tSNE) plot, based on our multiparameter flow cytometry data. All cluster-based UTC populations were present, and the ratio between recirculating and non-recirculating UTC populations as well as their absolute numbers remained largely unaltered when comparing various LNs from WT, *Tcrd*$^{-/-}$, *Mr1*$^{-/-}$, *Cd1d*$^{-/-}$, or triple KO (*Tcrd*$^{-/-}$/*Mr1*$^{-/-}$/*Cd1d*$^{-/-}$) animals (Figures 2H, 4D–4G, and S4E). Altogether, these data suggest that UTCs comprised interconnected populations that were maintained within shared homeostatic niches and were formed beyond the boundaries of their TCR-based lineage affiliations.

UTCs operate in functional units

Next, we assessed whether these interconnected populations not only shared the same homeostatic niche but also the same microanatomical location and a common functional output. To this end, we analyzed cytokine-driven immune responses of UTCs in the context of bacterial infections. We first focused on the Th17-polarized UTC populations and addressed their localization and migrational behavior in the sdLN. To define the localization of this group of cells, we generated IL18R^{Tom}/IL23R^{GFP} double reporter mice (Figure S5A) in which more than 90% of double positive cells in sdLNs were Th17-polarized UTCs, whereas the remaining population represented conventional T cells and ILCs (innate lymphoid cells) (Figure S5B). IL-18R^{+}/IL-23R^{+} UTCs homogeneously expressed ITGβ7^{+}, CXCR6^{+}, and high amounts of CD44 (Figure S5C), and, therefore, overlapped with previously defined Th17-polarized UTCs (Figures 3 and 4). When we analyzed tissue sections of sdLNs via confocal microscopy, IL-18R/IL-23R double positive cells were found in the subcapsular and interfollicular area (Figure 5A), in line with previous reports using CXCR6 reporter mice (Kastenmüller et al., 2012; Zhang et al., 2016) (Figure S5D). Among IL-18R/IL-23R double positive cells, $\alpha\beta$ and $\gamma\delta$ UTCs were similarly distributed within the interfollicular area (Figure S5E). In the LN, these UTCs were migrating at an $\approx$7 μm/min speed (Figures 5B and S5F; Videos S1 and S2). Following *S. aureus* infection *in vivo*, we did not observe cellular arrest or changes in migration speed as seen with classical antigen-specific $\alpha\beta$ T cells upon TCR-dependent activation but instead transient dynamic clustering reminiscent of a cytokine-mediated form of activation (Figures 5C and S5G; Videos S3 and S4) (Kastenmüller et al., 2013).

Having established a homogeneous intranodal migration pattern and shared localization of UTCs following infection, we next elucidated the functional output of UTCs during this cytokine-driven response using scRNA-seq of UTCs 4 h after *S. aureus* infection. Our scRNA-seq analysis revealed nine clusters of UTCs. The clustering differed from the steady-state condition (Figure 4A). All cells represented in various clusters appeared highly similar, had an activated phenotype, and showed a graded response ranging from *Gzmb*, *Il17a/f*, *Cxcl22*, and *Csf2* (GM-CSF) on one end to *S100a10* and *Hmgb2* at the other end of the spectrum (Figures 5D, S5H, and S5I; Table S1C). Plotting an activation score that consisted of several genes onto the UMAP supported this notion (Figure 5E; Table S1D). These data further supported the concept that the population of Th17-polarized UTCs in the sdLN formed a "functional unit" that comprised different lineages that shared the same homeostatic and microanatomical niche and a concerted cytokine-driven output. To further test the functional implications of this concept *in vivo*, we measured IL-17A and IL-17F production, which, based on our scRNA-seq data, appeared to be a representative read-out for UTC function upon *S. aureus* infection. Indeed, 4 h post infection in the skin, we detected robust IL-17A and IL-17F production within the dLN that was largely (>90%) restricted to UTCs (Figure 5F). All three lineages, produced and contributed to the overall amount of IL-17, albeit to varying degrees reflecting their relative abundance (Figure 5G). However, the total number of IL-17-producing cells remained unaltered in mice lacking either of these UTCs lineages, indicating functional compensation (Figure 5H). The functional activation and cytokine production by all UTCs under this experimental condition were dependent on IL-23 signals (Figure 5H). Next, we wished to extend our cytokine-driven functional concept to Th1-polarized UTCs and tested whether IFNγ production is also compensated among UTCs. To this end, we infected WT or lineage-deficient mice with *S. enterica* s.c. and probed the IFNγ response among UTCs in the sdLN 4 h later. The total IFNγ response among UTCs was also cytokine driven, depended on IL-18R1, and remained unaltered when comparing

(B) Flow cytometric phenotypic quantification and validation of the scRNA-seq of steady-state sdLN from C57BL/6J, *Tcrd*$^{-/-}$, *Cd1d*$^{-/-}$, *Mr1*$^{-/-}$, and B6-MAIT^{CAST} (CAST) mice.
(C) Flow cytometric quantification and statistical analysis of UTCs ITGβ7^{+} CXCR6^{+} in sdLN from different mice deficient for a single UTCs lineage, as indicated.
(D) Flow cytometric quantification and statistical analysis showing the two major UTCs clusters (CD62L^{+} and CD62L^{-} CD44^{+}; Figure S2C) in the LNs from different mice deficient for a single UTCs lineage, as indicated.
(E) t-SNE plot and statistical analysis of the detailed cluster distribution of CD62L^{+} UTCs in LNs of *Tcrd*$^{-/-}$, *Cd1d*$^{-/-}$, *Mr1*$^{-/-}$, and B6-MAIT^{CAST} (CAST) mice.
(F) t-SNE plot and statistical analysis of the detailed cluster distribution of CD62L^{-} CD44^{+} UTCs in LNs of *Tcrd*$^{-/-}$, *Cd1d*$^{-/-}$, *Mr1*$^{-/-}$, and B6-MAIT^{CAST} (CAST) mice.
(G) Statistical analysis of flow-cytometry-validated UTCs clusters in different mice deficient for a single UTCs lineage, as indicated. Data are showing one representative of three independent experiments (B and D, n = 3; C, n = 6) or pooled data from two independent experiments (D, E, and G, n = 6) or one experiment with pooled mice (A, n = 10). Error bars indicate the mean ± SEM. Comparison between groups was calculated (C [left], D, E, and F) using the one-way ANOVA; or (B) the two-way ANOVA, *** p = 0.0001, or (C [right]) the unpaired Mann-Whitney test.
See also Figure S4 and Table S1B.

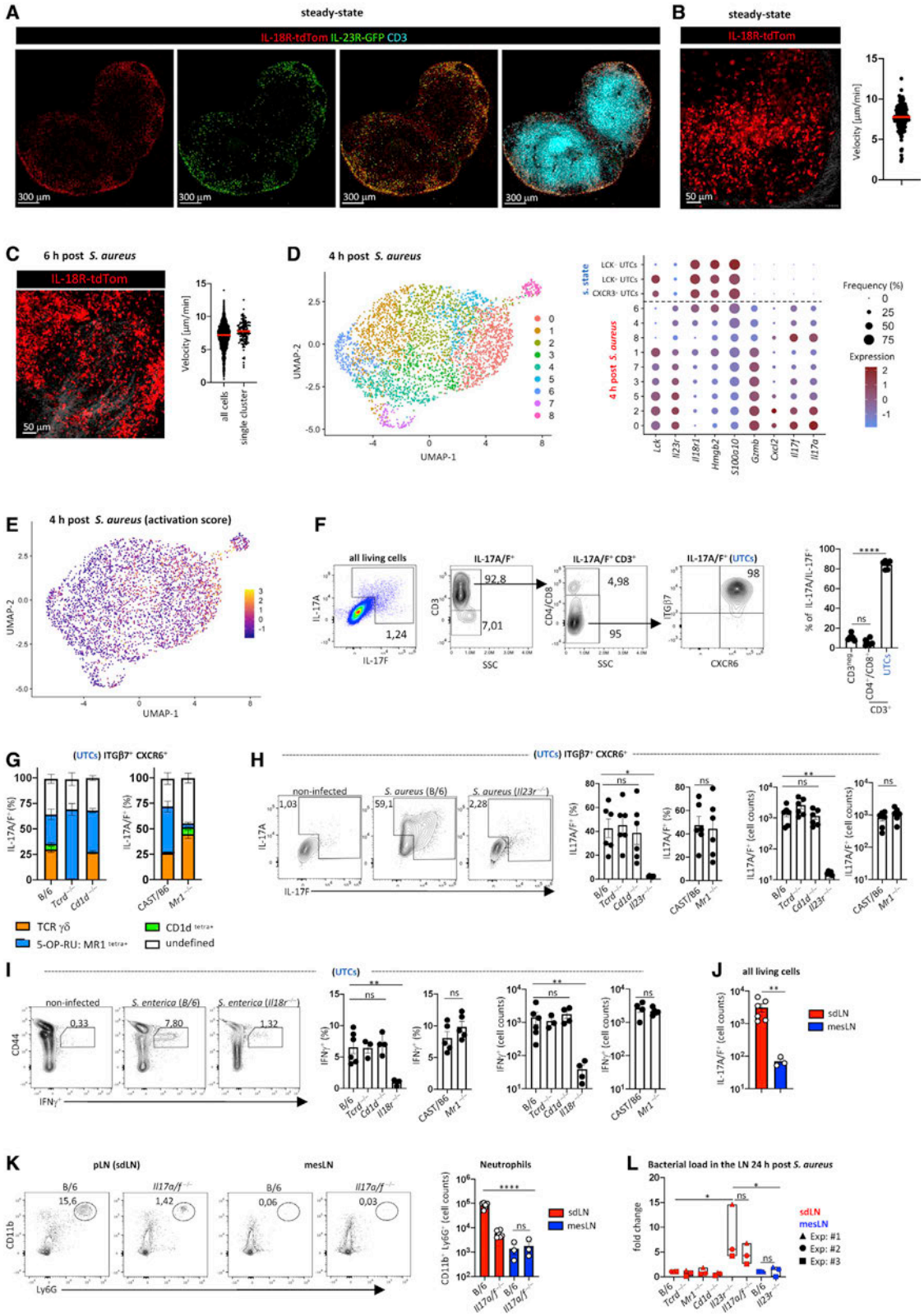

Figure 5. UTCs operate in functional units

(A) Confocal immunofluorescence image of a skin-draining LN (sdLN) showing the microanatomical localization of the IL18R^{Tom+} IL23R^{GFP+} CD3^{+} cells at steady state.

(legend continued on next page)

WT with *Tcrd*$^{-/-}$, *Mr1*$^{-/-}$, or *Cd1d*$^{-/-}$ mice (Figure 5I). Similar results were obtained when analyzing the spleen following i.v. infection with *S. enterica* (Figure S5J). Notably, we did not detect IL17-production among UTCs in the spleen following i.v. infection with *S. enterica* (data not shown). Together, these data supported the concept that categorizes UTCs as interconnected populations—functional units—across TCR-based lineage affiliations. These functional units shared four elements: (1) transcriptional identity, (2) homeostatic niche and numerical compensation, (3) microanatomical location and migratory behavior, and (4) cytokine-driven functional output.

Because we have shown that these local functional units differed between LNs, we wished to study the impact on bacterial resistance. Specifically, we compared mesLNs that lacked a Th17-polarized UTCs functional unit with sdLNs in which these cells were present (Figures 1A, 2D–2G, 3B, S2C, and S5B). S.c. or intraperitoneal (i.p.). injection with *S. aureus* led to similar and robust infection of sdLNs or mesLNs, respectively (Figure S5K). 4 h after infection, we detected a significant IL17-dependent neutrophil recruitment to sdLNs, whereas mesLNs remained largely devoid of neutrophils at this time point (Figure 5K). As expected, both IL23- and IL17-signals were critical to limit bacterial control in sdLNs. By contrast, IL-23 played no role in bacterial control in mesLNs, consistent with the absence of Th17-polarized UTCs in this LN (Figure 5L). In line with our functional unit concept, bacterial loads remained unaltered in sdLNs from single lineage-deficient mice (Figure 5L).

Together, these data demonstrated that UTCs are organized in functional units, which differed in their composition across lymph nodes. This inherent organization of LNs and their UTC populations directly impacted on the immune responses that are locally generated and the resistance toward pathogens that spread via the lymph.

DISCUSSION

In this study, we showed that UTCs constitutively migrated from tissues to locally draining LNs, establishing tissue-specific UTC populations across distinct LNs. As these cells are equipped with immediate innate-like effector functions, their tissue-specific composition and imprinting determined the local cytokine environment in LNs early during infection in a site-specific manner. As we showed, local differences in UTC composition differentially affected adaptive humoral immune responses initiated in distinct LNs, a finding that may have major implications for vaccines, especially those delivered through mucosal routes (Roco et al., 2019). Additionally, UTCs generated divergent cellular immune responses between LNs draining different tissues based on their capacity to clonally expand and the observed functionally relevant TCR repertoire differences. Together, our results established the concept that besides dendritic cells UTCs also critically link tissue immunity to lymph node function.

Our data further showed that UTC-dependent immunological differences between LNs were determined on two levels. First, developmentally due to the tissue-specific TCR-dependent seeding and effector polarization of UTCs (Salou et al., 2019). This process leads to significant heterogeneity of TCR repertoires and cytokine production capacity that differs between tissues and, due to their lymphatic migration, between dLNs that drain these tissues. Second, the functional output of UTCs remains stable due to their organization within functional units, even if their relative TCR-based composition within these units adapts to the local microbiota or tissue damage (Constantinides and Belkaid, 2021).

Key to the diverging immune responses in different LNs was the constitutive lymphatic migration of all UTCs revealed by our work. Lymphatic migration by a group of skin-derived γδ T cells has been observed before (Laidlaw et al., 2019; Zhang et al., 2016); however, here, we found that this was not a unique capacity of this subset. Instead, it was a general principle and reflected the common biology of all UTCs across tissues, TCR-based lineages, and differentiation states. Exceptions to this rule were intraepithelial UTCs, such as DETCs (dendritic epithelial γδ T cells), in the skin or CD8αα IEL in the gut, which we did not detect in dLNs (Chien et al., 2014; Olivares-Villagómez and Van Kaer, 2018). Conceptually, the lymphatic migration of UTCs served two important functions. First, it extended the

(B) Intravital microscopy sdLN image and statistical analysis of the migrational behavior of IL18R^{Tom+} cells at steady state.
(C) Intravital sdLN image and statistical analysis of the migrational behavior of IL18R^{Tom+} cells 6 h after footpad infection with *S. aureus*.
(D) (Left) UMAP displaying 3,555 scRNA-seq transcriptomes colored according to cluster classification of ITGβ7^{+} CXCR6^{+} sorted cells from popliteal LNs (sdLN) 4 h after subcutaneous (s.c.) infection with *S. aureus*. (Right) Dot plot of representative marker genes associated with the identified clusters, including steady-state clusters of UTCs (Figure 4A). Color indicates Z score mean expression across clusters and dot size represents fraction of cells in the cluster expressing respective genes.
(E) UMAP of 3555 scRNA-seq transcriptomes colored according to activation score.
(F–H) *Ex vivo* flow cytometric quantification and statistical analysis of the (F) IL-17A/F producing cells from C57BL/6 mice, (G) IL-17A/F producing UTCs lineages from *Tcrd*$^{-/-}$, *Cd1d*$^{-/-}$, *Mr1*$^{-/-}$, and B6-MAIT^{CAST} (CAST) mice, and (H) IL17A/F production in the sdLN after 4 h s.c. infection of *Tcrd*$^{-/-}$, *Cd1d*$^{-/-}$, *Mr1*$^{-/-}$, *Il23r*$^{-/-}$ and B6-MAIT^{CAST} (CAST) mice with 10^8 CFU *S. aureus*.
(I) *Ex vivo* flow cytometric quantification and statistical analysis of the IFNγ production in the sdLN 4 h after 10^7 CFU *S. typhimurium (Xen33)* subcutaneous infection of C57BL/6, *Tcrd*$^{-/-}$, *Cd1d*$^{-/-}$, *Mr1*$^{-/-}$, *Il18r*$^{-/-}$, and B6-MAIT^{CAST} (CAST) mice.
(J) *Ex vivo* flow cytometric quantification and statistical analysis of the IL-17A/F production in the sdLN and the mesLN of *Il17a/f* $^{-/-}$ and C57BL/6 mice 4 h after s.c. infection with 10^8 CFU *S. aureus*.
(K) *Ex vivo* flow cytometric quantification and statistical analysis of neutrophils in the sdLN and the mesLN of *Il17a/f* $^{-/-}$ and C57BL/6 mice 4 h after s.c. infection with 10^8 CFU *S. aureus*.
(L) Fold change of the colony-forming unit (CFU) in the sdLN and mesLN comparing *Tcrd*$^{-/-}$, *Cd1d*$^{-/-}$, *Mr1*$^{-/-}$, *Il23r*$^{-/-}$, and *Il17a/f* $^{-/-}$ with control mice 24 h after footpad infection with 10^8 CFU *S. aureus* (MRSA). Data are showing one representative of three independent experiments (A–C, n = 3; F–H, n = 6; I, n = 3–6; J and K, pLN (sdLN) n = 6, medLN, n = 3) or pooled data from three independent experiments (L, n = 3) or one experiment with pooled mice (D and E, n = 10). Error bars indicate the mean ± SEM. Comparison between groups (F, H–L) was calculated using the one-way ANOVA test. * $p \leq 0.01$; ** $p \leq 0.001$; **** $p < 0.0001$.
See also Figure S5; Table S1C and S1D; Videos S1, S2, and S3.

cytokine-driven innate function of UTCs from tissues to dLNs where they prevent systemic pathogen dissemination via the lymphatic route. Second, LNs in turn provide the optimal microenvironment for UTC proliferation following their adaptive TCR-based activation. Thereby, UTCs inherently linked tissue immunity to LN function. An important question is when after birth UTCs commence their lymphatic migration to draining LNs and whether insufficient UTCs migration may be related to the heightened susceptibility of infants to bacterial infections.

Notably, we were not able to detect a dedicated Th2-polarized UTC population outside the thymus. Instead, some Th1- and Th17-polarized UTCs had the capacity to additionally produce IL-4. This result is in line with a recent fate mapping study showing that NKT2 resemble a maturing progenitor population in the thymus that gradually diminishes at the expense of Th1 and Th17 polarized cells (Bortoluzzi et al., 2021). Although IL-17-polarized UTCs in different lymph nodes were distinct based on their tissue origin, this transcriptional sub-setting was not observed for Th1-polarized UTCs. This difference is likely based on the distinct anatomical localization of these various polarized UTC populations. Although Th17-polarized UTCs are found in the parenchyma, Th1-polarized NKT cells, at least in the lungs and the liver, are primarily localized within the vasculature (Geissmann et al., 2005; Scanlon et al., 2011). Elucidating the exact coordination between the local proliferation and lymphatic emigration under physiological and pathological conditions will be an exciting challenge for the future, in particular for UTCs residing intravascularly (Debes et al., 2005; Hunter et al., 2016).

Based on our data, we developed the concept that UTCs are organized in interconnected populations—functional units. Certainly, the members of these units express diverse TCRs allowing them to execute specific functions, such as the TCR-dependent production of IL-4 by NKT cells.

However, we believe that highlighting the shared and overlapping properties of UTCs and analyzing them as a population will help to uncover new biological functions of these groups of T cells during homeostasis and following infections. This concept also helps to explain previous findings on numerical compensation between UTC-lineage members, for example in a human with MR1 deficiency that exhibit numerical compensation of MAIT T cells by $\gamma\delta$ T cells (Howson et al., 2020). Transcriptional similarities among effector cells with similar functional polarization and among UTCs has been reported (Gutierrez-Arcelus et al., 2019; Lee et al., 2016). Our concept of functional units, however, goes beyond transcriptional homogeneity between UTCs. As such, we showed that the size and the functional output of these UTC units remained unaltered among lineage-deficient mice lacking single UTC lineages, arguing for shared homeostatic signals and potential quorum sensing mechanisms. However, this does not mean that the composition and size of functional units are absolutely fixed. On the contrary, functional units are likely dynamically regulated in the context of fundamental physiological processes. As such, homeostatic regulation of neutrophil production and vice versa the amount of IL-17-producing UTCs in the tissue is regulated via a feedback circuit (Stark et al., 2005). We believe that our approach to analyze UTCs as functional units will further reveal unknown physiological circuits in the future.

An important question that remained unresolved in our study is the function of the recirculating population of UTCs that consists of a large fraction of unpolarized cells. It seems likely that these cells have a more diverse TCR repertoire and higher functional plasticity than their tissue counterparts. Defining the exact role of the recirculating UTCs will be particularly relevant for human studies that primarily rely on blood samples for UTC analyses.

In summary, we showed that LNs that drain distinct tissues generated divergent immune responses based on the lymphatic migration pattern and rapid effector function of UTCs. This result established an additional cellular relay network that operates between tissues and dLNs, besides dendritic cells. Our data further revealed that UTCs are organized and function within common units that share specific anatomical niches and common homeostatic signals. We believe that our findings revealed a fundamental link between tissue immunity and LN function, which has important implications for vaccine application routes in particular those that aim at targeting UTCs.

Limitations of the study

We have shown different $\gamma\delta$ T cell responses in medLN versus sdLN versus spleen when comparing skin versus lung versus systemic infections with *S. aureus*. Unfortunately, for technical reasons, we are currently unable to manipulate the presence of distinct $\gamma\delta$ T cell populations in specific LNs. Therefore, we cannot exclude that other, T cell extrinsic factors contribute to the observed differences in $\gamma\delta$ T cell expansion between SLOs using different routes of infection. Also, we have shown that UTC lineages within the same functional unit share the same location within lymph nodes; yet, we cannot exclude more subtle microanatomical localization differences between various TCR-based lineages of UTCs. Finally, also other IL23R expressing cells, such as Th17 and ILC3, may contribute to heterogeneous immune responses between distinct LNs.

STAR★METHODS

Detailed methods are provided in the online version of this paper and include the following:

- KEY RESOURCES TABLE
- RESOURCE AVAILABILITY
  - Lead contact
  - Materials availability
  - Data and code availability
- EXPERIMENTAL MODEL AND SUBJECT DETAILS
  - Mice
  - Bacterial and viral strains
- METHOD DETAILS
  - Infections
  - Bacterial counts
  - Photoactivation of skin cells
  - FTY720 treatment
  - αCD62L *in vivo* blocking treatment
  - *In vitro* PMA-Ionomycin activation
  - Intravenous CD45 labeling
  - Flow cytometry
  - Isolation of mouse skin, lung and small intestine and adipose tissue-resident lymphocytes

- Cytokine measurement in the culture supernatants
- LN transplantation
- Confocal microscopy
- Intravital microscopy
- Hashtagging for scRNA-seq
- scRNA-seq library preparation and sequencing
- Sample demultiplexing and doublet identification
- scRNA-seq analysis

- QUANTIFICATION AND STATISTICAL ANALYSIS

SUPPLEMENTAL INFORMATION

Supplemental information can be found online at https://doi.org/10.1016/j.immuni.2022.07.019.

ACKNOWLEDGMENTS

We would like to thank Ronald N. Germain for critically reading the manuscript. The Core Unit for FACS and the Core Unit SysMed of the IZKF Würzburg have supported this study. The authors thank the Single-Cell Center Würzburg for technical support. The CD1d and MR1 tetramer were obtained through the NIH Tetramer Core Facility. This work was funded by grants through the German Research Foundation (DFG) under Germany's Excellence Strategy—EXC 2155 "RESIST"—project ID 390874280 to J.H., GRK2581 "SPHINGOINF" to W.K., and by grants of the European Research Council (ERC) to W.K. (819329—STEP2) and G.G. (759176-TissueLymphoContexts). W.K. and G.G. are supported by the Max Planck Society (Max Planck Research Groups).

AUTHOR CONTRIBUTIONS

M.A.A., K.K., P.C.d.C., and W.K. conceptualized the study and analyzed data. M.A.A., K.K., P.C.d.C., S.E., M.Z., A.T., H.S., T.Y., A.B., and A.G. planned and performed experiments and/or analyzed the data. K.K. analyzed scRNA-seq data. I.P., M.G., and K.O. provided critical reagents. J.H., M.G., A.-E.S., and W.K. supervised experiments. G.G. provided intellectual input and gave conceptual advice. W.K. and G.G. provided research funds.

DECLARATION OF INTERESTS

The authors declare no competing interests.

Received: February 4, 2022
Revised: June 6, 2022
Accepted: July 27, 2022
Published: August 23, 2022

REFERENCES

Ansaldo, E., Farley, T.K., and Belkaid, Y. (2021). Control of immunity by the microbiota. Annu. Rev. Immunol. *39*, 449–479. https://doi.org/10.1146/annurev-immunol-093019-112348.

Arlehamn, C.L., Seumois, G., Gerasimova, A., Huang, C., Fu, Z., Yue, X., Sette, A., Vijayanand, P., and Peters, B. (2014). Transcriptional profile of tuberculosis antigen-specific T cells reveals novel multifunctional features. J. Immunol. *193*, 2931–2940. https://doi.org/10.4049/jimmunol.1401151.

Audemard-Verger, A., Rivière, M., Durand, A., Peranzoni, E., Guichard, V., Hamon, P., Bonilla, N., Guilbert, T., Boissonnas, A., Auffray, C., et al. (2017). Macrophages induce long-term trapping of γδ T cells with innate-like properties within secondary lymphoid organs in the steady state. J. Immunol. *199*, 1998–2007. https://doi.org/10.4049/jimmunol.1700430.

Awasthi, A., Riol-Blanco, L., Jäger, A., Korn, T., Pot, C., Galileos, G., Bettelli, E., Kuchroo, V.K., and Oukka, M. (2009). Cutting edge: il-23 receptor gfp reporter mice reveal distinct populations of IL-17-producing cells. J. Immunol. *182*, 5904–5908. https://doi.org/10.4049/jimmunol.0900732.

Bendelac, A., Savage, P.B., and Teyton, L. (2007). The biology of NKT cells. Annu. Rev. Immunol. *25*, 297–336. https://doi.org/10.1146/annurev.immunol.25.022106.141711.

Bortoluzzi, S., Dashtsoodol, N., Engleitner, T., Drees, C., Helmrath, S., Mir, J., Toska, A., Flossdorf, M., Öllinger, R., Solovey, M., et al. (2021). Brief homogeneous TCR signals instruct common iNKT progenitors whose effector diversification is characterized by subsequent cytokine signaling. Immunity *54*, 2497–2513.e9. https://doi.org/10.1016/j.immuni.2021.09.003.

Brigl, M., Tatituri, R.V., Watts, G.F., Bhowruth, V., Leadbetter, E.A., Barton, N., Cohen, N.R., Hsu, F.F., Besra, G.S., and Brenner, M.B. (2011). Innate and cytokine-driven signals, rather than microbial antigens, dominate in natural killer T cell activation during microbial infection. J. Exp. Med. *208*, 1163–1177. https://doi.org/10.1084/jem.20102555.

Campbell, D.J., and Butcher, E.C. (2002). Rapid acquisition of tissue-specific homing phenotypes by CD4(+) T cells activated in cutaneous or mucosal lymphoid tissues. J. Exp. Med. *195*, 135–141. https://doi.org/10.1084/jem.20011502.

Chien, Y.H., and Konigshofer, Y. (2007). Antigen recognition by gammadelta T cells. Immunol. Rev. *215*, 46–58. https://doi.org/10.1111/j.1600-065X.2006.00470.x.

Chien, Y.H., Meyer, C., and Bonneville, M. (2014). γδ T cells: first line of defense and beyond. Annu. Rev. Immunol. *32*, 121–155. https://doi.org/10.1146/annurev-immunol-032713-120216.

Constantinides, M.G., and Belkaid, Y. (2021). Early-life imprinting of unconventional T cells and tissue homeostasis. Science *374*, eabf0095. https://doi.org/10.1126/science.abf0095.

Constantinides, M.G., Link, V.M., Tamoutounour, S., Wong, A.C., Perez-Chaparro, P.J., Han, S.J., Chen, Y.E., Li, K., Farhat, S., Weckel, A., et al. (2019). MAIT cells are imprinted by the microbiota in early life and promote tissue repair. Science *366*. https://doi.org/10.1126/science.aax6624.

Cording, S., Wahl, B., Kulkarni, D., Chopra, H., Pezoldt, J., Buettner, M., Dummer, A., Hadis, U., Heimesaat, M., Bereswill, S., et al. (2014). The intestinal micro-environment imprints stromal cells to promote efficient Treg induction in gut-draining lymph nodes. Mucosal Immunol. *7*, 359–368. https://doi.org/10.1038/mi.2013.54.

Cui, Y., Franciszkiewicz, K., Mburu, Y.K., Mondot, S., Le Bourhis, L., Premel, V., Martin, E., Kachaner, A., Duban, L., Ingersoll, M.A., et al. (2015). Mucosal-associated invariant T cell-rich congenic mouse strain allows functional evaluation. J. Clin. Invest. *125*, 4171–4185. https://doi.org/10.1172/JCI82424.

Debes, G.F., Arnold, C.N., Young, A.J., Krautwald, S., Lipp, M., Hay, J.B., and Butcher, E.C. (2005). Chemokine receptor CCR7 required for T lymphocyte exit from peripheral tissues. Nat. Immunol. *6*, 889–894. https://doi.org/10.1038/ni1238.

Dillen, C.A., Pinsker, B.L., Marusina, A.I., Merleev, A.A., Farber, O.N., Liu, H., Archer, N.K., Lee, D.B., Wang, Y., Ortines, R.V., et al. (2018). Clonally expanded γδ T cells protect against Staphylococcus aureus skin reinfection. J. Clin. Invest. *128*, 1026–1042. https://doi.org/10.1172/JCI96481.

Esterházy, D., Canesso, M.C.C., Mesin, L., Muller, P.A., de Castro, T.B.R., Lockhart, A., ElJalby, M., Faria, A.M.C., and Mucida, D. (2019). Compartmentalized gut lymph node drainage dictates adaptive immune responses. Nature *569*, 126–130. https://doi.org/10.1038/s41586-019-1125-3.

Everson, M.P., McDuffie, D.S., Lemak, D.G., Koopman, W.J., McGhee, J.R., and Beagley, K.W. (1996). Dendritic cells from different tissues induce production of different T cell cytokine profiles. J. Leukoc. Biol. *59*, 494–498. https://doi.org/10.1002/jlb.59.4.494.

Fiala, G.J., Schaffer, A.M., Merches, K., Morath, A., Swann, J., Herr, L.A., Hils, M., Esser, C., Minguet, S., and Schamel, W.W.A. (2019). Proximal Lck promotor-driven Cre function is limited in neonatal and ineffective in adult γδ T cell development. J. Immunol. *203*, 569–579. https://doi.org/10.4049/jimmunol.1701521.

Gaya, M., Barral, P., Burbage, M., Aggarwal, S., Montaner, B., Warren Navia, A., Aid, M., Tsui, C., Maldonado, P., Nair, U., et al. (2018). Initiation of antiviral B cell immunity relies on innate signals from spatially positioned NKT cells. Cell *172*, 517–533.e20. https://doi.org/10.1016/j.cell.2017.11.036.

Geissmann, F., Cameron, T.O., Sidobre, S., Manlongat, N., Kronenberg, M., Briskin, M.J., Dustin, M.L., and Littman, D.R. (2005). Intravascular immune surveillance by CXCR6+ NKT cells patrolling liver sinusoids. PLoS Biol. *3*, e113. https://doi.org/10.1371/journal.pbio.0030113.

Girard, J.P., Moussion, C., and Förster, R. (2012). HEVs, lymphatics and homeostatic immune cell trafficking in lymph nodes. Nat. Rev. Immunol. *12*, 762–773. https://doi.org/10.1038/nri3298.

Godfrey, D.I., Uldrich, A.P., McCluskey, J., Rossjohn, J., and Moody, D.B. (2015). The burgeoning family of unconventional T cells. Nat. Immunol. *16*, 1114–1123. https://doi.org/10.1038/ni.3298.

Gray, E.E., Friend, S., Suzuki, K., Phan, T.G., and Cyster, J.G. (2012). Subcapsular sinus macrophage fragmentation and CD169+ bleb acquisition by closely associated IL-17-committed innate-like lymphocytes. PLoS One *7*, e38258. https://doi.org/10.1371/journal.pone.0038258.

Gutierrez-Arcelus, M., Teslovich, N., Mola, A.R., Polidoro, R.B., Nathan, A., Kim, H., Hannes, S., Slowikowski, K., Watts, G.F.M., Korsunsky, I., et al. (2019). Lymphocyte innateness defined by transcriptional states reflects a balance between proliferation and effector functions. Nat. Commun. *10*, 687. https://doi.org/10.1038/s41467-019-08604-4.

Haas, J.D., Ravens, S., Düber, S., Sandrock, I., Oberdörfer, L., Kashani, E., Chennupati, V., Föhse, L., Naumann, R., Weiss, S., et al. (2012). Development of interleukin-17-producing γδ T cells is restricted to a functional embryonic wave. Immunity *37*, 48–59. https://doi.org/10.1016/j.immuni.2012.06.003.

Hammerschmidt, S.I., Ahrendt, M., Bode, U., Wahl, B., Kremmer, E., Förster, R., and Pabst, O. (2008). Stromal mesenteric lymph node cells are essential for the generation of gut-homing T cells in vivo. J. Exp. Med. *205*, 2483–2490. https://doi.org/10.1084/jem.20080039.

Hoebe, K., Du, X., Georgel, P., Janssen, E., Tabeta, K., Kim, S.O., Goode, J., Lin, P., Mann, N., Mudd, S., et al. (2003). Identification of *Lps2* as a key transducer of MyD88-independent TIR signalling. Nature *424*, 743–748. https://doi.org/10.1038/nature01889.

Houston, S.A., Cerovic, V., Thomson, C., Brewer, J., Mowat, A.M., and Milling, S. (2016). The lymph nodes draining the small intestine and colon are anatomically separate and immunologically distinct. Mucosal Immunol. *9*, 468–478. https://doi.org/10.1038/mi.2015.77.

Howson, L.J., Awad, W., von Borstel, A., Lim, H.J., McWilliam, H.E.G., Sandoval-Romero, M.L., Majumdar, S., Hamzeh, A.R., Andrews, T.D., McDermott, D.H., et al. (2020). Absence of mucosal-associated invariant T cells in a person with a homozygous point mutation in MR1. Sci. Immunol. *5*, eabc9492. https://doi.org/10.1126/sciimmunol.abc9492.

Hunter, M.C., Teijeira, A., and Halin, C. (2016). T cell trafficking through lymphatic vessels. Front. Immunol. *7*, 613. https://doi.org/10.3389/fimmu.2016.00613.

Ishigame, H., Kakuta, S., Nagai, T., Kadoki, M., Nambu, A., Komiyama, Y., Fujikado, N., Tanahashi, Y., Akitsu, A., Kotaki, H., et al. (2009). Differential Roles of Interleukin-17A and -17F in Host Defense against Mucoepithelial Bacterial Infection and Allergic Responses. Immunity *30*, 108–119. https://doi.org/10.1016/j.immuni.2008.11.009.

Itohara, S., Mombaerts, P., Lafaille, J., Iacomini, J., Nelson, A., Clarke, A.R., Hooper, M.L., Farr, A., and Tonegawa, S. (1993). T cell receptor delta gene mutant mice: independent generation of alpha beta T cells and programmed rearrangements of gamma delta TCR genes. Cell *72*, 337–348. https://doi.org/10.1016/0092-8674(93)90112-4.

Johansson-Lindbom, B., Svensson, M., Wurbel, M.A., Malissen, B., Márquez, G., and Agace, W. (2003). Selective generation of gut tropic T cells in gut-associated lymphoid tissue (GALT): requirement for GALT dendritic cells and adjuvant. J. Exp. Med. *198*, 963–969. https://doi.org/10.1084/jem.20031244.

Kastenmüller, W., Brandes, M., Wang, Z., Herz, J., Egen, J.G., and Germain, R.N. (2013). Peripheral prepositioning and local CXCL9 chemokine-mediated guidance orchestrate rapid memory CD8+ T cell responses in the lymph node. Immunity *38*, 502–513. https://doi.org/10.1016/j.immuni.2012.11.012.

Kastenmüller, W., Torabi-Parizi, P., Subramanian, N., Lämmermann, T., and Germain, R.N. (2012). A spatially-organized multicellular innate immune response in lymph nodes limits systemic pathogen spread. Cell *150*, 1235–1248. https://doi.org/10.1016/j.cell.2012.07.021.

Kucharzik, T., Hudson, J.T., III, Waikel, R.L., Martin, W.D., and Williams, I.R. (2002). CCR6 expression distinguishes mouse myeloid and lymphoid dendritic cell subsets: demonstration using a CCR6 EGFP knock-in mouse. Eur. J. Immunol. *32*, 104–112. https://doi.org/10.1002/1521-4141(200201)32:1<104::AID-IMMU104>3.0.CO;2-C.

Laidlaw, B.J., Gray, E.E., Zhang, Y., Ramírez-Valle, F., and Cyster, J.G. (2019). Sphingosine-1-phosphate receptor 2 restrains egress of γδ T cells from the skin. J. Exp. Med. *216*, 1487–1496. https://doi.org/10.1084/jem.20190114.

Lee, M., Lee, E., Han, S.K., Choi, Y.H., Kwon, D.I., Choi, H., Lee, K., Park, E.S., Rha, M.S., Joo, D.J., et al. (2020). Single-cell RNA sequencing identifies shared differentiation paths of mouse thymic innate T cells. Nat. Commun. *11*, 4367. https://doi.org/10.1038/s41467-020-18155-8.

Lee, Y.J., Holzapfel, K.L., Zhu, J., Jameson, S.C., and Hogquist, K.A. (2013). Steady-state production of IL-4 modulates immunity in mouse strains and is determined by lineage diversity of iNKT cells. Nat. Immunol. *14*, 1146–1154. https://doi.org/10.1038/ni.2731.

Lee, Y.J., Starrett, G.J., Lee, S.T., Yang, R., Henzler, C.M., Jameson, S.C., and Hogquist, K.A. (2016). Lineage-specific effector signatures of invariant NKT cells are shared amongst γδ T, innate lymphoid, and Th cells. J. Immunol. *197*, 1460–1470. https://doi.org/10.4049/jimmunol.1600643.

Legoux, F., Bellet, D., Daviaud, C., El Morr, Y., Darbois, A., Niort, K., Procopio, E., Salou, M., Gilet, J., Ryffel, B., et al. (2019). Microbial metabolites control the thymic development of mucosal-associated invariant T cells. Science *366*, 494–499. https://doi.org/10.1126/science.aaw2719.

Marchitto, M.C., Dillen, C.A., Liu, H., Miller, R.J., Archer, N.K., Ortines, R.V., Alphonse, M.P., Marusina, A.I., Merleev, A.A., Wang, Y., et al. (2019). Clonal Vγ6+Vδ4+ T cells promote IL-17-mediated immunity against Staphylococcus aureus skin infection. Proc. Natl. Acad. Sci. USA *116*, 10917–10926. https://doi.org/10.1073/pnas.1818256116.

McGinty, J.W., and von Moltke, J. (2020). A three course menu for ILC and bystander T cell activation. Curr. Opin. Immunol. *62*, 15–21. https://doi.org/10.1016/j.coi.2019.11.005.

McWilliam, H.E.G., and Villadangos, J.A. (2017). How MR1 presents a pathogen metabolic signature to mucosal-associated invariant T (MAIT) cells. Trends Immunol. *38*, 679–689. https://doi.org/10.1016/j.it.2017.06.005.

Mohrs, M., Shinkai, K., Mohrs, K., and Locksley, R.M. (2001). Analysis of type 2 immunity in vivo with a bicistronic IL-4 reporter. Immunity *15*, 303–311. https://doi.org/10.1016/s1074-7613(01)00186-8.

Mora, J.R., Cheng, G., Picarella, D., Briskin, M., Buchanan, N., and von Andrian, U.H. (2005). Reciprocal and dynamic control of CD8 T cell homing by dendritic cells from skin- and gut-associated lymphoid tissues. J. Exp. Med. *201*, 303–316. https://doi.org/10.1084/jem.20041645.

Nakae, S., Komiyama, Y., Nambu, A., Sudo, K., Iwase, M., Homma, I., Sekikawa, K., Asano, M., and Iwakura, Y. (2002). Antigen-Specific T Cell Sensitization Is Impaired in IL-17-Deficient Mice, Causing Suppression of Allergic Cellular and Humoral. Immunity *17*, 375–387. https://doi.org/10.1016/s1074-7613(02)00391-6.

Nakamizo, S., Egawa, G., Tomura, M., Sakai, S., Tsuchiya, S., Kitoh, A., Honda, T., Otsuka, A., Nakajima, S., Dainichi, T., et al. (2015). Dermal Vγ4(+) γδ T cells possess a migratory potency to the draining lymph nodes and modulate CD8(+) T-cell activity through TNF-alpha production. J. Invest. Dermatol. *135*, 1007–1015. https://doi.org/10.1038/jid.2014.516.

Oghumu, S., Dong, R., Varikuti, S., Shawler, T., Kampfrath, T., Terrazas, C.A., Lezama-Davila, C., Ahmer, B.M., Whitacre, C.C., Rajagopalan, S., et al. (2013). Distinct populations of innate CD8+ T cells revealed in a CXCR3 reporter mouse. J. Immunol. *190*, 2229–2240. https://doi.org/10.4049/jimmunol.1201170.

Olivares-Villagómez, D., and Van Kaer, L. (2018). Intestinal intraepithelial lymphocytes: sentinels of the mucosal barrier. Trends Immunol. *39*, 264–275. https://doi.org/10.1016/j.it.2017.11.003.

Parker, M.E., and Ciofani, M. (2020). Regulation of γδ T cell Effector Diversification in the Thymus. Front. Immunol. *11*, 42. https://doi.org/10.3389/fimmu.2020.00042.

Pellicci, D.G., Koay, H.F., and Berzins, S.P. (2020). Thymic development of unconventional T cells: how NKT cells, MAIT cells and γδ T cells emerge. Nat. Rev. Immunol. *20*, 756–770. https://doi.org/10.1038/s41577-020-0345-y.

Pezoldt, J., Pasztoi, M., Zou, M., Wiechers, C., Beckstette, M., Thierry, G.R., Vafadarnejad, E., Floess, S., Arampatzi, P., Buettner, M., et al. (2018). Neonatally imprinted stromal cell subsets induce tolerogenic dendritic cells in mesenteric lymph nodes. Nat. Commun. *9*, 3903. https://doi.org/10.1038/s41467-018-06423-7.

Pham, A.H., McCaffery, J.M., and Chan, D.C. (2012). Mouse lines with photo-activatable mitochondria to study mitochondrial dynamics. Genesis *50*, 833–843. https://doi.org/10.1002/dvg.22050.

Qi, H., Kastenmüller, W., and Germain, R.N. (2014). Spatiotemporal basis of innate and adaptive immunity in secondary lymphoid tissue. Annu. Rev. Cell Dev. Biol. *30*, 141–167. https://doi.org/10.1146/annurev-cellbio-100913-013254.

Ribot, J.C., Lopes, N., and Silva-Santos, B. (2021). γδ T cells in tissue physiology and surveillance. Nat. Rev. Immunol. *21*, 221–232. https://doi.org/10.1038/s41577-020-00452-4.

Roco, J.A., Mesin, L., Binder, S.C., Nefzger, C., Gonzalez-Figueroa, P., Canete, P.F., Ellyard, J., Shen, Q., Robert, P.A., Cappello, J., et al. (2019). Class-switch recombination occurs infrequently in germinal centers. Immunity *51*, 337–350.e7. https://doi.org/10.1016/j.immuni.2019.07.001.

Roozendaal, R., Mebius, R.E., and Kraal, G. (2008). The conduit system of the lymph node. Int. Immunol. *20*, 1483–1487. https://doi.org/10.1093/intimm/dxn110.

Salou, M., Legoux, F., Gilet, J., Darbois, A., du Halgouet, A., Alonso, R., Richer, W., Goubet, A.G., Daviaud, C., Menger, L., et al. (2019). A common transcriptomic program acquired in the thymus defines tissue residency of MAIT and NKT subsets. J. Exp. Med. *216*, 133–151. https://doi.org/10.1084/jem.20181483.

Scanlon, S.T., Thomas, S.Y., Ferreira, C.M., Bai, L., Krausz, T., Savage, P.B., and Bendelac, A. (2011). Airborne lipid antigens mobilize resident intravascular NKT cells to induce allergic airway inflammation. J. Exp. Med. *208*, 2113–2124. https://doi.org/10.1084/jem.20110522.

Schaefer, B.C., Schaefer, M.L., Kappler, J.W., Marrack, P., and Kedl, R.M. (2001). Observation of Antigen-Dependent $CD8^+$ T-Cell/ Dendritic Cell Interactions in Vivo. Cellular Immunology *214*, 110–122. https://doi.org/10.1006/cimm.2001.1895.

Shaikh, H., Vargas, J.G., Mokhtari, Z., Jarick, K.J., Ulbrich, M., Mosca, J.P., Viera, E.A., Graf, C., Le, D.D., Heinze, K.G., et al. (2021). Mesenteric lymph node transplantation in mice to study immune responses of the gastrointestinal tract. Front. Immunol. *12*, 689896. https://doi.org/10.3389/fimmu.2021.689896.

Smiley, S.T., Kaplan, M.H., and Grusby, M.J. (1997). Immunoglobulin E production in the absence of interleukin-4-secreting CD1-dependent cells. Science *275*, 977–979. https://doi.org/10.1126/science.275.5302.977.

Stark, M.A., Huo, Y., Burcin, T.L., Morris, M.A., Olson, T.S., and Ley, K. (2005). Phagocytosis of apoptotic neutrophils regulates granulopoiesis via IL-23 and IL-17. Immunity *22*, 285–294. https://doi.org/10.1016/j.immuni.2005.01.011.

Stoeckius, M., Zheng, S., Houck-Loomis, B., Hao, S., Yeung, B.Z., Mauck, W.M., 3rd, Smibert, P., and Satija, R. (2018). Cell Hashing with barcoded antibodies enables multiplexing and doublet detection for single cell genomics. Genome Biol. *19*, 224. https://doi.org/10.1186/s13059-018-1603-1.

Stuart, T., Butler, A., Hoffman, P., Hafemeister, C., Papalexi, E., Mauck, W.M., 3rd, Hao, Y., Stoeckius, M., Smibert, P., and Satija, R. (2019). Comprehensive integration of single-cell data. Cell *177*, 1888–1902.e21. https://doi.org/10.1016/j.cell.2019.05.031.

Thomas, S.N., Rohner, N.A., and Edwards, E.E. (2016). Implications of lymphatic transport to lymph nodes in immunity and immunotherapy. Annu. Rev. Biomed. Eng. *18*, 207–233. https://doi.org/10.1146/annurev-bioeng-101515-014413.

Thomas, S.Y., Scanlon, S.T., Griewank, K.G., Constantinides, M.G., Savage, A.K., Barr, K.A., Meng, F., Luster, A.D., and Bendelac, A. (2011). PLZF induces an intravascular surveillance program mediated by long-lived LFA-1-ICAM-1 interactions. J. Exp. Med. *208*, 1179–1188. https://doi.org/10.1084/jem.20102630.

Treiner, E., Duban, L., Bahram, S., Radosavljevic, M., Wanner, V., Tilloy, F., Affaticati, P., Gilfillan, S., and Lantz, O. (2003). Selection of evolutionarily conserved mucosal-associated invariant T cells by MR1. Nature *422*, 164–169. https://doi.org/10.1038/nature01433.

Ugur, M., Kaminski, A., and Pabst, O. (2018). Lymph node γδ and αβ CD8+ T cells share migratory properties. Sci. Rep. *8*, 8986. https://doi.org/10.1038/s41598-018-27339-8.

Unutmaz, D., Xiang, W., Sunshine, M.J., Campbell, J., Butcher, E., and Littman, D.R. (2000). The primate lentiviral receptor Bonzo/STRL33 is coordinately regulated with CCR5 and its expression pattern is conserved between human and mouse. J. Immunol. *165*, 3284–3292. https://doi.org/10.4049/jimmunol.165.6.3284.

Worbs, T., Bode, U., Yan, S., Hoffmann, M.W., Hintzen, G., Bernhardt, G., Förster, R., and Pabst, O. (2006). Oral tolerance originates in the intestinal immune system and relies on antigen carriage by dendritic cells. J. Exp. Med. *203*, 519–527. https://doi.org/10.1084/jem.20052016.

Zhang, Y., Roth, T.L., Gray, E.E., Chen, H., Rodda, L.B., Liang, Y., Ventura, P., Villeda, S., Crocker, P.R., and Cyster, J.G. (2016). Migratory and adhesive cues controlling innate-like lymphocyte surveillance of the pathogen-exposed surface of the lymph node. eLife *5*, e18156. https://doi.org/10.7554/eLife.18156.

STAR★METHODS

KEY RESOURCES TABLE

REAGENT or RESOURCE	SOURCE	IDENTIFIER
Antibodies		
Rat IgM 17D1 (unconjugated)	Kind gift from Robert Tigelaar, Yale	N/A
Armenian Hamster IgG anti-mouse CCR6 (CD196) (PE/Dazzle™ 594 conjugated)	29-2L17 BioLegend	Cat# 129822; RRID: AB_2687019
Armenian Hamster IgG anti-mouse CCR6 (CD196) (APC conjugated)	29-2L17 BioLegend	Cat# 129814; RRID: AB_1877147
Armenian Hamster IgG anti-mouse CCR6 (CD196) (PE conjugated)	29-2L17 BioLegend	Cat# 129804; RRID: AB_1279137
Mouse anti-mouse CCR9 (CD199) (FITC conjugated)	CW-1.2 BioLegend	Cat# 128706; RRID: AB_1186167
Rat IgG2b, κ CD3 (AF700 conjugated)	17A2 BioLegend	Cat# 100216; RRID: AB_493697
Armenian Hamster IgG CD3 (BV421 conjugated)	145-2C11 BioLegend	Cat# 100341; RRID: AB_2562556
Armenian Hamster IgG1, κ anti-mouse CD3e (BUV395 conjugated)	145-2C11 BD Biosciences	Cat# 563565; RRID: AB_2738278
Rat anti-mouse CD3e (BUV737 conjugated)	17A2 BD Biosciences	Cat# 612803; RRID: AB_2870130
Rat anti-mouse CD4 (BV605 conjugated)	RM4-5 BioLegend	Cat# 100547; RRID: AB_11125962
Rat anti-mouse CD4 (PE/Cyanine7 conjugated)	RM4-5 BioLegend	Cat# 100528; RRID: AB_312729
Rat anti-mouse CD4 (BV711 conjugated)	GK1-5 BioLegend	Cat# 100447; RRID: AB_2564586
Rat anti-mouse CD8α (BV605 conjugated)	53-6.7 BioLegend	Cat# 100744; RRID: AB_2562609
Rat anti-mouse CD8α (BV711 conjugated)	53-6.7 BioLegend	Cat# 100759; RRID: AB_2563510
Rat anti-human/mouse CD11b (eF450 conjugated)	M1/70 Thermo Fisher Scientific	Cat# 48-0112-82; RRID: AB_1582236
Rat anti-mouse CD19 (APC/Cyanine7 conjugated)	6D5 BioLegend	Cat# 115530; RRID: AB_830707
Rat anti-mouse CD38 (PE/Cyanine7 conjugated)	90 BioLegend	Cat# 102718; RRID: AB_2275531
Rat anti-mouse/human CD44 (BV785 conjugated)	IM7 BioLegend	Cat# 103059; RRID: AB_2571953
Rat anti-mouse/human CD44 (PE/Cyanine7 conjugated)	IM7 Thermo Fisher Scientific	Cat# 25-0441-82; RRID: AB_469623
Rat anti-mouse CD44 (BV786 conjugated)	IM7 BD Biosciences	Cat# 563736; RRID: AB_2738395
Rat anti-mouse CD45 (APC conjugated)	30-F11 BioLegend	Cat# 103112; RRID: AB_312977
Mouse anti-mouse CD45.2 (Pacific Blue conjugated)	104 BioLegend	Cat# 109820; RRID: AB_492872
Mouse anti-mouse CD45.2 (BV510 conjugated)	104 BioLegend	Cat# 109837; RRID: AB_2561393
Mouse anti-mouse CD45.2 (BUV563 conjugated)	104 BD Biosciences	Cat# 741273; RRID: AB_2870814

(*Continued on next page*)

Continued

REAGENT or RESOURCE	SOURCE	IDENTIFIER
Rat anti-mouse/human CD45R (B220) (APC/Cyanine7 conjugated)	RA3-6B2 BioLegend	Cat# 103224; RRID: AB_313007
Rat anti-mouse CD62L (BV510 conjugated)	MEL-14 BioLegend	Cat# 104441; RRID: AB_2561537
Rat anti-mouse CD62L (BV605 conjugated)	MEL-14 BioLegend	Cat# 104437; RRID: AB_11125577
Rat anti-mouse CD62L (APC/Cyanine7 conjugated)	MEL-14 BioLegend	Cat# 104428; RRID: AB_830799
Rat anti-mouse CD62L (APC conjugated)	MEL-14 BioLegend	Cat# 104412; RRID: AB_313099
Rat anti-mouse CD62L (PE/Cyanine7 conjugated)	MEL-14 BioLegend	Cat# 104418; RRID: AB_313103
Anti-mouse L-Selectin (CD62L) InVivoMAb	MEL-14 Bio X Cell	RRID: AB_1107665; Cat# BE0021
Rat IgG2a isotype control InVivoMAb	2A3 Bio X Cell	Cat# BXC-BE0089- 1MG-INDUSTRIAL
Rat anti-mouse CD93 (BV650 conjugated)	AA4.1 BD Biosciences	Cat# 563807; RRID: AB_2738432
Armenian Hamster anti-mouse CD95 (Fas) (BV605 conjugated)	Jo2 BD Biosciences	Cat# 740367; RRID: AB_2740099
Rat anti-mouse CD138 (Syndecan-1) (BV785 conjugated)	281-2 BioLegend	Cat# 142534; RRID: AB_2814047
Armenian Hamster anti-mouse CXCR3 (CD183) (BV510 conjugated)	CXCR3-173 BioLegend	Cat# 126528; RRID: AB_2650922
Rat anti-mouse CXCR5 (CD185) (AF647 conjugated)	L138D7 BioLegend	Cat# 145532; RRID: AB_2734209
Rat anti-mouse CXCR6 (CD186) (BV421 conjugated)	SA051D1 BioLegend	Cat# 151109; RRID: AB_2616760
Rat anti-mouse CXCR6 (CD186) (AF647 conjugated)	SA051D1 BioLegend	Cat# 151115; RRID: AB_2721358
Rat anti-mouse CXCR6 (CD186) (PE conjugated)	SA051D1 BioLegend	Cat# 151104; RRID: AB_2566546
Rat anti-mouse CXCR6 (CD186) (PE/Dazzle™ 594 conjugated)	SA051D1 BioLegend	Cat# 151117; RRID: AB_2721700
Rat anti-mouse Eomes (PE/Cyanine7 conjugated)	Dan1mag eBioscience	Cat# 25-4875-82; RRID: AB_2573454
Anti-GFP Polyclonal Antibody (AF488 conjugated)	Thermo Fisher Scientific	Cat# A-21311; RRID: AB_221477
Rat anti-mouse/human GL-7 (AF647 conjugated)	GL7 BioLegend	Cat# 144606; RRID: AB_2562185
Rat anti-mouse GM-CSF (PE conjugated)	MP1-22E9 eBioscience	Cat# 12-7331-82; RRID: AB_466205
Rat anti-mouse IgD (AF488 conjugated)	11-26c.2a BioLegend	Cat# 405718; RRID: AB_10730619
Rat anti-mouse IgG1 (V450 conjugated)	A85-1 BD Biosciences	Cat# 562107; RRID: AB_10894002
Mouse anti-rat IgM (PE conjugated)	RM-7B4 eBioscience	Cat# 12-4342-82; RRID: AB_10668833
Rat anti-mouse IL-4 (PE conjugated)	11B11 Biolegend	Cat# 504104; RRID: AB_315318
Rat anti-mouse IL-17A (FITC conjugated)	TC11-18H10.1 BioLegend	Cat# 506907; RRID: AB_536009
Rat anti-mouse IL-17A (APC conjugated)	TC11-18H10.1 BioLegend	Cat# 506916; RRID: AB_536018

(*Continued on next page*)

Continued

REAGENT or RESOURCE	SOURCE	IDENTIFIER
Rat anti-mouse IL-17A (AF700 conjugated)	TC11-18H10.1 BioLegend	Cat# 506914; RRID: AB_536016
Mouse anti-mouse IL-17F (PE conjugated)	9D3.1C8 BioLegend	Cat# 517008; RRID: AB_10690818
Mouse anti-mouse IL-17F (AF488 conjugated)	9D3.1C8 BioLegend	Cat# 517006; RRID: AB_10661903
Mouse anti-mouse IL-17F (AF647 conjugated)	9D3.1C8 BioLegend	Cat# 517004; RRID: AB_2249030
Rat anti-mouse IL-18Ra (eF450 conjugated)	P3TUNYA eBioscience	Cat# 48-5183-82; RRID: AB_2574069
Rat anti-mouse IL-7R (BV421 conjugated)	A7R34 BioLegend	Cat# 135024; RRID: AB_11218800
Rat anti-human/mouse ITGβ7 (PerCP/Cyanine5.5 conjugated)	FIB27 BioLegend	Cat# 121008; RRID: AB_2129312
Rat anti-mouse IFNγ (BV605 conjugated)	XMG1.2 BioLegend	Cat# 505839; RRID: AB_2561438
Rat anti-mouse IFNγ (BV421 conjugated)	XMG1.2 BioLegend	Cat# 505830; RRID: AB_2563105
Rat anti-human/mouse Ki-67 (PE conjugated)	SolA15 eBioscience	Cat# 12-5698-82; RRID: AB_11150954
Mouse anti-human Ki-67 (PE/Cyanine 7 conjugated)	B56 BD Biosciences	Cat# 561283; RRID: AB_10716060
Mouse anti-mouse/human/rat Lck (AF647 conjugated)	3A5 Santa Cruz	Cat# sc-433; RRID: AB_627880
Rat anti-mouse Ly-6G (APC conjugated)	1A8 BioLegend	Cat# 127614; RRID: AB_2227348
Rat anti-mouse PD-1 (CD279) (PE conjugated)	RMP1-14 BioLegend	Cat# 114118; RRID: AB_2566726
Mouse Anti-Mouse RORγt (BV421 conjugated)	Q31-378 BD Biosciences	Cat# 562894; RRID: AB_2687545
Mouse anti-mouse SLAMF6 (Ly-108) (BV711 conjugated)	13G3 BD Pharmingen	Cat# 740823; RRID: AB_2740481
Armenian Hamster anti-mouse TCR β (FITC conjugated)	H57-597 BioLegend	Cat# 109206; RRID: AB_313429
Armenian Hamster anti-mouse TCR γ/δ (AF488 conjugated)	GL3 Biolegend	Cat# 118128; RRID: AB_2562771
Armenian Hamster anti-mouse TCR γ/δ (BV421 conjugated)	GL3 BioLegend	Cat# 118119; RRID: AB_10896753
Armenian Hamster anti-mouse TCR γ/δ (BV605 conjugated)	GL3 Biolegend	Cat# 118129; RRID: AB_2563356
Armenian Hamster anti-mouse TCR γ/δ (BUV805 conjugated)	GL3 BD Biosciences	Cat# 748989; RRID: AB_2873388
TotalSeq™-A0301 anti-mouse Hashtag 1	BioLegend	Cat# 155801; RRID: AB_2750032
TotalSeq™-A0302 anti-mouse Hashtag 2	BioLegend	Cat# 155803; RRID: AB_2750033
TotalSeq™-A0303 anti-mouse Hashtag 3	BioLegend	Cat# 155805; RRID: AB_2750034
Bacterial and virus strains		
Salmonella enterica serovar Typhimurium *Xen-33* Strain 1189	PerkinElmer	Cat# 119235
Staphylococcus aureus strain HG001	Kind gift from Knut Ohlsen, Würzburg	N/A
S. aureus USA300 LAC	Kind gift from Knut Ohlsen, Würzburg	N/A
Vaccinia virus	Kind gift from Jonathan Yewdell, NIH	N/A

(*Continued on next page*)

Continued

REAGENT or RESOURCE	SOURCE	IDENTIFIER
Chemicals, peptides, and recombinant proteins		
Absorbable Catgut suture	Ethicon	Cat# V301G
Acepromycin	CP Pharma	N/A
ß-Mercaptoethanol	Gibco	Cat# 31350010
Baytril (Enrofloxacin, 0.05%)	Bayer	N/A
Brain-Heart-Infusion Broth	Carl Roth	Cat# X916.1
Brefeldin A	Sigma Aldrich	Cat# B7651-5MG
Carprofen	Midas Pharma GmbH	Cat# 53716-49-7
Collagenase D	Roche	Cat# 11088882001
Dispase II	Roche	Cat# 04942078001
DNase I	Sigma Aldrich	Cat# DN25
DTT	Sigma Aldrich	Cat# 1.11474
EDTA	Carl Roth	Cat# 8043.2
Fetal Bovine Serum	Sigma-Aldrich	Cat# F7524-500ML
Fibrin sealant (TISSEEL, Fibrin Sealant kit with DUPLOJECT system)	Baxter	Cat# 1504516
Fluoromount-G	Invitrogen	00-4958-02
FTY720	Sigma-Aldrich	SML0700-25MG
GCWFS	Sigma-Aldrich	Cat# G7041
HEPES	Sigma-Aldrich	Cat# H0887-100ML
Ionomycin	Sigma-Aldrich	Cat# I0634-1MG
Isoflurane CP 1mL/mL	Piramal	400806.00.00 G136k21B
Ketamine	Pfizer	N/A
LB Broth Base	Invitrogen	Cat# 12780029
Liberase TL	Roche	Cat# 05401020001
L-Lysine	Sigma-Aldrich	Cat# L5501-100G
Mouse CD1d (mCD1d) PBS-57 loaded (BV421-conjugated)	NIH Tetramer Core Facility	N/A
Mouse CD1d (mCD1d) unloaded (BV421-conjugated)	NIH Tetramer Core Facility	N/A
Mouse MR1 5-OP-RU loaded (PE-conjugated)	NIH Tetramer Core Facility	N/A
Mouse MR1 6-FP loaded (PE-conjugated)	NIH Tetramer Core Facility	N/A
$NaIO_4$	Sigma-Aldrich	Cat# S1878
Normal Mouse Serum	Invitrogen	Cat# 10410
OCT freezing media	Sakura Finetek	Cat# 12351753
Paraformaldehyde	Carl Roth	Cat# 0335.3
Patent blue V	Sigma-Aldrich	Cat# 21605
Penicillin/Streptomycin	Sigma-Aldrich	Cat# P4333
Percoll	Sigma-Aldrich	Cat# P1644-1L
Phorbol 12-Myristate 13-Acetate	Sigma-Aldrich	Cat# P8139-1MG
RPMI medium	Gibco	Cat# 72400021
Sucrose	Sigma-Aldrich	Cat# 1.07687
Superfrost Plus object slides	VWR	Cat# 631-0108
Suture, 6-0 with beveled needle	Ethicon	Cat# V301G
Thermo Scientific™ Columbia Blood Agar with Sheep Blood Medium	Thermo Scientific	Cat# PB5008A
Triton-X 100	Carl Roth	Cat# 3051.2
Xylazine	CP Pharma	N/A
Critical commercial assays		
Cytofix/ Cytoperm	BD Biosciences	Cat# 554714
Foxp3/Transcription Factor Staining Buffer Set	eBioscience	Cat# 00-5523-00
IC Fixation Buffer	eBioscience	Cat# 00-8222-49

(*Continued on next page*)

Continued

REAGENT or RESOURCE	SOURCE	IDENTIFIER
LEGENDplex™ Multiple Assays	BioLegend	Customized panel
Permeabilization Buffer	Invitrogen	Cat# 00-8333-56
Zombie NIR™ Fixable Viability Kit	BioLegend	Cat# 423106
Deposited data		
Raw and processed mouse scRNA-sequencing data	This paper	GEO: GSE174629
Experimental models: Organisms/strains		
Mouse: C57BL/6J	Janvier Laboratories	RRID: IMSR_JAX:000664
Mouse: B6.129P2 Tcrd$^{tm1\ Mom}$/J	Kind gift of Prinz, I. Itohara et al. (1993)	RRID: IMSR_JAX:002120
Mouse: B6.129P2-Mr1^{tm1Gfn}	Kind gift of Lantz, O. Treiner et al. (2003)	RRID: MGI:3688620
Mouse: B6.129S4-*Cxcr3*^{tm1Arsa}/SoghJ	Kind gift of Satoskar A. https://www.jax.org/strain/023337 Oghumuet al. (2013)	RRID: IMSR_JAX:023337
Mouse: C.129-Il4^{tm1Lky}/J	Kind gift of D. Voehringer https://www.jax.org/strain/004190	RRID: IMSR_JAX:004190
Mouse: *Il23r*^{tm1Kuch}/J	Kind gift of A. Zernecke Awasthi et al. (2009)	RRID: IMSR_JAX:035863
Mouse: B6-Cd1^{tm1Gru}/J	Jackson laboratories http://www.informatics.jax.org/allele/MGI:1857482 Smiley et al. (1997)	RRID: MGI:2653847
Mouse: B6.129P2-*Cxcr6*^{tm1Litt}/J	Jackson laboratories https://www.jax.org/strain/005693 Unutmaz et al. (2000).	RRID: IMSR_JAX:005693
Mouse: B6.129P2-Il17a^{tm1Yiw} Il17f^{tm2Yiw}	Jackson laboratories http://www.informatics.jax.org/strain/MGI:3830065 Nakae et al. (2002); Ishigame et al. (2009)	RRID: MGI:3830065
Mouse: C57BL/6-Tg(UBC-GFP)30Scha/J	Jackson laboratories https://www.jax.org/strain/004353 Schaefer et al. (2001)	RRID: IMSR_JAX:004353
Mouse: B6.tg (*Venus*)	Swanson et al., 2016	N/A
Mouse: Myd88/Trif-/-	Kind gift of M. Gómez de Agüero https://www.jax.org/strain/005037 Hoebe et al. (2003)	RRID: IMSR_JAX:005037
Mouse: B6.129S6-Ccr6tm1(EGFP)Irw/J	Jackson laboratories https://www.jax.org/strain/013061 Kucharzik et al. (2002)	RRID: IMSR_JAX:013061
Mouse: B6;129S-*Gt(ROSA)26Sor*$^{tm1(CAG-COX8A/Dendra2)Dcc}$/J	Kindly gift of Beilhack, A. Jackson laboratories https://www.jax.org/strain/018385 Pham et al. (2012)	RRID: IMSR_JAX:018385
Mouse: B6.IL18R^{Tom}	This paper; Generated in cooperation with Ozgene	N/A
Software and algorithms		
Attune NxT Software	Thermo Fisher Scientific	RRID: SCR_019590
BD FACSDiva Software	BD Biosciences	RRID: SCR_001456
Biorender	Biorender	RRID: SCR_018361
Flowjo v10	BD Biosciences	RRID: SCR_008520
GraphPad Prism	GraphPad	RRID: SCR_002798
Imaris v8.3	Bitplane	RRID: SCR_007370

(*Continued on next page*)

Continued

REAGENT or RESOURCE	SOURCE	IDENTIFIER
Leica Las X	Leica	RRID: SCR_013673
Microsoft Excel	Microsoft	RRID: SCR_016137
Seurat	Stuart et al., 2019	RRID: SCR_007322
SpectroFlo	Cytek	https://cytekbio.com/pages/spectro-flo

RESOURCE AVAILABILITY

Lead contact

Further information and requests for resources and reagents should be directed to and will be fulfilled by lead contact, Wolfgang Kastenmüller, (wolfgang.kastenmueller@uni-wuerzburg.de).

Materials availability

B6.IL18R^{Tom} mouse line was generated in this study and is available from the lead contact upon request.

Data and code availability

- Single-cell RNA-seq data have been deposited at GEO and are publicly available as of the date of publication. Accession numbers are listed in the key resources table.
- The paper does not report original code.
- Any additional information required to reanalyze the data reported in this paper is available from the lead contact upon request.

EXPERIMENTAL MODEL AND SUBJECT DETAILS

Mice

C57BL/6J and Balb/c were originally purchased from Janvier Laboratories. B6.129P2 Tcrdtm1 Mom/J, MR1 KO (Cui et al., 2015), CXCR3-*GFP* (Oghumu et al., 2013), IL4-*GFP* (Mohrs et al., 2001), IL23R-*GFP* (Awasthi et al., 2009) and Myd88/Trif DKO mice were provided by Prinz I., Lantz O., Satoskar A., D. Voehringer, A. Zernecke, and M. Gomez de Agüero, respectively. B6.CD1dKO (Smiley et al., 1997), CXCR6-GFP (Unutmaz et al., 2000), IL-17A/F DKO (Haas et al., 2012), B6.Ubc-GFP, B6.Venus, B6.129S6-Ccr6tm1(EGFP)Irw/J and B6;129S-Gt(ROSA)26Sortm1.1(CAG-COX8A/Dendra2)Dcc/J (Pham et al., 2012) were originally purchased from Jackson Laboratories, and provided by Beilhack, A. All mice were maintained in specific-pathogen-free conditions at an Association for Assessment and Accreditation of Laboratory Animal Care-accredited animal facility. All procedures were approved by the North Rhine-Westphalia State Environment Agency and/or the Lower Franconia Government.

B6.IL18R^{Tom} mouse line was generated in co-operation with Ozgene and maintained under specific-pathogen-free conditions. Therefore, heterozygous mice were used as reporter mice and homozygous as functional knock-out. B6.IL18R^{Tom} mice were genotyped via flow cytometry. Blood samples were stained with αIL18R (P3TUNYA, eBioscience) and analyzed for tdTomato expression. Homozygous B6.IL18R^{Tom} mice showed a reduced surface expression of IL-18R and a lower sensitivity towards IL-18. Both male and female mice were used for this study. All the experimental groups were age and sex-matched (8-16 weeks old).

Bacterial and viral strains

Salmonella enterica serovar Typhimurium *Xen-33* Strain 1189 was originally purchased from Perkin Elmer (Cat# 119235). *Staphylococcus aureus* HG001 or USA300 LAC and Vaccinia virus were provided by Ohlsen, K. and Yewdell, J.W., respectively.

METHOD DETAILS

Infections

Staphylococcus aureus HG001 or USA300 LAC were diluted in sterile PBS. Mice were injected with an infectious dose of 1x10^8 CFU subcutaneously or intraperitoneally for 4 h, 8 h or 24 h, or intranasally for 6 h, or subcutaneously, intranasally or intravenously infected with 1x10^6 CFU or 1x10^7 CFU for 3 days or 20 days. For ectopic infection mice were anaesthetized, the flank was shaved and tape-stripped six times. 1x10^8 CFU were applied to this skin area. The infected area was protected for 6 h with aluminium foil.

Vaccinia virus was diluted in sterile PBS. Mice were subcutaneously or intranasally infected with 200 PFU for 3 days or with 2 x 10^3 PFU for 9 days. *Salmonella enterica* serovar Typhimurium *Xen 33* was diluted in sterile PBS. Mice were injected with an infectious dose of 1x10^8 CFU intravenously or 1x10^7 CFU subcutaneously for 4 h.

Bacterial counts

Lymph nodes (popliteal LN (sdLN) and mesLN) were harvested 8 h and 24 h after infection and were collected into cold PBS. LN homogenates were plated on Columbia Blood Agar with Sheep Blood Medium (Thermo Scientific) and incubated at 37°C for 12-16 hours. Single colonies were counted.

Photoactivation of skin cells

To photoactivate the skin and oral cavity of Dendra2 mice, the mice were anesthetized using Isoflurane (Piramal). First, the footpad skin was exposed to 405nm light (405nm Silver LED, Prizmatix; 0.5 NA polymer fiber with 1500 μm core diameter, Prizmatix; F671SMA-405 collimator, Thorlabs) 3 times for 10 seconds. The illumination was performed by moving the light in a distance of 0.2 – 0.5 cm while the other body parts were shielded. For oral cavity illumination, the tongue and inner side of the mouth were exposed to 405 nm light for 40 sec or 30 sec, respectively. 24 h after illumination, mice were sacrificed and the tissue draining LNs were collected and processed for flow cytometry analysis. Non-illuminated mice served as control.

FTY720 treatment

FTY720 (Sigma Aldrich) was injected i. v. (25 μg/100 μl PBS per mouse) 4, 2 and 0 days before illuminating the footpad skin of Dendra2 mice.

αCD62L *in vivo* blocking treatment

Mice were treated intraperitoneally with 100ug/mouse of InVivoMAb anti-mouse L-Selectin (CD62L) (Clone Mel-14, Bio X Cell) or InVivoMAb rat IgG2α isotype control (2A3, Bio X Cell) every day for 5 days before the infection, the day of the infection and the 3 following days after the infection.

In vitro PMA-Ionomycin activation

Lymphocytes were isolated from popliteal, inguinal, mediastinal, mesenteric lymph nodes or spleen and plated in a 96-well plate (TPP) at a final concentration of $5x10^6$ cells/ml in 200uL. Cell suspensions in RPMI medium (Gibco) enriched with 1% P/S (Sigma-Aldrich), 10% FCS (Sigma-Aldrich), 50 μM ß-Mercaptoethanol (Gibco) were plated and activated using 0.025 μg/mL Phorbol Myristate Acetate (PMA, Sigma-Aldrich), 1 μg/mL Ionomycin (Sigma-Aldrich) and cultured for 4h hours at 37°C. 1 μg/mL Brefeldin A (BFA, Sigma-Aldrich) was added to the medium.

Intravenous CD45 labeling

αCD45.2 PB (104, BioLegend) was injected i.v. (2 μg/100 μl PBS) 5 min before sacrificing the mice.

Flow cytometry

Surface staining of single cell suspension was performed for 30 min at 4°C. Surface stainings including 17D1 clone unconjugated antibody were performed for 20 min at 4°C after pre-incubation with surface marker antibodies and αTCR γ/δ (GL3, BioLegend) antibody for 30 min at 4°C. The cells were then incubated with a secondary αRat IgM (RM-7B4, eBioscience). Surface stainings including MR1 tetramer were performed for 30 min at room temperature before incubation with other surface marker antibodies. For intracellular staining, surface-stained cells were fixed and permeabilized using the Cytofix/Cytoperm kit (BD Biosciences) or Foxp3 staining kit (Invitrogen) for 30 min at 4°C. Zombie NIR™ (BioLegend) dye was used to discriminate between living and non-living cells. The following antibodies were used for staining: αCCR6 (29-2L17, BioLegend), αCCR9 (CW-1.2, BioLegend), αCD3 (17A2 or 145-2C11, BioLegend and BD Biosciences), αCD4 (GK1-5 or RM4-5, BioLegend), αCD8α (53-6.7, BioLegend), αCD11b (M1/70, Thermo Fisher Scientific), αCD19 (6D5, BioLegend), αCD38 (90, BioLegend), αCD44 (IM7, BioLegend, BD Biosciences or Thermo Fisher Scientific), αCD45 (30-F11, BioLegend), αCD45.2 (104, BioLegend or BD Biosciences), αCD45R (RA3-6B2, BioLegend), αCD62L (MEL-14, BioLegend), αCD93 (AA4.1, BD Biosciences), αCD95 (Jo2, BD Biosciences), αCD138 (281-2, BioLegend), αCXCR3 (CXCR3-173, BioLegend), αCXCR5 (L138D7, BioLegend), αCXCR6 (SA051D1, BioLegend), αEomes (Dan11mag, eBioscience), αGFP (Thermo Fisher Scientific), αGL-7 (GL7, Biolegend), αGM-CSF (MP1-22E9, eBioscience), αIgD (11-26c.2a, BioLegend), αIgG1 (A85-1, BD Biosciences), αIL-4 (11B11, BioLegend), αIL-17A (TC11-18H10.1, BioLegend), αIL-17F (9D3.1C8, BioLegend), αIL-7R (A7R34, BioLegend), αITGβ7 (FIB27, BioLegend), αIFNγ (XMG1.2, BioLegend), αKi-67 (SolA15 or B56, eBioscience or BD Biosciences), αLck (3A5, Santa Cruz), αLy6G (1A8, BioLegend), αPD-1 (RMP1-14, BioLegend), αRORγt (Q31-378, BD Biosciences), αSLAMF6 (13G3, BD Pharmingen), αTCR β (H57-597, BioLegend), αTCR γ/δ (GL3, BioLegend or BD Biosciences). Cells were washed twice with Perm/Wash buffer (Invitrogen) and subsequently stained with antibodies in Perm/Wash solution for 30 min at 4°C. After washing twice, cells were kept in Perm/Wash buffer until acquisition at a LSRFortessa™, FACSCanto™ II or FACSCelesta™ with FACSDiva™ software, Attune NxT (Thermo Fisher Scientific) with Attune NxT Flowcytometry Software and Cytek Aurora 5-Laser or 4-Laser (Cytek Biosciences) with SpectroFlo Software. FlowJo™ (BD Biosciences) software was used for the analysis. The clone 17D1 (rat IgM) was a kind gift from Robert Tigelaar, Yale, and CD1d (BV421) and MR1 (PE) tetramers purchased from NIH Tetramer Core Facility.

Isolation of mouse skin, lung and small intestine and adipose tissue-resident lymphocytes

For isolation of resident cells from the skin, the ears of the mice were isolated and separated in order to expose the dermis. For isolating the lung-resident cells, the lungs were pre-washed in cold PBS and chopped into small pieces. The ear skin and the lungs

were digested using 12.5 mg/mL Liberase™ TL (Roche) for 90 min at 37°C and for 45 min at 37°C, respectively. The digestion was stopped by diluting with cold PBS supplemented with 50μM β-Mercaptoethanol (Gibco). For the lung, red blood cells were lysed. The isolation of small intestine-resident cells was performed after removing the fat, the Payer's patches and the feces, and by exposing the internal side of the intestine. To isolate the intraepithelial lymphocytes (IELs), the small intestine pieces were incubated in RPMI supplemented with 1mM EDTA (Carl Roth), 10mM HEPES (Sigma-Aldrich), 5% DTT (Sigma-Aldrich) for 30 min at 37°C. To isolate the lamina propria lymphocytes, the intestinal pieces were digested with 1.5 mg/mL Collagenase D (Roche), 0.5 mg/mL Dispase II (Roche) and 20 μg/mL DNase I (Sigma-Aldrich) for 30 min at 37°C. Density gradient centrifugation (Percoll, Sigma-Aldrich) was used to purify the lymphocytes obtained from every organ as indicated by the manufacturer.

For isolation of resident cells from the adipose tissue, the inguinal lymph node was removed and the embedding adipose tissue was isolated. Next, the adipose tissue was chopped into small pieces and digested using 1 mg/ml Collagenase D (Roche), 20 μg/mL DNase I (Sigma-Aldrich) and 10 mM HEPES (Sigma-Aldrich) for 40 min at 37°C. The digestion was stopped by diluting with cold PBS supplemented with 50 μM β-Mercaptoethanol (Gibco).

Cytokine measurement in the culture supernatants

Cytokine production was assessed in the supernatant of single cell suspension isolated from different LNs (see the In vitro PMA-ionomycin activation section) using a bead-based immunoassay (LEGENDplex™) following the manufacturer instructions.

LN transplantation

For transplantations of mesLN into the popliteal fossa, BALB/c recipient mice were first anesthetized with ketamine (Pfizer) and xylazine (CP Pharma), then the skin of the popliteal fossa of the right hind leg was opened and the endogenous pLN and surrounding fat tissue were removed. mesLN collected from BALB/c donor mice was placed into the popliteal fossa, and the cut was sewn with absorbable suture (Ethicon). After 8 weeks when all lymphatic and blood vessel connections to the transplanted LN restored, transplanted mesLN was harvested for flow cytometry analysis. Successful engraftment of transplanted mesLN was assessed by footpad injection of 20 μl Patent V (25 mg/ml, Sigma-Aldrich) into CO_2-euthanized mice.

The transplantation of sdLNs into the mesenteric tissue was previously described (Shaikh et al., 2021). Briefly, recipient C57BL/6 mice were first anesthetized with ketamine (Pfizer), xylazine (CP Pharma) and acepromycin (CP Pharma) and their abdomen shaved. Mice were s.c. injected with the perioperative analgesic Carprofen 5 mg/kg (Midas Pharma GmbH) to relieve pain 30 min before opening the abdominal cavity and every 12 h up to the third day after the surgery if required. A 1-1.5 cm midline incision was made in the skin and in the peritoneum on the linea alba and the mesLN of the mice were excised with minimal fat and connective tissue avoiding excessive bleeding. Donor sdLNs (inguinal, axillary, and brachial) collected from B6.Ubc-GFP or B6.Venus mice were placed into the recipient's mesenteric tissue and joined using two-component fibrin glue TISSEEL (Baxter). The peritoneum and skin were closed with three and four non-consecutive stitches with coated VICRYL® (polyglactin 910) suture, respectively. The drinking water was supplemented with Baytril (Enrofloxacin, 0.05%) for 7 days after surgery to avoid infections. After 8 weeks, when all lymphatic and blood vessel connections to the transplanted LN restored, transplanted sdLNs was harvested for flow cytometry analysis.

Confocal microscopy

To perform confocal microscopy, LNs were isolated and fixed in PLP buffer (0.05 M phosphate buffer containing 0.1 M L-lysine (pH 7.4, Sigma-Aldrich), 2 mg/ml $NaIO_4$ (Sigma-Aldrich) and 10 mg/ml paraformaldehyde (Carl Roth) for 12 h at 4°C. Samples were dehydrated with 30% sucrose (Sigma-Aldrich) at 4°C overnight. Organs were embedded in OCT freezing media (Sakura Finetek) and stored at -80°C. Serial 30 μm sections were cut on a CM3050S cryostat (Leica) and adhered to Superfrost Plus object slides (VWR). After rehydration with PBS for 10 min at RT, sections were permeabilized and blocked with PBS containing 1% FCS (Sigma-Aldrich), 1% GCWFS (Sigma Aldrich), 0.3% Triton-X 100 (Carl Roth) and 1% normal mouse serum (Invitrogen) for 30 min at RT. Staining was performed in blocking buffer at 4°C overnight. Sections were washed with 0.1 M Tris buffer and mounted with Fluoromount-G (Invitrogen). Acquisition was performed on a Zeiss LSM 710 confocal microscope with ZEN acquisition control software or a Leica SP8 confocal microscope with LasX software. Confocal images were imported into Imaris (v8.3, Bitplane) for further analysis. The following antibodies were used for staining: αB220 (RM2628; ThermoFisher), αCD3 (17A2), αERT-R7 (sc-73355, Santa Cruz), αGFP (A21311; ThermoFisher), αTCR γ/δ (GL3, BioLegend).

Intravital microscopy

Mice were anesthetized, popliteal LNs were exposed, and intravital microscopy was performed using a protocol modified from a previous report (Kastenmüller et al., 2013). Raw imaging data were processed and analyzed with Imaris (Bitplane).

Hashtagging for scRNA-seq

To combine different lymph nodes for scRNA sequencing, single cell suspensions were generated and together with the antibody mix for sorting, a specific TotalSeq™ Antibody mix (Biolegend) was added and incubated for 30 minutes at 4°C. After enriching for the populations of interest, the different samples were mixed in a 1:1:1 ratio and further processed for sequencing.

scRNA-seq library preparation and sequencing

The population of interest were enriched using FACSAria III (BD Biosciences), before being encapsulated into droplets with the ChromiumTM Controller (10x Genomics) and processed following manufacturer's specifications. Transcripts captured in all the cells encapsulated with a bead were uniquely barcoded using a combination of a 16 bp 10x Barcode and a 10 bp unique molecular identifier (UMI). cDNA libraries were generated using the Chromium™ Single Cell 3' Library & Gel Bead Kit v2 for the CXCR6^{high}/CD44+ cells (Figure 4A) or v3 for the other samples (Figures 5D and 2B) (10x Genomics) following the detailed protocol provided by the manufacturer. Libraries were quantified by QubitTM 3.0 Fluometer (ThermoFisher) and quality was checked using 2100 Bioanalyzer with High Sensitivity DNA kit (Agilent). Libraries were sequenced with the NovaSeq 6000 platform (S1 Cartridge, Illumina) in 50 bp paired-end mode. The sequencing data was demultiplexed using CellRanger software (version 2.0.2). The reads were aligned to mouse mm10 reference genome using STAR aligner. Aligned reads were used to quantify the expression of mouse genes and generation of gene-barcode matrix. Subsequent data analysis was performed using Seurat R package (version 3.2) (Stuart et al., 2019).

Sample demultiplexing and doublet identification

To demultiplex hashing tags for each cell HTODemux function in Seurat package was used with standard parameters. Cross-sample doublet cell detection was performed based on hashtag signal. Cells that were classified as 'singlet' and identified by hashtags were retained and used for downstream analysis (Stoeckius et al., 2018).

scRNA-seq analysis

Quality control was performed, and viable cells were selected by excluding cells with UMI counts lower than 1000 and above 27000, as well as cells having more than 5% of mitochondrial transcripts for the steady state CXCR6^{high} CD44^{+} cells. For the 4 h post infection data set (Figure 5D) cells with UMI counts lower than 1000 and above 3800, as well as cells having more than 6% of mitochondrial transcripts and more then 22000 total transcripts were excluded. For the data set comparing lymph nodes (Figure 2B) cells with UMI counts lower than 800 and above 3000, as well as cells having more than 6% of mitochondrial transcripts and more then 12000 (resident) or 10000 (circulating) total transcripts were excluded. Circulating and resident samples (Figure 2B) were combined using the merge function in Seurat. 2000 most variable genes were used for downstream analysis to calculate principal components, after log-normalization and scaling. Principle component analysis (PCA) was used for dimensionality reduction and to visualize a uniform manifold approximation and projection (UMAP) of the identified clusters. For the sample generated 4 h post infection (Figure 5D) and the samples comparing distinct lymph nodes (Figure 2B), contaminating clusters containing B cells, monocytes and classical T cells were removed from the analysis based on marker genes.

Activation and Th scores was calculated using gene lists (Table S1D) with AddModuleScore function from Seurat.

QUANTIFICATION AND STATISTICAL ANALYSIS

Apart of the genomic data, all the biological data were analyzed using Prism 8 software (GraphPad) by two-tailed unpaired Student's *t*-test, Mann-Whitney test, one-way ANOVA tests or two-way ANOVA tests.

Immunity, Volume *55*

Supplemental information

Lymphatic migration of unconventional T cells promotes site-specific immunity in distinct lymph nodes

Marco A. Ataide, Konrad Knöpper, Paulina Cruz de Casas, Milas Ugur, Sarah Eickhoff, Mangge Zou, Haroon Shaikh, Apurwa Trivedi, Anika Grafen, Tao Yang, Immo Prinz, Knut Ohlsen, Mercedes Gomez de Agüero, Andreas Beilhack, Jochen Huehn, Mauro Gaya, Antoine-Emmanuel Saliba, Georg Gasteiger, and Wolfgang Kastenmüller

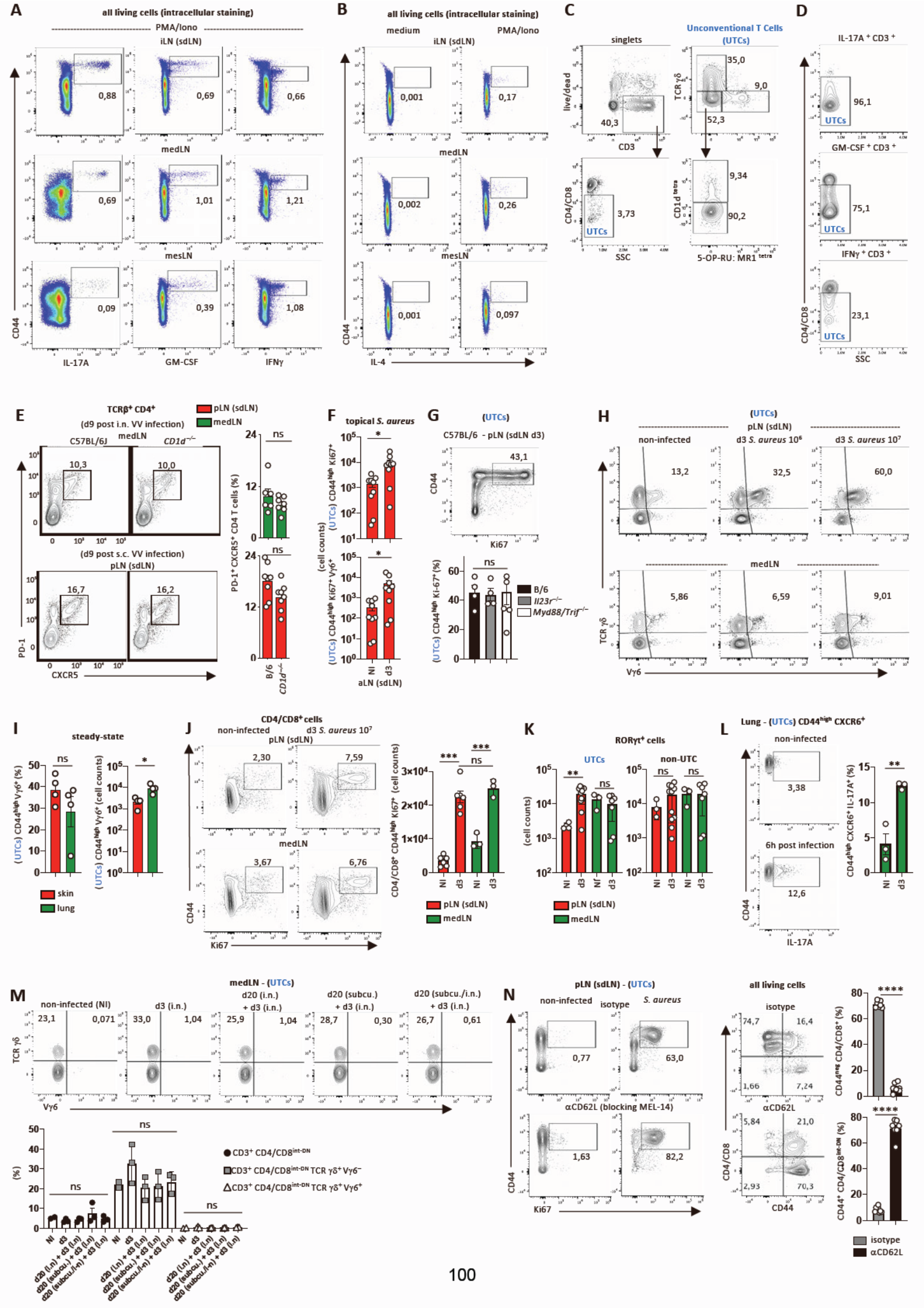
A
all living cells (intracellular staining)
PMA/Iono
iLN (sdLN)
medLN
mesLN
0,88
0,69
0,66
0,69
1,01
1,21
0,09
0,39
1,08
CD44
IL-17A
GM-CSF
IFNγ
B
all living cells (intracellular staining)
medium
PMA/Iono
iLN (sdLN)
medLN
mesLN
0,001
0,17
0,002
0,26
0,001
0,097
CD44
IL-4
C
singlets
Unconventional T Cells (UTCs)
live/dead
40,3
CD3
TCR γδ
35,0
9,0
52,3
CD4/CD8
3,73
UTCs
SSC
CD1d tetra
9,34
90,2
5-OP-RU: MR1 tetra
D
IL-17A + CD3 +
96,1
UTCs
GM-CSF + CD3 +
75,1
UTCs
IFNγ + CD3 +
23,1
UTCs
CD4/CD8
SSC
E
TCRβ+ CD4+
(d9 post i.n. VV infection)
pLN (sdLN)
medLN
C57BL/6J
CD1d−/−
10,3
10,0
(d9 post s.c. VV infection)
pLN (sdLN)
16,7
16,2
PD-1
CXCR5
PD-1+ CXCR5+ CD4 T cells (%)
ns
B/6
CD1d−/−
F
topical S. aureus
(UTCs) CD44high Ki67+
(UTCs) CD44high Ki67+ Vγ6+
(cell counts)
NI
d3
aLN (sdLN)
G
(UTCs)
C57BL/6 - pLN (sdLN d3)
43,1
CD44
Ki67
(UTCs) CD44high Ki-67+ (%)
ns
B/6
Il23r−/−
Myd88/Trif−/−
H
(UTCs)
pLN (sdLN)
non-infected
d3 S. aureus 10⁶
d3 S. aureus 10⁷
13,2
32,5
60,0
medLN
5,86
6,59
9,01
TCR γδ
Vγ6
I
steady-state
(UTCs) CD44high Vγ6+ (%)
(UTCs) CD44high Vγ6+ (cell counts)
skin
lung
J
CD4/CD8+ cells
non-infected
d3 S. aureus 10⁷
pLN (sdLN)
2,30
7,59
medLN
3,67
6,76
CD44
Ki67
CD4/CD8+ CD44high Ki67+ (cell counts)
pLN (sdLN)
medLN
K
RORγt+ cells
UTCs
non-UTC
(cell counts)
pLN (sdLN)
medLN
L
Lung - (UTCs) CD44high CXCR6+
non-infected
3,38
6h post infection
12,6
CD44
IL-17A
CD44high CXCR6+ IL-17A+ (%)
M
medLN - (UTCs)
non-infected (NI)
d3 (i.n.)
d20 (i.n.) + d3 (i.n.)
d20 (subcu.) + d3 (i.n.)
d20 (subcu./i.n.) + d3 (i.n.)
23,1
0,071
33,0
1,04
25,9
1,04
28,7
0,30
26,7
0,61
TCR γδ
Vγ6
(%)
CD3+ CD4/CD8int-DN
CD3+ CD4/CD8int-DN TCR γδ+ Vγ6−
CD3+ CD4/CD8int-DN TCR γδ+ Vγ6+
NI
d3
d20 (i.n.) + d3 (i.n.)
d20 (subcu.) + d3 (i.n.)
d20 (subcu./i.n.) + d3 (i.n.)
N
pLN (sdLN) - (UTCs)
non-infected
isotype
S. aureus
0,77
63,0
αCD62L (blocking MEL-14)
1,63
82,2
CD44
Ki67
all living cells
isotype
74,7
16,4
1,66
7,24
αCD62L
5,84
21,0
2,93
70,3
CD4/CD8
CD44
CD44neg CD4/CD8+ (%)
CD44+ CD4/CD8int-DN (%)
isotype
αCD62L

Supplementary Figure 1. Different LNs generate characteristic UTC-dependent immune responses, Related to Fig. 1

a/b) Flow cytometry-derived plots showing the cytokine production in all living cells from LNs (inguinal LN (sdLN), mediastinal LN (medLN) and mesenteric LN (mesLN)) stimulated with PMA (0,250 mg/ml) plus Ionomycin (1 mg/ml) for 4 h. **c/d)** Flow cytometry-derived plots showing the gating strategy used for UTCs, **c**) which are identified as $CD3^+$ CD4/$CD8^{int\text{-}DN}$ cells, and **d**) the UTCs % among the cytokine-producing cells. **e)** Flow cytometric quantification and statistical analysis of the T follicular helper cells (TfH; $CD4^+$ $CXCR5^+$ $PD\text{-}1^+$) in the sdLN and medLN from C57BL/6J and *Cd1d*$^{-/-}$ mice that were subcutaneously (s.c.) or intranasally (i.n.) infected with $2x10^3$ PFU of Vaccinia virus (VV) for 9 days. **f)** Statistical analysis of the flow cytometric quantification of proliferating UTCs from infected (d3) axillary LN (aLN) and control LN (NI) of C57BL/6J mice at 3 days post-topical infection with $1x10^8$ CFU of *S. aureus*. **g**) Flow cytometric quantification and statistical analysis of the proliferating UTCs in the sdLN from C57BL/6J, *Il23r* $^{-/-}$ and *Myd88/Trif* $^{-/-}$ mice that were s.c. infected with 10^7 CFU *S. aureus*. **h)** Representative plots from the flow cytometric analysis of proliferating UTCs in the pLN (sdLN) and medLN 3 days after s.c. or i.n. infection with 10^6 or 10^7 CFU *S. aureus.* **i)** Statistical analysis of the flow cytometric quantification of $V\gamma6^+$ γδ T cells in the footpad skin and the lung of C57BL/6J mice at steady state. The counts of $V\gamma6^+$ γδ T cells were normalized to number of cells per gram of tissue. **j)** Flow cytometric quantification and statistical analysis of the CD4/$CD8^+$ cells in the sdLN or medLN 3 days (d3) post-s.c. or -i.n. 10^7 CFU *S. aureus* infection of C57BL/6J mice. **k)** Statistical analysis of the flow cytometric quantification of sdLN and medLN lymph nodes of C57BL/6J mice that were not infected (NI) or intranasally or subcutaneously infected with $1x10^7$ CFU *S. aureus* for 3 days. **l)** Flow cytometric quantification and statistical analysis of the IL-17A-producing cells in the lung of C57BL/6J mice i.n. infected with 10^8 CFU *S. aureus* for 6 h. **m)** Flow cytometric and statistical analysis of the γδ T cells in the medLN of C57BL/6J mice that were infected s.c. ($1x10^7$ CFU) and/or i.n. ($1x10^6$ CFU) with *S. aureus* for 20 days (primary infection). Mice were re-challenged with *S. aureus* (10^6 CFU) i.n. (secondary infection), and 3 days after the medLN were harvested for analysis. **n)** Flow cytometric quantification and statistical analysis of the accumulation of $CD44^{high}$ $CD62L^-$ cells upon intraperitoneal (i.p.) anti-CD62L treatment and footpad infection of C57BL/6J mice with 10^7 CFU *S. aureus*. NI = non-infected. Data are showing one representative of two independent experiments (**a**, n = 3; **b**, n = 3; c, n = 4; **d,** n = 3 – 4; **e**, medLN B/6 n = 6; medLN *CD1d* $^{-/-}$ n = 7; pLN (sdLN) B/6 and *CD1d*$^{-/-}$, n = 8; **g**, B/6 and *Il23r* $^{-/-}$ n = 4, *Myd88* $^{-/-}$ n = 5; **h**, pLN (sdLN) n = 3; medLN n = 4; **i**, n = 4; **j,** pLN (sdLN) n = 6; medLN n = 3; **l**, n = 3; **m**, n = 3; **n**, NI n = 6; d3 n = 8) or three (**f,** n = 9), or two independent experiments (**k**, $n \geq 3$). Error bars indicate the mean ± s.e.m. Comparison between groups (**e, f, l, n**) was calculated using the unpaired Mann Whitney test $^{**}p \leq 0.001$; $^{****}p < 0.0001$or (**g, j, k, m**) the one-way ANOVA test. $^{**}p \leq 0.001$ $^{***}p \leq 0.0001$. See also Fig. 1.

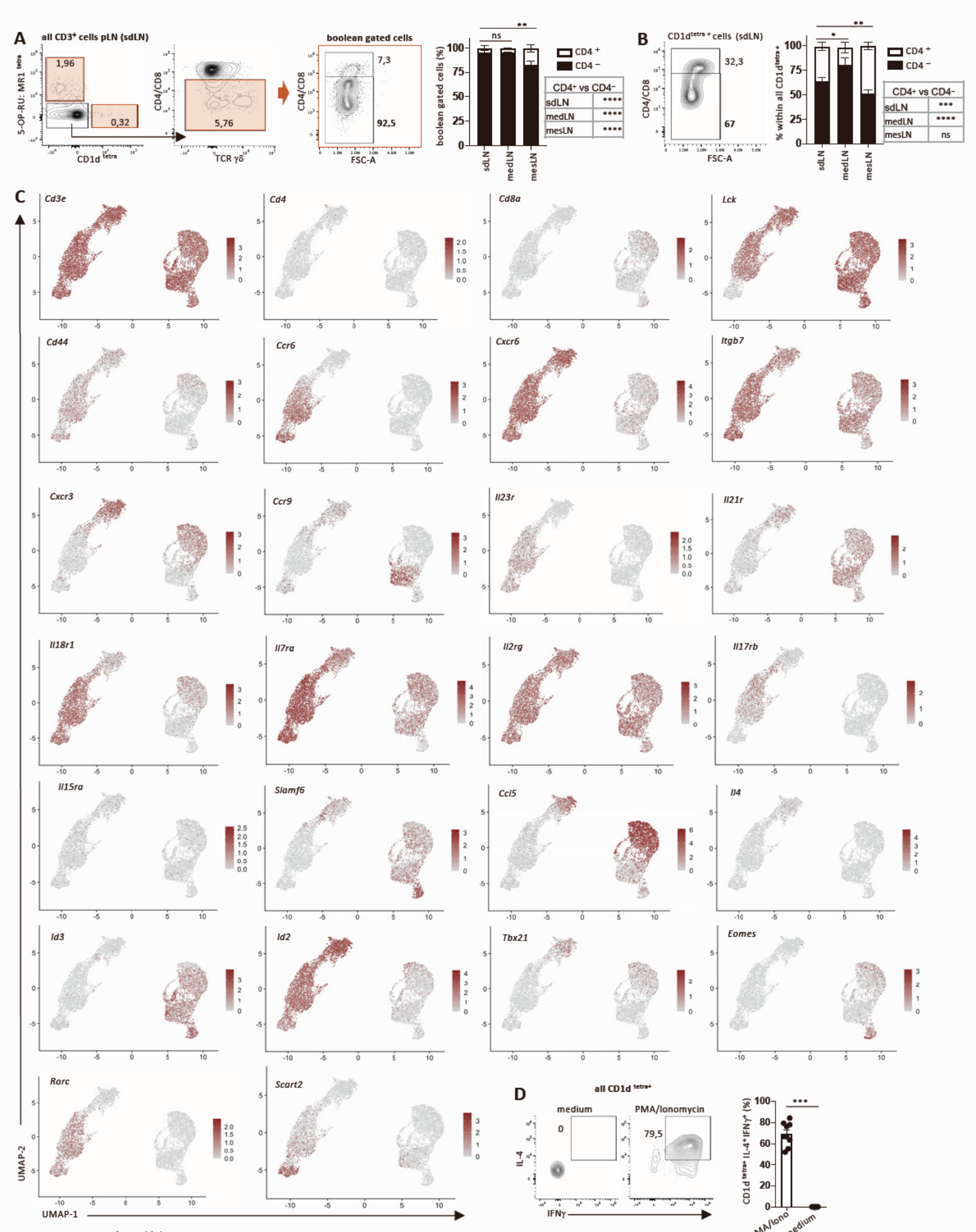
A
all CD3+ cells pLN (sdLN)
5-OP-RU: MR1 tetra
1,96
0,32
CD1d tetra
CD4/CD8
5,76
TCR γδ
boolean gated cells
7,3
92,5
FSC-A
boolean gated cells (%)
ns
**
CD4 +
CD4 −
CD4+ vs CD4−
sdLN ****
medLN ****
mesLN ****
B
CD1d tetra + cells (sdLN)
32,3
67
% within all CD1d tetra+
*
**
CD4+ vs CD4−
sdLN ***
medLN ****
mesLN ns
C
Cd3e
Cd4
Cd8a
Lck
Cd44
Ccr6
Cxcr6
Itgb7
Cxcr3
Ccr9
Il23r
Il21r
Il18r1
Il7ra
Il2rg
Il17rb
Il15ra
Slamf6
Ccl5
Il4
Id3
Id2
Tbx21
Eomes
Rorc
Scart2
UMAP-2
UMAP-1
D
all CD1d tetra+
medium
PMA/Ionomycin
0
79,5
IL-4
IFNγ
CD1d tetra+ IL-4+ IFNγ+ (%)
***
PMA/Iono
medium
E
CD3+ CD1d tetra+
(concatenated sdLN + medLN + mesLN)
47,1
CD4/CD8
CD1d tetra
clusters distribution CD1d tetra+ CD4+
(%)
CXCR3
CCR9
EOMES
remaining
CCR6
LCK neg
CXCR3
SLAMF6
remaining

Supplementary Figure 2. scRNA-seq reveals major differences in UTCs composition among lymph nodes, Related to Fig. 2

a/b) Flow cytometric analysis of CD4 expression among **a)** all UTCs in the skin draining LN (sdLN) and **b)** the $CD1d^{tetra+}$ cells in the sdLN, mediastinal LN (medLN) and mesenteric LN (mesLN) of C57BL/6J mice. **c)** Normalized gene-expression visualized for selected marker genes projected on the UMAP of all hashtagged and single cell-sequenced sdLN-, medLN- and mesLN- derived UTCs. **d)** Flow cytometric quantification and statistical analysis showing the IL-4 and IFNγ production in all $CD1d^{tetra+}$ cells stimulated with PMA (0,250 mg/ml) plus Ionomycin (1 mg/ml) for 4 h. Cells were isolated from the from the spleen of C57BL/6J mice. **e)** Flow cytometric quantification and statistical analysis of the CD4-expressing $CD1d^{tetra+}$ cells in the sdLN, medLN and mesLN of C57BL/6J mice. Data are showing one experiment from pooled mice (**c**, n = 10) or three independent experiments (**a**, **b,** n = 3; **d**, n = 9, **e**, n = 6). Error bars indicate the mean ± s.e.m. Comparison between groups was calculated (**a, b**) using the two-way ANOVA test. *$p \leq 0.01$; **$p \leq 0.001$; ****$p < 0.0001$; and (**d**) unpaired Mann Whitney test ***$p \leq 0.0001$. See also Fig. 2 and Table S1a.

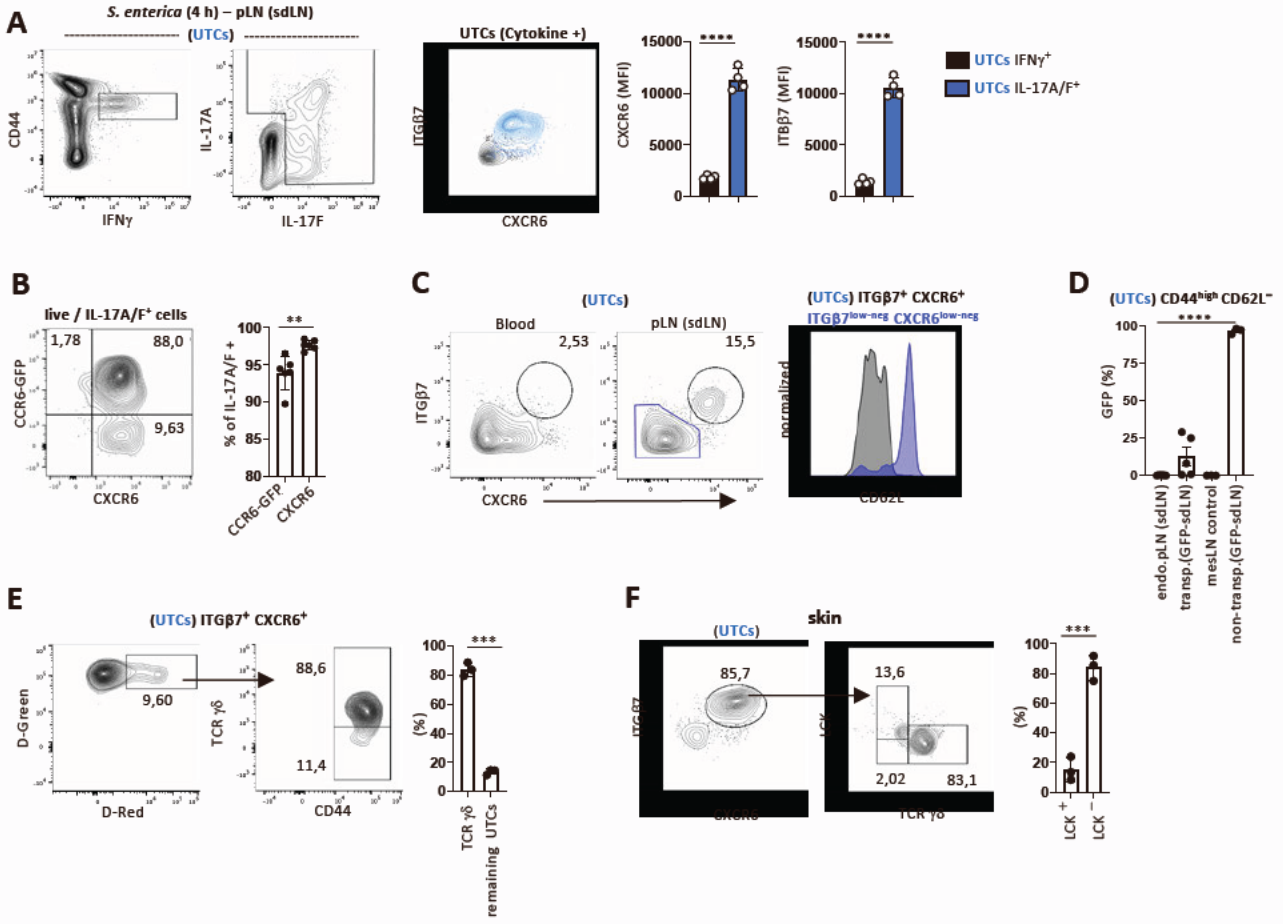
A
S. enterica (4 h) – pLN (sdLN)
(UTCs)
CD44
IFNγ
IL-17A
IL-17F
UTCs (Cytokine +)
ITGβ7
CXCR6
CXCR6 (MFI)
ITβ7 (MFI)
****
UTCs IFNγ+
UTCs IL-17A/F+
B
live / IL-17A/F+ cells
1,78
88,0
9,63
CCR6-GFP
CXCR6
% of IL-17A/F +
**
CCR6-GFP
CXCR6
C
(UTCs)
Blood
pLN (sdLN)
2,53
15,5
ITGβ7
CXCR6
(UTCs) ITGβ7+ CXCR6+
ITGβ7low-neg CXCR6low-neg
normalized
D
(UTCs) CD44high CD62L-
****
GFP (%)
endo.pLN (sdLN)
transp.(GFP-sdLN)
mesLN control
non-transp.(GFP-sdLN)
E
(UTCs) ITGβ7+ CXCR6+
9,60
D-Green
D-Red
88,6
11,4
TCR γδ
CD44
***
(%)
TCR γδ
remaining UTCs
F
skin
(UTCs)
85,7
13,6
2,02
83,1
LCK
TCR γδ
***
(%)
LCK+
LCK-

Supplementary Figure 3. UTCs continuously migrate from tissues to draining lymph nodes, Related to Fig. 3

a) Flow cytometric quantification and statistical analysis of pLN (sdLN) 4 h post- *S. enterica* infection. Contour plot (right) is the overlay of UTCs IL-17A/F^{+} (blue) and UTCs IFNγ^{+} (black) showing the CXCR6 and ITGβ7 expression. **b)** Flow cytometric quantification and statistical analysis of skin draining (sdLN) lymph nodes of C57BL/6J mice that were subcutaneously infected with 1x10^{7} CFU *S. aureus* for 4 h. **c)** Flow cytometry-derived plots comparing the relative frequency of the UTCs ITGβ7^{+} CXCR6^{+} in the popliteal LN (sdLN) and blood from C57BL/6J mice. Histograms show the CD62L expression among the UTC ITGβ7^{+} CXCR6^{+} population and within undefined UTCs. **d)** Statistical analysis comparing the frequency of GFP^{+} cells among the CD44^{high} CD62L^{-} UTCs of endogenous sdLN and control mesenteric LN (mesLN), and donor-derived sdLN transplanted into the mesenteries. The LNs were harvested and analyzed 8 weeks post-transplantation. **e)** Flow cytometric quantification and statistical analysis of the UTCs subsets among photoswitched (Dendra red^{+}) from the sdLN of Dendra2 mice. **f)** Flow cytometric quantification and statistical analysis of the LCK expression among UTCs from the skin of C57BL/6J mice. Data are showing one representative of two independent experiments (**a** = 4; **b**, n = 6; **c, d, f,** n = 3; **c**, n = 3 - 5). Error bars indicate the mean ± s.e.m. Comparison between groups was calculated (**c**) using the one-way ANOVA. ****$p < 0.0001$; and (**b, e, f**) using the unpaired Mann Whitney test **$p \leq 0.001$; ***$p \leq 0.0001$****$p < 0.0001$. See also Fig. 3

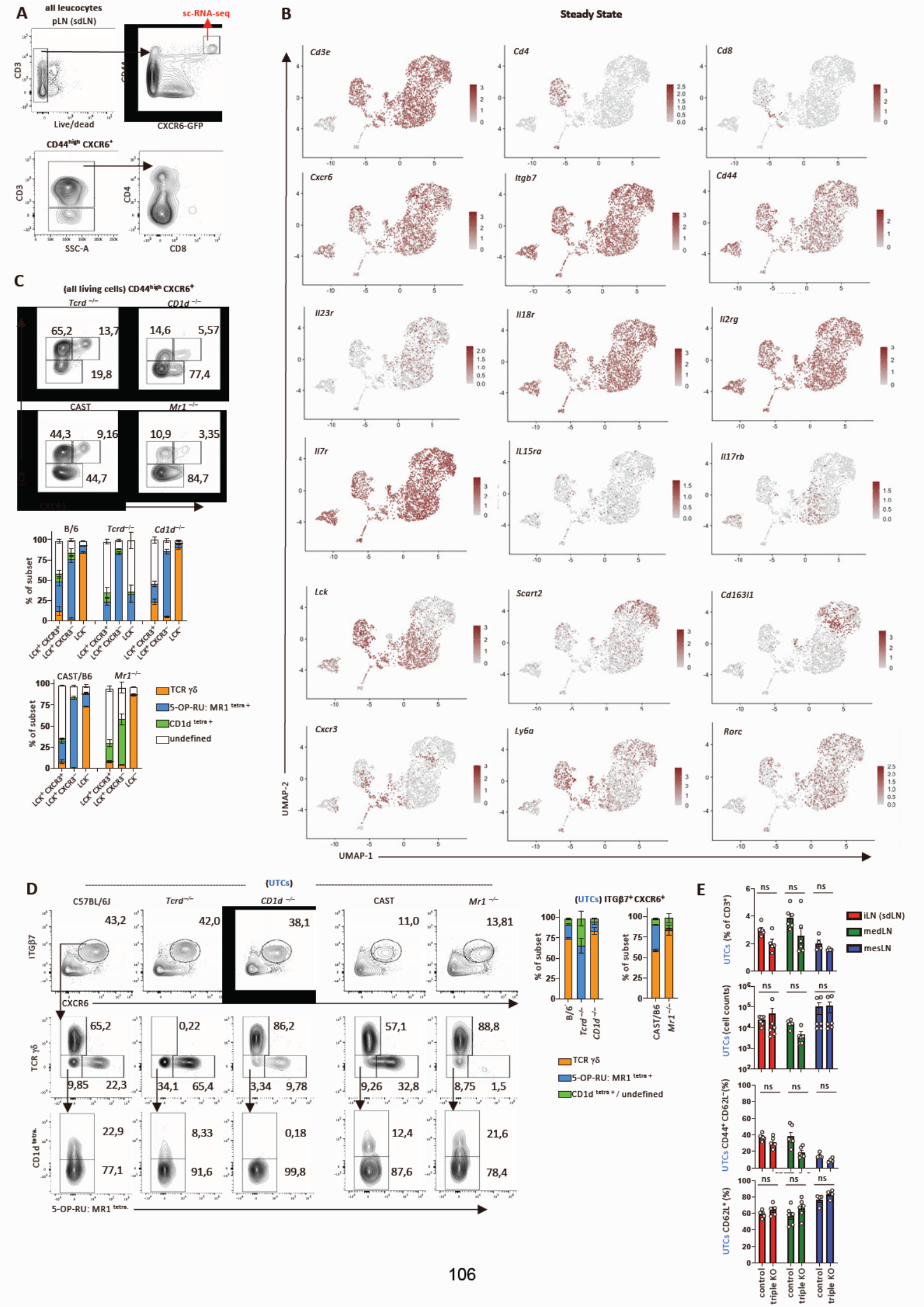
A
all leucocytes
pLN (sdLN)
sc-RNA-seq
CD3
Live/dead
CD4
CXCR6-GFP
CD44high CXCR6+
SSC-A
CD8
B
Steady State
Cd3e
Cd4
Cd8
Cxcr6
Itgb7
Cd44
Il23r
Il18r
Il2rg
Il7r
IL15ra
Il17rb
Lck
Scart2
Cd163l1
Cxcr3
Ly6a
Rorc
UMAP-2
UMAP-1
C
(all living cells) CD44high CXCR6+
Tcrd −/−
Cd1d −/−
65,2
13,7
19,8
14,6
5,57
77,4
CAST
Mr1 −/−
44,3
9,16
44,7
10,9
3,35
84,7
CXCR3
B/6
Tcrd−/−
Cd1d−/−
% of subset
LCK+ CXCR3+
LCK+ CXCR3−
LCK−
CAST/B6
Mr1−/−
TCR γδ
5-OP-RU: MR1 tetra +
CD1d tetra +
undefined
D
(UTCs)
C57BL/6J
Tcrd−/−
CD1d −/−
CAST
Mr1 −/−
ITGβ7
CXCR6
43,2
42,0
38,1
11,0
13,81
TCR γδ
65,2
0,22
86,2
57,1
88,8
9,85
22,3
34,1
65,4
3,34
9,78
9,26
32,8
8,75
1,5
CD1d tetra.
22,9
77,1
8,33
91,6
0,18
99,8
12,4
87,6
21,6
78,4
5-OP-RU: MR1 tetra.
(UTCs) ITGβ7+ CXCR6+
% of subset
B/6
Tcrd−/−
CD1d−/−
CAST/B6
Mr1−/−
TCR γδ
5-OP-RU: MR1 tetra +
CD1d tetra + / undefined
E
iLN (sdLN)
medLN
mesLN
UTCs (% of CD3+)
UTCs (cell counts)
UTCs CD44+ CD62L−(%)
UTCs CD62L+ (%)
ns
control
triple KO

Supplementary Figure 4. UTCs share the same homeostatic niche across lineages, Related to Fig. 4

a) Gating strategy used for sorting UTCs from popliteal LN (sdLN) for the steady-state scRNA-seq analysis. **b)** Normalized gene-expression visualized for selected marker genes projected on the UMAP of steady-state. **c)** Flow cytometric analysis showing the UTCs subsets and their lineage composition in steady-state sdLN (Fig. 4A) of C57BL/6J, *Tcrd*$^{-/-}$, *Cd1d*$^{-/-}$, *Mr1*$^{-/-}$, and B6-MAIT^{CAST} (CAST) mice. **d)** Flow cytometry-derived plots and quantification showing the refined gating strategy (CD3^{+} CD4/CD8$^{int\text{-}DN}$ ITGβ7^{+} CXCR6^{+}) and the lineage composition of UTCs in the skin draining LN (sdLN) at steady-state. Statistical analysis of the flow cytometric quantification of UTCs in the mesLN, medLN and sdLN from triple KO (*Tcrd*$^{-/-}$/*Mr1*$^{-/-}$/*Cd1d*$^{-/-}$) mice, and littermate control at steady-state. Data are showing pooled data from one experiment with pooled mice (**b,** n = 10), and one representative of three (**a, c, d,** n = 3) or two (**e**, n = ≥ 4) independent experiments. Error bars indicate the mean ± s.e.m. Comparison between groups was calculated (**e**) using the two-way ANOVA. See also Fig. 4 and Table S1b.

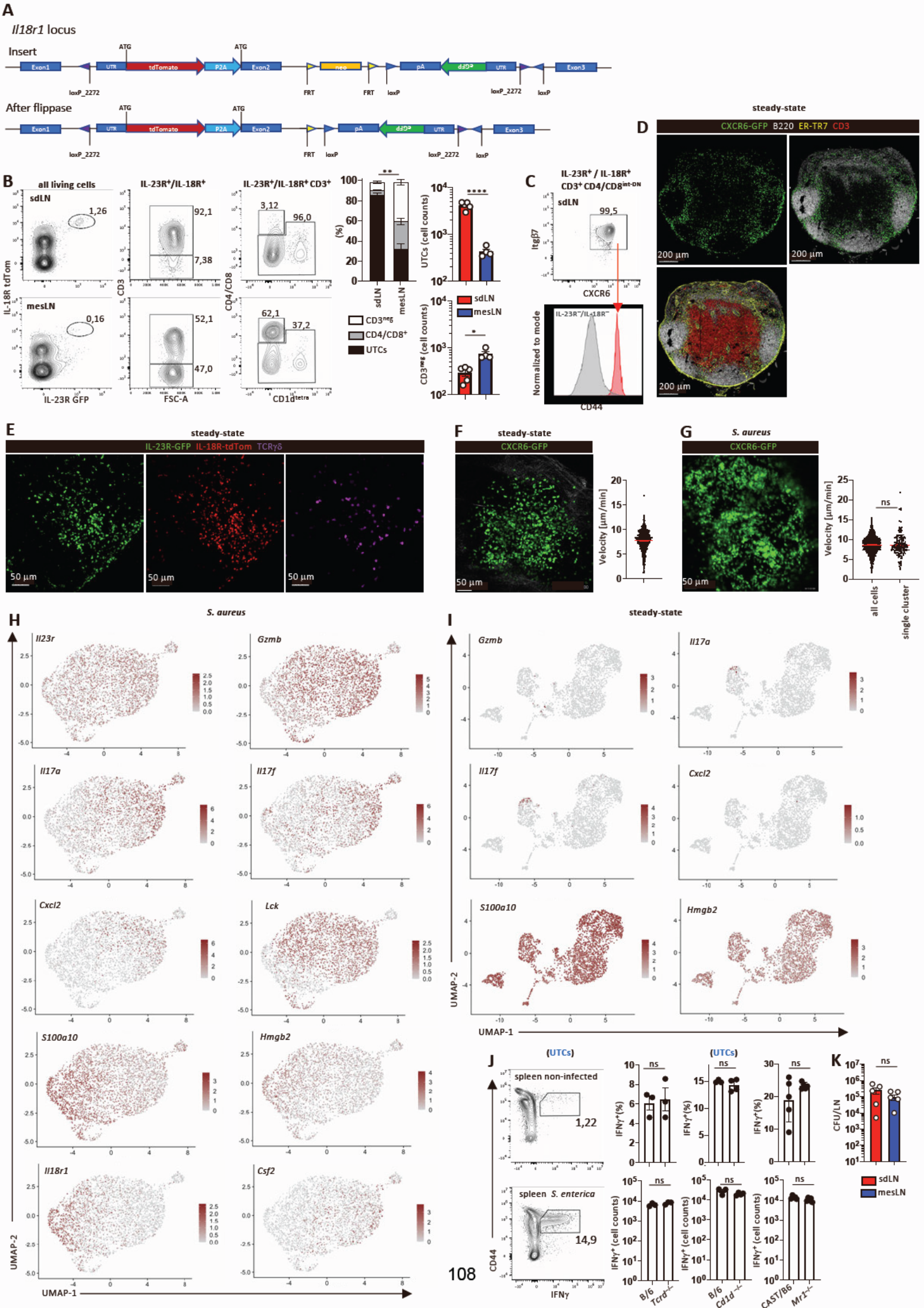
A
Il18r1 locus
Insert
After flippase
Exon1
Exon2
Exon3
tdTomato
P2A
neo
pA
eGFP
UTR
ATG
loxP_2272
FRT
loxP
B
all living cells
IL-23R+/IL-18R+
IL-23R+/IL-18R+ CD3+
sdLN
mesLN
IL-18R tdTom
IL-23R GFP
CD3
FSC-A
CD4/CD8
CD1d tetra
1,26
0,16
92,1
7,38
52,1
47,0
3,12
96,0
62,1
37,2
CD3neg
CD4/CD8+
UTCs
UTCs (cell counts)
CD3neg (cell counts)
C
IL-23R+ / IL-18R+
CD3+ CD4/CD8int-DN
Itgβ7
CXCR6
IL-23R−/IL-18R−
Normalized to mode
CD44
99,5
D
steady-state
CXCR6-GFP B220 ER-TR7 CD3
200 µm
E
steady-state
IL-23R-GFP IL-18R-tdTom TCRγδ
50 µm
F
steady-state
CXCR6-GFP
Velocity [µm/min]
G
S. aureus
CXCR6-GFP
ns
all cells
single cluster
H
S. aureus
Il23r
Gzmb
Il17a
Il17f
Cxcl2
Lck
S100a10
Hmgb2
Il18r1
Csf2
UMAP-1
UMAP-2
I
steady-state
Gzmb
Il17a
Il17f
Cxcl2
S100a10
Hmgb2
J
(UTCs)
spleen non-infected
1,22
spleen S. enterica
14,9
CD44
IFNγ
IFNγ+(%)
IFNγ+ (cell counts)
B/6
Tcrd−/−
B/6
Cd1d−/−
CAST/B6
Mr1−/−
K
CFU/LN
sdLN
mesLN
ns
108

Supplementary Figure 5. UTCs operate in functional units, Related to Fig. 5

a) Depiction of the modification of the *Il18r1* locus. The upper panel ("*Il18r1* locus") shows the original locus, the middle panel ("Insert") shows the locus after construct integration, containing a FRT-flanked neomycin-cassette. The lower panel ("After flippase") shows the construct after exertion of the neomycin. **b/c)** Flow cytometric quantification and statistical analysis of IL18R^{Tom+} IL23R^{GFP+} **b)** UTCs, conventional T and CD3 negative cells comparing the sdLN and the mesLN and **c)** the expression of ITGB7, CXCR6 and CD44 in the IL18R^{Tom+} IL23R^{GFP+} UTCs compartment. **d)** Confocal immunofluorescence image of a sdLN showing the microanatomical localization of CXCR6^{GFP+} CD3^{+} cells at steady state**. e)** Confocal immunofluorescence image of a skin-draining LN (sdLN) showing the microanatomical localization of the IL18R^{Tom+} IL23R^{GFP+} TCR γδ^{+} or TCR γδ $^{-}$ cells at steady state. **f)** Intravital sdLN image and statistical analysis of the migrational behavior of CXCR6^{GFP+} cells at steady state. **g)** Intravital sdLN image and statistical analysis of the migrational behavior of CXCR6^{GFP+} cells 4 h after *S. aureus* infection. **h/i)** Normalized gene-expression visualized for selected marker genes projected on the UMAP of **h)** 4 h post *S. aureus* infection and **i)** steady state scRNA-seq. **j)** *Ex vivo* flow cytometric analysis and statistical quantification of IFNγ production in the spleen 4 h after 10^8 CFU *S. enterica (Xen33)* intravenous infection of C57BL/6, *Tcrd*$^{-/-}$, *Cd1d*$^{-/-}$, *Mr1*$^{-/-}$, and B6-MAIT^{CAST} (CAST) mice. **k**) Colony-forming units (CFU) comparing the pLN (sdLN) and mesLN at 8 h post *S. aureus* (subcutaneous) and (intravenous) infection, respectively. Data are showing one representative of three independent experiments (**b**, sdLN n = 5, mesLN n = 4; **c**, n = 5; **d, f, g**, n = 3), or two independent experiments (**e**, n = 3; **j**, n = 3 - 5; **k**, n = 5), or one experiment with pooled mice (**h**, **i,** n = 10). Error bars indicate the mean ± s.e.m. Comparison between groups (**b, (left)**) was calculated using the one-way ANOVA test. ** $p \leq 0.001$; and (**b** (**right**)**, j, k**) using the unpaired Mann Whitney test * $p \leq 0.01$, **** $p < 0.0001$. See also Fig. 5, Table S1a/b and Videos S2/4.

Statement of individual author contributions and of legal second publication rights to manuscripts included in the dissertation

Manuscript 2 (complete reference): Ataide, M. A.*, Knöpper, K.*, Cruz de Casas, P.*,Ugur, M., Eickhoff, S., Zou, M., Shaikh, H., Trivedi, A., Grafen, A., Yang, T., Prinz, I., Ohlsen, K., Gomez de Agüero, M., Beilhack, A., Huehn, J., Gaya, M., Saliba, A. E., Gasteiger, G., Kastenmüller, W.; Lymphatic migration of unconventional T cells promotes site-specific immunity in distinct lymph nodes, *Immunity*, 2022, 55 (10): 1813-1828

*authors contributed equally

Participated in	**Author Initials,** Responsibility decreasing from left to right				
Study Design Methods Development	WK, MA, PCC, KK	MU, SE, AG, IP, AES	HS, AT, KO, MZ, MGA, AB, JH, MG, GG	TY	
Data Collection	PCC, KK, MA	HS, AT, AG, SE			
Data Analysis and Interpretation	MA, PCC, KK	MU, AT, MG, SE, AES, MZ			
Manuscript Writing Writing of Introduction Writing of Materials & Methods Writing of Discussion Writing of First Draft	WK, PCC, KK, MA	MU, GG			

Explanations (if applicable): PCC, KK and MA are the shared co-first authors, and contributed equally to each part of the manuscript preparation, revision and submission. WK is the primary supervisor.

If applicable, the doctoral researcher confirms that she/he has obtained permission from both the publishers (copyright) and the co-authors for legal second publication.

I hereby confirm that I have obtained permission from Elsevier publisher and shared first co-authors Marco Ataide and Konrad Knöpper for legal second publication. I also confirm Wolfgang Kastenmüller's (primary supervisor) acceptance.

The doctoral researcher and the primary supervisor confirm the correctness of the above mentioned assessment.

Paulina Cruz de Casas

Doctoral Researcher's Name | Date | Place | Signature

Konrad Knöpper

First co-author's name | Date | Place | Signature

Marco Ataide

First co-author's name | Date | Place | Signature

Prof. Dr. med. Wolfgang Kastenmüller

Primary Supervisor's Name | Date | Place | Signature

Statement of individual author contributions to figures/tables of manuscripts included in the dissertation

Manuscript 2 (complete reference): Ataide, M. A.*, Knöpper, K.*, Cruz de Casas, P.*,Ugur, M., Eickhoff, S., Zou, M., Shaikh, H., Trivedi, A., Grafen, A., Yang, T., Prinz, I., Ohlsen, K., Gomez de Agüero, M., Beilhack, A., Huehn, J., Gaya, M., Saliba, A. E., Gasteiger, G., Kastenmüller, W.; Lymphatic migration of unconventional T cells promotes site-specific immunity in distinct lymph nodes, *Immunity*, 2022, 55 (10): 1813-1828

*authors contributed equally

Figure	**Author Initials,** Responsibility decreasing from left to right				
1	MA, PC, KK	WK			
2	MA, PC, KK	WK			
3	MA, PC, KK	WK			
4	MA, PC, KK	WK			
5	MA, PC, KK	WK			
Table	**Author Initials,** Responsibility decreasing from left to right				
1 a-d	KK	WK, AES			
Videos	**Author Initials,** Responsibility decreasing from left to right				
S1 – S4	MA, SE	WK			

Explanations (if applicable): Main Figures 1-5 and associated Supplementary Figures 1-5, as well as Supplementary Tables 1 a-d, are considered in the contributions

If applicable, the doctoral researcher confirms that she/he has obtained permission from both the publishers (copyright) and the co-authors for legal second publication.

I hereby confirm that I have obtained permission from Elsevier publisher and co-authors Marco Ataide and Konrad Knöpper for legal second publication. I also confirm Wolfgang Kastenmüller's (primary supervisor) acceptance.

The doctoral researcher and the primary supervisor confirm the correctness of the above mentioned assessment.

Paulina Cruz de Casas

Doctoral Researcher's Name | Date | Place | Signature

Konrad Knöpper

Doctoral Researcher's Name | Date | Place | Signature

Marco Ataide

Doctoral Researcher's Name | Date | Place | Signature

Prof. Dr. med. Wolfgang Kastenmüller

Primary Supervisor's Name | Date | Place | Signature

Publishers copyright permissions

RightsLink

Sign in/Register

Lymphatic migration of unconventional T cells promotes site-specific immunity in distinct lymph nodes

Author:
Marco A. Ataide,Konrad Knöpper,Paulina Cruz de Casas,Milas Ugur,Sarah Eickhoff,Mangge Zou,Haroon Shaikh,Apurwa Trivedi,Anika Grafen,Tao Yang,Immo Prinz,Knut Ohlsen,Mercedes Gomez de Agüero,Andreas Beilhack,Jochen Huehn,Mauro Gaya et al.

Publication: Immunity

Publisher: Elsevier

Date: 11 October 2022

Journal Author Rights

Please note that, as the author of this Elsevier article, you retain the right to include it in a thesis or dissertation, provided it is not published commercially. Permission is not required, but please ensure that you reference the journal as the original source. For more information on this and on your other retained rights, please visit: https://www.elsevier.com/about/our-business/policies/copyright#Author-rights

BACK

CLOSE WINDOW

Summarising Discussion

Together, in our work we uncovered novel cell intrinsic and extrinsic roles of SL in modulating T cell function, thereby highlighting the importance of this pathway for lymphocyte biology. Previous studies have shown how the bioactive function of SL is dependent on their location within the cell or their secretion to the extracellular milieu. For these reasons, we hypothesized that PM SL would intrinsically modulate $CD8^+$ differentiation, whereas secreted SL would extrinsically regulate UTC migration. Our studies highlight the heterogeneous roles that one category of lipids can exert on T cell function. Here, we solely investigated the function of two members of the SL metabolism pathway in $CD8^+$ T cell differentiation and UTC migration, which are basic T cell functions. However, SL are comprised by numerous species and subspecies that should be investigated to understand the complete SL metabolism in T cells. Consistently, an in-depth characterization of the total lipidome in T cells would lay the foundation for the development of novel vaccination regimens and therapeutic approaches to treat various human conditions that involve the immune system.

Chapter I. The role of Smpdl3b in $CD8^+$ T cells.

Previous studies have depicted the role of various receptors, epigenetics, and metabolism in $CD8^+$ T cell differentiation from naïve to effector or memory populations[113]. However, the exact mechanism behind the fate decision of a naïve $CD8^+$ T cell is not completely clarified. Furthermore, limited studies have investigated the role of the PM in this process and have mainly focused on TCR activation events[175,184]. We hypothesized that SL metabolism could be involved in $CD8^+$ T cell differentiation since SM is the most abundant SL in the PM[185,186] and forms part of lipid rafts[127,128]. Therefore, we compared the SL profile of naïve, effector and memory (TCM and TEM) $CD8^+$ T cells and found a differing SL content between these populations. Moreover, we found that the enzyme sphingomyelin-phosphodiesterase acid-like 3b (Smpdl3b), a lipid-raft anchored phosphatase with supposed SMase activity, is crucial for the formation of memory $CD8^+$ T cells during an acute infection setting, and for the maintenance of $CX3CR1^-$ IL-$7R^+$ TCM and $CX3CR1^{int}$ IL-$7R^+$ TPM subpopulations. By making use of diverse functional assays, HPLC-MS/MS analysis and scRNA-seq datasets, we established that Smpdl3b regulates memory $CD8^+$ T cell survival via a SM-independent mechanism. Importantly, we and others have not been able to show SMase activity for Smpdl3b[187,188]. Nonetheless, our scRNA-seq data indicated that Smpdl3b regulates clathrin-mediated endocytosis and apoptosis processes by balancing the levels of *Hip1*, which encodes Huntingtin interacting protein 1 (Hip1). Hip1 modulates endocytosis and cell death by functioning as an adaptive protein between i) clathrin and other proteins involved in this endocytosis pathway[189], and ii) forming complexes where caspase 8 can be activated[190].

Recent studies have suggested functional similarities between Smpdl3b and its structural analog Smpdl3a[187]. Specifically, both enzymes act as phosphatases and nucleases[187,188,191], independent of SM. Interestingly, a new study from Hou *et al.* identified the physiological function of Smpdl3a as a cGAMP-degrading enzyme, hence regulating the cGAS-STING pathway and modulating innate immunity[192,193]. Moreover, Smpdl3b has also been described as a modulator of innate immunity through TLR3 and TLR4 signaling[188,194]. The similarities between Smpdl3a and Smpdl3b, in addition to the accumulation of Hip1 in Smpdl3b-deficient $CD8^+$ T cells, lead us to speculate its mechanism of

action. Likely, Smpdl3b acts as a protector of CD8$^+$ T cell memory formation during an acute infection by degrading extracellular cyclic dinucleotides (CDNs), such as cGAMP, released by apoptotic CD8$^+$ cells dying during the contraction phase, and by infected cells[113,195-197]. It has been shown that activation of the cGAS-STING pathway in CD8$^+$ T cells leads to apoptosis, following a similar kinetics than the Smpdl3b-deficient CD8$^+$ T cells (Chapter I. The role of Smpdl3b in CD8$^+$ T cells. Figure 3A)[198,199]. Hence, Smpdl3b might be expressed to protect the memory precursor and early memory CD8$^+$ T cells during the contraction phase of the CD8$^+$ T cell response, by degrading the large quantities of toxic CDNs released by dying cells, avoiding their internalization. Finally, Smpdl3b-deficiency leading to enhanced Hip1-mediated endocytosis, via a yet unknown mechanism, would lead to a defect in degrading these molecules and to the T cells endocytosing them, thus activating the STING pathway, leading to cell death. An additional mechanism could be the modulation of survival signaling pathways for memory CD8$^+$ T cells, such as IL-7 or IL-15. The loss of Smpdl3b leading to enhanced endocytosis could affect essential survival signaling pathways which rely on ligand-receptor endocytosis, thus leading to cell death[200-202].

Interestingly, the CX3CR1^{int} IL-7R$^+$ TPM subpopulation was most severely affected by the Smpdl3b-deficiency (Chapter I. The role of Smpdl3b in CD8$^+$ T cells. Figure 3A and Supplementary Figure 3F). Peripheral memory T cells (TPM) are defined as a self-renewing memory CD8$^+$ T cell subset that patrols non-peripheral tissues and SLO through CCR7[203]. Similarly, CX3CR1$^+$ non-classical monocytes express high levels of Smpdl3b[57,204] and patrol the microvasculature of non-lymphoid tissues[205-207]. Whether CX3CR1$^+$ monocytes are affected by Smpdl3b-deficiency is currently unknown and should be the focus of future studies. Nonetheless, the similar migratory behavior and role of these patrolling populations suggests that Smpdl3b could be important for their maintenance. Yet, our data indicates that Smpdl3b is not directly involved in cell migration, since the detected phenotype of the Smpdl3b-deficient CD8$^+$ T cells was equally observed in blood, SLO, salivary glands and small intestine (Chapter I. The role of Smpdl3b in CD8$^+$ T cells. Figure 3A and Supplementary Figure 3F). Interestingly, patrolling monocytes can be described as a more terminally differentiated population derived from their Ly6C$^+$ counterparts[208]. In accordance with our data, it is possible that Smpdl3b regulates the maintenance of less differentiated, stem-like populations such as Smpdl3b^{int} CX3CR1$^-$ IL-7R$^+$ TCM, Smpdl3b^{int} CX3CR1$^+$ IL-7R$^+$ TPM and Smpdl3b^{int} CX3CR1$^-$ Ly6C$^+$ monocytes by regulating their differentiation into more terminal populations, such as Smpdl3b^{high} CX3CR1$^+$ IL-7R$^-$ TEM and Smpdl3b^{high} CX3CR1$^+$ Ly6C$^-$ monocytes. The commonalities between T cell and monocyte populations deficient on Smpdl3b should be further investigated.

Chapter II. Lymphatic migration of unconventional T cells promotes site-specific immunity in distinct lymph nodes.

The configuration of the lymphatic system, with each tissue being connected to one or more dLNs, allows a constant flow of information reaching the LN and assessing the status of the tissue. MigDCs are the prime example of the importance of this connection, since they migrate via the afferent lymphatics to dLNs carrying tissue-specific antigens[23,51]. Furthermore, migDCs are imprinted by their tissue of origin, hence can program lymphocytes to specifically migrate to the affected tissue and exert their effector functions[65-67]. Our work shows how UTCs function as an additional link between tissues

and dLNs, and how they orchestrate LN-specific immune responses. In agreement with recent publications, we found that LNs draining distinct organs mount different immune responses, even towards the same stimulus or pathogen (Chapter II. Lymphatic migration of unconventional T cells promotes site-specific immunity in distinct lymph nodes. Figures 1 and 5; Appendix A. Review. Same yet different – how lymph node heterogeneity affects immune responses)[65,209]. Importantly, UTCs were largely responsible for the observed heterogeneous responses in distinct LNs. Intrigued by such a diverse group of cells influencing LN heterogeneity, we decided to further characterize UTCs in distinct tissues. As stated, UTCs differentiate already in the thymus into Th1-, Th2- and Th17-like cells[53,99]. Consistently with previous reports, we made use of scRNA-seq and flow cytometry to identify Th1-like UTCs in lung and small intestine, and Th17-like UTCs in skin and lung, and the respective dLNs of these organs[116,210,211] (Chapter II. Lymphatic migration of unconventional T cells promotes site-specific immunity in distinct lymph nodes. Figures 1, 2 and 3A). Hence, diverse UTC Th-like phenotypes reflect the observed cytokine profile of each dLN. Interestingly, we also found a naïve-like population of UTCs equally distributed in the analyzed LNs, suggesting no contribution to the observed LN heterogeneity. The origin of the Th-like differentiated UTCs in each dLN turned out to be the drained tissue. All UTC lineages (γδ T cells, MAIT and NKT) migrated through the lymphatics in a S1P/S1PR-dependent fashion, as previously reported for γδ T cells (Chapter II. Lymphatic migration of unconventional T cells promotes site-specific immunity in distinct lymph nodes. Figure 3)[33,68,69]. This striking finding is important because these cells are considered to be tissue-resident[27,53,99].

An additional interesting finding was that UTC individual lineages were not grouped as single clusters in our scRNA-seq analysis. Instead, each cluster contained a mixture of all lineages, and the segregation was due to other markers, such as chemokine or cytokine receptors. The observed homogeneity at a transcriptional level and shared migratory behavior (Chapter II. Lymphatic migration of unconventional T cells promotes site-specific immunity in distinct lymph nodes. Figures 2 and 3) indicated great similarities between UTC lineages. The different UTC lineages are historically studied as independent fields of research. However, recent studies suggest that these cells develop similarly and have overlapping functions in specific contexts[53,99,103,178]. Our work demonstrates that the distinct UTC lineages, including the less characterized αβ UTCs, are organized in functional units based on: i) transcriptional homogeneity (Chapter II. Lymphatic migration of unconventional T cells promotes site-specific immunity in distinct lymph nodes. Figure 2 and Supplementary Figure 2), ii) similar migratory behavior and location (Chapter II. Lymphatic migration of unconventional T cells promotes site-specific immunity in distinct lymph nodes. Figure 3E and G, Figure 5A and Supplementary Figure 5D-E), iii) cytokine-mediated activation and function (Chapter II. Lymphatic migration of unconventional T cells promotes site-specific immunity in distinct lymph nodes. Figure 5), and iiii) redundancy (Chapter II. Lymphatic migration of unconventional T cells promotes site-specific immunity in distinct lymph nodes. Figures 4 and 5).

In brief, our study shows how SL extrinsically mediate the migration of UTC functional units from tissues to dLNs via the S1P/S1PR1 axis in homeostatic conditions, and how this influences the heterogeneous immune responses mounted by individual LNs. Importantly, limited studies have studied the heterogeneity between distinct LNs[65-67], which lead us to write a Review to highlight the importance of this concept (Appendix A. Review. Same yet different – how lymph node heterogeneity affects

immune responses)[212]. Significantly, this ground-breaking study established how independently investigated cell lineages, that are considered tissue-resident populations, function as a group of cells that exhibit a common SL-dependent migratory pattern, both in homeostatic and inflammatory conditions. A comprehensive understanding of the physiological function of UTC migration from tissues to dLNs should be the focus of future studies.

Integration of chapters I and II: sphingolipid metabolism as a modulator of T cell biology via survival signaling pathways.

Taken together, our results highlight the importance of the SL metabolic pathway in modulating the basic biology of various T cell populations. Independently of regulating UTC migration from tissues to SLO, the S1P/S1PR1 signaling axis has been shown to modulate naïve and memory T cell survival[157,158]. Additionally, the survival roles of S1P have been reported in various settings[213-219]. Therefore, S1P is a crucial survival molecule for the homeostatic maintenance of naïve and memory Tconv. The high concentrations of S1P in blood and lymph modulate the transient migration of naïve Tconv that have reduced surface levels of S1PR1 (desensitization). Once naïve, and likely memory, Tconv access the LN, they stay for 12-24 hours searching for their cognate antigen[220]. When antigen is not encountered, Tconv upregulate S1PR1[138,143] in order to exit the LN by following the gradient towards the lymph. Importantly, within LNs a S1P gradient also exists, with low concentrations in the parenchyma and higher concentrations at exit sites – the cortical sinuses[136]. S1P also has important functions in positioning lymphocytes in the right location[42,221], similar to chemokines. Likely, the low-intermediate concentrations of LEC-derived S1P in LNs are enough for it to act as a survival factor, without inducing complete desensitization as in the blood and lymph[157,158]. Whether S1P/S1PR1 signaling is necessary for UTC survival is yet to be investigated. However, it could explain the migratory behavior of UTCs from tissues to dLNs during homeostatic conditions. Possibly, UTCs upregulate S1PR1 in tissues to migrate from a S1P-poor environment (tissues) via the S1P-rich lymphatics, where they downregulate surface S1PR1, similarly to naïve and memory Tconv. When accessing the S1P-low/intermediate dLNs, UTCs upregulate S1PR1. Hence, tissue-derived UTC migratory behavior (tissue-dLN.blood) might be essential to assure access to S1P, which acts as a survival molecule as it does for naïve and memory Tconv[157,158].

Considering that naïve CD8$^+$ T cells do not express Smpdl3b, whereas memory cells do, it is not obvious why Smpdl3b could be crucial for the S1P/S1PR1-mediated T cell survival (Chapter I. The role of Smpdl3b in CD8$^+$ T cells. Figure 2B). However, we and others have shown the phosphatase activity of Smpdl3b (Chapter I. The role of Smpdl3b in CD8$^+$ T cells. Figure 2E)[187,188]. Therefore, one possible mechanism could be that Smpdl3b degrades extracellular S1P to sphingosine to balance the S1P/S1PR signaling in the close proximity of the Smpdl3b$^+$ memory T cells, assuring the right amount of survival signaling and SLO egress. Nonetheless, the active site of Smpdl3b has not been reported to bind S1P[187], and sphingosine has been described as a pro-apoptotic molecule[120,222]. A more likely mechanism could be explained through the enhanced Hip1-mediated endocytosis suggested by our scRNA-seq analysis in the Smpdl3b KO cells. S1PR1 is internalized upon binding of S1P, but later recycled back into the cell surface[223,224]. Likely, the S1P/S1PR1 signaling axis could be affected in the Smpdl3b KO cells by enhanced internalization or impaired recycling back into the surface, thus hindering

this signaling pathway and provoking cell death. Accordingly, the need of S1P/S1PR1 signaling within the lymphatics for memory CD8$^+$ T cell survival matches the loss of TCM and TPM in Smpdl3b KO cells. TCM and TPM migrate between SLO and peripheral tissues, respectively. However, TEM exclusively recirculate between the blood and spleen[203], hence they might have distinct requirements for their maintenance. Finally, Smpdl3b could be exclusively required for memory CD8$^+$ T cells due to the differing membrane fluidity between naïve and memory populations. Memory CD8$^+$ T cells have been reported to have more and larger lipid rafts, thus different fluidity, when compared to their naïve counterparts[175]. By being a lipid-raft bound enzyme[187,188,225], Smpdl3b could be essential to guarantee adequate signaling events that would otherwise be altered by the presence of more lipid rafts in memory cells.

In line with the potential role of Smpdl3b affecting S1P-mediated signaling and survival, it has been shown that Smpdl3b$^+$ patrolling monocytes express S1PR5, while their classical counterparts do not[204]. Interestingly, one of the DEG between Smpdl3b WT and KO CD8$^+$ T cells from our scRNA-seq data was S1PR5, which is upregulated in the Smpdl3b KO cells (Chapter I. The role of Smpdl3b in CD8$^+$ T cells. Figure 6E). S1PR5 has the highest affinity for S1P[135] among all S1P receptors, and is essential for NK cell migration[226,227], the survival and circulation of patrolling monocytes[228], and an antagonist of TRM retention in tissues[229]. S1PR5 downregulation is induced by Tbet and Zeb2 to assure tissue residency of T cells[229]. In monocytes, Smpdl3b could be involved in regulating the intensity of the S1P/S1PR5 signaling pathway for migration and survival. Alternatively, Smpdl3b could be involved in modulating the surface levels of distinct S1PRs and balance these distinct signaling pathways in T cells and monocytes[135]. Thus, the loss of Smpdl3b could favor S1PR5 over S1PR1, hence affecting S1P/S1PR1 survival signaling in CD8$^+$ T cells. Describing whether S1PR5 is also downregulated in the presence of S1P, and whether it is involved in survival pathways, should be clarified.

Besides S1P acting as a pro-survival molecule, certain cytokines are crucial for the maintenance of distinct immune cell populations. For instance, IL-7 and IL-15 maintain memory CD8$^+$ T cells and UTCs homeostasis[10,230-234], while GM-CSF maintains monocytes[235]. Our data suggests that memory CD8$^+$ T cells, more specifically TCM and TPM, and UTCs require specific survival signaling, possibly via S1P or survival cytokines primarily in LNs. Thus, Smpdl3b could be involved in modulating this signaling axis in CD8$^+$ T cells by a yet unknown mechanism. Since patrolling monocytes do not access LNs in homeostatic conditions, it is likely that they are exposed to their survival molecules within the circulation. Importantly, the diverse function of each population is reflected in their location and migratory behavior, the latter assuring access to the required survival factors that would not be encountered by static populations.

Our findings reveal that utilizing the SL metabolism to modify T cell-mediated immune responses could be of great importance for improving the outcome of disease. Currently, several drugs have been approved to treat human diseases by manipulating the SL pathway. Examples are Fingolimod and Siponimod, used to treat MS by interfering with S1P-dependent migration of lymphocytes[152], or the off-target effects of antidepressants, such as amitriptyline, inhibiting acid sphingomyelinase (ASM)[182,236], which leads to a potential reduction of T cell-mediated inflammation[126]. An important recent publication by Zheng, X., *et al.* (2023) showed how the pharmacological modulation of ASM and neutral sphingomyelinase (NSM) activity in tumour infiltrating NK cells, in combination with immunotherapy,

improves the efficacy of antitumour immunity[237]. Another example is Rituximab, an approved monoclonal antibody (anti-CD20) used to treat B cell-mediated malignancies and to prevent antibody-mediated allograft rejection[238-240]. Off-targets of Rituximab are Smpdl3b *in vivo* and Asm *in vitro*[241,242]. Interestingly, some patients that experienced kidney transplantation and suffered of focal segmental glomerulosclerosis (FSGS) went into remission following Rituximab treatment. Smpdl3b is downregulated during FSGS, and the reversion of this phenotype by Rituximab seems to be beneficial[243]. Rituximab stabilizes Smpdl3b in the PM, having a protective effect for kidney diseases whose phenotype involves Smpdl3b downregulation[238,241,243]. Importantly, most of these treatments are used systemically. Hence, it is imperative to investigate their impact on specific T cell lineages (e.g. FTY720 and UTCs) and monocytes (Rituximab).

In conclusion, we propose that Smpdl3b activity and S1P-mediated migration from tissues to LNs are important for accessibility to survival signals required by memory $CD8^+$ T cells and tissue-derived UTCs, mainly within LNs. In depth characterisation of the SL pathway within distinct T cell populations during development, homeostasis, autoimmunity, and inflammation will allow the identification of potential specific targets to enhance or dampen T cell responses in a context-dependent and timely manner. Notably, the existence of already approved drugs directly or indirectly targeting this pathway, in combination with T cell specific-deficient models, will deepen our understanding in SL function in T cells. Remarkably, the development of molecules to specifically modulate the SL metabolism in T cells, rather than systemically, will only be achieved by understanding the SL metabolism in a spatiotemporal and context-specific fashion.

Limitations of the study

In this study, we unveiled novel intrinsic and extrinsic roles of SL for the basic biology of T cells. However, several limitations were encountered in both studies and will be highlighted in the following section.

Up to date, the SL research field still faces several technical challenges that limit our understanding of these molecules in distinct contexts. Methods for extracting and detecting whole cell-, organ-specific and organelle-specific SL are limited and require large cell numbers[125]. Additionally, specific antibodies targeting lipids for techniques such as imaging, flow cytometry or Western Blot are limited, owing to lipids being poorly immunogenic small molecules[244,245]. Besides these technical difficulties of the SL research field, an important biological challenge is the high interconnectivity of the SL pathway due to the various enzymes with opposing anabolic or catabolic functions on the same substrate (Chapter 1: Role of Smpdl3b in $CD8^+$ T cells. Figure 1A)[246-248]. As previously mentioned, several SL act as bioactive molecules in diverse contexts. Likely, the SL pathway is highly intertwined to facilitate the rapid production of certain species while bypassing the *de novo* synthesis pathway. Moreover, lipids are hydrophobic in nature, hence not easily secreted to the extracellular space to prevent disease-associated accumulation within the cell[122,248]. For instance, the Niemann-Pick disease is caused by mutations in the *ASM* gene provokes lysosomal SL accumulation and cellular disfunction[249]. Thus, the turnover and conversion of SL species function as a preventive mechanism for SL accumulation. However, this tight interconnection and precise regulation of the SL metabolism pose additional challenges for its comprehensive study. A main concern are compensatory mechanisms

between diverse isoforms of SL-modulating enzymes and various receptors for one same SL species expressed in mammalian cells[248,250-252]. In brief, the diversity and dynamics of the SL metabolism, alongside the technical limitations of lipid research, complicate their investigation in immune and non-immune cells. Despite the aforementioned limitations, we decided to investigate SL as modulators of basic T cell biology with two projects in which we also faced some challenges.

First, we describe the role of Smpdl3b as a modulator of memory and differentiation T cell survival in an acute infection setting. Here, we performed the first ever in-depth analysis comparing the sphingolipid profile of $CD8^+$ T cells with a distinct differentiation state. The aforementioned sphingolipidomics analysis was performed on SL extracted from whole cell lysates. Therefore, the organelle-specific differences within the SL composition of distinct populations of $CD8^+$ T cells, or between WT and Smpdl3b KO, cannot be directly appreciated in our setting. However, as we previously discussed, SL species are synthetized or degraded in specific location within cells, due to the defined location of the involved enzymes[253]. Hence, we could indirectly interpret that any potential differences in the amount of SM in, for instance the WT and Smpdl3b KO cells, would be due to the PM due to the location of the Smpdl3b within the membrane. Importantly, we saw no differences in any of the SL species between WT and KO cells. The greatest challenge of our sphingolipidomics analysis was the required number of cells. We performed our analysis on primary $CD8^+$ T cells isolated from spleen and LNs of acutely infected, or non-infected, mice. When isolating endogenous antigen-experienced $CD8^+$ T cells, obtaining the required numbers for naïve, effector and memory populations was not a limitation. Yet, for the comparison between WT and Smpdl3b KO cells we did not analyze the endogenous populations, but rather the TCR transgenic co-transferred cells. Thus, specially at a memory timepoint, obtaining the minimum number of cells required for the mass spectrometry analysis was difficult, specifically for Smpdl3b KO cells, and required pooling mice per each experiment. Moreover, each experiment was analyzed as an independent mass spectrometry run, hence the calibration of the standard controls might have differed, explaining the significant variation between WT and Smpdl3b KO sphingolipidomics experiments. A further limitation of this project was the lack of commercially available antibodies to validate the expression of Smpdl3b at a protein level via flow cytometry. Again, due to the cells being primary cells and being restricted by numbers, assessing protein expression via alternative methods (e.g. Western blot) would pose additional problems. Moreover, the information obtained at a single cell level with flow cytometry would also be lost with other techniques. Importantly, we validated that the enzyme is not only expressed, but also active, in $CD8^+$ T cells by using a phosphodiesterase activity assay. Overall, for this project, cell numbers were one of the greatest challenges and limitations. Unfortunately in this study we were not able to elucidate the mechanism and function of Smpdl3b. We and others exhaustively tested its sphingomyelinase or SL-degrading activities by using soluble, overexpressing, and physiological versions of the enzyme, yet were rather unsuccessful[187,188]. Owing to its structural similarity to Smpdl3a, and to both enzymes being phosphatases and nucleases, exploring the potential role of Smpdl3b as a cyclic di-nucleotide degrading enzyme should be considered[187,192]. One final important remark that has to be considered is that the Smpdl3b KO mice were generated within the European Conditional Mouse Mutagenesis Program (EUCOMM) in a C57BL6/N background[254] (Mouse Phenotype Database. “Gene Detail: MGI:1916022”. https://www.mousephenotype.org/data/genes/MGI:1916022). Then, we crossed them to P14.Venus

mice (B6.Cg-Tcra^{tm1Mom} Tg(TcrLCMV)327Sdz/TacMmjax x B6.tg (Venus)), which are in a C57BL6/J background. Therefore, our P14 Smpdl3b KO mice are in a mixed N and J background. By contrast, our P14 WT mice (B6.Cg-Tcra^{tm1Mom} Tg(TcrLCMV)327Sdz/TacMmjax x B6.tg (tdTomato)) were in a full C57BL/6J background. Despite the fact that these mouse strains are genetically very similar, they have some metabolic and behavioral differences[255]. Therefore, validating our experiments by using littermate controls or by backcrossing our WT and KO lines to have the same genetic backgrounds is crucial. Alternatively, confirming the Smpdl3b KO phenotype in endogenous CD8$^+$ T cells of full KO mice or bone marrow chimeras would clarify whether cells expressing TCRs with distinct affinities towards an antigen would be similarly affected by the lack of Smpdl3b.

Second, we delineated the S1P/S1PR-dependent migration of UTC functional units from tissues to dLNs in homeostatic conditions. As already mentioned, we investigated UTCs as a group, rather than separate entities. Since there are no specific markers that would allow us to selectively identify all of the UTC lineages while excluding other immune cell types, we are limited to define them as CD3$^+$ CD4$^-$ CD8$^-$. Additionally, we distinguish the different functional units based on classical markers for Th1 or Th17 conventional CD4$^+$ T cells, such as CXCR3 and CCR6, respectively[53,99], and on markers determined by our scRNA-seq data. In summary, a lack of UTC-functional unit exclusive markers hinders the development of mouse models to developmentally or conditionally knockout UTC functional units to further study their function. Another difficulty in this study was to show the direct evidence of S1P-dependent migration of UTCs from internal organs to their respective dLNs. As we showed, the skin and oral cavity photoconversion is easily accessible without the need for surgical intervention. However, the photoconversion of lung or small intestine UTCs to assess their presence in dLNs is technically challenging. Moreover, surgical intervention would induce inflammation and loss of homeostasis. An additional constraint for the UTC research field is that the physiological antigens recognized by the majority of UTCs have not yet been characterized[89]. Hence, studying the TCR-dependent immune responses of distinct UTC lineages within a functional unit is yet to be performed.

Both our studies on SL as modulators of T cell biology were exclusively performed using mouse models. Consequently, determining the translatability of our discoveries to humans is required and will be achieved by performing dedicated experiments using human samples. The murine and human immune systems differ in numerous aspects, such as genes and proteins expressed by immune cells, and also their function and abundance[88,89,256]. Additionally, the mice in our facility are kept in specific-pathogen free (SPF) conditions, meaning that the microbial agents that they are exposed to throughout their lives are defined. For our experiments, we typically infect animals with a single pathogen (e.g. LCMV or *S. aureus*) at a time to study the immune response. Evidently, this is not the reality in humans, given that throughout our lives we are constantly exposed to a great number of pathogens, even simultaneously[88]. For this reason, validating our findings by using mouse models that are closer to the human situation should be performed. An alternative could be using a model of laboratory mice denominated “wildlings”, which was recently developed by transferring embryos of C57BL/6 mice into wild mice[257]. The advantage of using the wildling mouse model is that they are genetically well-characterized, minimizing any genetic variations between littermates, while being exposed throughout their lives to a more “natural” microbiota mimicking the situation in humans. Hence, these mice seem to

be a more accurate model when studying translation to humans. Ultimately, assessing the SL profile and their effects in T cells from wildling mice should be considered.

Future directions

Evidently, the characterization of the SL profile of the various T cell lineages (Treg, Tconv, TRM, exhausted T cells, UTCs) during their development, differentiation and function ought to be the focus of subsequent studies. Furthermore, additional interesting studies could involve studying the SL profile mediating cell-to-cell interactions during, for example, antigen presentation.

Determining the physiological substrate and mechanism of action of Smpdl3b, and its connection to Hip1, is imperative. Likewise, studying the effects of its deficiency in additional cell types such as patrolling monocytes or $CD4^+$ T cells might help elucidating its physiological substrate and function. Particularly, studying the differentiation and function of Smpdl3b KO $CD4^+$ T cells would be of interest, since the kinetics of expression of *Smpdl3b* in this cell lineage is similar to $CD8^+$ T cells[204]. S1PR1/5 expression and downstream signaling events should be compared between Smpdl3b WT and deficient cell types, to identify its potential involvement in this survival signaling pathway[157,158].

Investigating whether UTCs require S1P signaling within dLNs for their survival, similarly to Tconv[157,158], should be clarified. Importantly, the rationale behind the homeostatic migration of UTCs from tissues to dLNs still has to be delineated. Likely, yet to be proven, the constant migration of UTCs to dLNs is a strategic mechanism to position rapid responders in the ideal environment to be activated and proliferate, to recruit other immune cells, and to prevent systemic spreading during an infection[37]. A follow-up query is the fate of tissue-derived UTCs in dLNs. Possibly, UTCs die, become LN-resident or egress dLNs to access the bloodstream and go back to the tissue of origin. In the context of acute inflammation of the skin, a specific subset of γδ T cells expands in dLNs and returns to the infected skin to fight the infection[258-260]. Conceivably, tissue-derived UTCs continuously migrate from tissues to dLNs and then return to their tissue of origin during homeostasis as an analogy to naïve Tconv that habitually patrol the bloodstream by circulating between SLOs. Finding recently recruited UTCs in tissues, following dLN egress during homeostasis is fairly challenging due to low cell numbers. Thus, manipulating UTCs migration by making use of S1PR1 and S1PR2 analogs or antagonists, respectively, might be an interesting strategy to increase their numbers and facilitate their identification[33].

In summary, SL research in immune cells is a field that should be pursued and be taken into consideration for the improvement of therapeutic and vaccination development and existing strategies.

References

1 LeBlanc, G., Kreissl, F. K., Melamed, J., Sobel, A. L. & Constantinides, M. G. The role of unconventional T cells in maintaining tissue homeostasis. *Semin Immunol* **61-64**, 101656 (2022). https://doi.org:10.1016/j.smim.2022.101656

2 Wynn, T. A. & Vannella, K. M. Macrophages in Tissue Repair, Regeneration, and Fibrosis. *Immunity* **44**, 450-462 (2016). https://doi.org:10.1016/j.immuni.2016.02.015

3 Julier, Z., Park, A. J., Briquez, P. S. & Martino, M. M. Promoting tissue regeneration by modulating the immune system. *Acta Biomater* **53**, 13-28 (2017). https://doi.org:10.1016/j.actbio.2017.01.056

4 Wiktor-Jedrzejczak, W. *et al.* Total absence of colony-stimulating factor 1 in the macrophage-deficient osteopetrotic (op/op) mouse. *Proceedings of the National Academy of Sciences* **87**, 4828-4832 (1990). https://doi.org:10.1073/pnas.87.12.4828

5 Reemst, K., Noctor, S. C., Lucassen, P. J. & Hol, E. M. The Indispensable Roles of Microglia and Astrocytes during Brain Development. *Frontiers in Human Neuroscience* **10** (2016). https://doi.org:10.3389/fnhum.2016.00566

6 Naik, S., Larsen, S. B., Cowley, C. J. & Fuchs, E. Two to Tango: Dialog between Immunity and Stem Cells in Health and Disease. *Cell* **175**, 908-920 (2018). https://doi.org:10.1016/j.cell.2018.08.071

7 Gonzalez, H., Hagerling, C. & Werb, Z. Roles of the immune system in cancer: from tumor initiation to metastatic progression. *Genes & Development* **32**, 1267-1284 (2018). https://doi.org:10.1101/gad.314617.118

8 Hiam-Galvez, K. J., Allen, B. M. & Spitzer, M. H. Systemic immunity in cancer. *Nature Reviews Cancer* **21**, 345-359 (2021). https://doi.org:10.1038/s41568-021-00347-z

9 Murphy, K., M., Weaver, Casey. *Janeway's immunobiology / Kenneth Murphy ; Casey Weaver. 9th edition.*, (New York : Garland Science, 2017, 2017).

10 Altan-Bonnet, G. & Mukherjee, R. Cytokine-mediated communication: a quantitative appraisal of immune complexity. *Nature Reviews Immunology* **19**, 205-217 (2019). https://doi.org:10.1038/s41577-019-0131-x

11 Legler, D. F. & Thelen, M. New insights in chemokine signaling. *F1000Research* **7**, 95 (2018). https://doi.org:10.12688/f1000research.13130.1

12 Hughes, C. E. & Nibbs, R. J. B. A guide to chemokines and their receptors. *The FEBS Journal* **285**, 2944-2971 (2018). https://doi.org:10.1111/febs.14466

13 Dustin, M. L. Integrins and Their Role in Immune Cell Adhesion. *Cell* **177**, 499-501 (2019). https://doi.org:10.1016/j.cell.2019.03.038

14 Luster, A. D., Alon, R. & Von Andrian, U. H. Immune cell migration in inflammation: present and future therapeutic targets. *Nature Immunology* **6**, 1182-1190 (2005). https://doi.org:10.1038/ni1275

15 Lianne *et al.* Yolk Sac Macrophages, Fetal Liver, and Adult Monocytes Can Colonize an Empty Niche and Develop into Functional Tissue-Resident Macrophages. *Immunity* **44**, 755-768 (2016). https://doi.org:10.1016/j.immuni.2016.02.017

16 Anderson, D. A., Dutertre, C.-A., Ginhoux, F. & Murphy, K. M. Genetic models of human and mouse dendritic cell development and function. *Nature Reviews Immunology* **21**, 101-115 (2021). https://doi.org:10.1038/s41577-020-00413-x

17 Radtke, D. & Voehringer, D. Granulocyte development, tissue recruitment, and function during allergic inflammation. *European Journal of Immunology* **53**, 2249977 (2023). https://doi.org:10.1002/eji.202249977

18 Sun, J. C. & Lanier, L. L. NK cell development, homeostasis and function: parallels with CD8+ T cells. *Nature Reviews Immunology* **11**, 645-657 (2011). https://doi.org:10.1038/nri3044

19 Lebien, T. W. & Tedder, T. F. B lymphocytes: how they develop and function. *Blood* **112**, 1570-1580 (2008). https://doi.org:10.1182/blood-2008-02-078071

20 Germain, R. N. T-cell development and the CD4–CD8 lineage decision. *Nature Reviews Immunology* **2**, 309-322 (2002). https://doi.org:10.1038/nri798

21 Ashby, K. M. & Hogquist, K. A. A guide to thymic selection of T cells. *Nature Reviews Immunology* (2023). https://doi.org:10.1038/s41577-023-00911-8
22 Ugur, M. *et al.* Lymph node medulla regulates the spatiotemporal unfolding of resident dendritic cell networks. *Immunity* **56**, 1778-1793.e1710 (2023). https://doi.org:10.1016/j.immuni.2023.06.020
23 Worbs, T., Hammerschmidt, S. I. & Förster, R. Dendritic cell migration in health and disease. *Nature Reviews Immunology* **17**, 30-48 (2017). https://doi.org:10.1038/nri.2016.116
24 Mass, E., Nimmerjahn, F., Kierdorf, K. & Schlitzer, A. Tissue-specific macrophages: how they develop and choreograph tissue biology. *Nature Reviews Immunology* **23**, 563-579 (2023). https://doi.org:10.1038/s41577-023-00848-y
25 Masopust, D. & Soerens, A. G. Tissue-Resident T Cells and Other Resident Leukocytes. *Annual Review of Immunology* **37**, 521-546 (2019). https://doi.org:10.1146/annurev-immunol-042617-053214
26 Ghaedi, M. & Takei, F. Innate lymphoid cell development. *J Allergy Clin Immunol* **147**, 1549-1560 (2021). https://doi.org:10.1016/j.jaci.2021.03.009
27 Fan, X. & Alexander. Hallmarks of Tissue-Resident Lymphocytes. *Cell* **164**, 1198-1211 (2016). https://doi.org:10.1016/j.cell.2016.02.048
28 Thomas, G., Tacke, R., Hedrick, C. C. & Hanna, R. N. Nonclassical Patrolling Monocyte Function in the Vasculature. *Arteriosclerosis, Thrombosis, and Vascular Biology* **35**, 1306-1316 (2015). https://doi.org:10.1161/atvbaha.114.304650
29 Merad, M., Sathe, P., Helft, J., Miller, J. & Mortha, A. The Dendritic Cell Lineage: Ontogeny and Function of Dendritic Cells and Their Subsets in the Steady State and the Inflamed Setting. *Annual Review of Immunology* **31**, 563-604 (2013). https://doi.org:10.1146/annurev-immunol-020711-074950
30 Stewart, R. H. A Modern View of the Interstitial Space in Health and Disease. *Frontiers in Veterinary Science* **7** (2020). https://doi.org:10.3389/fvets.2020.609583
31 Petrova, T. V. & Koh, G. Y. Biological functions of lymphatic vessels. *Science* **369** (2020). https://doi.org:10.1126/science.aax4063
32 Von Andrian, U. H. & Mempel, T. R. Homing and cellular traffic in lymph nodes. *Nature Reviews Immunology* **3**, 867-878 (2003). https://doi.org:10.1038/nri1222
33 Laidlaw, B. J., Gray, E. E., Zhang, Y., Ramírez-Valle, F. & Cyster, J. G. Sphingosine-1-phosphate receptor 2 restrains egress of γδ T cells from the skin. *Journal of Experimental Medicine* **216**, 1487-1496 (2019). https://doi.org:10.1084/jem.20190114
34 Zhang, Y. *et al.* Migratory and adhesive cues controlling innate-like lymphocyte surveillance of the pathogen-exposed surface of the lymph node. *Elife* **5** (2016). https://doi.org:10.7554/eLife.18156
35 Junt, T. *et al.* Subcapsular sinus macrophages in lymph nodes clear lymph-borne viruses and present them to antiviral B cells. *Nature* **450**, 110-114 (2007). https://doi.org:10.1038/nature06287
36 Cabeza-Cabrerizo, M., Cardoso, A., Minutti, C. M., Pereira Da Costa, M. & Reis E Sousa, C. Dendritic Cells Revisited. *Annual Review of Immunology* **39**, 131-166 (2021). https://doi.org:10.1146/annurev-immunol-061020-053707
37 Gasteiger, G., Ataide, M. & Kastenmüller, W. Lymph node – an organ for T-cell activation and pathogen defense. *Immunological Reviews* **271**, 200-220 (2016). https://doi.org:10.1111/imr.12399
38 Heesters, B. A., Myers, R. C. & Carroll, M. C. Follicular dendritic cells: dynamic antigen libraries. *Nature Reviews Immunology* **14**, 495-504 (2014). https://doi.org:10.1038/nri3689
39 Fletcher, A. L., Acton, S. E. & Knoblich, K. Lymph node fibroblastic reticular cells in health and disease. *Nature Reviews Immunology* **15**, 350-361 (2015). https://doi.org:10.1038/nri3846
40 Kastenmüller, W., Torabi-Parizi, P., Subramanian, N., Lämmermann, T. & Ronald. A Spatially-Organized Multicellular Innate Immune Response in Lymph Nodes Limits Systemic Pathogen Spread. *Cell* **150**, 1235-1248 (2012). https://doi.org:10.1016/j.cell.2012.07.021

41 Gray, E. E., Friend, S., Suzuki, K., Phan, T. G. & Cyster, J. G. Subcapsular Sinus Macrophage Fragmentation and CD169+ Bleb Acquisition by Closely Associated IL-17-Committed Innate-Like Lymphocytes. *PLoS ONE* **7**, e38258 (2012). https://doi.org:10.1371/journal.pone.0038258
42 Fang, V. *et al.* Gradients of the signaling lipid S1P in lymph nodes position natural killer cells and regulate their interferon-γ response. *Nature Immunology* **18**, 15-25 (2017). https://doi.org:10.1038/ni.3619
43 Qi, H., Kastenmüller, W. & Germain, R. N. Spatiotemporal Basis of Innate and Adaptive Immunity in Secondary Lymphoid Tissue. *Annual Review of Cell and Developmental Biology* **30**, 141-167 (2014). https://doi.org:10.1146/annurev-cellbio-100913-013254
44 Baratin, M. *et al.* T Cell Zone Resident Macrophages Silently Dispose of Apoptotic Cells in the Lymph Node. *Immunity* **47**, 349-362.e345 (2017). https://doi.org:10.1016/j.immuni.2017.07.019
45 Gray, E. E. & Cyster, J. G. Lymph Node Macrophages. *Journal of Innate Immunity* **4**, 424-436 (2012). https://doi.org:10.1159/000337007
46 Lewis, S. M., Williams, A. & Eisenbarth, S. C. Structure and function of the immune system in the spleen. *Science Immunology* **4**, eaau6085 (2019). https://doi.org:10.1126/sciimmunol.aau6085
47 Bronte, V. & Mikael. The Spleen in Local and Systemic Regulation of Immunity. *Immunity* **39**, 806-818 (2013). https://doi.org:10.1016/j.immuni.2013.10.010
48 Epelman, S., Kory & Gwendalyn. Origin and Functions of Tissue Macrophages. *Immunity* **41**, 21-35 (2014). https://doi.org:10.1016/j.immuni.2014.06.013
49 Lendeckel, U., Venz, S. & Wolke, C. Macrophages: shapes and functions. *ChemTexts* **8** (2022). https://doi.org:10.1007/s40828-022-00163-4
50 Sixt, M. *et al.* The Conduit System Transports Soluble Antigens from the Afferent Lymph to Resident Dendritic Cells in the T Cell Area of the Lymph Node. *Immunity* **22**, 19-29 (2005). https://doi.org:10.1016/j.immuni.2004.11.013
51 Itano, A. A. *et al.* Distinct Dendritic Cell Populations Sequentially Present Antigen to CD4 T Cells and Stimulate Different Aspects of Cell-Mediated Immunity. *Immunity* **19**, 47-57 (2003). https://doi.org:10.1016/s1074-7613(03)00175-4
52 Gasteiger, G., Fan, X., Dikiy, S., Lee, S. Y. & Rudensky, A. Y. Tissue residency of innate lymphoid cells in lymphoid and nonlymphoid organs. *Science* **350**, 981-985 (2015). https://doi.org:10.1126/science.aac9593
53 Constantinides, M. G. & Belkaid, Y. Early-life imprinting of unconventional T cells and tissue homeostasis. *Science* **374**, eabf0095 (2021). https://doi.org:10.1126/science.abf0095
54 Torcellan, T. *et al.* Circulating NK cells establish tissue residency upon acute infection of skin and mediate accelerated effector responses to secondary infection. *Immunity* (2023). https://doi.org:10.1016/j.immuni.2023.11.018
55 Schuster, I. S. *et al.* Infection induces tissue-resident memory NK cells that safeguard tissue health. *Immunity* **56**, 531-546 e536 (2023). https://doi.org:10.1016/j.immuni.2023.01.016
56 Mueller, S. N. & Mackay, L. K. Tissue-resident memory T cells: local specialists in immune defence. *Nature Reviews Immunology* **16**, 79-89 (2016). https://doi.org:10.1038/nri.2015.3
57 Auffray, C. *et al.* Monitoring of blood vessels and tissues by a population of monocytes with patrolling behavior. *Science* **317**, 666-670 (2007). https://doi.org:10.1126/science.1142883
58 Ginhoux, F. & Jung, S. Monocytes and macrophages: developmental pathways and tissue homeostasis. *Nature Reviews Immunology* **14**, 392-404 (2014). https://doi.org:10.1038/nri3671
59 Palomino-Segura, M., Sicilia, J., Ballesteros, I. & Hidalgo, A. Strategies of neutrophil diversification. *Nature Immunology* **24**, 575-584 (2023). https://doi.org:10.1038/s41590-023-01452-x
60 Aroca-Crevillén, A., Adrover, J. M. & Hidalgo, A. Circadian Features of Neutrophil Biology. *Frontiers in Immunology* **11** (2020). https://doi.org:10.3389/fimmu.2020.00576

61 Shi, F.-D., Ljunggren, H.-G., La Cava, A. & Van Kaer, L. Organ-specific features of natural killer cells. *Nature Reviews Immunology* **11**, 658-671 (2011). https://doi.org:10.1038/nri3065
62 Gallatin, W. M., Weissman, I. L. & Butcher, E. C. A cell-surface molecule involved in organ-specific homing of lymphocytes. *Nature* **304**, 30-34 (1983). https://doi.org:10.1038/304030a0
63 Druzd, D. *et al.* Lymphocyte Circadian Clocks Control Lymph Node Trafficking and Adaptive Immune Responses. *Immunity* **46**, 120-132 (2017). https://doi.org:10.1016/j.immuni.2016.12.011
64 Ugur, M., Kaminski, A. & Pabst, O. Lymph node γδ and αβ CD8+ T cells share migratory properties. *Scientific Reports* **8** (2018). https://doi.org:10.1038/s41598-018-27339-8
65 Brown, H., Komnick, M. R., Brigleb, P. H., Dermody, T. S. & Esterhazy, D. Lymph node sharing between pancreas, gut, and liver leads to immune crosstalk and regulation of pancreatic autoimmunity. *Immunity* **56**, 2070-2085 e2011 (2023). https://doi.org:10.1016/j.immuni.2023.07.008
66 Campbell, D. J. & Butcher, E. C. Rapid Acquisition of Tissue-specific Homing Phenotypes by CD4+ T Cells Activated in Cutaneous or Mucosal Lymphoid Tissues. *The Journal of Experimental Medicine* **195**, 135-141 (2002). https://doi.org:10.1084/jem.20011502
67 Mora, J. R. *et al.* Selective imprinting of gut-homing T cells by Peyer's patch dendritic cells. *Nature* **424**, 88-93 (2003). https://doi.org:10.1038/nature01726
68 Gray, E. E. *et al.* Deficiency in IL-17-committed Vγ4+ γδ T cells in a spontaneous Sox13-mutant CD45.1+ congenic mouse substrain provides protection from dermatitis. *Nature Immunology* **14**, 584-592 (2013). https://doi.org:10.1038/ni.2585
69 Nakamizo, S. *et al.* Dermal Vγ4 + γδ T Cells Possess a Migratory Potency to the Draining Lymph Nodes and Modulate CD8 + T-Cell Activity through TNF-α Production. *Journal of Investigative Dermatology* **135**, 1007-1015 (2015). https://doi.org:10.1038/jid.2014.516
70 Tomura, M. *et al.* Tracking and quantification of dendritic cell migration and antigen trafficking between the skin and lymph nodes. *Scientific Reports* **4** (2014). https://doi.org:10.1038/srep06030
71 Sheng, J. *et al.* Fate mapping analysis reveals a novel murine dermal migratory Langerhans-like cell population. *Elife* **10** (2021). https://doi.org:10.7554/eLife.65412
72 Abramson, J., Dobeš, J., Lyu, M. & Sonnenberg, G. F. The emerging family of RORγt+ antigen-presenting cells. *Nature Reviews Immunology* **24**, 64-77 (2024). https://doi.org:10.1038/s41577-023-00906-5
73 Tang, D., Kang, R., Coyne, C. B., Zeh, H. J. & Lotze, M. T. <scp>PAMP</scp>s and <scp>DAMP</scp>s: signal 0s that spur autophagy and immunity. *Immunological Reviews* **249**, 158-175 (2012). https://doi.org:10.1111/j.1600-065x.2012.01146.x
74 Fitzgerald, K. A. & Kagan, J. C. Toll-like Receptors and the Control of Immunity. *Cell* **180**, 1044-1066 (2020). https://doi.org:10.1016/j.cell.2020.02.041
75 Rehwinkel, J. & Gack, M. U. RIG-I-like receptors: their regulation and roles in RNA sensing. *Nature Reviews Immunology* **20**, 537-551 (2020). https://doi.org:10.1038/s41577-020-0288-3
76 Brunette, R. L. *et al.* Extensive evolutionary and functional diversity among mammalian AIM2-like receptors. *Journal of Experimental Medicine* **209**, 1969-1983 (2012). https://doi.org:10.1084/jem.20121960
77 Platnich, J. M. & Muruve, D. A. NOD-like receptors and inflammasomes: A review of their canonical and non-canonical signaling pathways. *Arch Biochem Biophys* **670**, 4-14 (2019). https://doi.org:10.1016/j.abb.2019.02.008
78 Janeway, C. A. & Medzhitov, R. Innate Immune Recognition. *Annual Review of Immunology* **20**, 197-216 (2002). https://doi.org:10.1146/annurev.immunol.20.083001.084359
79 Akira, S., Uematsu, S. & Takeuchi, O. Pathogen Recognition and Innate Immunity. *Cell* **124**, 783-801 (2006). https://doi.org:10.1016/j.cell.2006.02.015

80 Mogensen, T. H. Pathogen Recognition and Inflammatory Signaling in Innate Immune Defenses. *Clinical Microbiology Reviews* **22**, 240-273 (2009). https://doi.org:10.1128/cmr.00046-08
81 Hirayama, D., Iida, T. & Nakase, H. The Phagocytic Function of Macrophage-Enforcing Innate Immunity and Tissue Homeostasis. *International Journal of Molecular Sciences* **19**, 92 (2017). https://doi.org:10.3390/ijms19010092
82 Klose, C. S. N. & Artis, D. Innate lymphoid cells control signaling circuits to regulate tissue-specific immunity. *Cell Research* **30**, 475-491 (2020). https://doi.org:10.1038/s41422-020-0323-8
83 Vivier, E. & Malissen, B. Innate and adaptive immunity: specificities and signaling hierarchies revisited. *Nature Immunology* **6**, 17-21 (2005). https://doi.org:10.1038/ni1153
84 Chaplin, D. D. Overview of the immune response. *Journal of Allergy and Clinical Immunology* **125**, S3-S23 (2010). https://doi.org:10.1016/j.jaci.2009.12.980
85 Akkaya, M., Kwak, K. & Pierce, S. K. B cell memory: building two walls of protection against pathogens. *Nat Rev Immunol* **20**, 229-238 (2020). https://doi.org:10.1038/s41577-019-0244-2
86 Jameson, S. C. & Masopust, D. Understanding Subset Diversity in T Cell Memory. *Immunity* **48**, 214-226 (2018). https://doi.org:10.1016/j.immuni.2018.02.010
87 Sebina, I. & Pepper, M. Humoral immune responses to infection: common mechanisms and unique strategies to combat pathogen immune evasion tactics. *Current Opinion in Immunology* **51**, 46-54 (2018). https://doi.org:10.1016/j.coi.2018.02.001
88 Kumar, B. V., Connors, T. J. & Farber, D. L. Human T Cell Development, Localization, and Function throughout Life. *Immunity* **48**, 202-213 (2018). https://doi.org:10.1016/j.immuni.2018.01.007
89 Godfrey, D. I., Uldrich, A. P., McCluskey, J., Rossjohn, J. & Moody, D. B. The burgeoning family of unconventional T cells. *Nature Immunology* **16**, 1114-1123 (2015). https://doi.org:10.1038/ni.3298
90 van der Meer, J. W., Joosten, L. A., Riksen, N. & Netea, M. G. Trained immunity: A smart way to enhance innate immune defence. *Mol Immunol* **68**, 40-44 (2015). https://doi.org:10.1016/j.molimm.2015.06.019
91 Ratajczak, W., Niedzwiedzka-Rystwej, P., Tokarz-Deptula, B. & Deptula, W. Immunological memory cells. *Cent Eur J Immunol* **43**, 194-203 (2018). https://doi.org:10.5114/ceji.2018.77390
92 Bedoui, S., Gebhardt, T., Gasteiger, G. & Kastenmüller, W. Parallels and differences between innate and adaptive lymphocytes. *Nature Immunology* **17**, 490-494 (2016). https://doi.org:10.1038/ni.3432
93 Krangel, M. S. Mechanics of T cell receptor gene rearrangement. *Current Opinion in Immunology* **21**, 133-139 (2009). https://doi.org:10.1016/j.coi.2009.03.009
94 Melandri, D. *et al.* The gammadeltaTCR combines innate immunity with adaptive immunity by utilizing spatially distinct regions for agonist selection and antigen responsiveness. *Nat Immunol* **19**, 1352-1365 (2018). https://doi.org:10.1038/s41590-018-0253-5
95 Rigau, M. *et al.* Butyrophilin 2A1 is essential for phosphoantigen reactivity by gammadelta T cells. *Science* **367** (2020). https://doi.org:10.1126/science.aay5516
96 Chien, Y.-H., Meyer, C. & Bonneville, M. <scp>γδ</scp>T Cells: First Line of Defense and Beyond. *Annual Review of Immunology* **32**, 121-155 (2014). https://doi.org:10.1146/annurev-immunol-032713-120216
97 Silva-Santos, B., Pennington, D. J. & Hayday, A. C. Lymphotoxin-mediated regulation of gammadelta cell differentiation by alphabeta T cell progenitors. *Science* **307**, 925-928 (2005). https://doi.org:10.1126/science.1103978
98 Schmolka, N., Wencker, M., Hayday, A. C. & Silva-Santos, B. Epigenetic and transcriptional regulation of gammadelta T cell differentiation: Programming cells for responses in time and space. *Semin Immunol* **27**, 19-25 (2015). https://doi.org:10.1016/j.smim.2015.01.001

99 Pellicci, D. G., Koay, H.-F. & Berzins, S. P. Thymic development of unconventional T cells: how NKT cells, MAIT cells and γδ T cells emerge. *Nature Reviews Immunology* **20**, 756-770 (2020). https://doi.org:10.1038/s41577-020-0345-y
100 Van Rhijn, I., Godfrey, D. I., Rossjohn, J. & Moody, D. B. Lipid and small-molecule display by CD1 and MR1. *Nature Reviews Immunology* **15**, 643-654 (2015). https://doi.org:10.1038/nri3889
101 Bendelac, A. Positive selection of mouse NK1+ T cells by CD1-expressing cortical thymocytes. *The Journal of experimental medicine* **182**, 2091-2096 (1995). https://doi.org:10.1084/jem.182.6.2091
102 Seach, N. *et al.* Double Positive Thymocytes Select Mucosal-Associated Invariant T Cells. *The Journal of Immunology* **191**, 6002-6009 (2013). https://doi.org:10.4049/jimmunol.1301212
103 Legoux, F. *et al.* Microbial metabolites control the thymic development of mucosal-associated invariant T cells. *Science* **366**, 494-499 (2019). https://doi.org:10.1126/science.aaw2719
104 Lee, M. *et al.* Single-cell RNA sequencing identifies shared differentiation paths of mouse thymic innate T cells. *Nature Communications* **11** (2020). https://doi.org:10.1038/s41467-020-18155-8
105 Roche, P. A. & Furuta, K. The ins and outs of MHC class II-mediated antigen processing and presentation. *Nature Reviews Immunology* **15**, 203-216 (2015). https://doi.org:10.1038/nri3818
106 Zhu, J., Yamane, H. & Paul, W. E. Differentiation of Effector CD4 T Cell Populations. *Annual Review of Immunology* **28**, 445-489 (2010). https://doi.org:10.1146/annurev-immunol-030409-101212
107 Hsieh, C. S. *et al.* Development of TH1 CD4+ T cells through IL-12 produced by Listeria-induced macrophages. *Science* **260**, 547-549 (1993). https://doi.org:10.1126/science.8097338
108 Zheng, W.-P. & Flavell, R. A. The Transcription Factor GATA-3 Is Necessary and Sufficient for Th2 Cytokine Gene Expression in CD4 T Cells. *Cell* **89**, 587-596 (1997). https://doi.org:10.1016/s0092-8674(00)80240-8
109 Allen, J. E. & Sutherland, T. E. Host protective roles of type 2 immunity: parasite killing and tissue repair, flip sides of the same coin. *Semin Immunol* **26**, 329-340 (2014). https://doi.org:10.1016/j.smim.2014.06.003
110 Harrington, L. E. *et al.* Interleukin 17–producing CD4+ effector T cells develop via a lineage distinct from the T helper type 1 and 2 lineages. *Nature Immunology* **6**, 1123-1132 (2005). https://doi.org:10.1038/ni1254
111 Van Stipdonk, M. J. B., Lemmens, E. E. & Schoenberger, S. P. Naïve CTLs require a single brief period of antigenic stimulation for clonal expansion and differentiation. *Nature Immunology* **2**, 423-429 (2001). https://doi.org:10.1038/87730
112 Eickhoff, S. *et al.* Robust Anti-viral Immunity Requires Multiple Distinct T Cell-Dendritic Cell Interactions. *Cell* **162**, 1322-1337 (2015). https://doi.org:10.1016/j.cell.2015.08.004
113 Kaech, S. M. & Cui, W. Transcriptional control of effector and memory CD8+ T cell differentiation. *Nat Rev Immunol* **12**, 749-761 (2012). https://doi.org:10.1038/nri3307
114 Hansen, T. H. & Bouvier, M. MHC class I antigen presentation: learning from viral evasion strategies. *Nature Reviews Immunology* **9**, 503-513 (2009). https://doi.org:10.1038/nri2575
115 Ribot, J. C., Lopes, N. & Silva-Santos, B. γδ T cells in tissue physiology and surveillance. *Nature Reviews Immunology* **21**, 221-232 (2021). https://doi.org:10.1038/s41577-020-00452-4
116 Salou, M. *et al.* A common transcriptomic program acquired in the thymus defines tissue residency of MAIT and NKT subsets. *Journal of Experimental Medicine* **216**, 133-151 (2019). https://doi.org:10.1084/jem.20181483
117 Olszak, T. *et al.* Microbial exposure during early life has persistent effects on natural killer T cell function. *Science* **336**, 489-493 (2012). https://doi.org:10.1126/science.1219328

118 Sun, L., Su, Y., Jiao, A., Wang, X. & Zhang, B. T cells in health and disease. *Signal Transduction and Targeted Therapy* **8** (2023). https://doi.org:10.1038/s41392-023-01471-y
119 Ruterbusch, M., Pruner, K. B., Shehata, L. & Pepper, M. In Vivo CD4⁺T Cell Differentiation and Function: Revisiting the Th1/Th2 Paradigm. *Annual Review of Immunology* **38**, 705-725 (2020). https://doi.org:10.1146/annurev-immunol-103019-085803
120 Hannun, Y. A. & Obeid, L. M. Sphingolipids and their metabolism in physiology and disease. *Nature Reviews Molecular Cell Biology* **19**, 175-191 (2018). https://doi.org:10.1038/nrm.2017.107
121 Mielke, M. M. *et al.* Plasma Sphingomyelins are Associated with Cognitive Progression in Alzheimer's Disease. *Journal of Alzheimer's Disease* **27**, 259-269 (2011). https://doi.org:10.3233/jad-2011-110405
122 Gomez-Larrauri, A. *et al.* Role of bioactive sphingolipids in physiology and pathology. *Essays in Biochemistry* **64**, 579-589 (2020). https://doi.org:10.1042/ebc20190091
123 Peters, S., Fohmann, I., Rudel, T. & Schubert-Unkmeir, A. A Comprehensive Review on the Interplay between Neisseria spp. and Host Sphingolipid Metabolites. *Cells* **10** (2021). https://doi.org:10.3390/cells10113201
124 Merrill, A. H. De Novo Sphingolipid Biosynthesis: A Necessary, but Dangerous, Pathway. *Journal of Biological Chemistry* **277**, 25843-25846 (2002). https://doi.org:10.1074/jbc.r200009200
125 Lee, M., Lee, S. Y. & Bae, Y. S. Functional roles of sphingolipids in immunity and their implication in disease. *Exp Mol Med* **55**, 1110-1130 (2023). https://doi.org:10.1038/s12276-023-01018-9
126 Hartel, J. C., Merz, N. & Grosch, S. How sphingolipids affect T cells in the resolution of inflammation. *Front Pharmacol* **13**, 1002915 (2022). https://doi.org:10.3389/fphar.2022.1002915
127 Chiantia, S. & London, E. Sphingolipids and membrane domains: recent advances. *Handb Exp Pharmacol*, 33-55 (2013). https://doi.org:10.1007/978-3-7091-1368-4_2
128 Lingwood, D. & Simons, K. Lipid rafts as a membrane-organizing principle. *Science* **327**, 46-50 (2010). https://doi.org:10.1126/science.1174621
129 Canals, D., Salamone, S. & Hannun, Y. A. Visualizing bioactive ceramides. *Chem Phys Lipids* **216**, 142-151 (2018). https://doi.org:10.1016/j.chemphyslip.2018.09.013
130 Blitterswijk, W. J. V., Luit, A. H. V. D., Veldman, R. J., Verheij, M. & Borst, J. Ceramide: second messenger or modulator of membrane structure and dynamics? *Biochemical Journal* **369**, 199-211 (2003). https://doi.org:10.1042/bj20021528
131 Trajkovic, K. *et al.* Ceramide triggers budding of exosome vesicles into multivesicular endosomes. *Science* **319**, 1244-1247 (2008). https://doi.org:10.1126/science.1153124
132 Dadsena, S. *et al.* Ceramides bind VDAC2 to trigger mitochondrial apoptosis. *Nature Communications* **10** (2019). https://doi.org:10.1038/s41467-019-09654-4
133 Colombini, M. Ceramide channels and their role in mitochondria-mediated apoptosis. *Biochim Biophys Acta* **1797**, 1239-1244 (2010). https://doi.org:10.1016/j.bbabio.2010.01.021
134 Von Haefen, C. *et al.* Ceramide induces mitochondrial activation and apoptosis via a Bax-dependent pathway in human carcinoma cells. *Oncogene* **21**, 4009-4019 (2002). https://doi.org:10.1038/sj.onc.1205497
135 J. Watters, R., Wang, H.-G., Sung, S.-S., P. Loughran, T. & Liu, X. Targeting Sphingosine-1-Phosphate Receptors in Cancer. *Anti-Cancer Agents in Medicinal Chemistry* **11**, 810-817 (2011). https://doi.org:10.2174/187152011797655041
136 Cyster, J. G. & Schwab, S. R. Sphingosine-1-Phosphate and Lymphocyte Egress from Lymphoid Organs. *Annual Review of Immunology* **30**, 69-94 (2012). https://doi.org:10.1146/annurev-immunol-020711-075011
137 Matloubian, M. *et al.* Lymphocyte egress from thymus and peripheral lymphoid organs is dependent on S1P receptor 1. *Nature* **427**, 355-360 (2004). https://doi.org:10.1038/nature02284

138 Baeyens, A. A. L. & Schwab, S. R. Finding a Way Out: S1P Signaling and Immune Cell Migration. *Annual Review of Immunology* **38**, 759-784 (2020). https://doi.org:10.1146/annurev-immunol-081519-083952
139 Pappu, R. *et al.* Promotion of lymphocyte egress into blood and lymph by distinct sources of sphingosine-1-phosphate. *Science* **316**, 295-298 (2007). https://doi.org:10.1126/science.1139221
140 Serra, M. & Saba, J. D. Sphingosine 1-phosphate lyase, a key regulator of sphingosine 1-phosphate signaling and function. *Advances in Enzyme Regulation* **50**, 349-362 (2010). https://doi.org:10.1016/j.advenzreg.2009.10.024
141 Schwab, S. R. *et al.* Lymphocyte sequestration through S1P lyase inhibition and disruption of S1P gradients. *Science* **309**, 1735-1739 (2005). https://doi.org:10.1126/science.1113640
142 Arnon, T. I. *et al.* GRK2-Dependent S1PR1 Desensitization Is Required for Lymphocytes to Overcome Their Attraction to Blood. *Science* **333**, 1898-1903 (2011). https://doi.org:10.1126/science.1208248
143 Lo, C. G., Xu, Y., Proia, R. L. & Cyster, J. G. Cyclical modulation of sphingosine-1-phosphate receptor 1 surface expression during lymphocyte recirculation and relationship to lymphoid organ transit. *The Journal of Experimental Medicine* **201**, 291-301 (2005). https://doi.org:10.1084/jem.20041509
144 Allende, M. L. *et al.* S1P₁receptor expression regulates emergence of NKT cells in peripheral tissues. *The FASEB Journal* **22**, 307-315 (2008). https://doi.org:10.1096/fj.07-9087com
145 Odumade, O. A., Weinreich, M. A., Jameson, S. C. & Hogquist, K. A. Krüppel-Like Factor 2 Regulates Trafficking and Homeostasis of γδ T Cells. *The Journal of Immunology* **184**, 6060-6066 (2010). https://doi.org:10.4049/jimmunol.1000511
146 Shiow, L. R. *et al.* CD69 acts downstream of interferon-α/β to inhibit S1P1 and lymphocyte egress from lymphoid organs. *Nature* **440**, 540-544 (2006). https://doi.org:10.1038/nature04606
147 Cibrián, D. & Sánchez-Madrid, F. CD69: from activation marker to metabolic gatekeeper. *European Journal of Immunology* **47**, 946-953 (2017). https://doi.org:10.1002/eji.201646837
148 Bankovich, A. J., Shiow, L. R. & Cyster, J. G. CD69 Suppresses Sphingosine 1-Phosophate Receptor-1 (S1P1) Function through Interaction with Membrane Helix 4. *Journal of Biological Chemistry* **285**, 22328-22337 (2010). https://doi.org:10.1074/jbc.m110.123299
149 Breart, B. & Bousso, P. S1P₁ downregulation tailors CD8⁺ T-cell residence time in lymph nodes to the strength of the antigenic stimulation. *European Journal of Immunology* **46**, 2730-2736 (2016). https://doi.org:10.1002/eji.201646550
150 Mempel, T. R., Henrickson, S. E. & Von Andrian, U. H. T-cell priming by dendritic cells in lymph nodes occurs in three distinct phases. *Nature* **427**, 154-159 (2004). https://doi.org:10.1038/nature02238
151 Baeyens, A. *et al.* Monocyte-derived S1P in the lymph node regulates immune responses. *Nature* **592**, 290-295 (2021). https://doi.org:10.1038/s41586-021-03227-6
152 Bigaud, M. *et al.* Central Versus Peripheral Drug Exposure Ratio, a Key Differentiator for Siponimod Over Fingolimod? *Neurology and Therapy* **12**, 1187-1203 (2023). https://doi.org:10.1007/s40120-023-00487-4
153 Sharma, S., Mathur, A. G., Pradhan, S., Singh, D. B. & Gupta, S. Fingolimod (FTY720): First approved oral therapy for multiple sclerosis. *J Pharmacol Pharmacother* **2**, 49-51 (2011). https://doi.org:10.4103/0976-500X.77118
154 Maceyka, M. & Spiegel, S. Sphingolipid metabolites in inflammatory disease. *Nature* **510**, 58-67 (2014). https://doi.org:10.1038/nature13475
155 Sun, Y. *et al.* Ozanimod for Treatment of Relapsing-Remitting Multiple Sclerosis in Adults: A Systematic Review and Meta-Analysis of Randomized Controlled Trials. *Frontiers in Pharmacology* **11** (2020). https://doi.org:10.3389/fphar.2020.589146

156 Van Langelaar, J., Rijvers, L., Smolders, J. & Van Luijn, M. M. B and T Cells Driving Multiple Sclerosis: Identity, Mechanisms and Potential Triggers. *Frontiers in Immunology* **11** (2020). https://doi.org:10.3389/fimmu.2020.00760
157 Dixit, D. *et al.* S1PR1 inhibition induces pro-apoptotic signaling in T cells and limits humoral responses within lymph nodes. *Journal of Clinical Investigation* (2024). https://doi.org:10.1172/jci174984
158 Mendoza, A. *et al.* Lymphatic endothelial S1P promotes mitochondrial function and survival in naive T cells. *Nature* **546**, 158-161 (2017). https://doi.org:10.1038/nature22352
159 Liu, G. *et al.* The receptor S1P1 overrides regulatory T cell–mediated immune suppression through Akt-mTOR. *Nature Immunology* **10**, 769-777 (2009). https://doi.org:10.1038/ni.1743
160 Liu, G., Yang, K., Burns, S., Shrestha, S. & Chi, H. The S1P1-mTOR axis directs the reciprocal differentiation of TH1 and Treg cells. *Nature Immunology* **11**, 1047-1056 (2010). https://doi.org:10.1038/ni.1939
161 Garris, C. S. *et al.* Defective sphingosine 1-phosphate receptor 1 (S1P1) phosphorylation exacerbates TH17-mediated autoimmune neuroinflammation. *Nature Immunology* **14**, 1166-1172 (2013). https://doi.org:10.1038/ni.2730
162 Tonnetti, L., Verí, M.-C., Bonvini, E. & D'Adamio, L. A Role for Neutral Sphingomyelinase-mediated Ceramide Production in T Cell Receptor–induced Apoptosis and Mitogen-activated Protein Kinase–mediated Signal Transduction. *The Journal of Experimental Medicine* **189**, 1581-1589 (1999). https://doi.org:10.1084/jem.189.10.1581
163 Bai, A., Kokkotou, E., Zheng, Y. & Robson, S. C. Role of acid sphingomyelinase bioactivity in human CD4+ T-cell activation and immune responses. *Cell Death Dis* **6**, e1828 (2015). https://doi.org:10.1038/cddis.2015.178
164 Chan, G. & Ochi, A. Sphingomyelin-ceramide turnover in CD28 costimulatory signaling. *European Journal of Immunology* **25**, 1999-2004 (1995). https://doi.org:10.1002/eji.1830250730
165 Stoffel, B., Bauer, P., Nix, M., Deres, K. & Stoffel, W. Ceramide-independent CD28 and TCR signaling but reduced IL-2 secretion in T cells of acid sphingomyelinase-deficient mice. *European Journal of Immunology* **28**, 874-880 (1998). https://doi.org:10.1002/(sici)1521-4141(199803)28:03<874::aid-immu874>3.0.co;2-t
166 Bai, A. *et al.* CD39 and CD161 Modulate Th17 Responses in Crohn's Disease. *The Journal of Immunology* **193**, 3366-3377 (2014). https://doi.org:10.4049/jimmunol.1400346
167 Hose, M. *et al.* T Cell-Specific Overexpression of Acid Sphingomyelinase Results in Elevated T Cell Activation and Reduced Parasitemia During Plasmodium yoelii Infection. *Front Immunol* **10**, 1225 (2019). https://doi.org:10.3389/fimmu.2019.01225
168 Hose, M. *et al.* Cell-intrinsic ceramides determine T cell function during melanoma progression. *Elife* **11** (2022). https://doi.org:10.7554/eLife.83073
169 Avota, E., de Lira, M. N. & Schneider-Schaulies, S. Sphingomyelin Breakdown in T Cells: Role of Membrane Compartmentalization in T Cell Signaling and Interference by a Pathogen. *Front Cell Dev Biol* **7**, 152 (2019). https://doi.org:10.3389/fcell.2019.00152
170 Wiese, T. *et al.* Inhibition of acid sphingomyelinase increases regulatory T cells in humans. *Brain Commun* **3**, fcab020 (2021). https://doi.org:10.1093/braincomms/fcab020
171 Hollmann, C. *et al.* Inhibition of Acid Sphingomyelinase Allows for Selective Targeting of CD4+ Conventional versus Foxp3+ Regulatory T Cells. *J Immunol* **197**, 3130-3141 (2016). https://doi.org:10.4049/jimmunol.1600691
172 Hollmann, C. *et al.* Translational Approaches Targeting Ceramide Generation From Sphingomyelin in T Cells to Modulate Immunity in Humans. *Front Immunol* **10**, 2363 (2019). https://doi.org:10.3389/fimmu.2019.02363
173 Park, A. Y. *et al.* GIMAP5 deficiency reveals a mammalian ceramide-driven longevity assurance pathway. *Nature Immunology* (2024). https://doi.org:10.1038/s41590-023-01691-y

174 Nagafuku, M. *et al.* CD4 and CD8 T cells require different membrane gangliosides for activation. *Proceedings of the National Academy of Sciences* **109**, E336-E342 (2012). https://doi.org:10.1073/pnas.1114965109
175 Kersh, E. N. *et al.* TCR signal transduction in antigen-specific memory CD8 T cells. *J Immunol* **170**, 5455-5463 (2003). https://doi.org:10.4049/jimmunol.170.11.5455
176 Dinic, J., Riehl, A., Adler, J. & Parmryd, I. The T cell receptor resides in ordered plasma membrane nanodomains that aggregate upon patching of the receptor. *Sci Rep* **5**, 10082 (2015). https://doi.org:10.1038/srep10082
177 Grassme, H., Cremesti, A., Kolesnick, R. & Gulbins, E. Ceramide-mediated clustering is required for CD95-DISC formation. *Oncogene* **22**, 5457-5470 (2003). https://doi.org:10.1038/sj.onc.1206540
178 Xu, C. *et al.* Expansion of MAIT cells in the combined absence of NKT and γδ-T cells. *Mucosal Immunology* **16**, 446-461 (2023). https://doi.org:10.1016/j.mucimm.2023.05.003
179 Canals, D., Perry, D. M., Jenkins, R. W. & Hannun, Y. A. Drug targeting of sphingolipid metabolism: sphingomyelinases and ceramidases. *British Journal of Pharmacology* **163**, 694-712 (2011). https://doi.org:10.1111/j.1476-5381.2011.01279.x
180 Bhabak, K. P. & Arenz, C. Novel drugs targeting sphingolipid metabolism. *Handb Exp Pharmacol*, 187-196 (2013). https://doi.org:10.1007/978-3-7091-1368-4_10
181 Companioni, O., Mir, C., Garcia-Mayea, Y. & Lleonart, M. E. Targeting Sphingolipids for Cancer Therapy. *Frontiers in Oncology* **11** (2021). https://doi.org:10.3389/fonc.2021.745092
182 Beckmann, N., Sharma, D., Gulbins, E., Becker, K. A. & Edelmann, B. R. Inhibition of acid sphingomyelinase by tricyclic antidepressants and analogons. *Frontiers in Physiology* **5** (2014). https://doi.org:10.3389/fphys.2014.00331
183 Ataide, M. A. *et al.* Lymphatic migration of unconventional T cells promotes site-specific immunity in distinct lymph nodes. *Immunity* **55**, 1813-1828 e1819 (2022). https://doi.org:10.1016/j.immuni.2022.07.019
184 Edwards-Hicks, J. *et al.* Phosphoinositide acyl chain saturation drives CD8(+) effector T cell signaling and function. *Nat Immunol* **24**, 516-530 (2023). https://doi.org:10.1038/s41590-023-01419-y
185 Slotte, J. P. Biological functions of sphingomyelins. *Prog Lipid Res* **52**, 424-437 (2013). https://doi.org:10.1016/j.plipres.2013.05.001
186 Milhas, D., Clarke, C. J. & Hannun, Y. A. Sphingomyelin metabolism at the plasma membrane: implications for bioactive sphingolipids. *FEBS Lett* **584**, 1887-1894 (2010). https://doi.org:10.1016/j.febslet.2009.10.058
187 Gorelik, A., Heinz, L. X., Illes, K., Superti-Furga, G. & Nagar, B. Crystal Structure of the Acid Sphingomyelinase-like Phosphodiesterase SMPDL3B Provides Insights into Determinants of Substrate Specificity. *J Biol Chem* **291**, 24054-24064 (2016). https://doi.org:10.1074/jbc.M116.755801
188 Heinz, L. X. *et al.* The Lipid-Modifying Enzyme SMPDL3B Negatively Regulates Innate Immunity. *Cell Rep* **11**, 1919-1928 (2015). https://doi.org:10.1016/j.celrep.2015.05.006
189 Waelter, S. *et al.* The huntingtin interacting protein HIP1 is a clathrin and alpha-adaptin-binding protein involved in receptor-mediated endocytosis. *Hum Mol Genet* **10**, 1807-1817 (2001). https://doi.org:10.1093/hmg/10.17.1807
190 Gervais, F. G. *et al.* Recruitment and activation of caspase-8 by the Huntingtin-interacting protein Hip-1 and a novel partner Hippi. *Nature Cell Biology* **4**, 95-105 (2002). https://doi.org:10.1038/ncb735
191 Traini, M. *et al.* Sphingomyelin Phosphodiesterase Acid-like 3A (SMPDL3A) Is a Novel Nucleotide Phosphodiesterase Regulated by Cholesterol in Human Macrophages. *Journal of Biological Chemistry* **289**, 32895-32913 (2014). https://doi.org:10.1074/jbc.m114.612341
192 Hou, Y. *et al.* SMPDL3A is a cGAMP-degrading enzyme induced by LXR-mediated lipid metabolism to restrict cGAS-STING DNA sensing. *Immunity* **56**, 2492-2507 e2410 (2023). https://doi.org:10.1016/j.immuni.2023.10.001

193 Decout, A., Katz, J. D., Venkatraman, S. & Ablasser, A. The cGAS–STING pathway as a therapeutic target in inflammatory diseases. *Nature Reviews Immunology* **21**, 548-569 (2021). https://doi.org:10.1038/s41577-021-00524-z
194 Watanabe, S. *et al.* Sphingomyelin Phosphodiesterase Acid-Like 3b is Essential for Toll-Like Receptor 3 Signaling in Human Podocytes. *J Membr Biol* **255**, 117-122 (2022). https://doi.org:10.1007/s00232-021-00206-w
195 Elliott, M. R. *et al.* Nucleotides released by apoptotic cells act as a find-me signal to promote phagocytic clearance. *Nature* **461**, 282-286 (2009). https://doi.org:10.1038/nature08296
196 Liu, H. *et al.* cGAS facilitates sensing of extracellular cyclic dinucleotides to activate innate immunity. *EMBO Rep* **20** (2019). https://doi.org:10.15252/embr.201846293
197 Luteijn, R. D. *et al.* SLC19A1 transports immunoreactive cyclic dinucleotides. *Nature* **573**, 434-438 (2019). https://doi.org:10.1038/s41586-019-1553-0
198 Larkin, B. *et al.* Cutting Edge: Activation of STING in T Cells Induces Type I IFN Responses and Cell Death. *The Journal of Immunology* **199**, 397-402 (2017). https://doi.org:10.4049/jimmunol.1601999
199 Quaney, M. J. *et al.* STING controls T cell memory fitness during infection through T cell-intrinsic and IDO-dependent mechanisms. *Proceedings of the National Academy of Sciences* **120** (2023). https://doi.org:10.1073/pnas.2205049120
200 Faller, E. M., Ghazawi, F. M., Cavar, M. & Macpherson, P. A. IL-7 induces clathrin-mediated endocytosis of CD127 and subsequent degradation by the proteasome in primary human CD8 T cells. *Immunology & Cell Biology* **94**, 196-207 (2016). https://doi.org:10.1038/icb.2015.80
201 Henriques, C. M., Rino, J., Nibbs, R. J., Graham, G. J. & Barata, J. T. IL-7 induces rapid clathrin-mediated internalization and JAK3-dependent degradation of IL-7Rα in T cells. *Blood* **115**, 3269-3277 (2010). https://doi.org:10.1182/blood-2009-10-246876
202 Waldmann, T. A., Miljkovic, M. D. & Conlon, K. C. Interleukin-15 (dys)regulation of lymphoid homeostasis: Implications for therapy of autoimmunity and cancer. *Journal of Experimental Medicine* **217** (2020). https://doi.org:10.1084/jem.20191062
203 Gerlach, C. *et al.* The Chemokine Receptor CX3CR1 Defines Three Antigen-Experienced CD8 T Cell Subsets with Distinct Roles in Immune Surveillance and Homeostasis. *Immunity* **45**, 1270-1284 (2016). https://doi.org:10.1016/j.immuni.2016.10.018
204 ImmGen, C. Open-source ImmGen: mononuclear phagocytes. *Nat Immunol* **17**, 741 (2016). https://doi.org:10.1038/ni.3478
205 Moreno-Cañadas, R., Luque-Martín, L. & Arroyo, A. G. Intravascular Crawling of Patrolling Monocytes: A Lèvy-Like Motility for Unique Search Functions? *Frontiers in Immunology* **12** (2021). https://doi.org:10.3389/fimmu.2021.730835
206 Buscher, K., Marcovecchio, P., Hedrick, C. C. & Ley, K. Patrolling Mechanics of Non-Classical Monocytes in Vascular Inflammation. *Frontiers in Cardiovascular Medicine* **4** (2017). https://doi.org:10.3389/fcvm.2017.00080
207 Carlin, L. M., Auffray, C. & Geissmann, F. Measuring Intravascular Migration of Mouse Ly6C^{low} Monocytes In Vivo Using Intravital Microscopy. *Current Protocols in Immunology* **101**, 14.33.11-14.33.11 (2013). https://doi.org:10.1002/0471142735.im1433s101
208 Yona, S. *et al.* Fate Mapping Reveals Origins and Dynamics of Monocytes and Tissue Macrophages under Homeostasis. *Immunity* **38**, 79-91 (2013). https://doi.org:10.1016/j.immuni.2012.12.001
209 Clement, R. L. *et al.* Follicular regulatory T cells control humoral and allergic immunity by restraining early B cell responses. *Nature Immunology* **20**, 1360-1371 (2019). https://doi.org:10.1038/s41590-019-0472-4
210 Prinz, I., Silva-Santos, B. & Pennington, D. J. Functional development of γδ <scp>T</scp> cells. *European Journal of Immunology* **43**, 1988-1994 (2013). https://doi.org:10.1002/eji.201343759
211 You *et al.* Tissue-Specific Distribution of iNKT Cells Impacts Their Cytokine Response. *Immunity* **43**, 566-578 (2015). https://doi.org:10.1016/j.immuni.2015.06.025

212 Cruz De Casas, P., Knöpper, K., Dey Sarkar, R. & Kastenmüller, W. Same yet different — how lymph node heterogeneity affects immune responses. *Nature Reviews Immunology* (2023). https://doi.org:10.1038/s41577-023-00965-8
213 An, S., Zheng, Y. & Bleu, T. Sphingosine 1-Phosphate-induced Cell Proliferation, Survival, and Related Signaling Events Mediated by G Protein-coupled Receptors Edg3 and Edg5. *Journal of Biological Chemistry* **275**, 288-296 (2000). https://doi.org:10.1074/jbc.275.1.288
214 Blom, T. *et al.* An autocrine sphingosine-1-phosphate signaling loop enhances NF-κB-activation and survival. *BMC Cell Biology* **11**, 45 (2010). https://doi.org:10.1186/1471-2121-11-45
215 Donati, C. *et al.* Sphingosine 1-Phosphate Mediates Proliferation and Survival of Mesoangioblasts. *STEM CELLS* **25**, 1713-1719 (2007). https://doi.org:10.1634/stemcells.2006-0725
216 Edsall, L. C., Pirianov, G. G. & Spiegel, S. Involvement of Sphingosine 1-Phosphate in Nerve Growth Factor-Mediated Neuronal Survival and Differentiation. *The Journal of Neuroscience* **17**, 6952-6960 (1997). https://doi.org:10.1523/jneurosci.17-18-06952.1997
217 Kim, D. S., Hwang, E. S., Lee, J. E., Kim, S. Y. & Park, K. C. Sphingosine-1-phosphate promotes mouse melanocyte survival via ERK and Akt activation. *Cell Signal* **15**, 919-926 (2003). https://doi.org:10.1016/s0898-6568(03)00055-x
218 Weigert, A. *et al.* Apoptotic cells promote macrophage survival by releasing the antiapoptotic mediator sphingosine-1-phosphate. *Blood* **108**, 1635-1642 (2006). https://doi.org:10.1182/blood-2006-04-014852
219 Rutherford, C. *et al.* Regulation of cell survival by sphingosine-1-phosphate receptor S1P1 via reciprocal ERK-dependent suppression of Bim and PI-3-kinase/protein kinase C-mediated upregulation of Mcl-1. *Cell Death & Disease* **4**, e927-e927 (2013). https://doi.org:10.1038/cddis.2013.455
220 Mandl, J. N. *et al.* Quantification of lymph node transit times reveals differences in antigen surveillance strategies of naive CD4+ and CD8+ T cells. *Proc Natl Acad Sci U S A* **109**, 18036-18041 (2012). https://doi.org:10.1073/pnas.1211717109
221 Green, J. A. *et al.* The sphingosine 1-phosphate receptor S1P(2) maintains the homeostasis of germinal center B cells and promotes niche confinement. *Nat Immunol* **12**, 672-680 (2011). https://doi.org:10.1038/ni.2047
222 Suzuki, E., Handa, K., Toledo, M. S. & Hakomori, S. Sphingosine-dependent apoptosis: a unified concept based on multiple mechanisms operating in concert. *Proc Natl Acad Sci U S A* **101**, 14788-14793 (2004). https://doi.org:10.1073/pnas.0406536101
223 Park, S.-J. & Im, D.-S. Sphingosine 1-Phosphate Receptor Modulators and Drug Discovery. *Biomolecules & Therapeutics* **25**, 80-90 (2017). https://doi.org:10.4062/biomolther.2016.160
224 Pérez-Jeldres, T. *et al.* Targeting Cytokine Signaling and Lymphocyte Traffic via Small Molecules in Inflammatory Bowel Disease: JAK Inhibitors and S1PR Agonists. *Frontiers in Pharmacology* **10** (2019). https://doi.org:10.3389/fphar.2019.00212
225 Masuishi, Y. *et al.* Mass spectrometric identification of glycosylphosphatidylinositol-anchored peptides. *J Proteome Res* **12**, 4617-4626 (2013). https://doi.org:10.1021/pr4004807
226 Walzer, T. *et al.* Natural killer cell trafficking in vivo requires a dedicated sphingosine 1-phosphate receptor. *Nature Immunology* **8**, 1337-1344 (2007). https://doi.org:10.1038/ni1523
227 Jenne, C. N. *et al.* T-bet–dependent S1P5 expression in NK cells promotes egress from lymph nodes and bone marrow. *Journal of Experimental Medicine* **206**, 2469-2481 (2009). https://doi.org:10.1084/jem.20090525
228 Debien, E. *et al.* S1PR5 is pivotal for the homeostasis of patrolling monocytes. *European Journal of Immunology* **43**, 1667-1675 (2013). https://doi.org:10.1002/eji.201343312

229 Evrard, M. *et al.* Sphingosine 1-phosphate receptor 5 (S1PR5) regulates the peripheral retention of tissue-resident lymphocytes. *Journal of Experimental Medicine* **219** (2022). https://doi.org:10.1084/jem.20210116
230 Schluns, K. S. & Lefrançois, L. Cytokine control of memory T-cell development and survival. *Nature Reviews Immunology* **3**, 269-279 (2003). https://doi.org:10.1038/nri1052
231 Kelly, E., Won, A., Refaeli, Y. & Van Parijs, L. IL-2 and Related Cytokines Can Promote T Cell Survival by Activating AKT. *The Journal of Immunology* **168**, 597-603 (2002). https://doi.org:10.4049/jimmunol.168.2.597
232 Baccala, R. *et al.* γδ T Cell Homeostasis Is Controlled by IL-7 and IL-15 Together with Subset-Specific Factors. *The Journal of Immunology* **174**, 4606-4612 (2005). https://doi.org:10.4049/jimmunol.174.8.4606
233 Webster, K. E. *et al.* IL-17-producing NKT cells depend exclusively on IL-7 for homeostasis and survival. *Mucosal Immunology* **7**, 1058-1067 (2014). https://doi.org:10.1038/mi.2013.122
234 Gordy, L. E. *et al.* IL-15 Regulates Homeostasis and Terminal Maturation of NKT Cells. *The Journal of Immunology* **187**, 6335-6345 (2011). https://doi.org:10.4049/jimmunol.1003965
235 Hunter, M. Survival of monocytes and macrophages and their role in health and disease. *Frontiers in Bioscience* **Volume**, 4079 (2009). https://doi.org:10.2741/3514
236 Kornhuber, J. *et al.* Identification of new functional inhibitors of acid sphingomyelinase using a structure-property-activity relation model. *J Med Chem* **51**, 219-237 (2008). https://doi.org:10.1021/jm070524a
237 Zheng, X. *et al.* Tumors evade immune cytotoxicity by altering the surface topology of NK cells. *Nature Immunology* **24**, 802-813 (2023). https://doi.org:10.1038/s41590-023-01462-9
238 Leget, G. A. & Czuczman, M. S. Use of rituximab, the new FDA-approved antibody. *Curr Opin Oncol* **10**, 548-551 (1998). https://doi.org:10.1097/00001622-199811000-00012
239 Parajuli, S. *et al.* Rituximab and Monitoring Strategies for Late Antibody-Mediated Rejection After Kidney Transplantation. *Transplantation Direct* **3**, e227 (2017). https://doi.org:10.1097/txd.0000000000000746
240 Ravichandran, A. K. *et al.* Rituximab is associated with improved survival in cardiac allograft patients with antibody-mediated rejection: a single center review. *Clinical Transplantation* **27**, 961-967 (2013). https://doi.org:10.1111/ctr.12277
241 Perosa, F., Favoino, E., Caragnano, M. A. & Dammacco, F. Generation of biologically active linear and cyclic peptides has revealed a unique fine specificity of rituximab and its possible cross-reactivity with acid sphingomyelinase-like phosphodiesterase 3b precursor. *Blood* **107**, 1070-1077 (2006). https://doi.org:10.1182/blood-2005-04-1769
242 Bezombes, C. Rituximab antiproliferative effect in B-lymphoma cells is associated with acid-sphingomyelinase activation in raft microdomains. *Blood* **104**, 1166-1173 (2004). https://doi.org:10.1182/blood-2004-01-0277
243 Fornoni, A. *et al.* Rituximab targets podocytes in recurrent focal segmental glomerulosclerosis. *Sci Transl Med* **3**, 85ra46 (2011). https://doi.org:10.1126/scitranslmed.3002231
244 Maekawa, M. & Fairn, G. D. Molecular probes to visualize the location, organization and dynamics of lipids. *Journal of Cell Science* **127**, 4801-4812 (2014). https://doi.org:10.1242/jcs.150524
245 Boumelhem, B. B. *et al.* Intracellular flow cytometric lipid analysis – a multiparametric system to assess distinct lipid classes in live cells. *Journal of Cell Science* **135** (2022). https://doi.org:10.1242/jcs.258322
246 Snider, J. M., Luberto, C. & Hannun, Y. A. Approaches for probing and evaluating mammalian sphingolipid metabolism. *Analytical Biochemistry* **575**, 70-86 (2019). https://doi.org:10.1016/j.ab.2019.03.014
247 Lewis, A. C., Wallington-Beddoe, C. T., Powell, J. A. & Pitson, S. M. Targeting sphingolipid metabolism as an approach for combination therapies in haematological

malignancies. *Cell Death Discovery* **4** (2018). https://doi.org:10.1038/s41420-018-0075-0
248 Gault, C. R., Obeid, L. M. & Hannun, Y. A. An overview of sphingolipid metabolism: from synthesis to breakdown. *Adv Exp Med Biol* **688**, 1-23 (2010). https://doi.org:10.1007/978-1-4419-6741-1_1
249 Vanier, M. T. Niemann-Pick diseases. *Handb Clin Neurol* **113**, 1717-1721 (2013). https://doi.org:10.1016/B978-0-444-59565-2.00041-1
250 Goñi, F. M. & Alonso, A. Sphingomyelinases: enzymology and membrane activity. *FEBS Letters* **531**, 38-46 (2002). https://doi.org:10.1016/s0014-5793(02)03482-8
251 Cartier, A. & Hla, T. Sphingosine 1-phosphate: Lipid signaling in pathology and therapy. *Science* **366**, eaar5551 (2019). https://doi.org:10.1126/science.aar5551
252 Fohmann, I. *et al.* Sphingosine kinase 1/S1P receptor signaling axis is essential for cellular uptake of Neisseria meningitidis in brain endothelial cells. *PLOS Pathogens* **19**, e1011842 (2023). https://doi.org:10.1371/journal.ppat.1011842
253 Van Meer, G. & Hoetzl, S. Sphingolipid topology and the dynamic organization and function of membrane proteins. *FEBS Letters* **584**, 1800-1805 (2010). https://doi.org:10.1016/j.febslet.2009.10.020
254 Friedel, R. H., Seisenberger, C., Kaloff, C. & Wurst, W. EUCOMM the European Conditional Mouse Mutagenesis Program. *Briefings in Functional Genomics and Proteomics* **6**, 180-185 (2007). https://doi.org:10.1093/bfgp/elm022
255 Mekada, K. & Yoshiki, A. Substrains matter in phenotyping of C57BL/6 mice. *Experimental Animals* **70**, 145-160 (2021). https://doi.org:10.1538/expanim.20-0158
256 Sellers, R. S. Translating Mouse Models. *Toxicologic Pathology* **45**, 134-145 (2017). https://doi.org:10.1177/0192623316675767
257 Rosshart, S. P. *et al.* Laboratory mice born to wild mice have natural microbiota and model human immune responses. *Science* **365**, eaaw4361 (2019). https://doi.org:10.1126/science.aaw4361
258 Marchitto, M. C. *et al.* Clonal Vγ6 ⁺ Vδ4 ⁺ T cells promote IL-17–mediated immunity against Staphylococcus aureus skin infection. *Proceedings of the National Academy of Sciences* **116**, 10917-10926 (2019). https://doi.org:10.1073/pnas.1818256116
259 Ramírez-Valle, F., Gray, E. E. & Cyster, J. G. Inflammation induces dermal Vγ4 ⁺ γδT17 memory-like cells that travel to distant skin and accelerate secondary IL-17–driven responses. *Proceedings of the National Academy of Sciences* **112**, 8046-8051 (2015). https://doi.org:10.1073/pnas.1508990112
260 Murphy, A. G. *et al.* Staphylococcus aureus Infection of Mice Expands a Population of Memory γδ T Cells That Are Protective against Subsequent Infection. *The Journal of Immunology* **192**, 3697-3708 (2014). https://doi.org:10.4049/jimmunol.1303420

Appendix A

Review

“Same yet different – how lymph node heterogeneity affects immune responses”[212]

nature reviews immunology

https://doi.org/10.1038/s41577-023-00965-8

Review article

Check for updates

Same yet different — how lymph node heterogeneity affects immune responses

Paulina Cruz de Casas[1], Konrad Knöpper[2,3], Rupak Dey Sarkar[1] & Wolfgang Kastenmüller[1]

Abstract

Lymph nodes are secondary lymphoid organs in which immune responses of the adaptive immune system are initiated and regulated. Distributed throughout the body and embedded in the lymphatic system, local lymph nodes are continuously informed about the state of the organs owing to a constant drainage of lymph. The tissue-derived lymph carries products of cell metabolism, proteins, carbohydrates, lipids, pathogens and circulating immune cells. Notably, there is a growing body of evidence that individual lymph nodes differ from each other in their capacity to generate immune responses. Here, we review the structure and function of the lymphatic system and then focus on the factors that lead to functional heterogeneity among different lymph nodes. We will discuss how lymph node heterogeneity impacts on cellular and humoral immune responses and the implications for vaccination, tumour development and tumour control by immunotherapy.

Sections

[1]Max Planck Research Group, Würzburg Institute of Systems Immunology, Julius-Maximilians-Universität Würzburg, Würzburg, Germany. [2]Howard Hughes Medical Institute, University of California, San Francisco, San Francisco, CA, USA. [3]Department of Microbiology and Immunology, University of California, San Francisco, San Francisco, CA, USA. e-mail: wolfgang.kastenmueller@uni-wuerzburg.de

Introduction

In the body of mammals, there are two major circulatory systems. The first one is the cardiovascular system, which is responsible for transporting nutrients and oxygen throughout the body. The second is the lymphatic vascular system (LVS)[1] (Box 1). The LVS collects interstitial fluid from the tissues it drains and transports it back into the bloodstream via the lymphatic vessels and through lymph nodes (LNs). Owing to the hydrostatic and osmotic pressure of the blood in the capillaries, interstitial fluid accumulates in tissues[2] and must be removed to avoid oedema and impaired tissue function. Once interstitial fluid has entered the lymphatic vessels, it is referred to as lymph. In humans, about 3–4 l of lymph are returned to the bloodstream each day[3]. Most tissues of the body contain lymphatic structures with the exception of the brain. In the brain, exchange between interstitial and cerebrospinal fluid takes place through the lymphatic vessels of the meninges[4]. Recent data suggest that this is crucial for eliminating protein accumulation that occurs, for example, in Alzheimer's disease[5].

Besides acting as a draining system for molecules derived from tissues, lymph also contains various cell populations, such as lymphocytes, myeloid cells and stem cells[6,7]. These cells leave the tissues through the lymphatic vessels and migrate to reach the blood system or immigrate to secondary lymphoid organs (SLOs), such as LNs, which are located along the lymphatic vessels[8,9]. Consequently, LNs concentrate molecules and cells derived from the local tissues they drain.

LNs are of critical importance in triggering adaptive immune responses and are, therefore, connected to both circulatory systems. It is becoming increasingly clear that distinct LNs differ in their ability to support specific immune responses and that this heterogeneity is primarily because of their lymphatic connection. This feature has important implications for understanding the nature of tissue-specific immune responses.

In this Review, we highlight the cell types and molecular factors that contribute to LN heterogeneity during homoeostatic conditions and cancer and explain how they shape the nature of the immune responses generated at these sites. Furthermore, we discuss the clinical implications of understanding LN heterogeneity, for instance, in the settings of cancer immunotherapy and vaccination.

Lymph nodes: structure and function

LNs are SLOs that have a variable, usually ovoid or bean-shaped appearance (Fig. 1). Estimates of LN numbers in humans are roughly 450, the majority of which are found in the abdomen, pelvis and mediastinum[10,11]. LNs are critical elements of the LVS (Box 1) and serve two essential functions. Firstly, they act as filtering and defence organs for microbes and microbial components that are drained from the tissues via the lymph. Because of the open-ended funnel-like structure of the lymphatic capillaries, pathogens that infect barrier tissues such as the skin, lungs or intestines can easily access the lymphatic vessels. Therefore, the filter function of LNs is essential to limit pathogens from spreading from the tissue via the lymph and ultimately through the blood system[12]. The second essential task of LNs is the organization and initiation of adaptive immune responses. To this end, LNs need to compartmentalize lymphocytes in B cell and T cell areas but must also promote the interaction of these lymphocytes and other immune cells to orchestrate immune responses in space and time[13]. Therefore, to fulfill these functions, LNs require a sophisticated and specialized structure, as briefly outlined in the following passages.

LNs are encased in a connective tissue capsule consisting predominantly of fibre-rich collagenous connective tissue with elastic fibres and individual smooth muscle cells[14]. From the capsule, connective tissue septa, known as trabeculae, radiate into the interior of the LN and subdivide it in segments (Fig. 1). The capsule is pierced by several afferent lymphatic vessels. The lymph pours out of the afferent lymphatic vessel into a cleft space, the subcapsular sinus (SCS) located beneath the entire capsule. From here, the lymph percolates through a system of internodal or perinodal sinuses to larger medullary sinuses. At the hilum, the lymph is collected and leaves via the efferent lymphatic vessels. In order to serve its filtering function, the lymphatic sinuses are populated by specialized macrophage populations that scavenge microbes and clear microbial products from the lymph[15]. Upon infection or activation, these macrophages rapidly orchestrate a local immune response to enforce the barrier function of the LN[16] and to initiate humoral and cellular immune responses to clear infections[12,17].

The basic framework and compartmentalization of the LN is organized by fibroblastic reticular cells (FRCs) and follicular dendritic cells (FDCs). The FRCs, which comprise several subtypes, constitute the major parenchymal component of the T cell zone and form a tightly meshed hollow conduit network by producing and enveloping extracellular matrix with widely ramified, interconnected projections[18]. The entrance to the conduit system is restricted by sinus-lining lymphatic endothelial cells (LECs) that form fenestrae that contain radicular diaphragms. These diaphragms function as filters formed by plasmalemma vesicle-associated protein fibrils[19], which limit the access of lymphatic components into the parenchyma and into the conduits running under the marginal sinus according to their molecular size (maximum 70 kDa)[20–23]. Therefore, the conduit system transports lymphatic fluid containing low molecular weight components from the marginal and intermediate sinuses through the parenchyma and to the high endothelial venules (HEVs) and into the medullary sinuses. HEVs emerge from arteries that enter the hilum of LNs and branch in the cortex, forming arterioles and dense plexuses of capillaries around the B cell follicles. Here, these vessels form loops and turn into specialized postcapillary venules characterized by cuboidal (as opposed to flattened) endothelial cells, hence the name HEVs. On the way back towards the hilum, the HEVs merge into larger vessels to further exit the LN as medullary venules and finally as draining veins (Fig. 1). This structure allows for the rapid display of chemokines[24] that are transported from the tissue to the draining LN (DLN) HEVs, that consequently allows for the prompt recruitment of immigrating leukocytes from the bloodstream. This allows LNs to respond quickly to inflammation and microbial infections in tissues before they spread.

Compartmentalization of the LN into T cell and B cell domains is controlled by the selective expression of chemokines by the underlying reticular cell network. The FRC network, which braids the T cell-rich paracortex, produces CC-chemokine ligand 19 (CCL19) and CCL21. These chemokines recruit and promote the migration of dendritic cells (DCs) and T cells via CC-chemokine receptor 7 (CCR7). By contrast, the FDC network that extends through the follicles produces CXC-chemokine ligand 13 (CXCL13), which regulates the migratory activity of B cells via CXCR5 (Fig. 1). In addition to these, other chemoattractant fields locally regulate the precise localization of certain lymphocytes. Prime examples are the oxysterols that bind GPR183 to recruit lymphocytes to the interfollicular areas (IFA) of the LN cortex and CCL20, which attracts lymphocytes to the SCS via CCR6 (ref. 16). For further details, we refer the reader to specialized reviews on this topic[25,26]. Following infection, local chemoattractant fields naturally become much more complex, giving rise to microdomains that promote specific interactions or direct lymphocyte differentiation in specific directions[27].

Box 1

The lymphatic vascular system

The lymphatic vascular system (LVS) is the second circulatory system, with the first being the blood vascular system. The LVS consists of lymphatic vessels that sprout from peripheral tissues to collect the lymph and transport it into the blood. The lymphatic vascular tree comprises various subregions with specific functions and specializations[220]. Lymphatic vessels arise in the tissue from blind-ending funnel-shaped structures and are called lymphatic capillaries. These capillaries are characterized by a fenestrated basement membrane, anchorage in the extracellular matrix (ECM), and overlapping, loosely connected lymphatic endothelial cells (LECs) that have an 'oak leaf' appearance[221]. The following segment of the lymphatic vascular tree is composed of collector vessels. Unlike the lymphatic capillaries, the collector vessels are characterized by a continuous basement membrane and tightly interconnected, elongated LECs. Smooth muscle cells surround the basement membrane, and their constriction mediates lymphatic flow and regulates the lymphatic pressure. The interior of the collecting vessels is lined with valves that ensure unidirectional flow of lymph, from tissues to lymph nodes (LNs). The lymph flows from the tissues via the lymphatic vessels through the thoracic or the right lymphatic duct, wherein it is returned to the bloodstream[220].

The interstitial fluid is largely a filtrate of the blood and, therefore, contains soluble proteins, lipids, carbohydrates, metabolites and electrolytes. Its exact composition depends on the tissue in which it is formed and reflects the specific structure, function and metabolic activity of each organ[3]. Increased pressure within the tissue widens the connection between the LECs forming the capillary lymphatics owing to their anchoring with the extracellular matrix. Thereby, macromolecules can bypass the fenestrated basal membrane of the LECs and form the lymph. Therefore, the LVS actively participates in the transport and distribution of metabolites and other molecules[222]. A notable example is the lymphatic system which drains the digestive tract. Long-chain fatty acids, as well as fat-soluble vitamins, are not directly released into the bloodstream after absorption in the intestines, as is the case with other nutrients. Instead, they are packaged into chylomicrons, which are transported via the lymphatic vessels and enter the bloodstream via the thoracic duct[223]. This leads to a particular composition of lymph, which is called chyle, whereas the lymph vessels that transport this fluid are called lacteals. In addition to transporting metabolites, the LVS also serves as a transport system enabling immune cells derived from the peripheral tissue to access the draining LNs.

As mentioned, HEVs connect LNs to the bloodstream. Hence, in addition to being supplied by the tissue-derived lymph, LNs receive blood-derived components. Importantly, HEVs in the IFA serve as entry portals for lymphocytes that are circulating in the blood. At the molecular level, glycosylation-dependent cell adhesion molecule 1 on the HEV surface interacts with CD62L (also known as L-selectin) on circulating lymphocytes[28]. The interaction of CD62L and its ligands, and additional factors including chemokines[29] and integrins[30], supports the rolling and arrest of lymphocytes on the endothelium and their subsequent extravasation into LNs[6]. Upon entry of lymphocytes to the IFA, they can interact with DCs that have migrated from the tissue via the lymph[31]. Remarkably, afferent lymphatic vessels project directly to the IFA (Fig. 1), thereby guiding newly arriving migratory DCs directly to this critical interaction zone. If lymphocytes are not activated by their cognate antigen, they exit the LN by entering the cortical sinuses and are subsequently flushed out via the efferent lymphatic vessel. The transit time of lymphocytes depends on the subset, ranging from approximately 6 to 24 h, and is primarily controlled by a sphingosine-1-phosphate (S1P) gradient that extends across the lymphatic endothelium[32].

Detailed analyses have revealed significant functional differences between LNs draining different organs. This heterogeneity is partly owing to the LN structural components and resident immune cell populations, and partly a consequence of its connection to the tissues. Each tissue harbours distinct immune cell populations that differ in phenotype and function (Supplementary Table 1, Fig. 2), and some of these cells continuously immigrate to DLNs in which they generate and influence immune responses. Additionally, each tissue has its own unique metabolism and releases distinct molecules that modulate the function and differentiation of immune cells in the LN (Supplementary Table 1, Fig. 2). Therefore, the function of LNs draining different tissues is dictated by the associated tissue with its unique properties and function and, in the case of barrier tissues, its microbial composition. In humans, the situation is even more complex because LNs are often arranged in chains and, thus, receive information from both the drained tissue and the upstream LNs[33] (Fig. 3). Importantly, the cellular composition of a LN can be modified by its individual immune history. In the following sections, we will focus on how cellular compositions differ between distinct LNs, ranging from structural cells (stromal) to immigrating and LN-resident immune cells.

Cells can immigrate into LNs either via the blood, as is the case for recirculating cells that are largely shared between LNs, or via the lymph, as is the case for tissue-derived cells that typically differ between LNs. It is the latter population that primarily contributes to LN heterogeneity (Fig. 2) and these tissue-derived cells are the main focus of this Review. We will also discuss the role of soluble tissue-derived factors in shaping lymph node heterogeneity. However, owing to the limited knowledge on this subject (see Supplementary Table 1) and it being an emerging topic, we concentrate on how soluble factors from the tissues control immune responses in the associated LNs using three key examples: the drainage of the intestine, the skin and tumour tissues.

Cell populations and lymph node heterogeneity

The lymphatic system is important for immune cell migration and has two main purposes. First, it enables lymphocyte recirculation and return to the bloodstream. Second, it supports information relay from the tissue to its DLN. Lymphocytes that enter LNs via the bloodstream are

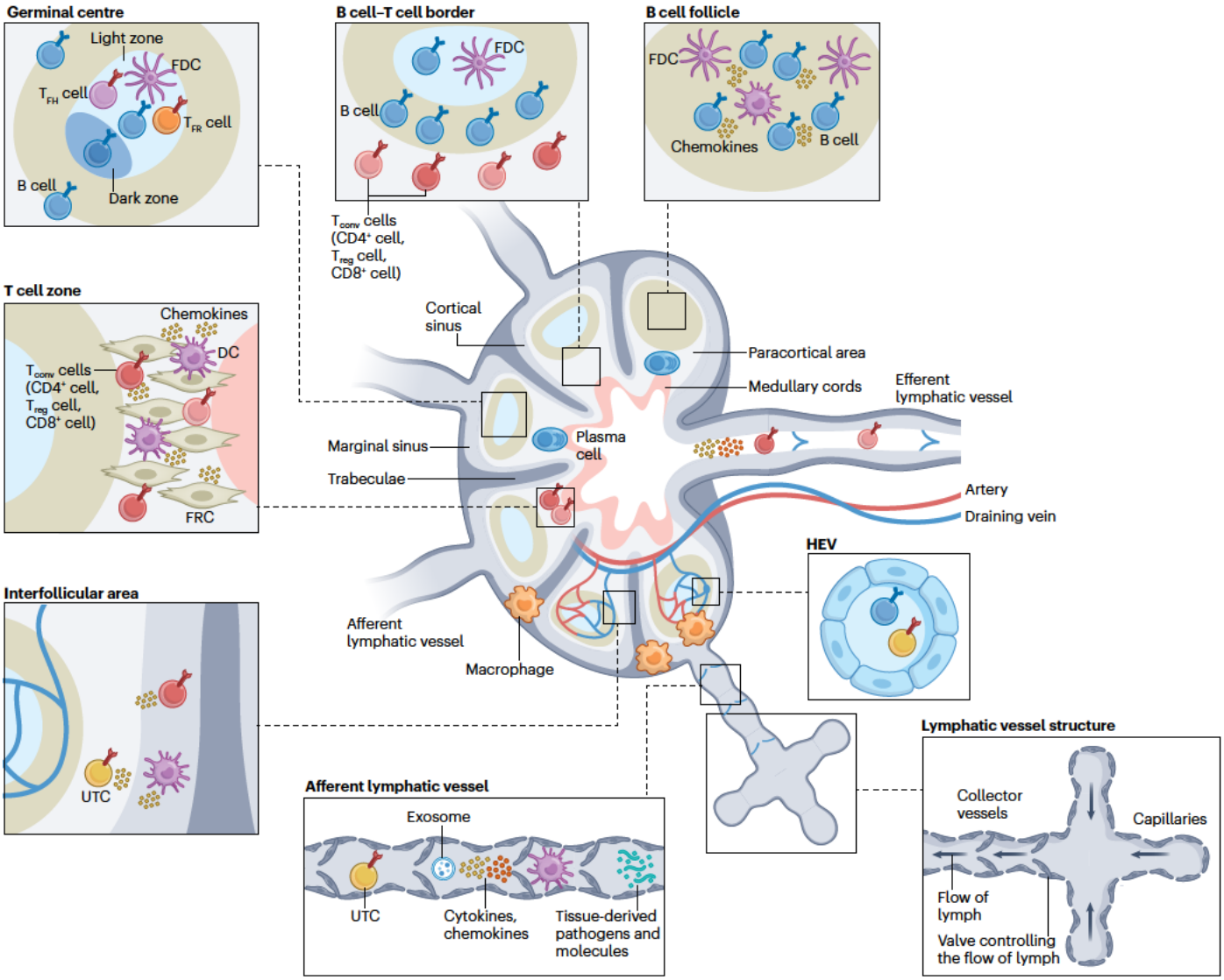

Fig. 1 | Lymph node structure and cellular and molecular composition. The structure of lymph nodes (LNs) is essential for their roles in filtering lymph-borne compounds derived from the tissue and in initiating adaptive immune responses. Funnel-shaped afferent lymphatics emerge in tissues. Fine-structured lymphatics merge to larger collector vessels, which mediate lymphatic flow by containing valves that secure the unidirectional flow of lymph towards the LN. Afferent lymphatics penetrate the capsule of LNs, which is composed of a collagen-rich connective tissue and smooth muscle cells that cover the LNs. From there, the afferent lymphatics extend into the internal LN and reach the subcapsular sinus, which is composed of lymphatic endothelial cells and mainly populated by macrophages. Blood-borne lymphocytes enter LNs via the high endothelial venules (HEVs), partly located in the intrafollicular area, wherein dendritic cells (DCs) and unconventional T cells (UTCs) are located. Fibroblastic reticular cells (FRCs) are responsible for compartmentalizing the LN paracortex into the T cell zone, wherein conventional T (T_{conv}) cells ($CD4^+$ T cells, $CD8^+$ T cells and regulatory T (T_{reg}) cells) and DCs interact. Follicular dendritic cells (FDCs) compartmentalize the follicles into B cell zones, wherein germinal centres are formed, and follicular helper T (T_{FH}) and follicular regulatory T (T_{FR}) cells are localized. Plasma cells are located in the medullary cords of LN. Distinct tissue-derived compounds (chemokines, cytokines, antigens, exosomes and even pathogens) can be passively drained via the lymphatic vessels to the LNs, reaching the sinuses and, depending on the molecular size, also deeper areas of the LN.

transient visitors who continuously patrol and recirculate between SLOs and are, therefore, evenly distributed among LNs draining distinct tissues (for example, naive T cells and B cells). Also, some DCs immigrate as pre-DCs via the bloodstream, proliferate, develop in the LN medulla and execute their function as resident DCs, but they are short-lived and continuously replenished[34]. These cell types probably have a rather small influence on LN heterogeneity. By contrast, cell types that immigrate via the lymph, such as migratory DCs that developed in the tissues and integrate inflammatory and antigenic cues, or unconventional T cells (UTCs) that can directly execute effector functions, significantly contribute to diverging immune response in the LNs (Fig. 2). Additionally, long-lived LN-resident cells contribute to LN heterogeneity.

These cells include stromal cells and endothelial cells that give LNs their structure and anatomy, or lymphocytes that settle after their local stimulation. In the following section, we will discuss these different cell types and explain the mechanisms by which they contribute to functional differences among LNs.

Stromal and endothelial cells

The LN stroma mainly comprises FRCs, FDCs, LECs and blood vessel endothelial cells. These cells influence immune responses and interact with immune cells by the expression of adhesion molecules, chemokines and cytokines, and their phenotype differs between distinct LNs. For example, lower frequencies of cytokine-producing and chemokine-producing FRCs[35] and phenotypically distinct parenchymal reticular cells are found in gut-draining mesenteric LNs (MLNs) than in skin-draining LNs[36]. Given the role of FRCs in regulating T cell zone organization in LNs, heterogeneity among this cell type could potentially lead to diverging immune responses[18]. Indeed, the heterogeneity of stromal cells between LNs further impacts the local induction of regulatory T (T_{reg}) cells and the imprinting of tissue-homing receptors on activated T cells and B cells[37,38]. Experimental evidence for this conclusion was provided by elegant LN transplantation experiments in which popliteal LNs have been transplanted to the mesenteries, or MLNs to the popliteal fossa[37,38]. Importantly, whereas some features of LN stromal cells are plastic and will be rewired by components of the lymph that are unique to the drained tissues, other features of LN stromal cells, such as the capacity to induce tolerance, seem to be imprinted early during development and are maintained following transplantation[39]. These features could potentially be harnessed to prevent or treat autoimmunity.

Given the distinct roles and interactions of the stromal compartment with immune cells[19,37,38,40], a systematic comparison between distinct LNs would help to further delineate local effects on LN-specific immunity. This includes LECs which, as recently reviewed[41,42], differ in their expression of Toll-like receptors, cytokines, chemokines and adhesion molecules[43]. Unfortunately, to date, few studies have directly compared the stromal cell composition between different LNs.

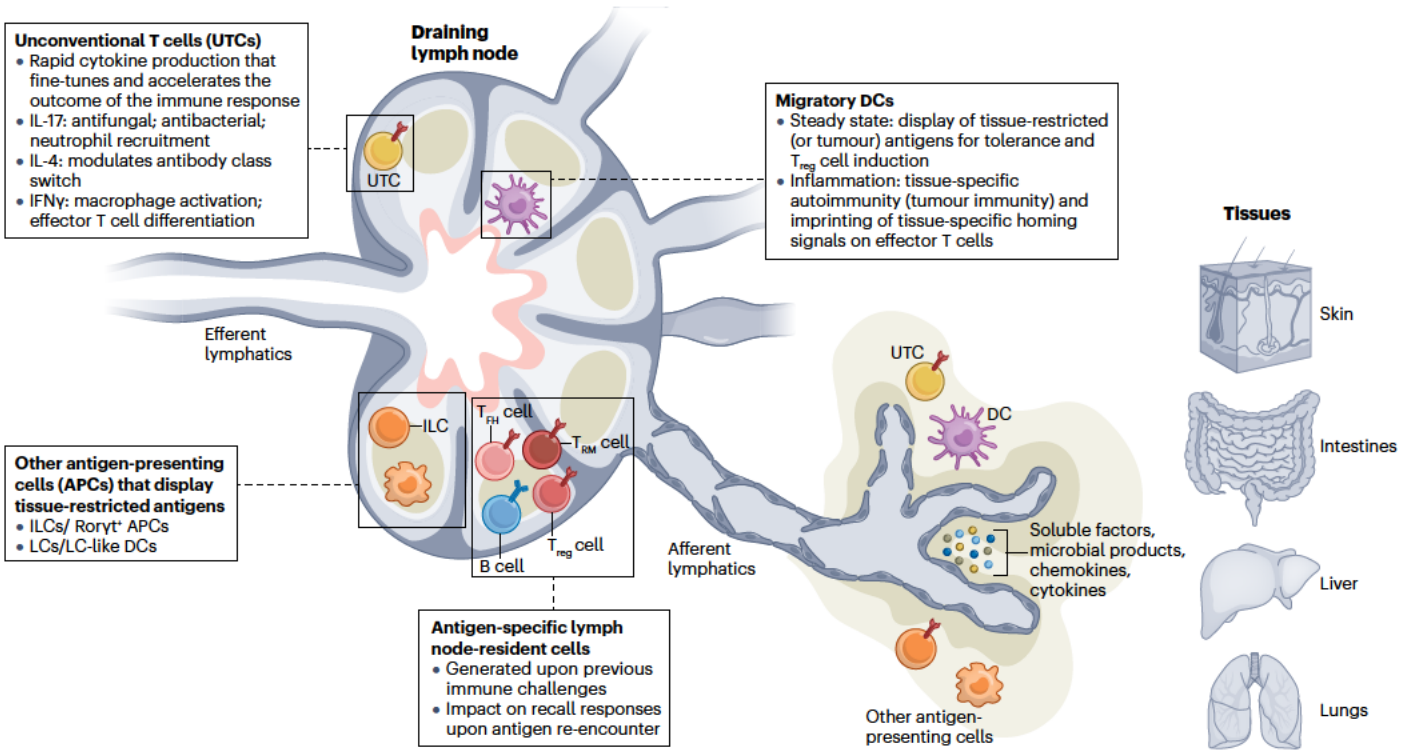

Fig. 2 | Mechanisms underlying lymph node heterogeneity. Lymph nodes are connected to tissues via the afferent lymphatics, wherein lymph flows in a unidirectional manner from the tissue to the lymph node. The lymph composition varies between tissues, owing to its enrichment in metabolites and immune cells derived from the tissue in which it is formed. Lymph serves as a means of transport for tissue-derived migratory immune cells, such as dendritic cells (DCs), unconventional T cells (UTCs), Langerhans cell (LC)-like DCs and RORγt⁺ antigen-presenting cells (APCs). Migratory DCs influence lymph node heterogeneity owing to the transport of tissue-derived antigens that will be presented to T cells, and to their tissue-imprinted transcriptional program to induce tissue-homing signals on effector T cells. Moreover, DCs orchestrate the differentiation of effector regulatory T (T_{reg}) cells by presenting tissue-restricted antigens for the induction of tolerance. Tissue-derived UTCs possess a distinct effector differentiation status depending on the tissue of origin (for example, there are more Th17-like cells in the skin and Th1-like cells in the small intestine). Therefore, they set distinct inflammatory environments in the draining lymph nodes owing to the production of different cytokines that will fine-tune and accelerate specific immune responses in distinct lymph nodes. Additionally, within the lymph, tissue-derived soluble factors such as cytokines, chemokines and microbial products are also drained to lymph nodes. Soluble factors and other molecules drained from tissues to lymph nodes will influence immune responses to various degrees, but the details are largely unknown. In addition to lymph-derived immune cells and soluble factors, antigen-specific lymph node-resident cells such as resident memory T (T_{RM}) cells, follicular helper T (T_{FH}) cells, T_{reg} cells and B cells partake in lymph node heterogeneity upon re-encounter with their cognate antigen, facilitating and modulating secondary immune responses. ILC, innate lymphoid cell.

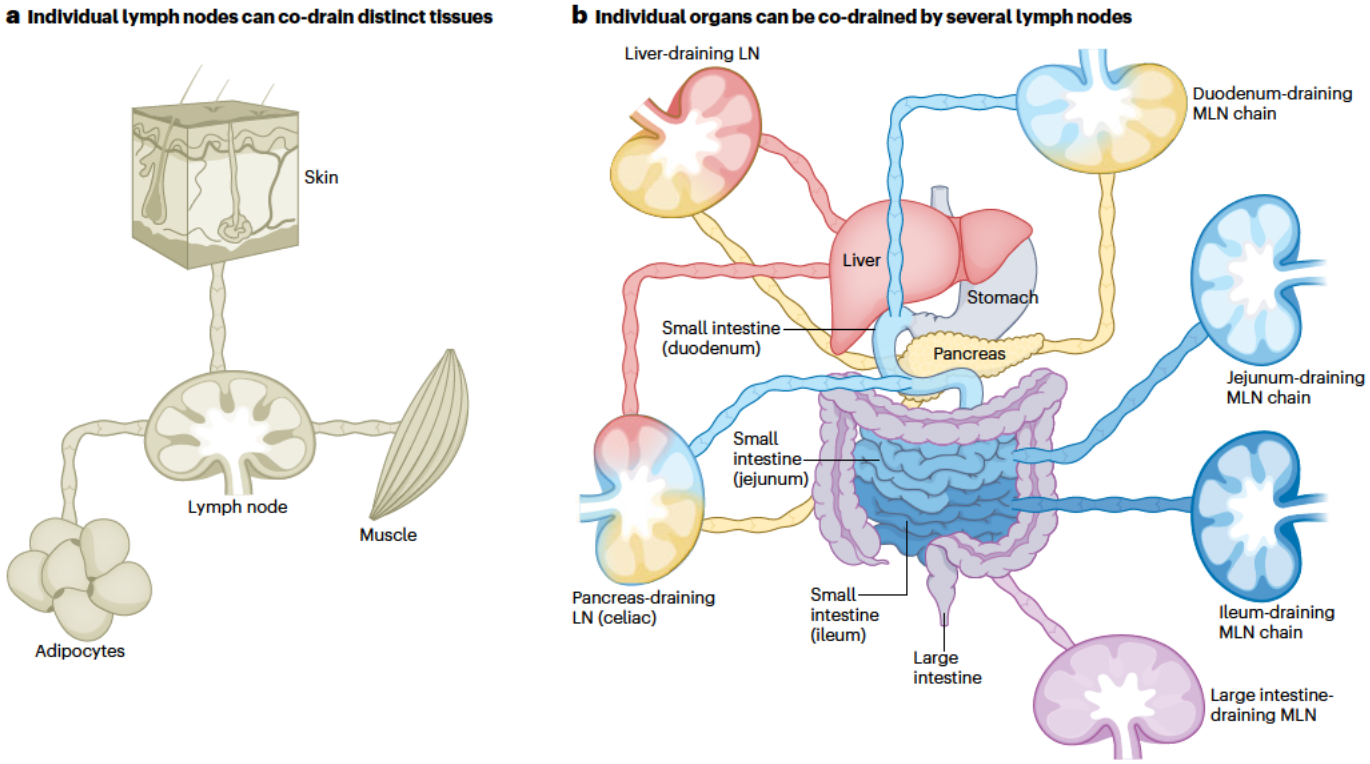

Fig. 3 | Complexity of lymph drainage. a, The way an individual lymph node type, such as the skin-draining lymph nodes, can co-drain multiple organs or tissues is depicted — here, the lymph node shown is draining the skin, fat and muscle tissues. **b**, Furthermore, and particularly in humans, individual organs are co-drained by more than one lymph node in a hierarchical manner. In mice, the pancreas-draining lymph node co-drains the pancreas, the liver and the duodenum, whereas the pancreas is additionally drained by duodenum-draining and liver-draining lymph nodes. Naturally, lymph node co-drainage will influence the cellular and molecular composition of the lymph drained to distinct lymph nodes. Therefore, the immune responses will be defined by a mixture of tissue-derived cellular and molecular factors from distinct origins. LN, lymph node; MLN, mesenteric LN.

Dendritic cells

Conventional DCs (cDCs) are myeloid cells that are specialized in activating lymphocytes[44]. cDCs excel in antigen uptake and antigen presentation, express a plethora of costimulatory and co-inhibitory molecules, and produce numerous immunomodulatory mediators[45]. The expression of these molecules by DCs is regulated by pattern recognition receptors, cytokine receptors and G protein-coupled receptors, which allow cDCs to sense environmental changes, in particular infections, damage and other inflammatory mediators[46]. The activation of cDCs, which also continuously occurs during homoeostasis, has been termed cDC maturation[45]. Conceptually, it is helpful to discriminate between homoeostatic versus inflammatory cDC maturation. However, at the molecular level, both processes are largely identical[47]. The prevailing view is that homoeostatic maturation of cDCs serves to maintain immunotolerance. However, the mechanistic basis of how cDCs mature during homoeostasis and how they mediate their tolerogenic function is still largely unknown. Clearly, cDCs are critical cellular platforms on which various sources of information are received, processed, integrated and further transmitted to lymphocytes in order to initiate and guide immune responses that are tailored towards the specific challenge[48]. Thus, cDCs are critical to maintain and reestablish homoeostasis following immune challenges.

On the basis of the structure of the lymphatic system, inflammatory mediators, antigens and pathogens can directly gain access to the DLNs. LN-resident cDCs can access the lymph and initiate adaptive or tolerogenic immune responses. However, this pathway alone seems to be insufficient to fully inform the DLN on the status and critical changes within tissues. Therefore, cDCs in tissues not only access and integrate local information but also deliver it to the DLN. They do this actively by CCR7-dependent migration via lymphatic vessels. CCR7 is upregulated during both inflammatory and homoeostatic cDC maturation[48]. Therefore, cDCs continuously migrate to DLNs, in which they constantly report the status of the tissue during homoeostatic or inflammatory conditions. In the DLN, they can interact directly with lymphocytes or relay information to other cDC populations residing in the LN, as has been demonstrated in the context of herpes simplex virus infections[49]. Following the discovery of cDCs in 1973[50], the question on whether these cells functionally differ between lymphoid tissues arose. It was anticipated that lymphoid tissues that drain mucosal sites would need to induce B cells that switch to IgA synthesis for optimal protection, and it was indeed found that T cells and cDCs isolated from Peyer's patches (PPs) have a much higher capacity for doing this[51]. Later, it was shown that cDC-derived retinoic acid together with IL-6 played a critical part in inducing IgA class switching in gut-associated lymphoid tissues. This provided a first molecular explanation for the divergent immune response induced in different lymphoid organs by migratory cDCs[52].

As different tissues are exposed to different levels of foreign proteins and commensal organisms, it would make sense for their

associated DLNs to show varying capacity to induce tolerogenic immune responses. In 1996, it was reported that DCs isolated from PPs and the spleen differed in their capacity to induce Th1 versus Th2 cell responses, with PP-derived DCs showing greater induction of Th2 cell responses[53]. From today's point of view, this and other early studies have significant limitations because CD11c was used as the sole marker to identify DCs and the distinction from macrophages was, thus, unclear. Additionally, there was a lack of awareness of additional $CD4^+$ T cell differentiation states such as T_{reg} cells and Th17 cells. However, this basic idea turned out to be correct and was elegantly demonstrated two decades later. Specifically, it was shown that LNs that drain different segments of the gut promote either T_{reg} cell or Th17 cell differentiation in response to the same model antigen[54]. This was associated with distinct gene signatures in the cDCs and stromal cells that populated these lymphoid tissues. Moreover, it was recently shown that a subpopulation of migratory DCs, cDC1s, show transcriptional distinctions that are based on their tissue of origin. Liver-derived and pancreas-derived migratory cDC1s present a pro-inflammatory phenotype, whereas duodenum-derived cDC1s are more tolerogenic[55].

As well as showing different capacities to instruct tolerogenic or inflammatory B cell and T cell responses, migratory cDCs from different LNs vary in their ability to upregulate trafficking molecules, such as chemokine receptors and adhesion molecules on T cells[56–58]. For example, T cells primed by cDCs isolated from PPs, but not cDCs from the spleen or skin-draining LNs, upregulate CCR9 and the gut-homing integrin α4β7. These studies have established the concept that migratory cDCs imprint a specific tissue-homing program during T cell activation, which promotes T cell migration to the affected tissue. Migratory cDCs also seem to imprint naive T cells in the steady state, with a more recent study showing that the capacity of naive CD8 T cells to differentiate into tissue-resident memory T (T_{RM}) cells depends on their prior interaction with migratory cDCs derived from the aforementioned tissue[59].

Further work is needed to address tissue-specific imprinting, especially by migratory cDCs, because previous studies are largely limited to the comparison of cDCs from LNs with cDCs from PPs and the spleen, which are SLOs but differ from LNs in several aspects (Box 2). Also, the exact molecular mechanism of how distinct tissue derived-signals lead to a heterogeneous DC function (for instance, immunogenic versus tolerogenic) in steady state requires further research. Nevertheless, it is clear that migratory cDCs are crucial for tailoring lymphocyte responses in DLNs to the associated tissue and, hence, contribute significantly to LN heterogeneity (Supplementary Table 1, Fig. 2).

Unconventional T cells

UTCs are a heterogenous group of cells that include three major lineages — γδ T cells, mucosal-associated invariant T (MAIT) cells and natural killer T (NKT) cells. Like conventional T cells, UTCs originate from the thymus but have several properties that differ from those of conventional αβ T cells. Firstly, UTCs are restricted to non-polymorphic antigen-presenting molecules, such as MR1 for MAIT cells[60–62] and CD1d for NKT cells[63–65]. In fact, the majority of γδ T cells are not restricted to a particular antigen-presenting molecule but can bind unprocessed antigens in a similar manner to B cells[66]. Secondly, the antigens that are recognized by UTCs are typically not derived from proteins. MR1 binds and presents bacterial metabolites[67], whereas CD1d presents diverse lipid species[64,68,69]. The antigens that are recognized by murine and human γδ T cells are largely unknown. However, a subset of humans γδ T cells can recognize phosphoantigens presented by butyrophilins[66,70]. Lastly, a large fraction of UTCs differentiate into effector subsets during their development in the thymus and subsequently seed various tissues in developmental waves[71].

Functionally, tissue UTCs interact with commensal organisms, maintain tissue homoeostasis and participate in tissue healing and pathogen defence[69,71–75]. To execute these functions, UTCs can be activated via their specific T cell receptor (TCR) or via specific cytokines. Therefore, they are often described as a bridge between innate and adaptive immunity. Accordingly, we and others have shown that despite their division into distinct lineages based on their TCR sequence, the UTC family members (NKT cells, MAIT cells and γδ T cells) are transcriptionally and functionally highly similar and can compensate for each other if they have the same effector differentiation, for instance, if they are Th1-like, Th2-like or Th17-like[76–79].

On the basis of parabiosis experiments, tissue subsets of UTCs have been considered to be tissue-resident, similar to innate lymphoid cells (ILCs)[80–82]. However, it has been shown that some Th17-like γδ T cells can migrate from the skin to the associated DLNs via lymphatics in an S1P receptor (S1PR)-dependent manner[83,84]. Our own group has recently shown that the lymphatic migration of Th17-like γδ T cells from the skin is not an exception but instead represents a general principle for UTCs across tissues and differentiation states[79]. As different tissues

Box 2

The spleen and Peyer's patches

The spleen and Peyer's patches (PPs) are secondary lymphoid organs (SLOs) but they differ in several aspects from lymph nodes (LNs). The spleen can be divided into the red pulp and the white pulp, separated by either the marginal zone in rodents or the perifollicular zone in humans[224]. The spleen lacks afferent lymphatic vessels, and in contrast to LNs, immune cells and antigens enter via the blood, which is connected to the red pulp via an open circulation[225]. An important cell type in the red pulp are macrophages, which filter the blood and remove aged erythrocytes from the circulation[226]. Lymphocytes, such as T cells, enter the white pulp via perivascular migration[227], whereas their exit route is still unclear. The white pulp is structured similar to LNs, containing B cell follicles and a central T cell zone to initiate adaptive immune response against blood-borne pathogens[228].

PPs line the wall of the small intestine[229]. Their development depends on the microbiota and their numbers can vary between individuals (humans have approximately 100–200 PPs, whereas mice have 6–12 PPs)[230–232]. PPs are structurally organized like LNs, harbouring large B cell follicles and T cell zones, but they lack a capsule. Functionally, this is critical because it enables a direct access to gut antigens. Specifically, PPs are lined with follicle-associated epithelium containing microfold cells (M cells) that are specialized to transport antigens from the mucosa and transmit them to the underlying B cells. Lymphocytes immigrate to PPs in a similar manner as to LNs via high endothelial venules (HEVs) and exit via lymphatic vessels[233], although certain differences do exist. A functional hallmark of the PPs is the generation of IgA-switched plasma cells, which regulate the interplay and homoeostasis with the microbiome[234].

Glossary

Affinity maturation and antibody class switching
Affinity maturation and antibody class switching are two important mechanisms B cells use to improve the efficacy of the antibody response. Once B cells have recognized their cognate antigen through the B cell receptor (BCR), they start producing IgM antibodies and this is known as the primary response. To increase the binding affinity of the BCR to cognate antigen, B cells introduce mutations into the complementarity-determining region of the BCR via a process known as somatic hypermutation (SHM). SHM produces B cells with varying affinities of BCRs, and only the ones with the strongest affinity are positively selected by follicular helper T cells in germinal centres. During antibody class switching, changes occur in the heavy-chain domain of the antibody, creating antibodies with similar affinity but different effector functions. This process involves recombining the exon clusters on the IgH locus, enabling antibody isotype switching (for example, from IgM to IgG, IgE or IgA).

Aryl hydrocarbon receptor
(AhR). A ligand-activated transcription factor, which upon ligand binding translocates from the cytoplasm to the nucleus, forms a complex with aryl hydrocarbon receptor nuclear translocator and induces transcription of target genes. In its inactive state, it forms a protein dimer complex with HSP90, XAP2, p23 and SRC. AhR has diverse roles in adaptive immune responses, such as promoting Th17 cell induction or T_{reg} cell stabilization.

Central T_{reg} cells
T_{reg} cells can be classified either on their developmental origin — as tT_{reg} and pT_{reg} cells — or based on their migratory pattern — as central T_{reg} and effector T_{reg} cells. Central T_{reg} cells primarily recirculate in the blood and SLOs. They are characterized by a $CD4^+CD25^+FOXP3^+CD44^{low}CD62L^{high}CCR7^+$ phenotype and primarily localize to the T cell zone in the spleen and lymph nodes. They require IL-2 for their homoeostasis and survival and serve as a pool of long-lived recirculating T_{reg} cells in SLOs.

Effector T_{reg} cells
Effector T_{reg} cells develop from central T_{reg} cells in a BATF-dependent manner and require ICOS signalling for their survival. Even though inflammatory signals primarily drive the differentiation of effector T_{reg} cells from central T_{reg} cells, constant T cell receptor stimulation is required for the maintenance of effector T_{reg} cells. These T_{reg} cells have a $CD4^+CD25^+FOXP3^+CD44^{high}CD62L^{low}CCR7^-$ phenotype and primarily localize to non-lymphoid tissues.

Exosomes
Exosomes are single-membraned extracellular vesicles that are produced by cells in the endoplasmic reticulum and can carry different types of cargo from nucleic acids to proteins or metabolites. They are critical components in cellular communications both over short and long distances.

Hyaluronic acid
Hyaluronic acid is a large polysaccharide formed of glucuronic acid and glucosamine, with an approximate relative molecular weight of 10^5–10^7 (ratio of the molecular weights of hyaluronic acid and carbon). It is produced by distinct cell types and is the main component of the extracellular matrix.

Sphingosine-1-phosphate
(S1P). A sphingolipid that is formed from ceramide by the action of ceramidase and sphingosine kinases (SK1 and SK2). S1P acts as a crucial mediator in lymphocyte trafficking, vascular development and heart development via its receptors S1PR1–S1PR5.

Tumour secretome
The tumour secretome is the entire collection of macromolecules — including both soluble proteins and insoluble vesicles — that take part in cell–cell communication in the tumour (for example, growth factors, lipids and exosomes).

are developmentally seeded by different UTC subsets and lineages with distinct TCR repertoires, they vastly differ regarding their specific composition and function. Owing to their migratory behaviour, this heterogeneity is also reflected in the DLNs[79] (Supplementary Table 1, Fig. 2). Based on cytokine production and cellular immune responses, we have shown that UTCs from distinct LNs drive different cellular and humoral immune responses, which contributes significantly to the functional heterogeneity among these LNs. For example, Th17-like UTCs are largely absent in MLNs, but they are abundant in skin-draining LNs and lung-draining LNs. As a result, IL-17-dependent neutrophil recruitment to the MLNs is markedly reduced and delayed following bacterial spread via the lymph as compared with the skin-draining LNs[79]. Conversely, there are hardly any IL-4-producing NKT cells in the skin or in the skin-draining LNs, whereas they are numerous in the lung and lung-draining LNs. Functionally, these IL-4-producing NKT cells are important for IgG1 production after infection with influenza or vaccinia viruses[79,85]. A caveat is that most of the data so far are derived from animal models. Therefore, a validation of the migratory route of UTCs and their functional impact on LNs in humans is urgently needed.

Lymph node-resident memory T cells

Following activation by their specific antigen, T cells undergo clonal expansion and differentiate into effector T cells, including different helper T cell subsets[86]. Activated T cells also give rise to a spectrum of effector states ranging from short-lived terminally differentiated cells to effector memory T (T_{EM}) cells and long-lived central memory T (T_{CM}) cells[87,88]. Some effector T cells persist in specialized niches in peripheral organs as the so-called tissue-resident memory T cells[89]. LNs typically contain T_{CM} cells, which recirculate between SLOs, albeit at slower kinetics than their naive counterparts[90,91]. LNs may also contain T_{EM} cell populations that scan tissues and enter via the lymphatic vessels on their way to the bloodstream. Both T_{CM} and T_{EM} cell populations are expected to equally distribute between SLOs following the resolution of infections. However, tracking studies have found that up to 50% of $CD4^+$ T_{EM} cells in lymphoid organs are retained for several weeks[92,93]. These locally retained antigen-specific $CD4^+$ T cells comprise a heterogeneous population including T follicular helper (T_{FH}) cells[94]. $CD8^+$ T_{RM} cells have been shown to immigrate to DLNs via the lymphatic route, wherein they can be locally maintained and partially retain their tissue imprinted signature[30,95–97]. As a consequence, different LNs contain distinct sets of resident $CD4^+$ and $CD8^+$ T cells that differ in their effector functions and in their TCR repertoires, based on the distinct immune history of each LN and its associated tissue. Therefore, localized populations of memory T cells contribute significantly to the heterogeneity seen between LNs and continue to be shaped and adapted throughout life.

Regulatory T cells

T_{reg} cells are a specialized subpopulation of $CD4^+$ T cells that express the transcription factor FOXP3 and are essential for preventing autoimmunity and maintaining homoeostasis[98,99]. T_{reg} cells are typically divided into thymic (tT_{reg}) and peripheral (pT_{reg}) subsets based on their developmental origin[100]. Additionally, T_{reg} cells can be divided into central T_{reg} cells,

which express CD62L and recirculate between SLOs, and effector T_{reg} cells, which populate peripheral tissues. Importantly, LNs also contain a sizeable population of effector T_{reg} cells (in the MLNs, for example, these cells constitute up to 60% of total $CD4^+FOXP3^+$ T cells)[101] and the size of this population differs between LNs that drain different sites and further increases with age[102]. Additionally, we recently found that 10–20% of all T_{reg} cells in LNs are memory-like resident cells[103]. Importantly, resident and circulating T_{reg} cells had distinct TCR repertoires, and each LN contained exclusive clonal subpopulations of resident T_{reg} cells. Because the TCR specificity of T cells and their effector differentiation program bestows them with different capacities and mechanisms to suppress specific immune responses[104], individual LNs probably differ in their function to suppress specific immune responses. Indeed, it was recently shown that skin-draining LNs contain fewer Th1-like effector T_{reg} cells than lung-draining LNs and that this impacts the antitumour responses that are generated in these respective LNs[105]. Regarding autoimmunity, even more subtle shifts in T_{reg} cell parameter values can initiate autoimmune states because this mechanism is based on negative feedback by regulating IL-2 availability[106,107]. Therefore, local changes in T_{reg} cell density (less than twofold) or expression of suppressive molecules may shift the equilibrium in individual LNs towards immune activation by DCs presenting distinct tissue-restricted antigens from the draining site[108,109]. In summary, there is clear evidence that T_{reg} cell populations differ between LNs and that these differences also have a functional impact on locally emerging immune responses (Fig. 2). We suspect that this will have a particular impact on autoimmunity and on immune control of tumours.

Follicular B cells and T cells

An essential function of LNs is to support antibody responses. Activated B cells interact with T_{FH} cells to form germinal centres (GCs) and undergo affinity maturation and class switch recombination. Within the GC, B cells can become either memory B cells or high-affinity long-lived plasma cells. B cell responses can be heterogeneous based on the antigen (protein or not protein) and the costimulatory input that naive B cells receive upon activation[110]. This affinity maturation and antibody class switching is influenced by local factors and interactions with cell types, which differ across LNs. For example, gut-associated lymphoid tissues display a preference in inducing IgA-producing plasma cells, which is at least partly supported by cDC-derived retinoic acid and IL-6 (ref. 52).

T_{FH} cells are a subset of $CCR7^-CXCR5^+$ $CD4^+$ T cells that support B cell maturation and antibody class switching[111]. They are recruited and retained in the B cell follicles of LNs via the CXCR5–CXCL13 axis[112]. Upon activation, some high-affinity naive $CD4^+$ T cells upregulate CXCR5, differentiate into T_{FH} cells and permanently reside in DLNs as long-lived T_{FH} cells[113,114]. At the molecular level, T_{FH} cells guide B cell maturation via their expression of costimulatory molecules (such as CD40L, ICOS and OX40) and cytokines (such as IL-4 and IL-10), which recruit B cells into GCs to generate long-lived memory B cells and promote their antibody class switching[115]. Antigen-specific T_{FH} cells, B cells and antibody-secreting cells seem to preferentially establish and persist in the DLN of the tissue wherein antigen is initially encountered because they are not found in non-draining LNs or the spleen[93]. Moreover, T_{FH} cell function depends on their location; for instance, splenic and MLN-resident T_{FH} cells dramatically differ in the amount of IL-4 they produce[94]. Importantly, T_{FH} cell-mediated B cell responses are regulated by antigen-specific follicular regulatory T (T_{FR}) cells[116,117], which suppress humoral responses and autoreactive B cells[118]. Clearly, following a germinal centre reaction, LNs generate and locally maintain unique T_{FH} and T_{FR} cell populations that may impact on future immune responses initiated in these LNs.

However, there is also evidence that even unchallenged LNs differ in their capacity to generate distinct T_{FH} and T_{FR} cell populations. One group has used RNA sequencing to compare T_{FH} and T_{FR} cells in DLNs following subcutaneous or intranasal immunization. They found several differentially expressed genes when comparing T_{FH} or T_{FR} cells from skin-draining LNs with their counterparts in lung-draining LNs. For instance, lung-draining LN T_{FH} cells from the intranasally immunized mice had a Th2-like gene signature (*Gfi1*, *Gata3*, *Il13*), whereas T_{FH} cells from skin-draining LNs expressed *Icos*, *Id2*, *Id3*, *Batf3* and *Il17re*. T_{FR} cells from lung-draining LNs and skin-draining LNs did not express a Th2-like gene signature but differed in the expression of other genes, such as *Itga4*, *Fan1*, *F13a1* and *Klf11* (ref. 119). A caveat of the comparison is that different antigens were used for the intranasal and subcutaneous immunization. In summary, distinct LNs differ in their capacity and function to induce humoral immune responses, and this appears to be owing, at least in part, to differences in their local resident T_{FH} and T_{FR} cell populations.

Other cell types

It is possible that other cell populations also contribute to LN heterogeneity. For example, Langerhans cells (LCs) reside in the stratified epithelium of mucosal surfaces and migrate to DLNs but are absent in LNs draining internal organs. A recent study challenges the capability of LCs to migrate to the DLN describing a population of LC-like DCs[120]. Also, a new population of $ROR\gamma t^+$ antigen-presenting cells was identified in skin-draining LNs and mucosal tissue-draining LNs[121–123]. Profiling of these cells indicated an ambivalent identity showing factors associated with both cDCs (for example, Zbtb46) and type III innate lymphoid cells (for example, *Il7r* and *Rorc*)[124–126]. Some of these cells also express the autoimmune regulator (AIRE) and are, therefore, classified as extrathymic AIRE-expressing cells (eTACs)[127]. Importantly, like cDCs, eTACs migrate from tissues to DLNs in a CCR7-dependent manner and appear to have a critical role in regulating immune homoeostasis[121]. Although we are only beginning to understand the exact function of these cells, it is clear that their abundance differs between distinct LNs[122] and they appear to be enriched in LNs draining mucosal tissues. Overall, which myeloid cell subsets migrate to the DLN from distinct tissues and how they influence the local immune response remain to be investigated further.

Additionally, lymphoid, innate-like immune cells, such as ILCs and B1 cells, can also be detected in LNs and may contribute to shaping immune responses within them, especially because it has been demonstrated that B1 cells can migrate from the tissue to the DLN in a similar manner to UTCs[128].

Conclusions on lymph node cellular heterogeneity

The majority of immune cells populating the LNs recirculate between them, resulting in a regular distribution of these cells. However, some cell types like cDCs and UTCs continuously migrate from tissue to the DLNs and, thereby, import tissue-specific information that helps to generate LN-specific immune responses (Supplementary Table 1, Fig. 2). In addition, the local immune history induces LN-resident immune cell populations, such as memory T cell subsets, T_{reg} cells, T_{FH} cells and B cells. These populations further modulate the immune response that is generated in distinct LNs. It is becoming more evident that, in addition to LN-resident immune cell populations, local stromal cells also display LN-based heterogeneity. Initial studies have demonstrated

that these differences could impact the immune response and future studies will shed more light on its influences. Addressing the contributions of distinct cell types in a detailed manner will be important for fully understanding the cellular factors that shape LN heterogeneity. In the following sections, we will focus on the soluble factors that are found in the lymph and how these further diversify immune responses that are generated in specific LNs.

Soluble factors contributing to lymph node heterogeneity

Several studies have characterized the molecules that are transported from tissues via the lymph in homoeostatic conditions[129,130]. These molecules include proteins[23,131], hyaluronic acid[132–134], exosomes[135–137], enzymes[138], lipoproteins[139], amino acids[140], glycoproteins and lipids[141], nitric oxide[142,143], and cytokines and chemokines[144] (Fig. 2). Further studies will be needed to elucidate the direct lymphatic drainage of other tissue-derived molecules, such as ions, neurotransmitters (for example, serotonin[145]) and hormones, considering their abundance in tissues. Many of these molecules have a well-documented role in modulating immune cells[142]. For instance, several amino acids have been shown to influence immune cells in different manners. Tryptophan catalysis by the enzyme indoleamine 2,3-dioxygenase (IDO) enhances the differentiation of naive $CD4^+$ T cells to T_{reg} cells[146], whereas arginine is an important factor for T cell and myeloid cell activation and function[147–149]. Additionally, glutamine regulates Th1 versus T_{reg} cell differentiation[150], and the breakdown of arginine and tryptophan in cDCs promotes their immunosuppressive function[151]. Similarly, hormones and neuropeptides regulate immune responses. Oestrogen influences myeloid cell function and regulates T_{reg} cell differentiation[152,153], whereas serotonin executes a wide spectrum of immune functions as recently reviewed[145].

On the basis of the insights from the field of immunometabolism, it is obvious that molecules and metabolites found in lymph significantly influence and control the differentiation and function of immune cells. Therefore, fluctuations in the abundance and composition of these metabolites will probably impact immune cell function, particularly during their activation under inflammatory conditions. Indeed, there is data suggesting that the environment in which $CD4^+$ T cells are primed (for example, skin-draining LNs versus MLNs) has a direct impact on their phenotype and their role during autoimmunity[154]. Nevertheless, whether the metabolites significantly differ between lymph drained from different tissues and, hence, in the associated LNs still needs to be addressed systematically (Supplementary Table 1).

In multicellular organisms, organs have a distinct structure and function and, therefore, the products of their metabolism also largely differ. This was elegantly demonstrated by a group who quantified the production and consumption of metabolites by measuring their abundance in arterial and venous blood in several distinct organs in pigs[155]. They found that these different organs release numerous metabolites related to their specific anabolism and catabolism. Of course, this study focused on analysing the blood and not the lymph, yet it is fair to assume that the lymph of these tissues shows comparable changes in their metabolic composition as the venous blood.

Moreover, it has been shown that LNs are very effective in clearing tissue-derived metabolites and proteins transported via the lymph[156,157]. This suggests that the DLN cells are exposed to tissue-drained metabolites that do not access other LNs and, probably, have distinct effects on them. A few studies have directly determined the composition of the lymph derived from distinct tissues in homoeostatic conditions during infection and diseases using bovine, rodent, canine and human samples[131,158–160]. Together, these studies have shown that the molecular composition of the lymph indeed mirrors the drained tissue. Thus, the lymph can be used as an important tool to study the tissue-specific physiological or pathological state[3,161,162]. Unfortunately, the focus of most of these studies has been limited to analysing the lymph composition from a specific site rather than directly comparing lymph derived from distinct tissues. Accordingly, there are currently no studies that have systematically compared the functional impact of soluble factors from lymph of various sites on immune responses. Nevertheless, the role of some individual molecules in influencing local immune responses in specific LNs has been clarified (Supplementary Table 1). In the following section, we will review how some of these soluble factors contribute to the functional heterogeneity between distinct DLNs. Finally, we will discuss how solid tumours manipulate immune responses by releasing distinct molecules to the lymph and the DLN.

Gut-draining and liver-draining lymph nodes

The intestine serves as an essential organ for the absorption of nutrients and, consistently, the metabolic products that are generated during this process are also found in the lymph and the DLNs. Naturally, these metabolic products are distributed systemically, but their concentrations differ between organs and LNs. For example, metabolites absorbed via the intestine and microbial products have an increased concentration within the mesenteries. Additionally, the individual intestinal segments have specialized functions for the absorption of certain substances and harbour different microbial communities. Proteins and carbohydrates are absorbed in the small intestine. Lipids, bile acids and lipid-soluble vitamins (vitamin A, vitamin D, vitamin E and vitamin K) are primarily absorbed in the terminal ileum. The large intestine is important for the recovery of water and electrolytes, as well as the fermentation of some of the indigestible food matter by bacteria. Therefore, different segments of the gut and their associated LNs have distinct requirements regarding tolerance towards food antigens and the local microbiota. Accordingly, the LNs draining the small and large intestines are anatomically and immunologically distinct[163]. Even within the small intestine, there are differences, with LNs draining the proximal part preferentially eliciting tolerogenic responses. By contrast, the LNs draining the distal part has a higher tendency to elicit pro-inflammatory T cell responses[54]. Importantly, microbial-derived metabolites in the gut differ based on their origin: there are metabolites that bacteria produce from the diet (for example, short-chain fatty acids (SCFAs)), host-produced metabolites that are modified by bacteria (for example, secondary bile acids), and metabolites that are de novo synthesized by bacteria (for example, branched-chain amino acids)[164].

One group of bacteria-derived metabolites are products of tryptophan metabolism and these can bind and activate the aryl hydrocarbon receptor (AhR)[165]. Ligands for the AhR are prominently produced by *Lactobacillus* during the degradation of tryptophan[166] or directly obtained through ingestion of AhR ligand-containing food such as broccoli or brussel sprouts, among others[167]. Activation of AhR has been shown to influence the activation and differentiation of several immune cells including ILCs[168], T cells[169] and cDCs[170]. Deficiency of AhR or lack of its ligands owing to overexpression of their degrading enzymes[171] disturbs intestinal homoeostasis leading to barrier dysfunction. It is clear that AhR ligands act systemically, but it is possible that the concentration of these ligands varies greatly depending on the tissue and, thus, on the DLN. Therefore, we hypothesize that these differences will affect the local immune responses generated in the respective LNs.

Vitamin A is another metabolite that has been shown to regulate local immune responses in various studies. Vitamin A is a lipid-soluble vitamin that is transported as retinyl esters in the form of chylomicrons from the intestine to the draining MLNs via the lacteals, and it is drained into the blood circulation afterwards[172]. Chylomicrons are responsible for distributing lipids and fat-soluble vitamins to tissues. Therefore, they are hydrolysed in tissues and reduced in size and density before their final catabolism in the liver. These smaller residual chylomicrons are referred to as chylomicron remnants, which contain high amounts of vitamin A metabolites (retinyl esters) that rapidly accumulate in the hepatic stellate cells. Hence, this organ is the major site of vitamin A accumulation across species, from which it can be redistributed to other tissues when required[173,174]. The MLNs have high levels of the vitamin A metabolite retinoic acid, which in turn promotes the induction of pT_{reg} cells[175]. As mentioned earlier, retinoic acid is also important for imprinting gut-homing receptors on T cells[32]. Therefore, variations in retinoic acid concentrations can contribute to local differences in effector T cells and T_{reg} cells in LNs[38]. When TCR transgenic ovalbumin (OVA)-specific $CD4^+$ T cells were adoptively transferred to mice prior to oral or intravenous immunization with OVA peptide, higher numbers and frequencies of T_{reg} cells were observed in mesenteric and liver-draining coeliac LNs than in popliteal LNs, regardless of the immunization route. This difference was attributed to early-life imprinting of LN stromal cells by retinoic acid and the microbiota[38]. Notably, retinoic acid was shown to be dispensable for T_{reg} cell induction in MLNs, whereas the microbiota was essential. Opposingly, retinoic acid was indispensable for T_{reg} cell induction in coeliac LNs, whereas the microbiota was not.

As well as retinoic acid, microbiota-derived SCFAs — such as acetate, propionate and butyrate — are produced in the small intestine by fermentation of soluble dietary fibres by the microbiota. Several recent studies have shown how microbiota-derived SCFAs influence immune responses[176], including pT_{reg} cell induction[177], $CD8^+$ memory T cell formation[178], B cell differentiation and antibody production[179] and $CD4^+$ T cell differentiation[180]. For a summary of the effects of other lipids on immune cells, we refer the reader to an in-depth review on this topic[181]. These lipids probably have a concentration-dependent function and, therefore, their impact on immunity probably differs among LNs draining distinct tissues. Overall, in-depth studies delineating the amount of intestinal microbiota-derived and food-derived metabolites in distinct LNs and their effects on immune cells are required to better understand the development of tolerance and tissue-homing immune cells.

Subcutaneous lymph nodes

Subcutaneous LNs drain the skin, fat tissue and muscles and are, therefore, rich in soluble metabolites that are generated in these tissues. Hyaluronic acid or hyaluronan is widely distributed throughout all the tissues in the body, but the skin represents a major reservoir. It can be catabolized either locally in tissues or in the DLNs after being transported via the lymph[132]. Therefore, the hyaluronic acid content in the pre-nodal lymph varies depending on the site of collection[133,134].

During immune responses, hyaluronic acid can serve distinct functions. As a large ECM component, hyaluronic acid promotes the adhesion and activation of immune cells, whereas if broken down into smaller fragments, it can mediate pro-inflammatory signals[182]. Hyaluronic acid-interacting receptors are CD44, its analogue LYVE1 (which is expressed by LECs) and ICAM1. Macrophage-expressed CD44 is thought to have an important role in hyaluronic acid uptake and in the clearance of hyaluronic acid fragments during inflammation. This function of CD44 may be important for tissue homoeostasis, as hyaluronic acid fragments and its complexes formed with other proteins may activate cDCs and promote inflammation[183]. However, most studies on hyaluronic acid have been performed in vitro or using peripheral tissues rather than LNs. In this respect, our current insights on the role of hyaluronic acid in LNs and potential differences between distinct LNs are largely rudimentary and remain speculative[183].

The situation is similar with another important metabolite — lactate. Lactate is mainly formed during anaerobic glycolysis, particularly in muscles after exercise when high amounts of ATP are rapidly required. Interestingly, it was shown that exercise can promote survival in a breast cancer model in mice[184]. This effect was based on an altered carbon metabolism in $CD8^+$ T cells, which altered their redox state, promoted their stemness and ultimately improved their antitumoural efficacy[185,186]. It is very possible that muscle-draining subcutaneous LNs are exposed to particularly high concentrations of lactate after exercise since it has been shown that lactate can be drained via the lymph in the context of tumours[187]. On account of its immune regulatory functions, elucidating lactate abundance in distinct LNs during homoeostasis, exercising and disease contexts will be important.

Similar to gut and liver DLNs, metabolites derived from tissues such as the skin or the muscle also influence immune cell responses. Therefore, studies analysing the effect of these molecules in the LNs draining these tissues can shed new light on their local influences in the context of inflammation, vaccination and therapy. Importantly, as discussed in this section, some LNs drain more than one organ. For example, the subcutaneous LNs are co-draining the skin, fat tissue and muscles, whereas the pancreas, liver and duodenum are co-drained by the liver, coeliac and duodenal DLNs in mice[55] (Fig. 3). Therefore, these LNs are exposed to certain combinations of migratory cell types and metabolites that might have synergistic or opposing effects when regulating immune responses. This drainage of several tissues by distinct LNs further increases the functional heterogeneity of these organs. It was recently shown that certain LNs are drained by the pancreas, liver and duodenum in a hierarchical manner in which the hierarchy refers to the relative amount of lymph received from each of the aforementioned tissues[55]. Consequently, migratory DCs from these tissues coalesced in the shared DLNs during homoeostatic and inflammatory conditions, and influenced each other to induce tolerogenic, inflammatory or autoimmune T cell responses (for example, autoimmune T cells targeting pancreatic antigens can be activated in the pancreas-draining lymph node as a result of gut inflammation)[55]. Thus, lymph co-drainage is a complex phenomenon influencing LN heterogeneity owing to (1) individual LNs being drained by several organs or (2) the same organ being drained by several LNs (Fig. 3). Further studies into the subject will probably reveal novel insights into which tissue is drained by which LN, expanding our understating of LN heterogeneity. This knowledge, specifically in humans, will be invaluable for diagnosis and treatment of patients.

Tumour-draining lymph nodes

In the previous sections, we have discussed how soluble factors that drain from tissues to LNs under homoeostatic conditions can affect the LN immune response. In the following section, we will focus on soluble factors generated by tumours that affect responses in the tumour-draining LNs. Primary tumours secrete distinct molecules and extracellular vesicles (referred to as the tumour secretome) that favour

their growth, progression and, eventually, dissemination throughout the body. These soluble factors promote immune evasion, mainly in LNs, by disrupting the 'cancer–immunity cycle'[188]. In principle, this cycle is self-reinforcing as it increases the amount of tumour antigens produced, which amplifies the immune response. However, cancer cells can disrupt this cycle via several mechanisms, mainly by targeting the DLNs.

The first LNs receiving direct drainage from a tumour site are referred to as sentinel lymph nodes (SLNs), which are usually identified by visualizing the lymphatic collecting vessels via dynamic imaging (lymphoscintigraphy) of tracers that can be detected in lymph fluid[189]. SLNs are also important sites for immunotherapy[190–195]. Vascular remodelling-related growth factors, such as vascular endothelial growth factor A (VEGFA) and VEGFC, are prominent tumour cell-derived molecules that are initially drained to SLNs[196–198]. In fact, expanded LECs and LN stromal cells in SLNs induced tolerogenic antigen-specific T cell responses[197,199]. Similarly, proliferating, activated FRCs affected immune cell recruitment and activation in SLNs[200]. Importantly, VEGFs are drained together with cytokines, such as granulocyte–macrophage colony-stimulating factor (GM-CSF), M-CSF and IL-3, and can exert immunosuppressive effects by promoting the survival and differentiation of immature myeloid cells. These cells promote an immunosuppressive environment in SLNs through various mechanisms[201]. Additionally, tumours and their microenvironment can also produce immunosuppressive cytokines, including IL-10 and TGFβ, and other mediators also contribute to the immunosuppressive environment of SLNs that can inhibit DC migration, induce T cell anergy, limit inflammatory macrophage activity and inhibit cytotoxic NK cell and T cell responses[202–205]. Indeed, the SLNs of patients with non-metastatic melanoma were shown to be enriched in IL-10, GM-CSF and IDO[206,207]. In the future, it will be interesting to elucidate the individual effects of locally produced cytokines in SLNs as compared with those drained directly from the tumour microenvironment.

The tumour and its microenvironment also produce metabolites that modify immune responses in the SLNs. It was reported that tumour-derived lactic acid is drained to the DLNs and affects the mitochondrial function and metabolism of FRCs in the LN[187]. Metabolites such as lactate and lactic acid also directly affect T cell function and could contribute to an immunosuppressive T cell response in SLNs[208].

Extracellular vesicles, such as exosomes, also form part of the tumour secretome. These vesicles are probably means of cell–cell communication whose composition and cargo vary depending on the releasing cell and its functional state[209]. Therefore, different cancer cells also secrete exosomes — which have been referred to as oncosomes — for immune evasion[135,136]. Exosomes are drained to the SLNs[210,211] and have been shown to suppress T cell activation[212,213], NK cell proliferation and cytotoxic function, such as perforin release[214], and even to induce a protumorigenic B cell response in the absence of the $CD169^+$ SCS macrophages in the SLN[211]. Therefore, it is not surprising that the immunosuppressive mechanisms provoked by melanoma or breast cancer tumour cells are dependent on the extent to which the LN drains the tumour directly. In humans, LNs are organized in chains, and the LNs that drain the tumour directly are more immunosuppressed and have lower numbers of cDCs, for example, than the LNs further up the chain[215].

Cancers have different cellular origins, develop in various tissues, and significantly differ with regard to the molecules and vesicles that they release into their environment. Naturally, this heterogeneity also influences the SLNs, which are directly exposed to these factors. Yet even the same tumours induce distinct immune responses when implanted into different sites. In fact, following implantation of a lung adenocarcinoma line in the skin or the lung, different $CD8^+$ T cell responses were generated in the respective SLNs, which in turn controlled tumour growth to different extents. This elegant study has shown that this difference was based on the different abundances of effector T_{reg} cells found in the lung-draining LNs compared with the skin-draining LNs. Microbiota-induced IFNɣ has a critical role in driving effector T_{reg} cell generation in lung-draining LNs and these cells inhibited cDC1-dependent $CD8^+$ T cell priming[105].

Overall, SLNs draining tumours are exposed to a plethora of soluble factors that modulate and typically suppress antitumour immunity[200]. This is a dynamic process that allows cancer cells to survive and grow and lays the ground for future lymphatic metastasis.

Box 3

Vaccination

The goal of vaccination is to induce pathogen-specific memory cells in the form of T cells, providing cell-mediated protection, and B cells for neutralizing antibodies. The importance of local immune protection in tissues is an emerging aspect that is a focus of future vaccine strategies. In the prominent case of COVID-19, the available vaccines succeeded in inducing a protective, systemic immune response[235] but failed in generating local immunity via lung-resident memory cells in contrast to the infection with the virus[236–239]. This is an important limitation because the protection against severe COVID-19 infection not only requires neutralizing antibodies but is also associated with the presence of $CD8^+$ T_{RM} cells in the lung[240,241]. Also, the local immune compartment, composed of IgA-producing plasma cells and tissue-resident memory B and T cells, has been shown to be essential for long-lasting protection against infections[242–244].

Nasal vaccinations are being developed to overcome this limitation and have been shown to be superior in inducing local memory formation in animal models[239,245–252]. Nevertheless, this approach comes with several drawbacks, including increased production costs, limited induction of systemic immunity and uncertainty regarding the actual dose administered to individual patients. Accordingly, only one intranasal vaccine was approved by the FDA (FluMist by AstraZeneca in 2018) before the COVID-19 pandemic. Notably, despite encouraging results of the nasal ChAdOx1 nCoV-19 AZD1222 vaccine in animal models[239,253], this agent failed in a phase I human trial[239,254]. Currently, 16 mucosal vaccines against SARS-CoV-2 are in clinical trial phases I–III or have been registered to be further reviewed by regulatory agencies. For further details regarding the ongoing clinical trials, we would like to direct the readers to a dedicated review[239].

For prophylactic vaccinations, which need to be applied to a large population in a simple and safe way, targeting organs other than the lungs, intestine and skin to induce local immune protection is probably not feasible. However, in certain diseases such as tumours or autoimmune disorders, therapy that targets specific tissues and their associated lymph nodes may be a promising strategy that could be worth the challenge of site-specific application.

Conclusions on soluble factors and lymph node heterogeneity

The lymph transported from different organs and tissue drainage sites to the associated LNs differs substantially in the composition of its soluble constituents. Some of these molecules, present in varying degrees, have been shown to have a marked impact on emerging immune responses. The regional influence of some of these substances, such as SCFAs and vitamin A, has already been clearly demonstrated in vivo. Overall, however, our knowledge in this research area is still rudimentary and largely limited to homoeostatic situations (Supplementary Table 1). As such, many key questions remain to be addressed. To what extent do physiological processes, such as the circadian rhythm, affect the fluctuations of soluble compounds in specific LNs? How do these soluble compounds change during development, puberty and ageing? What are the concentrations of metabolites and inflammatory mediators in lymph following injuries or during chronic diseases? Which of these factors functionally impact the immune responses that are generated in draining LNs and which of these factors act locally? Answering these questions would not only increase our basic understanding of the generation of immune responses and the role of local factors but would also have direct implications for the prophylaxis and therapy of diseases in humans.

Outlook and perspectives

The central task of the immune system is to protect the host from pathogens, while maintaining tolerance and tissue integrity. The structure of the lymphatic system inevitably leads to heterogeneity of the lymphatic fluid and the cells it contains, and thus to functional differences between different LNs. We assume that the system is optimized owing to evolutionary pressure. Accordingly, all LNs must be able to robustly generate fundamentally similar immune responses. At the same time, there is local adaptation to generate tailored immune responses against specific classes of pathogens in different tissues. Importantly, in this Review, we focused on individual LNs draining individual tissues, but as previously mentioned, one LN can drain more than one organ (Fig. 3). Therefore, the level of heterogeneity will also rely on the 'drained organ combination' or co-drainage. To date, our knowledge about inter-lymph node differences is limited, yet a profound understanding of the molecular mechanisms at play would give us the opportunity to harness them optimally. Hence, better treatment strategies for patients could be designed.

Specifically, the design of vaccinations and cancer immunotherapy treatments could be significantly improved by harnessing the system to our advantage. Currently, standard vaccines, whether intramuscular or subcutaneous (live vaccines), induce immune responses in the skin-draining LNs. Some mucosal vaccines are already in use, and with new developments in mRNA-based vaccines and biomaterials for targeted approaches, we may anticipate breakthroughs in the near future[216,217]. Importantly, the rationale for mucosal vaccination is to induce local immunity at barrier sites including secreted IgA antibodies and resident populations of $CD4^+$ and $CD8^+$ T cells[218]. However, targeting mucosal-associated lymphoid tissues and other LNs with their unique properties may further allow us to generate tailored and efficient immune responses against specific classes of pathogens by stimulating the 'ideal responders' in their 'right environment' (Box 3). Profound insights into which immune responses are optimally triggered in which LNs will be critical to this endeavour. To achieve this goal, future studies need to systematically investigate functional differences between LNs, particularly in humans, under several conditions (homoeostasis, infection and disease). The Human Cell Atlas initiative[219] is an important step towards this goal and should incorporate the 300–400 individual LNs, optimally from the same patient or organ donor. This accumulation of comparable data and further mechanistic research will be helpful to develop new strategies to safely target specific LNs to optimize vaccination and immunotherapy approaches against cancer.

Published online: 14 December 2023

References

1. Randolph, G. J., Ivanov, S., Zinselmeyer, B. H. & Scallan, J. P. The lymphatic system: integral roles in immunity. *Annu. Rev. Immunol.* **35**, 31–52 (2017).
2. Levick, J. R. & Michel, C. C. Microvascular fluid exchange and the revised Starling principle. *Cardiovasc. Res.* **87**, 198–210 (2010).
3. Santambrogio, L. The lymphatic fluid. *Int. Rev. Cell Mol. Biol.* **337**, 111–133 (2018).
4. Louveau, A. et al. Structural and functional features of central nervous system lymphatic vessels. *Nature* **523**, 337–341 (2015).
5. Da Mesquita, S., Fu, Z. & Kipnis, J. The meningeal lymphatic system: a new player in neurophysiology. *Neuron* **100**, 375–388 (2018).
6. von Andrian, U. H. & Mempel, T. R. Homing and cellular traffic in lymph nodes. *Nat. Rev. Immunol.* **3**, 867–878 (2003).
7. Welner, R. S. & Kincade, P. W. Stem cells on patrol. *Cell* **131**, 842–844 (2007).
8. Collado-Diaz, V., Medina-Sanchez, J. D., Gkountidi, A. O. & Halin, C. Imaging leukocyte migration through afferent lymphatics. *Immunol. Rev.* **306**, 43–57 (2022).
9. von Andrian, U. H. & Mackay, C. R. T-cell function and migration — two sides of the same coin. *N. Engl. J. Med.* **343**, 1020–1034 (2000).
10. Girard, J. P., Moussion, C. & Förster, R. HEVs, lymphatics and homeostatic immune cell trafficking in lymph nodes. *Nat. Rev. Immunol.* **12**, 762–773 (2012).
11. Gray, H. *Gray's Anatomy: the Anatomical Basis of Clinical Practice* (Elsevier Health Sciences, 2015).
12. Junt, T. et al. Subcapsular sinus macrophages in lymph nodes clear lymph-borne viruses and present them to antiviral B cells. *Nature* **450**, 110–114 (2007).
13. Qi, H., Kastenmüller, W. & Germain, R. N. Spatiotemporal basis of innate and adaptive immunity in secondary lymphoid tissue. *Annu. Rev. Cell Dev. Biol.* **30**, 141–167 (2014).
14. Acton, S. E., Onder, L., Novkovic, M., Martinez, V. G. & Ludewig, B. Communication, construction, and fluid control: lymphoid organ fibroblastic reticular cell and conduit networks. *Trends Immunol.* **42**, 782–794 (2021).
15. Iannacone, M. et al. Subcapsular sinus macrophages prevent CNS invasion on peripheral infection with a neurotropic virus. *Nature* **465**, 1079–1083 (2010).
16. Zhang, Y. et al. Migratory and adhesive cues controlling innate-like lymphocyte surveillance of the pathogen-exposed surface of the lymph node. *eLife* **5**, e18156 (2016).
17. Muntjewerff, E. M., Meesters, L. D. & van den Bogaart, G. Antigen cross-presentation by macrophages. *Front. Immunol.* **11**, 1276 (2020).
18. Bajénoff, M. et al. Stromal cell networks regulate lymphocyte entry, migration, and territoriality in lymph nodes. *Immunity* **25**, 989–1001 (2006).
19. Jalkanen, S. & Salmi, M. Lymphatic endothelial cells of the lymph node. *Nat. Rev. Immunol.* **20**, 566–578 (2020).
20. Itano, A. A. et al. Distinct dendritic cell populations sequentially present antigen to CD4 T cells and stimulate different aspects of cell-mediated immunity. *Immunity* **19**, 47–57 (2003).
21. Sixt, M. et al. The conduit system transports soluble antigens from the afferent lymph to resident dendritic cells in the T cell area of the lymph node. *Immunity* **22**, 19–29 (2005).
22. Roozendaal, R. et al. Conduits mediate transport of low-molecular-weight antigen to lymph node follicles. *Immunity* **30**, 264–276 (2009).
23. Clement, C. C. et al. Protein expression profiles of human lymph and plasma mapped by 2D-DIGE and 1D SDS-PAGE coupled with nanoLC-ESI-MS/MS bottom-up proteomics. *J. Proteom.* **78**, 172–187 (2013).
24. Palframan, R. T. et al. Inflammatory chemokine transport and presentation in HEV: a remote control mechanism for monocyte recruitment to lymph nodes in inflamed tissues. *J. Exp. Med.* **194**, 1361–1373 (2001).
25. Huang, J. Y., Lyons-Cohen, M. R. & Gerner, M. Y. Information flow in the spatiotemporal organization of immune responses. *Immunol. Rev.* **306**, 93–107 (2022).
26. Gasteiger, G., Ataide, M. & Kastenmüller, W. Lymph node — an organ for T-cell activation and pathogen defense. *Immunol. Rev.* **271**, 200–220 (2016).
27. Duckworth, B. C. & Groom, J. R. Conversations that count: cellular interactions that drive T cell fate. *Immunol. Rev.* **300**, 203–219 (2021).
28. Springer, T. A. Traffic signals on endothelium for lymphocyte recirculation and leukocyte emigration. *Annu. Rev. Physiol.* **57**, 827–872 (1995).
29. Okada, T. et al. Chemokine requirements for B cell entry to lymph nodes and Peyer's patches. *J. Exp. Med.* **196**, 65–75 (2002).
30. Faveeuw, C., Di Mauro, M. E., Price, A. A. & Ager, A. Roles of α4 integrins/VCAM-1 and LFA-1/ICAM-1 in the binding and transendothelial migration of T lymphocytes and T lymphoblasts across high endothelial venules. *Int. Immunol.* **12**, 241–251 (2000).
31. Bajénoff, M., Granjeaud, S. & Guerder, S. The strategy of T cell antigen-presenting cell encounter in antigen-draining lymph nodes revealed by imaging of initial T cell activation. *J. Exp. Med.* **198**, 715–724 (2003).
32. Druzd, D. et al. Lymphocyte circadian clocks control lymph node trafficking and adaptive immune responses. *Immunity* **46**, 120–132 (2017).

33. Braun, A. et al. Afferent lymph-derived T cells and DCs use different chemokine receptor CCR7-dependent routes for entry into the lymph node and intranodal migration. *Nat. Immunol.* **12**, 879–887 (2011).
34. Ugur, M. et al. Lymph node medulla regulates the spatiotemporal unfolding of resident dendritic cell networks. *Immunity* **56**, 1778–1793.e10 (2023).
35. Fletcher, A. L. et al. Reproducible isolation of lymph node stromal cells reveals site-dependent differences in fibroblastic reticular cells. *Front. Immunol.* **2**, 35 (2011).
36. Pezoldt, J. et al. Neonatally imprinted stromal cell subsets induce tolerogenic dendritic cells in mesenteric lymph nodes. *Nat. Commun.* **9**, 3903 (2018).
37. Hammerschmidt, S. I. et al. Stromal mesenteric lymph node cells are essential for the generation of gut-homing T cells in vivo. *J. Exp. Med.* **205**, 2483–2490 (2008).
This study shows that lymph node stromal cells instruct tissue-homing signals in T cells in a lymph node-specific manner.
38. Cording, S. et al. The intestinal micro-environment imprints stromal cells to promote efficient T_{reg} induction in gut-draining lymph nodes. *Mucosal Immunol.* **7**, 359–368 (2014).
This study shows that stromal cells from lymph nodes draining distinct sites differ in their capacity to induce regulatory T cells.
39. Wolvers, D. A. et al. Intranasally induced immunological tolerance is determined by characteristics of the draining lymph nodes: studies with OVA and human cartilage gp-39. *J. Immunol.* **162**, 1994–1998 (1999).
40. Podgrabinska, S. et al. Inflamed lymphatic endothelium suppresses dendritic cell maturation and function via Mac-1/ICAM-1-dependent mechanism. *J. Immunol.* **183**, 1767–1779 (2009).
41. Ulvmar, M. H. & Mäkinen, T. Heterogeneity in the lymphatic vascular system and its origin. *Cardiovasc. Res.* **111**, 310–321 (2016).
42. Miyasaka, M. A short review on lymphatic endothelial cell heterogeneity. *Inflamm. Regen.* **41**, 21–23 (2021).
43. Pegu, A. et al. Human lymphatic endothelial cells express multiple functional TLRs. *J. Immunol.* **180**, 3399–3405 (2008).
44. Steinman, R. M. Decisions about dendritic cells: past, present, and future. *Annu. Rev. Immunol.* **30**, 1–22 (2012).
45. Cabeza-Cabrerizo, M. et al. Dendritic cells revisited. *Annu. Rev. Immunol.* **39**, 131–166 (2021).
46. Joffre, O., Nolte, M. A., Spörri, R. & Sousa, C. R. E. Inflammatory signals in dendritic cell activation and the induction of adaptive immunity. *Immunol. Rev.* **227**, 234–247 (2009).
47. Ardouin, L. et al. Broad and largely concordant molecular changes characterize tolerogenic and immunogenic dendritic cell maturation in thymus and periphery. *Immunity* **45**, 305–318 (2016).
48. Worbs, T., Hammerschmidt, S. I. & Förster, R. Dendritic cell migration in health and disease. *Nat. Rev. Immunol.* **17**, 30–48 (2017).
49. Allan, R. S. et al. Migratory dendritic cells transfer antigen to a lymph node-resident dendritic cell population for efficient CTL priming. *Immunity* **25**, 153–162 (2006).
50. Steinman, R. M. & Cohn, Z. A. Identification of a novel cell type in peripheral lymphoid organs of mice: I. Morphology, quantitation, tissue distribution. *J. Exp. Med.* **137**, 1142–1162 (1973).
51. Spalding, D. M. & Griffin, J. A. Different pathways of differentiation of pre-B cell lines are induced by dendritic cells and T cells from different lymphoid tissues. *Cell* **44**, 507–515 (1986).
52. Mora, J. R. et al. Generation of gut-homing IgA-secreting B cells by intestinal dendritic cells. *Science* **314**, 1157–1160 (2006).
This study identifies retinoic acid as part of a molecular mechanism of imprinting of gut-homing IgA-secreting cells.
53. Everson, M. P. et al. Dendritic cells from different tissues induce production of different T cell cytokine profiles. *J. Leukoc. Biol.* **59**, 494–498 (1996).
54. Esterházy, D. et al. Compartmentalized gut lymph node drainage dictates adaptive immune responses. *Nature* **569**, 126–130 (2019).
This work demonstrates that the gut-draining lymph nodes are immunologically adapted to the particular intestinal segment they drain and, accordingly, preferentially elicit inflammatory or tolerogenic immune responses.
55. Brown, H., Komnick, M. R., Brigleb, P. H., Dermody, T. S. & Esterházy, D. Lymph node sharing between pancreas, gut, and liver leads to immune crosstalk and regulation of pancreatic autoimmunity. *Immunity* https://doi.org/10.1016/j.immuni.2023.07.008 (2023).
This study demonstrates how lymph node co-drainage of tissues impacts the tolerance towards self-antigens.
56. Campbell, D. J. & Butcher, E. C. Rapid acquisition of tissue-specific homing phenotypes by $CD4^+$ T cells activated in cutaneous or mucosal lymphoid tissues. *J. Exp. Med.* **195**, 135–141 (2002).
This landmark study shows a differential imprinting of homing receptors in CD4 T cells in different lymph nodes.
57. Johansson-Lindbom, B. et al. Selective generation of gut tropic T cells in gut-associated lymphoid tissue (GALT): requirement for GALT dendritic cells and adjuvant. *J. Exp. Med.* **198**, 963–969 (2003).
58. Mora, J. R. et al. Selective imprinting of gut-homing T cells by Peyer's patch dendritic cells. *Nature* **424**, 88–93 (2003).
This landmark study shows a differential imprinting of homing receptors in CD8 T cells in different lymph nodes.
59. Mani, V. et al. Migratory DCs activate TGF-b to precondition naïve $CD8^+$ T cells for tissue-resident memory fate. *Science* **366**, https://doi.org/10.1126/science.aav5728 (2019).
This study shows that tissue-derived migratory dendritic cells pre-condition naive $CD8^+$ T cells to adopt a tissue-residency program after infection.
60. Lantz, O. & Bendelac, A. An invariant T cell receptor α chain is used by a unique subset of major histocompatibility complex class I-specific CD4+ and CD4-8- T cells in mice and humans. *J. Exp. Med.* **180**, 1077–1106 (1994).
61. Tilloy, F. et al. An invariant T cell receptor α chain defines a novel TAP-independent major histocompatibility complex class Ib-restricted α/β T cell subpopulation in mammals. *J. Exp. Med.* **189**, 1907–1921 (1999).
62. Treiner, E. et al. Selection of evolutionarily conserved mucosal-associated invariant T cells by MR1. *Nature* **422**, 164–169 (2003); erratum **423**, 1018 (2003).
63. Bendelac, A. et al. CD1 recognition by mouse $NK1^+$ T lymphocytes. *Science* **268**, 863–865 (1995).
64. Gumperz, J. E. et al. Murine CD1d-restricted T cell recognition of cellular lipids. *Immunity* **12**, 211–221 (2000).
65. Godfrey, D. I. et al. Antigen recognition by CD1d-restricted NKT T cell receptors. *Semin. Immunol.* **22**, 61–67 (2010).
66. Deseke, M. & Prinz, I. Ligand recognition by the γδ TCR and discrimination between homeostasis and stress conditions. *Cell. Mol. Immunol.* **17**, 914–924 (2020).
67. Kjer-Nielsen, L. et al. MR1 presents microbial vitamin B metabolites to MAIT cells. *Nature* **491**, 717–723 (2012).
68. Kinjo, Y. et al. Recognition of bacterial glycosphingolipids by natural killer T cells. *Nature* **434**, 520–525 (2005).
69. Mattner, J. et al. Exogenous and endogenous glycolipid antigens activate NKT cells during microbial infections. *Nature* **434**, 525–529 (2005).
70. Herrmann, T. & Karunakaran, M. M. Butyrophilins: γδ T cell receptor ligands, immunomodulators and more. *Front. Immunol.* **13**, 876493 (2022).
71. Ribot, J. C., Lopes, N. & Silva-Santos, B. γδ T cells in tissue physiology and surveillance. *Nat. Rev. Immunol.* **21**, 221–232 (2021).
72. Schneider, D. F. et al. A novel role for NKT cells in cutaneous wound repair. *J. Surg. Res.* **168**, 325–333.e1 (2011).
73. Tanno, H. et al. Contribution of invariant natural killer T cells to skin wound healing. *Am. J. Pathol.* **185**, 3248–3257 (2015).
74. Legoux, F., Salou, M. & Lantz, O. MAIT cell development and functions: the microbial connection. *Immunity* **53**, 710–723 (2020).
75. Zhang, Y. et al. Mucosal-associated invariant T cells restrict reactive oxidative damage and preserve meningeal barrier integrity and cognitive function. *Nat. Immunol.* **23**, 1714–1725 (2022).
76. Constantinides, M. G. & Belkaid, Y. Early-life imprinting of unconventional T cells and tissue homeostasis. *Science* **374**, eabf0095 (2021).
77. Constantinides, M. G. et al. MAIT cells are imprinted by the microbiota in early life and promote tissue repair. *Science* **366**, eaax6624 (2019).
78. Howson, L. J. et al. Absence of mucosal-associated invariant T cells in a person with a homozygous point mutation in MR1. *Sci. Immunol.* **5**, eabc9492 (2020).
79. Ataide, M. A. et al. Lymphatic migration of unconventional T cells promotes site-specific immunity in distinct lymph nodes. *Immunity* **55**, 1813–1828.e9 (2022).
This study demonstrates that lymph nodes draining different barrier tissues mount distinct innate and adaptive immune responses owing to their unconventional T cell composition.
80. Fan, X. & Rudensky, A. Y. Hallmarks of tissue-resident lymphocytes. *Cell* **164**, 1198–1211 (2016).
81. Salou, M. et al. A common transcriptomic program acquired in the thymus defines tissue residency of MAIT and NKT subsets. *J. Exp. Med.* **216**, 133–151 (2019).
82. Tan, L. et al. Single-cell transcriptomics identifies the adaptation of $Scart1^+$ $Vγ6^+$ T cells to skin residency as activated effector cells. *Cell Rep.* **27**, 3657–3671.e4 (2019).
83. Gray, E. E. et al. Deficiency in IL-17-committed $Vγ4^+$ γδ T cells in a spontaneous Sox13-mutant $CD45.1^+$ congenic mouse substrain provides protection from dermatitis. *Nat. Immunol.* **14**, 584–592 (2013).
84. Nakamizo, S. et al. Dermal $Vγ4^+$ γδ T cells possess a migratory potency to the draining lymph nodes and modulate $CD8^+$ T-cell activity through TNF-α production. *J. Invest. Dermatol.* **135**, 1007–1015 (2015).
85. Gaya, M. et al. Initiation of antiviral B cell immunity relies on innate signals from spatially positioned NKT cells. *Cell* **172**, 517–533.e20 (2018).
86. Williams, M. A. & Bevan, M. J. Effector and memory CTL differentiation. *Annu. Rev. Immunol.* **25**, 171–192 (2007).
87. Buchholz, V. R., Schumacher, T. N. M. & Busch, D. H. T cell fate at the single-cell level. *Annu. Rev. Immunol.* **34**, 65–92 (2016).
88. Zhu, J., Yamane, H. & Paul, W. E. Differentiation of effector $CD4^+$ T cell populations. *Annu. Rev. Immunol.* **28**, 445–489 (2010).
89. Mueller, S. N. & Mackay, L. K. Tissue-resident memory T cells: local specialists in immune defence. *Nat. Rev. Immunol.* **16**, 79–89 (2016).
90. Ugur, M., Kaminski, A. & Pabst, O. Lymph node γδ and αβ $CD8^+$ T cells share migratory properties. *Sci. Rep.* **8**, 8986 (2018).
91. Mandl, J. N. et al. Quantification of lymph node transit times reveals differences in antigen surveillance strategies of naïve $CD4^+$ and $CD8^+$ T cells. *Proc. Natl Acad. Sci. USA* **109**, 18036–18041 (2012).

92. Ugur, M., Schulz, O., Menon, M. B., Krueger, A. & Pabst, O. Resident CD4$^+$ T cells accumulate in lymphoid organs after prolonged antigen exposure. *Nat. Commun.* **5**, 4821 (2014).
93. Fazilleau, N. et al. Lymphoid reservoirs of antigen-specific memory T helper cells. *Nat. Immunol.* **8**, 753–761 (2007).
94. Cucak, H., Yrlid, U., Reizis, B., Kalinke, U. & Johansson-Lindbom, B. Type I interferon signaling in dendritic cells stimulates the development of lymph-node-resident T follicular helper cells. *Immunity* **31**, 491–501 (2009).
95. Beura, L. K. et al. CD4$^+$ resident memory T cells dominate immunosurveillance and orchestrate local recall responses. *J. Exp. Med.* **216**, 1214–1229 (2019).
96. Stolley, J. M. et al. Retrograde migration supplies resident memory T cells to lung-draining LN after influenza infection. *J. Exp. Med.* **217**, e20192197 (2020).
97. Beura, L. K. et al. T cells in nonlymphoid tissues give rise to lymph-node-resident memory T cells. *Immunity* **48**, 327–338.e5 (2018).
98. Campbell, C. & Rudensky, A. Roles of regulatory T cells in tissue pathophysiology and metabolism. *Cell Metab.* **31**, 18–25 (2020).
99. Dikiy, S. & Rudensky, A. Y. Principles of regulatory T cell function. *Immunity* **56**, 240–255 (2023).
100. Lee, H. M., Bautista, J. L. & Hsieh, C. S. Thymic and peripheral differentiation of regulatory T cells. *Adv. Immunol.* **112**, 25–71 (2011).
101. Vaeth, M. et al. Tissue resident and follicular T_{reg} cell differentiation is regulated by CRAC channels. *Nat. Commun.* **10**, 1183 (2019).
102. Miragaia, R. J. et al. Single-cell transcriptomics of regulatory T cells reveals trajectories of tissue adaptation. *Immunity* **50**, 493–504.e7 (2019).
103. Kaminski, A. et al. Resident regulatory T cells reflect the immune history of individual lymph nodes. *Sci. Immunol.* https://doi.org/10.1126/sciimmunol.adj5789 (2023).
This study identifies lymph node-resident T_{reg} cells that possess lymph node-specific TCR repertoires as a consequence of the local immune history.
104. Josefowicz, S. Z., Lu, L.-F. & Rudensky, A. Y. Regulatory T cells: mechanisms of differentiation and function. *Annu. Rev. Immunol.* **30**, 531–564 (2012).
105. Zagorulya, M. et al. Tissue-specific abundance of interferon-gamma drives regulatory T cells to restrain DC1-mediated priming of cytotoxic T cells against lung cancer. *Immunity* **56**, 386–405.e10 (2023).
This study shows that lung-draining versus skin-draining lymph nodes differ in their ability to elicit an antitumor immune response owing to their T_{reg} cell composition.
106. Oyler-Yaniv, A. et al. A tunable diffusion-consumption mechanism of cytokine propagation enables plasticity in cell-to-cell communication in the immune system. *Immunity* **46**, 609–620 (2017).
107. Chinen, T. et al. An essential role for the IL-2 receptor in T_{reg} cell function. *Nat. Immunol.* **17**, 1322–1333 (2016).
108. Simeonov, D. R. et al. Non-coding sequence variation reveals fragility within interleukin 2 feedback circuitry and shapes autoimmune disease risk. Preprint at *bioRxiv* https://doi.org/10.1101/2023.06.17.545426 (2023).
109. Wong, H. S. et al. A local regulatory T cell feedback circuit maintains immune homeostasis by pruning self-activated T cells. *Cell* **184**, 3981–3997.e22 (2021).
110. Nutt, S. L., Hodgkin, P. D., Tarlinton, D. M. & Corcoran, L. M. The generation of antibody-secreting plasma cells. *Nat. Rev. Immunol.* **15**, 160–171 (2015).
111. Breitfeld, D. et al. Follicular B helper T cells express CXC chemokine receptor 5, localize to B cell follicles, and support immunoglobulin production. *J. Exp. Med.* **192**, 1545–1552 (2000).
112. Cyster, J. G. et al. Follicular stromal cells and lymphocyte homing to follicles. *Immunol. Rev.* **176**, 181–193 (2000).
113. Fazilleau, N., McHeyzer-Williams, L. J., Rosen, H. & McHeyzer-Williams, M. G. The function of follicular helper T cells is regulated by the strength of T cell antigen receptor binding. *Nat. Immunol.* **10**, 375–384 (2009).
114. Vogelzang, A. et al. A fundamental role for interleukin-21 in the generation of T follicular helper cells. *Immunity* **29**, 127–137 (2008).
115. Grewal, I. S. & Flavell, R. A. CD40 and CD154 in cell-mediated immunity. *Annu. Rev. Immunol.* **16**, 111–135 (1998).
116. Lim, H. W., Hillsamer, P. & Kim, C. H. Regulatory T cells can migrate to follicles upon T cell activation and suppress GC-Th cells and GC-Th cell-driven B cell responses. *J. Clin. Invest.* **114**, 1640–1649 (2004).
117. Aloulou, M. et al. Follicular regulatory T cells can be specific for the immunizing antigen and derive from naive T cells. *Nat. Commun.* **7**, 10579 (2016).
118. Botta, D. et al. Dynamic regulation of T follicular regulatory cell responses by interleukin 2 during influenza infection. *Nat. Immunol.* **18**, 1249–1260 (2017).
119. Clement, R. L. et al. Follicular regulatory T cells control humoral and allergic immunity by restraining early B cell responses. *Nat. Immunol.* **20**, 1360–1371 (2019).
120. Sheng, J. et al. Fate mapping analysis reveals a novel murine dermal migratory Langerhans-like cell population. *eLife* **10**, e65412 (2021).
121. Mackley, E. C. et al. CCR7-dependent trafficking of RORγ+ ILCs creates a unique microenvironment within mucosal draining lymph nodes. *Nat. Commun.* **6**, 5862 (2015).
122. Yamano, T. et al. Aire-expressing ILC3-like cells in the lymph node display potent APC features. *J. Exp. Med.* **216**, 1027–1037 (2019).
123. Abramson, J., Dobeš, J., Lyu, M. & Sonnenberg, G. F. The emerging family of RORγt+ antigen-presenting cells. *Nat. Rev. Immunol.* https://doi.org/10.1038/s41577-023-00906-5 (2023).
124. Lyu, M. et al. ILC3s select microbiota-specific regulatory T cells to establish tolerance in the gut. *Nature* **610**, 744–751 (2022).
125. Akagbosu, B. et al. Novel antigen-presenting cell imparts T_{reg}-dependent tolerance to gut microbiota. *Nature* **610**, 752–760 (2022).
126. Kedmi, R. et al. A RORγt+ cell instructs gut microbiota-specific T_{reg} cell differentiation. *Nature* **610**, 737–743 (2022).
127. Wang, J. et al. Single-cell multiomics defines tolerogenic extrathymic Aire-expressing populations with unique homology to thymic epithelium. *Sci. Immunol.* **6**, eabl5053 (2021).
128. Waffarn, E. E. et al. Infection-induced type I interferons activate CD11b on B-1 cells for subsequent lymph node accumulation. *Nat. Commun.* **6**, 8991 (2015).
129. Wiig, H. & Swartz, M. A. Interstitial fluid and lymph formation and transport: physiological regulation and roles in inflammation and cancer. *Physiol. Rev.* **92**, 1005–1060 (2012).
130. Aukland, K. & Reed, R. K. Interstitial-lymphatic mechanisms in the control of extracellular fluid volume. *Physiol. Rev.* **73**, 1–78 (1993).
131. Clement, C. C. et al. An expanded self-antigen peptidome is carried by the human lymph as compared to the plasma. *PLoS One* **5**, e9863 (2010).
The study provides a comparative, quantitative analysis of peptide fragments found in human lymph.
132. Fraser, J. R. E., Laurent, T. C. & Laurent, U. B. G. Hyaluronan: its nature, distribution, functions and turnover. *J. Intern. Med.* **242**, 27–33 (1997).
133. Tengblad, A. et al. Concentration and relative molecular mass of hyaluronate in lymph and blood. *Biochem. J.* **236**, 521–525 (1986).
134. Fraser, J. R. E., Kimpton, W. G., Laurent, T. C., Cahill, R. N. P. & Vakakis, N. Uptake and degradation of hyaluronan in lymphatic tissue. *Biochem. J.* **256**, 153–158 (1988).
135. Srinivasan, S., Vannberg, F. O. & Dixon, J. B. Lymphatic transport of exosomes as a rapid route of information dissemination to the lymph node. *Sci. Rep.* **6**, 24436 (2016).
136. Hood, J. L. The association of exosomes with lymph nodes. *Semin. Cell Dev. Biol.* **67**, 29–38 (2017).
137. Zhang, W. et al. Exosomes in pathogen infections: a bridge to deliver molecules and link functions. *Front. Immunol.* **9**, 90 (2018).
138. Shannon, A. D., Quin, J. W. & Courtice, F. C. Lysosomal enzyme activities in sheep plasma and lymph. *Res. Vet. Sci.* **22**, 209–215 (1977).
139. Reichl, D., Hathaway, C. B., Sterchi, J. M. & Miller, N. E. Lipoproteins of human peripheral lymph. Apolipoprotein AI-containing lipoprotein with alpha-2 electrophoretic mobility. *Eur. J. Clin. Invest.* **21**, 638–643 (1991).
140. Jacobs, F. A. & Largis, E. E. Transport of amino acids via the mesenteric lymph duct in rats. *Proc. Soc. Exp. Biol. Med.* **130**, 692–696 (1969).
141. Nanjee, M. N., Cooke, C. J., Olszewski, W. L. & Miller, N. E. Lipid and apolipoprotein concentrations in prenodal leg lymph of fasted humans: associations with plasma concentrations in normal subjects, lipoprotein lipase deficiency, and LCAT deficiency. *J. Lipid Res.* **41**, 1317–1327 (2000).
142. O'Sullivan, D., Sanin, D. E., Pearce, E. J. & Pearce, E. L. Metabolic interventions in the immune response to cancer. *Nat. Rev. Immunol.* **19**, 324–335 (2019).
143. Ohhashi, T., Kawai, Y., Maejima, D., Hayashi, M. & Watanabe-Asaka, T. Physiological roles of lymph flow-mediated nitric oxide in lymphatic system. *Lymphat. Res. Biol.* **21**, 253–261 (2023).
144. Olszewski, W. L. The lymphatic system in body homeostasis: physiological conditions. *Lymphat. Res. Biol.* **1**, 11–21 (2003).
145. Wu, H., Denna, T. H., Storkersen, J. N. & Gerriets, V. A. Beyond a neurotransmitter: the role of serotonin in inflammation and immunity. *Pharmacol. Res.* **140**, 100–114 (2019).
146. Munn, D. H. & Mellor, A. L. Indoleamine 2,3 dioxygenase and metabolic control of immune responses. *Trends Immunol.* **34**, 137–143 (2013).
147. Fletcher, M. et al. L-Arginine depletion blunts antitumor T-cell responses by inducing myeloid-derived suppressor cells. *Cancer Res.* **75**, 275–283 (2015).
148. Geiger, R. et al. L-Arginine modulates T cell metabolism and enhances survival and anti-tumor activity. *Cell* **167**, 829–842.e13 (2016).
149. Steggerda, S. M. et al. Inhibition of arginase by CB-1158 blocks myeloid cell-mediated immune suppression in the tumor microenvironment. *J. Immunother. Cancer* **5**, 101 (2017).
150. Klysz, D. et al. Glutamine-dependent α-ketoglutarate production regulates the balance between T helper 1 cell and regulatory T cell generation. *Sci. Signal.* **8**, ra97 (2015).
151. Mondanelli, G. et al. A relay pathway between arginine and tryptophan metabolism confers immunosuppressive properties on dendritic cells. *Immunity* **46**, 233–244 (2017).
152. Svoronos, N. et al. Tumor cell-independent estrogen signaling drives disease progression through mobilization of myeloid-derived suppressor cells. *Cancer Discov.* **7**, 72–85 (2017).
153. Vasanthakumar, A. et al. Sex-specific adipose tissue imprinting of regulatory T cells. *Nature* **579**, 581–585 (2020).
154. Hiltensperger, M. et al. Skin and gut imprinted helper T cell subsets exhibit distinct functional phenotypes in central nervous system autoimmunity. *Nat. Immunol.* **22**, 880–892 (2021).
This study shows that helper T cells primed in different lymph nodes are phenotypically distinct and home to distinct areas of tissues during inflammation.
155. Jang, C. et al. Metabolite exchange between mammalian organs quantified in pigs. *Cell Metab.* **30**, 594–606.e3 (2019).
156. Clement, C. C. et al. Quantitative profiling of the lymph node clearance capacity. *Sci. Rep.* **8**, 11253 (2018).
157. Zawieja, D. C. et al. Lymphatic cannulation for lymph sampling and molecular delivery. *J. Immunol.* **203**, 2339–2350 (2019).

158. Reichl, D., Simons, L. A., Myant, N. B., Pflug, J. J. & Mills, G. L. The lipids and lipoproteins of human peripheral lymph, with observations on the transport of cholesterol from plasma and tissues into lymph. *Clin. Sci. Mol. Med.* **45**, 313–329 (1973).
159. Sloop, C. H., Castle, C. K., Lefevre, M. & Wong, L. Comparison of the lipid and apolipoprotein composition of skeletal muscle and peripheral lymph in control dogs and in dogs fed a high fat, high cholesterol, hypothyroid-inducing diet. *Biochim. Biophys. Acta* **1169**, 196–201 (1993).
160. Julien, P., Fong, B. & Angel, A. Cardiac and peripheral lymph lipoproteins in dogs fed cholesterol and saturated fat. *Arteriosclerosis* **4**, 435–442 (1984).
161. Santambrogio, L. & Rammensee, H. G. Contribution of the plasma and lymph degradome and peptidome to the MHC ligandome. *Immunogenetics* **71**, 203–216 (2019).
162. Clement, C. C. et al. The dendritic cell major histocompatibility complex II (MHC II) peptidome derives from a variety of processing pathways and includes peptides with a broad spectrum of HLA-DM sensitivity. *J. Biol. Chem.* **291**, 5576–5595 (2016).
163. Houston, S. A. et al. The lymph nodes draining the small intestine and colon are anatomically separate and immunologically distinct. *Mucosal Immunol.* **9**, 468–478 (2016).
This study shows that migratory dendritic cells from the small intestine-draining lymph nodes and colon-draining lymph nodes differ phenotypically and differentially imprint T cells for tissue-specific homing.
164. Yang, W. & Cong, Y. Gut microbiota-derived metabolites in the regulation of host immune responses and immune-related inflammatory diseases. *Cell. Mol. Immunol.* **18**, 866–877 (2021).
165. Gutiérrez-Vázquez, C. & Quintana, F. J. Regulation of the immune response by the aryl hydrocarbon receptor. *Immunity* **48**, 19–33 (2018).
166. Lamas, B. et al. CARD9 impacts colitis by altering gut microbiota metabolism of tryptophan into aryl hydrocarbon receptor ligands. *Nat. Med.* **22**, 598–605 (2016).
167. Nguyen, L. P. & Bradfield, C. A. The search for endogenous activators of the aryl hydrocarbon receptor. *Chem. Res. Toxicol.* **21**, 102–116 (2008).
168. Li, S. et al. Aryl hydrocarbon receptor signaling cell intrinsically inhibits intestinal group 2 innate lymphoid cell function. *Immunity* **49**, 915–928.e5 (2018).
169. Quintana, F. J. et al. Control of T_{reg} and T_H17 cell differentiation by the aryl hydrocarbon receptor. *Nature* **453**, 65–71 (2008).
170. Chng, S. H. et al. Ablating the aryl hydrocarbon receptor (AhR) in CD11c$^+$ cells perturbs intestinal epithelium development and intestinal immunity. *Sci. Rep.* **6**, 23820 (2016).
171. Schiering, C. et al. Feedback control of AHR signalling regulates intestinal immunity. *Nature* **542**, 242–245 (2017).
172. Cifarelli, V. & Eichmann, A. The intestinal lymphatic system: functions and metabolic implications. *Cell. Mol. Gastroenterol. Hepatol.* **7**, 503–513 (2019).
173. D'Ambrosio, D. N., Clugston, R. D. & Blaner, W. S. Vitamin A metabolism: an update. *Nutrients* **3**, 63–103 (2011).
174. Eroglu, A. & Harrison, E. H. Carotenoid metabolism in mammals, including man: formation, occurrence, and function of apocarotenoids. *J. Lipid Res.* **54**, 1719–1730 (2013).
175. Sun, C. M. et al. Small intestine lamina propria dendritic cells promote de novo generation of Foxp3 T_{reg} cells via retinoic acid. *J. Exp. Med.* **204**, 1775–1785 (2007).
176. Kim, C. H. Control of lymphocyte functions by gut microbiota-derived short-chain fatty acids. *Cell. Mol. Immunol.* **18**, 1161–1171 (2021).
177. Arpaia, N. et al. Metabolites produced by commensal bacteria promote peripheral regulatory T-cell generation. *Nature* **504**, 451–455 (2013).
178. Bachem, A. et al. Microbiota-derived short-chain fatty acids promote the memory potential of antigen-activated CD8$^+$ T cells. *Immunity* **51**, 285–297.e5 (2019).
179. Kim, M., Qie, Y., Park, J. & Kim, C. H. Gut microbial metabolites fuel host antibody responses. *Cell Host Microbe* **20**, 202–214 (2016).
180. Haghikia, A. et al. Dietary fatty acids directly impact central nervous system autoimmunity via the small intestine. *Immunity* **43**, 817–829 (2015).
181. Buck, M. D., Sowell, R. T., Kaech, S. M. & Pearce, E. L. Metabolic instruction of immunity. *Cell* **169**, 570–586 (2017).
182. Kobayashi, T., Chanmee, T. & Itano, N. Hyaluronan: metabolism and function. *Biomolecules* **10**, 1525 (2020).
183. Lee-Sayer, S. S. M. et al. The where, when, how and why of hyaluronan binding by immune cells. *Front. Immunol.* **6**, 150 (2015).
184. Rundqvist, H. et al. Cytotoxic T-cells mediate exercise-induced reductions in tumor growth. *eLife* **9**, e59996 (2020).
185. Quinn, W. J. et al. Lactate limits T cell proliferation via the NAD(H) redox state. *Cell Rep.* **33**, 108500 (2020).
186. Feng, Q. et al. Lactate increases stemness of CD8+ T cells to augment anti-tumor immunity. *Nat. Commun.* **13**, 4981 (2022).
187. Riedel, A. et al. Tumor-derived lactic acid modulates activation and metabolic status of draining lymph node stroma. *Cancer Immunol. Res.* **10**, 482–497 (2022).
188. Chen, D. S. & Mellman, I. Oncology meets immunology: the cancer-immunity cycle. *Immunity* **39**, 1–10 (2013).
189. Uren, R. F., Howman-Giles, R. & Thompson, J. F. Patterns of lymphatic drainage of the skin in patients with melanoma. *J. Nucl. Med.* **44**, 570–582 (2003).
190. Connolly, K. A. et al. A reservoir of stem-like CD8$^+$ T cells in the tumor-draining lymph node preserves the ongoing antitumor immune response. *Sci. Immunol.* **6**, eabg7836 (2021).
191. Schenkel, J. M. et al. Conventional type I dendritic cells maintain a reservoir of proliferative tumor-antigen specific TCF-1+ CD8+ T cells in tumor-draining lymph nodes. *Immunity* **54**, 2338–2353.e6 (2021).
192. Thomas, S. N., Vokali, E., Lund, A. W., Hubbell, J. A. & Swartz, M. A. Targeting the tumor-draining lymph node with adjuvanted nanoparticles reshapes the anti-tumor immune response. *Biomaterials* **35**, 814–824 (2014).
193. Koster, B. D. et al. Local adjuvant treatment with low-dose CpG-B offers durable protection against disease recurrence in clinical stage I-II melanoma: data from two randomized phase II trials. *Clin. Cancer Res.* **23**, 5679–5686 (2017).
194. Ji, P. et al. Smart exosomes with lymph node homing and immune-amplifying capacities for enhanced immunotherapy of metastatic breast cancer. *Mol. Ther. Nucleic Acids* **26**, 987–996 (2021).
195. Dammeijer, F. et al. The PD-1/PD-L1-checkpoint restrains T cell immunity in tumor-draining lymph nodes. *Cancer Cell* **38**, 685–700.e8 (2020).
196. Hirakawa, S. et al. VEGF-A induces tumor and sentinel lymph node lymphangiogenesis and promotes lymphatic metastasis. *J. Exp. Med.* **201**, 1089–1099 (2005).
197. Lund, A. W. et al. VEGF-C promotes immune tolerance in B16 melanomas and cross-presentation of tumor antigen by lymph node lymphatics. *Cell Rep.* **1**, 191–199 (2012).
198. Farnsworth, R. H., Lackmann, M., Achen, M. G. & Stacker, S. A. Vascular remodeling in cancer. *Oncogene* **33**, 3496–3505 (2014).
199. Dubrot, J. et al. Lymph node stromal cells acquire peptide-MHCII complexes from dendritic cells and induce antigen-specific CD4$^+$ T cell tolerance. *J. Exp. Med.* **211**, 1153–1166 (2014).
200. Riedel, A., Shorthouse, D., Haas, L., Hall, B. A. & Shields, J. Tumor-induced stromal reprogramming drives lymph node transformation. *Nat. Immunol.* **17**, 1118–1127 (2016).
201. Gillot, L., Baudin, L., Rouaud, L., Kridelka, F. & Noël, A. The pre-metastatic niche in lymph nodes: formation and characteristics. *Cell. Mol. Life Sci.* **78**, 5987–6002 (2021).
202. Cochran, A. J. et al. Tumour-induced immune modulation of sentinel lymph nodes. *Nat. Rev. Immunol.* **6**, 659–670 (2006).
203. Mannino, M. H. et al. The paradoxical role of IL-10 in immunity and cancer. *Cancer Lett.* **367**, 103–107 (2015).
204. Batlle, E. & Massagué, J. Transforming growth factor-β signaling in immunity and cancer. *Immunity* **50**, 924–940 (2019).
205. Ito, M. et al. Tumor-derived TGFβ-1 induces dendritic cell apoptosis in the sentinel lymph node. *J. Immunol.* **176**, 5637–5643 (2006).
206. Lee, J. H. et al. Quantitative analysis of melanoma-induced cytokine-mediated immunosuppression in melanoma sentinel nodes. *Clin. Cancer Res.* **11**, 107–112 (2005).
207. Botella-Estrada, R. et al. Cytokine expression and dendritic cell density in melanoma sentinel nodes. *Melanoma Res.* **15**, 99–106 (2005).
208. Watson, M. J. et al. Metabolic support of tumour-infiltrating regulatory T cells by lactic acid. *Nature* **591**, 645–651 (2021).
209. Buzas, E. I. The roles of extracellular vesicles in the immune system. *Nat. Rev. Immunol.* **23**, 236–250 (2022).
210. Hu, L., Wickline, S. A. & Hood, J. L. Magnetic resonance imaging of melanoma exosomes in lymph nodes. *Magn. Reson. Med.* **74**, 266–271 (2015).
211. Pucci, F. et al. SCS macrophages suppress melanoma by restricting tumor-derived vesicle-B cell interactions. *Science* **352**, 242–246 (2016).
212. Taylor, D. D. & Gerçel-Taylor, C. Tumour-derived exosomes and their role in cancer-associated T-cell signalling defects. *Br. J. Cancer* **92**, 305–311 (2005).
213. Czystowska-Kuzmicz, M. et al. Small extracellular vesicles containing arginase-1 suppress T-cell responses and promote tumor growth in ovarian carcinoma. *Nat. Commun.* **10**, 3000 (2019).
214. Liu, C. et al. Murine mammary carcinoma exosomes promote tumor growth by suppression of NK cell function. *J. Immunol.* **176**, 1375–1385 (2006).
215. Cochran, A. J., Pihl, E., Wen, D. R., Hoon, D. S. & Korn, E. L. Zoned immune suppression of lymph nodes draining malignant melanoma: histologic and immunohistologic studies. *J. Natl Cancer Inst.* **78**, 399–405 (1987).
216. Chaudhary, N., Weissman, D. & Whitehead, K. A. mRNA vaccines for infectious diseases: principles, delivery and clinical translation. *Nat. Rev. Drug Discov.* **20**, 817–838 (2021).
217. Backlund, C., Jalili-Firoozinezhad, S., Kim, B. & Irvine, D. J. Biomaterials-mediated engineering of the immune system. *Annu. Rev. Immunol.* **41**, 153–179 (2023).
218. Lavelle, E. C. & Ward, R. W. Mucosal vaccines — fortifying the frontiers. *Nat. Rev. Immunol.* **22**, 236–250 (2022).
219. Regev, A. et al. The Human Cell Atlas white paper. Preprint at *arXiv* https://doi.org/10.48550/arXiv.1810.05192 (2018).
220. Petrova, T. V. & Koh, G. Y. Biological functions of lymphatic vessels. *Science* **369**, eaax4063 (2020).
221. Baluk, P. et al. Functionally specialized junctions between endothelial cells of lymphatic vessels. *J. Exp. Med.* **204**, 2349–2362 (2007).
222. Oliver, G., Kipnis, J., Randolph, G. J. & Harvey, N. L. The lymphatic vasculature in the 21st century: novel functional roles in homeostasis and disease. *Cell* **182**, 270–296 (2020).
223. Randolph, G. J. & Miller, N. E. Lymphatic transport of high-density lipoproteins and chylomicrons. *J. Clin. Invest.* **124**, 929–935 (2014).
224. Lewis, S. M., Williams, A. & Eisenbarth, S. C. Structure and function of the immune system in the spleen. *Sci. Immunol.* **4**, eaau6085 (2019).
225. Mebius, R. E. & Kraal, G. Structure and function of the spleen. *Nat. Rev. Immunol.* **5**, 606–616 (2005).
226. Oldenborg, P. A. et al. Role of CD47 as a marker of self on red blood cells. *Science* **288**, 2051–2054 (2000).
227. Chauveau, A. et al. Visualization of T cell migration in the spleen reveals a network of perivascular pathways that guide entry into T zones. *Immunity* **52**, 794–807.e7 (2020).

228. Bronte, V. & Pittet, M. J. The spleen in local and systemic regulation of immunity. *Immunity* **39**, 806–818 (2013).
229. Reboldi, A. & Cyster, J. G. Peyer's patches: organizing B-cell responses at the intestinal frontier. *Immunol. Rev.* **271**, 230–245 (2016).
230. Heel, K. A., McCauley, R. D., Papadimitriou, J. M. & Hall, J. C. Review: Peyer's patches. *J. Gastroenterol. Hepatol.* **12**, 122–136 (1997).
231. Cornes, J. S. Peyer's patches in the human gut. *Proc. R. Soc. Med.* **58**, 716 (1965).
232. Cerutti, A. & Rescigno, M. The biology of intestinal immunoglobulin A responses. *Immunity* **28**, 740–750 (2008).
233. Cyster, J. G. & Von Andrian, U. H. Dynamics of B cell migration to and within secondary lymphoid organs. in *Molecular Biology of B Cells* (eds Honjo, T., Alt, F. W. & Neuberger, M. S.) 203–221 (Elsevier, 2004).
234. Travis, M. A. et al. Loss of integrin αvβ8 on dendritic cells causes autoimmunity and colitis in mice. *Nature* **449**, 361–365 (2007).
235. Polack, F. P. et al. Safety and efficacy of the BNT162b2 mRNA Covid-19 vaccine. *N. Engl. J. Med.* **383**, 2603–2615 (2020).
236. Sheikh-Mohamed, S. et al. Systemic and mucosal IgA responses are variably induced in response to SARS-CoV-2 mRNA vaccination and are associated with protection against subsequent infection. *Mucosal Immunol.* **15**, 799–808 (2022).
237. Poon, M. M. L. et al. SARS-CoV-2 infection generates tissue-localized immunological memory in humans. *Sci. Immunol.* **6**, eabl9105 (2021).
238. Tang, J. et al. Respiratory mucosal immunity against SARS-CoV-2 after mRNA vaccination. *Sci. Immunol.* **7**, eadd4853 (2022).
239. Knisely, J. M. et al. Mucosal vaccines for SARS-CoV-2: scientific gaps and opportunities — workshop report. *NPJ Vaccines* **8**, 53 (2023).
240. Liao, M. et al. Single-cell landscape of bronchoalveolar immune cells in patients with COVID-19. *Nat. Med.* **26**, 842–844 (2020).
241. Grau-Expósito, J. et al. Peripheral and lung resident memory T cell responses against SARS-CoV-2. *Nat. Commun.* **12**, 3010 (2021).
242. Onodera, T. et al. Memory B cells in the lung participate in protective humoral immune responses to pulmonary influenza virus reinfection. *Proc. Natl Acad. Sci. USA* **109**, 2485–2490 (2012).
243. Schenkel, J. M. & Masopust, D. Tissue-resident memory T cells. *Immunity* **41**, 886–897 (2014).
244. Son, Y. M. et al. Tissue-resident CD4+ T helper cells assist the development of protective respiratory B and CD8+ T cell memory responses. *Sci. Immunol.* **6**, eabb6852 (2021).
245. Kingstad-Bakke, B. et al. Vaccine-induced systemic and mucosal T cell immunity to SARS-CoV-2 viral variants. *Proc. Natl Acad. Sci. USA* **119**, e2118312119 (2022).
246. Nouailles, G. et al. Live-attenuated vaccine sCPD9 elicits superior mucosal and systemic immunity to SARS-CoV-2 variants in hamsters. *Nat. Microbiol.* **8**, 860–874 (2023).
247. Lapuente, D. et al. Protective mucosal immunity against SARS-CoV-2 after heterologous systemic prime-mucosal boost immunization. *Nat. Commun.* **12**, 6871 (2021).
248. Mao, T. et al. Unadjuvanted intranasal spike vaccine elicits protective mucosal immunity against sarbecoviruses. *Science* **378**, eabo2523 (2022).
249. Hassan, A. O. et al. A single-dose intranasal ChAd vaccine protects upper and lower respiratory tracts against SARS-CoV-2. *Cell* **183**, 169–184.e13 (2020).
250. King, R. G. et al. Single-dose intranasal administration of AdCOVID elicits systemic and mucosal immunity against SARS-CoV-2 and fully protects mice from lethal challenge. *Vaccines* **9**, 881 (2021).
251. Hassan, A. O. et al. An intranasal vaccine durably protects against SARS-CoV-2 variants in mice. *Cell Rep.* **36**, 109452 (2021).
252. Afkhami, S. et al. Respiratory mucosal delivery of next-generation COVID-19 vaccine provides robust protection against both ancestral and variant strains of SARS-CoV-2. *Cell* **185**, 896–915.e19 (2022).
253. van Doremalen, N. et al. Intranasal ChAdOx1 nCoV-19/AZD1222 vaccination reduces viral shedding after SARS-CoV-2 D614G challenge in preclinical models. *Sci. Transl. Med.* **13**, eabh0755 (2021).
254. Madhavan, M. et al. Tolerability and immunogenicity of an intranasally-administered adenovirus-vectored COVID-19 vaccine: an open-label partially-randomised ascending dose phase I trial. *eBioMedicine* **85**, 104298 (2022).

Acknowledgements
The authors thank the WÜSI principal investigators, A. Riedel, M. Bajénoff and the Kastenmüller Lab for the critical reading of the manuscript. Our research is supported by the European Research Council (ERC) (819329- STEP2), the German Research Foundation (DFG) (SFB 1583- DECIDE and GRK2581 'SPHINGOINF') and the Max Planck Society (Max Planck Research Groups).

Author contributions
The authors contributed equally to all aspects of the article.

Competing interests
The authors declare no competing interests.

Additional information
Supplementary information The online version contains supplementary material available at https://doi.org/10.1038/s41577-023-00965-8.

Peer review information *Nature Reviews Immunology* thanks A. Andrusaite, V. Cerovic, S. Milling and the other, anonymous, reviewer(s) for their contribution to the peer review of this work.

Publisher's note Springer Nature remains neutral with regard to jurisdictional claims in published maps and institutional affiliations.

Statement of individual author contributions and of legal second publication rights to manuscripts included in the dissertation

Manuscript 3 (complete reference): Cruz de Casas, P., Knöpper, K., Dey Sarkar, R., Kastenmüller, W.; Same yet different – how lymph node heterogeneity affects immune responses, *Nat Rev Immunol*, 2023, online ahead of print					
Participated in	**Author Initials,** Responsibility decreasing from left to right				
Data Collection	PCC, KK, RDS, WK				
Manuscript Writing Writing of Introduction Writing of Discussion Writing of First Draft	PCC, KK, RDS, WK				

Explanations (if applicable): the figures of this manuscript were designed and drafted by PCC, RDS, KK and WK. However, the published figures were created by the journal itself.

If applicable, the doctoral researcher confirms that she/he has obtained permission from both the publishers (copyright) and the co-authors for legal second publication.

I hereby confirm that I have obtained permission from Springer Nature publisher and co-authors Konrad Knöpper and Rupak Dey Sarkar for legal second publication. I also confirm Wolfgang Kastenmüller's (primary supervisor) acceptance.

The doctoral researcher and the primary supervisor confirm the correctness of the above mentioned assessment.

Paulina Cruz de Casas

Doctoral Researcher's Name | Date | Place | Signature

Konrad Knöpper

Co-authors Name | Date | Place | Signature

Rupak Dey Sarkar

Co-authors Name | Date | Place | Signature

Prof. Dr. med. Wolfgang Kastenmüller

Primary Supervisor's Name | Date | Place | Signature

Appendix B

Abbreviations

ACK: Ammonium-Chloride-Potassium
ADP: adenosine di-phopshate
APC(s): antigen presenting cell(s)
APM: antigen presenting molecule
ASM: acid sphingomyelinase
ATP: adenosine tri-phosphate
BCR: B cell receptor
BFA: Brefeldin A
bis-pNPP: bis(4-nitrophenyl) phosphate
BM: bone marrow
BSA: bovine serum albumin
C1P: ceramide-1-phosphate
CCL: C-C motif chemokine ligand
CCR: C-C motif chemokine receptor
CD: cluster of differentiation
cDCs: conventional dendritic cells
CDN(s): cyclic dinucleotide(s)
cDNA: complementary desoxyribonucleic acid
Cer: ceramide
cGAMP: cyclic guanosine monophosphate-adenosine monophosphate
cGAS: nucleotidyl transferase cyclic GMP-AMP synthase
CITE-seq: Cellular Indexing of Transcriptomes and Epitopes
CFU: colony forming units
CLPs: common lymphoid progenitor cells
CNS: central nervous system
CTL: cytotoxic lymphocytes
CXCL: C-X-C motif chemokine ligand
CXCR: C-X-C motif chemokine receptor
DAMPs: damage-associated molecular patterns
DCs: dendritic cells
DEGs: differentially expressed genes
dhCer: dihydroceramide
dhSM: dihydrosphingomyelin
dLN(s): draining lymph node(s)
DMSO: dimethylsulfoxid
DN: double negative
DP: double positive
DTT: diethiothreitol
EE: early effector cells

ENPP1: ectonucleotide pyrophosphatase/phosphodiesterase I
EUCOMM: European Conditional Mouse Mutagenesis
FACS: fluorescence-activated cell sorting
FDCs: follicular dendritic cells
FRCs: fibroblastic reticular cells
FSGS: focal segmental glomerulosclerosis
GM1: monosialotetrahexosylganglioside
GPI: glycosylphosphatidylinositol
hexCer: hexosylceramides
Hip1: Huntington-interacting protein 1
HPLC-MS/MS: high-performance liquid chromatography tandem mass spectrometry
IELs: intraephitelial lymphocytes
IFNγ: interferon-γ
ILCs: innate lymphoid cells
iLN: inguinal lymph node
i.n.: intranasal
IL-: interleukin
i.p.: intraperitoneal
IS: immune system
ISF: interstitial fluid
i.v.: intravenous
KO: knock-out
KS: 3-ketosphinganine
lacCer: lactosylceramides
LCs: Langerhans cells
LCMV: lymphocytic choriomeningitis virus
LEC(s): lymphatic endothelial cell(s)
LN(s): lymph node(s)
LP: lamina propria
LXR: liver X receptor
MAIT: mucosal-associated invariant T cells
medLN(s): mediastinal lymph node(s)
mesLN(s): mesenteric lymph node(s)
MFI: mean fluorescence intensity
MHC: major histocompatibility complex
MHC-I: major histocompatibility complex class I
MHC-II: major histocompatibility complex class II
migDC(s): migratory dendritic cell(s)
MPEC: memory precursor effector cells
MR1: major histocompatibility complex class I-related gene protein
MRSA: methicillin-resistant *Staphylococcus aureus*

MS: multiple sclerosis
NK cells: natural killer cells
NKT: natural killer T cells
NSM: neutral sphingomyelinase
P14: T cell receptor (TCR)-transgenic gp33-specific $CD8^+$ T cells
PAMPs: pathogen-associated molecular patterns
PCA: principal component analysis
PCR: polymerase chain reaction
PFU: plaque forming units
PLO: primary lymphoid organs
PM: plasma membrane
PMA: phorbol myristate acetate
pNP: 4-Nitrophenol
pre-DCs: precursors of dendritic cells
PRRs: pattern-recognition receptors
PRRSV: porcine reproductive and respiratory syndrome virus
RNA-seq: RNA sequencing
rpm: rotations per minute
RT: room temperature
S1P: sphingosine-1-phosphate
S1PR(s): sphingosine-1-phosphate receptor(s)
S. aureus: Staphylococcus aureus
s.c.: subcutaneous
scRNA-seq: single-cell RNA sequencing
sdLN(s): skin-draining lymph node(s)
SEM: standard error of the mean
SG: salivary gland
SL: sphingolipids
SLEC: short-lived effector memory
SLO: secondary lymphoid organs
SM: sphingomyelin
SMase(s): sphingomyelinase(s)
Smpd: sphingomyelin phosphodiesterase
Smpdl: sphingomyelin phosphodiesterase acid-like
Smpdl3a: sphingomyelin phosphodiesterase acid-like 3a
Smpdl3b: sphingomyelin phosphodiesterase acid-like 3b
SP: single positive
SPT: serine palmitoyltransferase
STING: stimulator of interferon genes
TCM: central memory T cells
TCR: T cell receptor

Tconv: conventional T cells

T_{eff}: effector T cells

TEM: effector memory T cells

Th: T helper cell

TLR: toll-like receptor

T_{mem}: memory T cells

TNFα: tumor necrosis factor-α

TPM: peripheral memory T cells

Treg: regulatory T cells

TRM: tissue-resident memory T cells

tSNE: t-distributed stochastic neighbor embedding

UMAP: uniform manifold approximation and projection

UMI: unique molecular identifier

UTC(s): unconventional T cell(s)

v:v : volume:volume

VVG2: Vaccinia virus expressing LCMV-GP protein

WT: wild-type

Acknowledgements

My period as a PhD student has been a rollercoaster ride, with several ups and downs from the beginning up until today. However, every day I look back and realize that I would not want it to have been any different. My PhD adventure started roughly at the same time as the COVID-19 pandemic, in April 2020. I was still living in France when, around 2-3 weeks before the starting date of my contract, the president announced a complete lockdown of the country, which would include closing the borders between France and Germany, for an undefined period of time. I was lucky to have such a good German friend, Aristea, living in Maastricht (Netherlands), who contacted me to offer me a home with her during the pandemic. If it wasn't for Aristea, I would not have managed to go to Germany on time. So I would always be very grateful for this. Thank you Aristea.

Wolfgang Kastenmüller, my PhD supervisor, is the person I would like to thank the most. Mainly, I would like to thank him for giving me the opportunity to join his group, despite me joining as a surprise. Along the way, Wolfgang gave me the opportunity to work on very exciting and fun projects, for which I am extremely grateful. I would also like to thank Wolfgang for always supporting me during every step of my PhD, and for always being there for me to discuss the big picture of our projects and the technicalities of our experiments. More importantly, I will always be grateful because Wolfgang gave me all his trust and patience to evolve to the scientist that I have become today, and for his guidance and advice. I also want to thank Wolfgang for all the fun get-togethers he organized for our team. I will always cherish these memories. Thank you for everything Wolfgang.

The next person I would like to thank is Niklas Beyerdorf. Niklas was who first allowed me to join one of the projects of our training group. Also, he guided me on how to get started as a PhD student in the University of Würzburg. Thank you Niklas for always being so enthusiastic about science, and for always being there to support me and the project. Thank you for your trust, mentorship and guidance throughout our annual meetings. Thank you Niklas. I would also like to extend my gratitude to the additional members of my thesis advisory committee, Andreas Beilhack and Thomas Rudel, for all their useful feedback and enthusiasm during our annual meetings. Thank you Andreas and Thomas.

My PhD would not have been what it was without one of my best friends, Konrad. Konrad taught me pretty much everything I know about Immunology, including many of the techniques and methods we use in our lab. Moreover, Konrad taught me something I had not had in a very long time, and that is the true meaning of friendship. Konrad and I shared thousands of hours together in the lab working on the beautiful UTC story I share with you as part of this compilation. Konrad was not only my colleague, but also the person that made all this possible. Thank you Konrad for your time, your advice and all the fun moments and conversations we had. Thank you for your advice, for your patience and your friendship. I am happy to know that, wherever we both go, I will always have the best friend to count on, and I hope he knows it is the same from my side. Thank you for forgiving me when I almost killed you during our little bike ride to Eibelstadt. Thank you Konrad.

My biggest gratitude lies with my mom, my sister, and my partner. I do not have enough words to express how grateful I am every single day to know I have such an amazing team backing me up whenever I need it. Thank you for showing me the meaning of trust, loyalty, and love. I would like to thank my mom, Lucero, and my sister, Andrea, for always being there for me and holding me when I needed it the most. Thank you for making me the person who I am today. I am also very grateful to have

met Ingo during the course of my PhD. Thank you Ingo for your patience and care, your advice, and for teaching me so many things (including how to use EndNote). Without the three of you, I would not have managed to make it until today. So, again, thank you mom, Andrea and Ingo. I, of course, also thank the rest of my family, Elena, Mayela, all my cousins, and my dog, Sansa. Thank you for always caring for me and supporting me.

Marco is one of the persons to whom I will always be very grateful. Marco was my first mentor in the lab. He trained me from the very beginning and trusted me blindly to perform every experiment we had to perform. Despite not having worked with him in the lab for long, we continued working together to finalize the UTC project that he started. Without him, this project would not have developed as it did. Marco is one of the most positive and enthusiastic scientists I have ever met, and I am grateful that I had the opportunity to learn so much from him. Thank you Marco.

During my PhD, I was very lucky to have colleagues who rapidly became my friends. I thank Chloe and Ana for being so welcoming and friendly since the first day. I thank them also for all the laughter, the fun, the adventures, and the happy moments we shared together (I also thank that we are alive after our little bike accident!). Without them, my PhD would not have been so much fun. Thank you Ana and Chloe. Another colleague that became a very good friend is Augusto. Augusto was always there to listen to me and to support me whenever I needed it. Thank you for all the laughs and the fun moments we had. Thank you for helping me balance the emotional environment in our office. Thank you for being so authentic and for all the Switch nights. Thank you Augusto.

Anika is someone who made my PhD a very fun and amazing time. I thank Anika for always being there for me when I needed it. I thank her for guiding me so much when I first came to Germany. I would also like to thank Anika for her positive energy every single day, and for being the bright light in the room to make everything better. Thank you Anika.

My gratitude extends to all the members of the Kamü lab with whom I have the honor to work during my PhD. Thank you Lennart, Annerose, Deeksha, Milas, Rupak, Kasia, Sawako, Jacob, Katya, Anfei, Defne, Karen, Kathrin and Andrea. Thank you for all the discussions, help when doing experiments, fun at the social gatherings. Thank you for being a great and fun team to work with.

I would like to thank Martin for always making the time to give me advice and for the fruitful scientific discussions we had. I additionally would like to thank other members of the Institute of Systems Immunology. Thank you Christin, Sigrun, Sofie, Ye, Christian, Rémi, Alex, Gabi, Miriam C., Miriam E., Katrin, Sophia, Hao, Stella, Mariachiara, Mercedes, Georg, Gosia, Katja, Christina Sabine, Sarah, Janine, Katerina, Galina, Jasmina, Stefan and Kim. Thank you for all your organizational, technical and intellectual support. Thank you for making me feel like we are all part of one big team.

Finally, I would like to thank the members of my training group and external collaborators. I thank Jürgen for having invited me to form part of the PhD program. I thank Putri for being my friend within the training group. I thank Fabian, Dominik and Burkhard for all the collaborations and support. I thank the rest of the training group for our meetings and the feedback for the Smpdl3b project. I also thank Leonhard Heinz for his help and support for the Smpdl3b project.

Looking back to the past 4 years, I can say I have been privileged to be surrounded by amazing scientists and friends, whose lessons and wisdom I will carry with me for the rest of my life. Thank you.

Affidavit

I hereby confirm that my thesis entitled “Sphingolipids as modulators of T cell function” is the result of my own work. I did not receive any help or support from commercial consultants. All sources and / or materials applied are listed and specified in the thesis. Furthermore, I confirm that this thesis has not yet been submitted as part of another examination process neither in identical nor in similar form.

Place, Date

Signature

Eidesstattliche Erklärung

Hiermit erkläre ich an Eides statt, die Dissertation „Sphingolipide als Modulatoren der T-Zell-Funktion“, d.h. insbesondere selbständig und ohne Hilfe eines kommerziellen Promotionsberaters, angefertigt und keine anderen als die von mir angegebenen Quellen und Hilfsmittel verwendet zu haben. Ich erkläre außerdem, dass die Dissertation weder in gleicher noch in ähnlicher Form bereits in einem anderen Prüfungsverfahren vorgelegen hat.

Place, Date

Signature

Publication list

- Cruz de Casas, P., et al. (2023). Same yet different – how lymph node heterogeneity affects immune responses. *Nat. Rev. Immunology.*

- Ataíde, M., Knöpper, K., Cruz de Casas, P., et al. (2022). Lymphatic migration of unconventional T cells promotes site-specific immunity in distinct lymph nodes. *Immunity*. 55: 1813-1828. https://doi.org/10.1016/j.immuni.2022.07.019 (shared first authorship)

- Lesire, L., Chaput, L., Cruz De Casas, P., et al. (2020). High-Throughput Image-Based Aggresome Quantification. *SLAS Discovery*. 25: 783-791. https://doi.org/10.1177/2472555220919708